AN ISOFORM-SPECIFIC ROLE OF FYNT IN ALZHEIMER'S DISEASE AND ITS RELEVANCE IN NEUROINFLAMMATION

LEE CHING LI
(B.Sc. (Hons.), NUS)

A THESIS SUBMITTED FOR THE DEGREE OF DOCTOR OF PHILOSOPHY

DEPARTMENT OF PHARMACOLOGY

NATIONAL UNIVERSITY OF SINGAPORE

2016

DECLARATION

I hereby declare that the thesis is my original work and it has been written by me in its entirety. I have duly acknowledged all the sources of the information which have been used in the thesis.

This thesis has also not been submitted for any degree in any university previously.

Lee Ching Li
21st January 2016

ACKNOWLEDGEMENTS

I would like to thank my supervisor, Dr Mitchell Lai, for giving me the opportunity to take up this project, providing encouragement and insightful ideas during the course of my study.

I would like to thank my co-supervisor Dr Michelle Tan, who closely supervised me throughout all these years. I am grateful for her invaluable advices, detailed guidance, patience and understanding.

I would like to thank my co-supervisor Prof Peter Wong for giving me positive feedback and helpful pointers.

I would like to thank Clara, for all her help, encouragement and quirky pranks that brighten up the lab.

I would like to thank Jasinda and Yuek Ling for their constant morale support and ideas.

I would like to thank Ezan, Su Jing, Mrs Ting, Andrea and Siew Ying for their guidance in animal work and also the VanDongen Laboratory from Duke-NUS for their valuable advice and demonstration on neuronal culture.

I am also grateful to have met many wonderful friends and colleagues in the Department of Clinical Translational Research, SGH and in NUS who were extremely supportive and encouraging throughout the course of my study.

I thank all my friends (Sarisblingbling, L4, ASG, Dramaclub, Kahyee, Duan, FYP mates and many more) who always shower me with care and concern.

Lastly, I thank my dearest family for their support and prayers. Without them (especially my grandfather), this would not have been possible.

TABLE OF CONTENTS

SUMMARY

Alzheimer's disease (AD) is a progressive neurodegenerative disease characterized by neuropathological hallmarks that include accumulation of amyloid-beta (Aβ) plaques and neurofibrillary tangles, neuroinflammation and neuronal loss. Recent studies have found that Fyn tyrosine kinase is implicated in the pathogenesis of AD, mediating Aβ toxicity and tau hyperphosphorylation. However, no study has attempted to delineate isoform-specific roles of Fyn in association with AD. Our preliminary data from exon arrays demonstrated differential alternative splicing of Fyn in AD, with significant increase of FynT but no change of brain-predominant FynB isoform in AD as compared to control brain samples. Furthermore, gene ontology term enrichment analyses of the exon array data and cellular markers correlation revealed that FynT was positively correlated with markers associated to reactive astrogliosis and negatively correlated with neuronal genes.

This thesis thus aims to identify the isoform-specific role of FynT in AD brain and the possible impacts of FynT induction to the progression of AD. We hypothesized that FynT induction may be associated with pathological features in AD. In this thesis, the flow of my research follows a post-mortem-to-bench approach, where we first identified our research target from post-mortem brain tissues (Chapter 3) and then investigated and validated its function using primary cell culture (Chapter 4) and recombinant approaches (Chapter 5).

In summary, using post-mortem brain tissues, we validated specific increase of FynT mRNA and protein expression in AD brains and determined that FynT induction in AD was independently associated with neurofibrillary degeneration and reactive astrogliosis (Chapter 3). Thus, we speculated that the expression of FynT and FynB may be differentially regulated by pathological conditions associated with AD. Primary rat mixed cortical cultures treated with Aβ and primary rat astrocyte cultures treated with TNFα demonstrated that FynT but not FynB could be specifically induced by both *in vitro* systems associated with AD in astrocytes. Furthermore, FynT was positively correlated with astrocytic markers in increasing populations of astrocytes from mixed cortical cultures (Chapter 4). Taking into account that previous studies have reported Fyn involvement in cytokines expression in immune cells, we hypothesized that FynT kinase activity can modulate inflammatory response in astrocytes. By employing recombinant FynT mutant approaches, FynT kinase activity was found to facilitate TNFα-induced expression of inflammatory markers in immortalized normal human astrocyte (iNHA), likely through modulating NF-κB signalling pathway (Chapter 5).

In conclusion, our findings have added new perspectives to the isoform-specific role of FynT in AD, particularly the role of FynT in modulating neuroinflammatory responses in astrocytes. Therefore, we speculate that the aberrant increased expression of FynT in AD may be targeted as a therapeutic approach in alleviating neuroinflammation and possibly tau pathology in AD.

LIST OF TABLES

LIST OF FIGURES

LIST OF ABBREVIATIONS

18S rRNA	18S ribosomal RNA
AD	Alzheimer's disease
ANOVA	Analysis of variance
APOE4	Apolipoprotein E *epsilon* 4
APP	Amyloid precursor protein
AraC	Cytosine ß-D-arabinofuronoside
Aβ	Amyloid-beta
BA9/22	Brodmann area 9 or 22
BBB	Blood brain barrier
BDR	Brains for Dementia Research
CCK-8	Cell counting kit-8
CCL2	Chemokine (C-C motif) ligand 2 also known as monocyte chemotactic protein 1 (MCP-1)
CCL3	Chemokine (C-C Motif) ligand 3 also known as macrophage inflammatory protein 1 alpha (MIP-1α)
CCL4	Chemokine (C-C Motif) ligand 4 also known as macrophage inflammatory protein 1-beta (MIP-1β)
CCL5	Chemokine (C-C Motif) ligand 5 also known as regulated on activation, normal T cell expressed and secreted (RANTES)
CCL7	Chemokine (C-C Motif) ligand 7 also known as monocyte chemoattractant protein 3 (MCP-3)
CD11B	CD11 antigen-like family member B
cDNA	Complementary DNA
CERAD	Consortium to Establish a Registry for AD
CHX	Cycloheximide
CNS	Central nervous system
CSF	Cerebrospinal fluid
CSF2	Colony stimulating factor 2 also known as granulocyte-macrophage colony stimulating factor (GM-CSF)

CSF3	Colony Stimulating Factor 3 also known as granulocyte colony stimulating factor (G-CSF)
CXCL10	Chemokine (C-X-C Motif) ligand 10 also known as interferon-inducible cytokine (IP-10)
CXCL12	Chemokine (C-X-C Motif) ligand 12 also known as stromal cell derived factor 1 (SDF-1)
DAMP	Danger-associated molecular patterns
DIV	Days *in vitro*
DMEM	Dulbecco's modified eagle medium
DMSO	Dimethyl sulfoxide
DNA	Deoxyribonucleic acid
DNase	Deoxyribonuclease
DsiRNA	Dicer-substrate RNAs
EDTA	Ethylenediaminetetraacetic acid
ELISA	Enzyme-linked immunosorbent assay
ENO2	Neuron-specific enolase
EV	Empty vector
FBS	Fetal bovine serum
FGF-2	Fibroblast growth factor 2
FTDP-17T	Familial frontotemporal dementia with Parkinsonism linked to chromosome 17
FynB	Fyn tyrosine kinase isoform B
FynT	Fyn tyrosine kinase isoform T
FynT-CA	Fyn tyrosine kinase isoform T, constitutively active
FynT-KD	Fyn tyrosine kinase isoform T, kinase dead
FynT-WT	Fyn tyrosine kinase isoform T, wild-type
GAPDH	Glyceraldehyde-3-phosphate dehydrogenase
GFAP	Glial fibrillary acidic protein
GLAST	Solute carrier family 1 (glial high affinity glutamate transporter), member 3

GLT-1	Solute carrier family 1 (glial high affinity glutamate transporter), member 2
GO	Gene ontology
hTERT	Human telomerase reverse transcriptase
IF	Immunofluoresence
IκB	Inhibitor of kappa B
IKK	IκB kinase
IL-1	Interleukin 1
IL-1α	Interleukin 1 alpha
IL1B/ IL-1β	Interleukin 1 beta
IL1ra/ IL-1ra	Interleukin 1 receptor antagonist
IL23	Interleukin 23
IL6/ IL-6	Interleukin 6
IL8/ IL-8	Interleukin 8
iNHA	Immortalized normal human astrocytes
JNK	c-Jun N-terminal kinase
LIF	Leukemia inhibitory factor
LPS	Lipopolysaccharide
LTP	Long-term potentiation
MAP	Microtubule associated protein
MAPK	Mitogen-activated protein kinases
MAPT	Microtubule associated protein tau
MCI	Mild cognitive impairment
mRNA	Messenger RNA
NB	Neurobasal
NBTR	Newcastle Brain Tissue Resource
NeuN	Neuronal Nuclei, also known as RNA binding protein fox-1 homolog 3 (RBFOX3)

NFT	Neurofibrillary tangles
NF-κB	Nuclear factor-kappa B
NMDA	N-methyl-D-aspartate
NSAID	Non-steroidal anti-inflammatories
OCT	Optimal cutting temperature compound
OPTIMA	Oxford Project to Investigate Memory and Ageing
PBS	Phosphate buffer saline
PCR	Polymerase chain reaction
PHF	Paired helical filaments
PMI	Post-mortem interval
PrP^{C}	Cellular prion protein
PSEN1/2	Presenilin-1/2
RNA	Ribonucleic acid
RNase	Ribonuclease
ROS	Reactive oxygen species
RT	Room temperature
RT-PCR	Reverse transcription polymerase chain reaction
sAPPα	Secreted amyloid precursor protein-α
SEM	Standard error of the mean
SFK	Src family kinase
SH1/2/3	Src Homology 1, 2 or 3
TGFβ	Transforming growth factor beta
TLR	Toll-like receptors
TNFR1	Tumour necrosis factor receptor 1
TNFα	Tumour necrosis factor alpha
TREM2	Triggering receptor expressed on myeloid cells 2
TUBB3	Tubulin, beta 3 class III

CHAPTER 1- Introduction

CHAPTER 1- Introduction

1.1 Alzheimer's disease (AD)

Alzheimer's disease (AD) is a neurodegenerative disease that is characterized by severe progressive loss of memory and cognitive abilities such as language, problem-solving skills and even one's ability to conduct daily tasks. It is the most common form of dementia (up to 80%) that mainly affects the aged (Alzheimer's, 2015). A small proportion of patients diagnosed with early-onset AD before the age of 65 are often linked to genetic mutations of Amyloid precursor protein (APP), Presenilin-1 (PSEN1) and Presenilin-2 (PSEN2) (Selkoe, 1991, Cras et al., 1998, Brouwers et al., 2008). The exact etiology of AD is still unclear but possible risk factors include aging, genetic predisposition (e.g. Apolipoprotein E epsilon 4 (APOE4)) and also environmental risk factors such as lifestyle and history of head trauma (Tilley et al., 1998, Guo et al., 2000, Xu et al., 2015).

Currently, the global prevalence of dementia among people above 60 years of age has been reported to be about 5%, which is estimated to be over 46 million. The number is expected to double every 20 years, spiralling to approximately 131 million in 2050. Furthermore, the prevalence of AD increases exponentially after the age of 65 (Qiu et al., 2009). The disease has cost huge economic burden globally, rounding to about US$ 818 billion in 2015 (Martin Prince, 2015). In Singapore, the prevalence of dementia among people above 60 years of age as of 2015 was reported to be 10%, double the percentage of global prevalence (Subramaniam et al., 2015). This could be attributed to the rapid ageing population as well as higher prevalence of risk factors for

dementia, such as diabetes, hypertension and obesity (Subramaniam et al., 2015).

At present, there is no cure for AD and the progression from diagnosis to death takes about seven to ten years, with pneumonia or sepsis as the common causes of death (Brookmeyer et al., 2002). With the acceleration of worldwide population aging, there is a compelling need to develop new treatments that can effectively delay the onset of AD or prevent the disease.

1.1.1 Histopathological hallmarks of AD

Dr. Alois Alzheimer first described the case of AD in Auguste Deter, who displayed profound memory loss and worsening psychosocial changes before her death in 1906. Upon autopsy, he found extensive neuronal loss and abnormal deposits in and around nerve cells (Dahm, 2006). These deposits, namely amyloid plaques and neurofibrillary tangles (NFT), are the classical hallmarks of AD which are still used as post-mortem histological markers for definitive diagnosis of AD (Perl, 2010). Apart from amyloid plaques which are composed of aggregated amyloid-beta (Aβ) peptides and NFT that are made up of hyperphosphorylated tau protein, neuronal loss, synaptic dysfunction and reactive gliosis are also neuropathological features of AD (Beach et al., 1989, Itagaki et al., 1989, Fuller et al., 2010, Serrano-Pozo et al., 2011). Several of these hallmarks (e.g., Aβ accumulation, synaptic dysfunction) can be observed even before the onset of clinical symptoms and are characteristic in different stages of the disease (see Figure 1.1) (Braak and Braak, 1991, Lichtenstein et al., 2010, Sperling et al., 2011).

In recent years, more research has been focussed on the earlier stage of AD, the mild cognitive impairment (MCI) stage, where subtle changes in memory

can be observed yet patients are not labelled demented clinically (Petersen et al., 1999). Synaptic loss that has been observed in the MCI stage (Scheff et al., 2006) is known to be the best pathological correlation of cognitive dysfunction in AD thus far (Terry et al., 1991, Koffie et al., 2011).

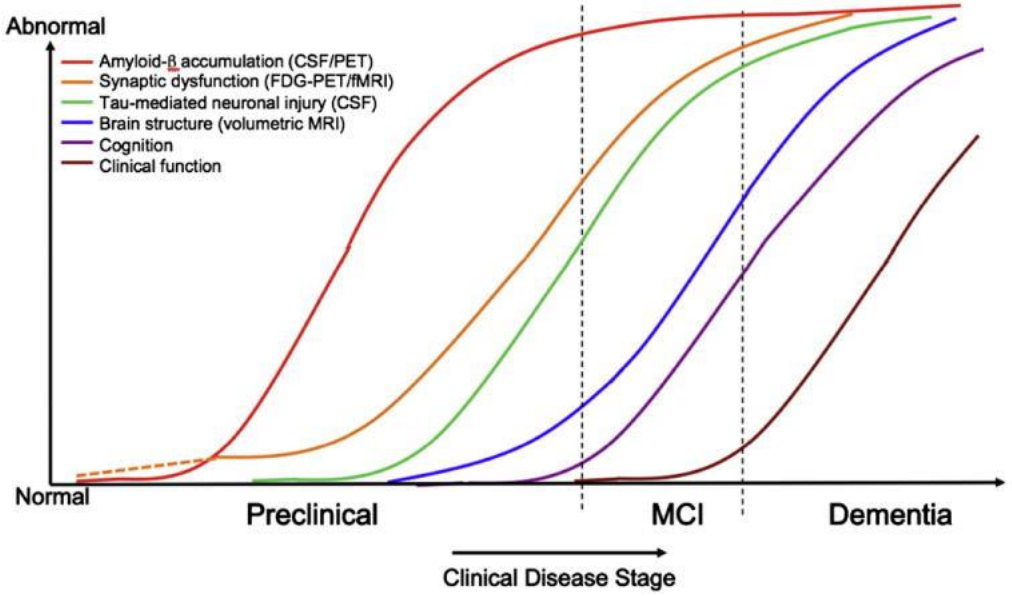

Figure 1.1 Hypothetical model of biomarkers in AD to illustrate the preclinical phase of AD. Biomarkers emerging at different stages of AD progression; from preclinical to MCI and subsequently dementia. Changes plotted from maximally normal to maximally abnormal (y axis) as a function of disease stage (x axis). Figure adapted from (Sperling et al., 2011) with permission from Elsevier.

1.1.2 Amyloid beta (Aβ)

Aβ, the major component of aggregated extracellular plaques is derived from its precursor, APP (Masters et al., 1985, Goldgaber et al., 1987). APP is a transmembrane protein expressed abundantly in the brain (Zheng and Koo, 2011). Full-length APP can be processed by the non-amyloidogenic or amyloidogenic pathways. Under physiological condition, APP undergoes processing predominantly via the non-amyloidogenic pathway. However in AD, there is a shift towards the amyloidogenic pathway (Fukumoto et al., 2002, Platt et al., 2013). In the non-amyloidogenic pathway, APP is cleaved

by α-secretase, yielding soluble APP derivative, secreted Amyloid precursor protein-α (sAPPα). sAPPα has been found to be involved in several cellular processes including neuroprotection, possibly memory enhancement and modulates synaptic plasticity and excitability (Turner et al., 2003, Reinhard et al., 2005, Ring et al., 2007, Zheng and Koo, 2011). On the other hand, sequential processing of APP by β-secretase and γ-secretase generally yields 40-42 kDa Aβ peptides. The neurotoxic $A\beta_{1-42}$ peptide is highly hydrophobic and therefore more prone to self-aggregation, resulting in oligomerization, insoluble fibrils formation and subsequently formation of amyloid plaques mainly in the neocortex (See Figure 1.2) (Selkoe, 2002, Serrano-Pozo et al., 2011). The toxic moiety of $A\beta_{1-42}$ responsible for its neurotoxic properties has been identified to be $A\beta_{25-35}$, the shortest fragment capable of forming large β-sheet yet retaining toxicity of the full-length peptide (McLaurin and Chakrabartty, 1997, Stepanichev et al., 2006, Millucci et al., 2010). While less well-studied in the field, this short fragment has been reported to be detected in both subiculum and entorhinal cortex of AD brains (Kubo et al., 2003).

Although amyloid plaques do not correlate well with the severity of AD, *in vivo* and *in vitro* experiments have demonstrated that aggregated Aβ can induce oxidative stress in neurons (Pike et al., 1993, Matsuoka et al., 2001). Earlier studies suggested that Aβ-induced neurotoxicity requires fibrillar aggregation of Aβ *in vitro* (Pike et al., 1993, Lorenzo and Yankner, 1994). However, increasing evidence has also revealed that soluble oligomeric species of Aβ can exert greater cytotoxic effects and induce synaptic dysfunction in neurons (Lambert et al., 1998, Klein et al., 2001, Dahlgren et

al., 2002, Lacor et al., 2007). Possible mechanisms of how oligomeric Aβ exerts neurotoxicity include direct perturbation of the membrane lipid bilayer and affecting ion homeostasis, impairing mitochondria function, inducing tau hyperphosphorylation and enhancing excitotoxic N-methyl-D-aspartate (NMDA) receptors mediated signalling by activating signalling pathways through engagement of PrP^{C}-Fyn (Zheng et al., 2002, Du et al., 2008, Butterfield and Lashuel, 2010, Um et al., 2012). In addition, the neurotoxic Aβ has also been shown to activate both microglial and astrocytes resulting in increased expression of inflammatory mediators and accumulation of reactive oxygen species (ROS) (El Khoury et al., 1996, Simpson et al., 2010, Heneka et al., 2015).

Many genetic risk factors of AD are related to APP mutations and APP processing genes like PSEN1 and PSEN2 of the γ-secretase (Tilley et al., 1998, Selkoe, 2002). Mutations in these deterministic genes lead to accelerated accumulation of Aβ plaques, resulting in early onset, autosomal dominant familial AD (Musiek and Holtzman, 2015). Furthermore, because the APP gene is localized on chromosome 21, neuropathology of AD can also be observed in trisomy 21 (Down syndrome) (Iwatsubo et al., 1995). These genetic evidences have provided framework for the amyloid hypothesis of AD, where Aβ accumulation in the brain is the primary driver of AD pathogenesis (Hardy and Selkoe, 2002).

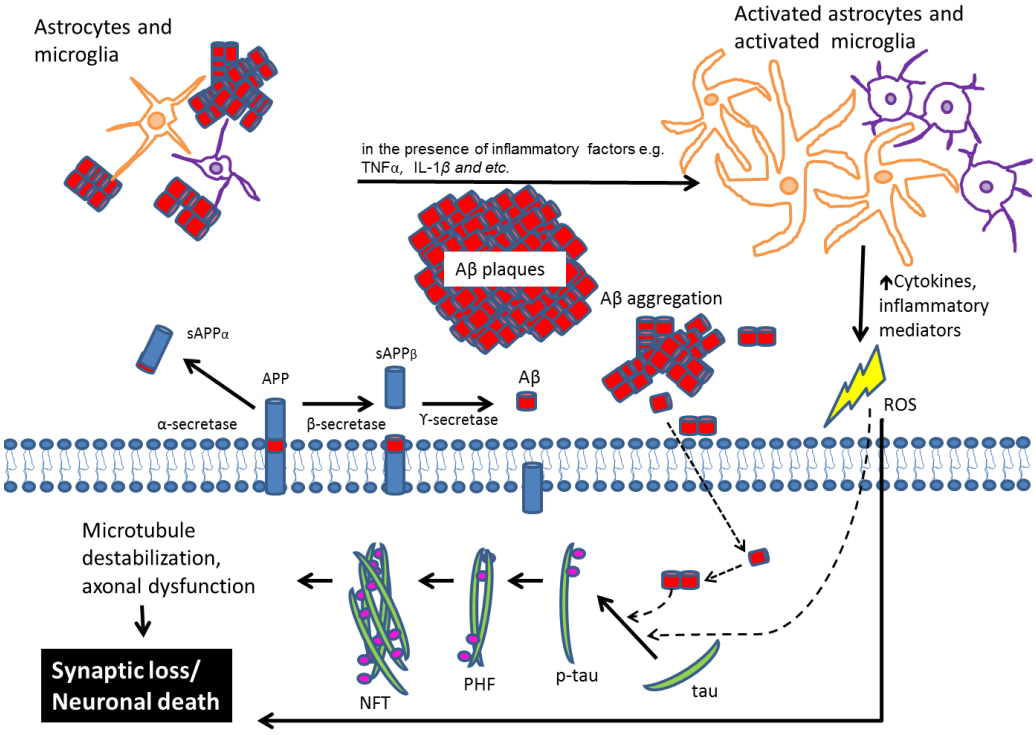

Figure 1.2 A pictorial summary of neuropathological events in AD. Transmembrane APP in neurons can be processed by non-amyloidogenic pathway to give sAPPα or amyloidogenic pathway in AD through β-sceretase and γ-secretase to give Aβ. Aβ peptides, particularly $A\beta_{1\text{-}42}$, are prone to aggregation giving rise to extracellular Aβ plaque- a hallmark of AD. Aβ can also accumulate intracellularly in neurons and may facilitate tau phosphorylation. Glial cells, such as microglia and astrocytes, are activated in the presence of aggregated Aβ and secrete more inflammatory cytokines to propagate glial activation. Increased inflammatory mediators facilitate ROS production in the brain, resulting in tau hyperphosphorylation, synaptic loss and neuronal death.

1.1.3 Neurofibrillary tangles (NFTs)

Apart from Aβ, the other pathological protein that undergoes aggregation in AD is tau. Tau is a microtubule associated protein (MAP) that is essential for the assembly and stabilization of microtubules in neurons (Weingarten et al., 1975). There are at least 58 reported phosphorylation sites in tau which consist of a majority of serine/threonine sites as well as tyrosine sites (Wang et al., 2013b). Abnormal phosphorylation of tau proteins causes microtubule destabilization which results in the aggregation of hyperphosphorylated tau seen in paired helical filaments (PHF). These aggregated proteins eventually form neuropil threads in axonal and dendritic segments, neurofibrillary tangles in somatodendritic compartments of neurons, and dystrophic neurites in AD (Iqbal et al., 2009, Serrano-Pozo et al., 2011). Unlike the less predictable spatiotemporal progression of amyloid deposition in AD, the pattern of spreading of NFT pathology is much more predictable and correlates better clinically with the severity and the progression of dementia in AD (Braak and Braak, 1991, Serrano-Pozo et al., 2011). Clinicopathological staging of NFT in AD by Braak and Braak (Braak and Braak, 1991) can be distinguished into six stages based on the extent of NFT distribution in the brain. Briefly, the first two stages involved the alteration of the entorhinal cortex, followed by limbic and hippocampal accumulation of NFT (stages three and four) and subsequently spreading to the neocortex as seen in Figure 1.3 (Braak and Braak, 1991, Serrano-Pozo et al., 2011).

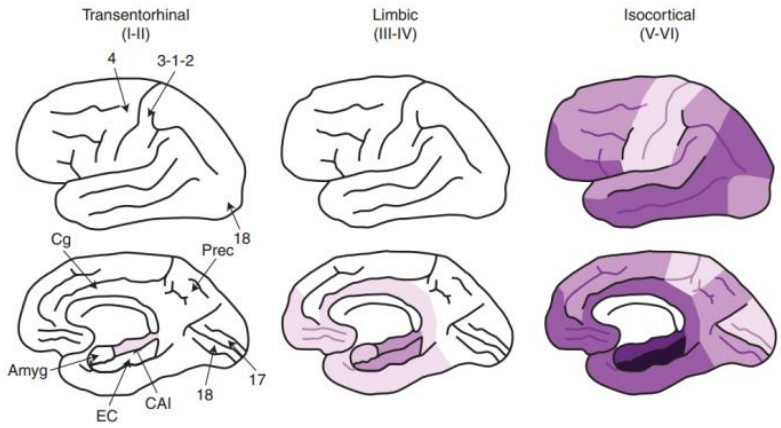

Figure 1.3 Spatiotemporal pattern of NFT distribution in AD. Purple shading with increasing intensity indicates increasing NFT densities distribution. Amyg: Amygdala; EC: Entorhinal cortex; CA1: Cornus ammonis 1; Cg: Cingulate cortex; Prec: Precuneus; 4: Primary motor cortex; 3-1-2: Primary sensory cortex; 17: Primary visual cortex; 18: Secondary visual cortex. Figure adapted with permission from Cold Spring Harb Perspect Med 2011;1:a006189 with copyright to Cold Spring Harbor Laboratory Press.

The loss of neurons parallels with NFTs pathology especially in the entorhinal cortex (Gomez-Isla et al., 1996). Although NFT pathology demonstrates better clinical correlation with AD progression as compared to Aβ plaques, the status of tau gene, MAPT, as a risk factor for AD is not as established as the APP gene. Till date, tau mutations have not been identified and linked to familial forms of AD other than in familial frontotemporal dementia with Parkinsonism linked to chromosome 17 (FTDP-17T) (Wolfe, 2009). Nevertheless, increasing evidence based on several genomic studies suggest that certain MAPT variants could be associated with increased risk of AD (Coppola et al., 2012, Desikan et al., 2015).

1.1.4 Treatment of AD

At present, there is no cure for AD and current available treatments only temporarily lessen or stabilize the clinical deterioration of the disease. Cholinesterase inhibitors (e.g. donepezil, rivastigmine) and the NMDA receptor antagonist memantine are as of now the key drug treatments for AD that have been approved by the Food and Drug Administration (Farlow and Cummings, 2007). New therapies targeting the Aβ and its precursor proteins, cholesterol reducing statins, other NMDA receptor antagonists and anti-inflammatory drugs are currently under clinical trials (Helmuth, 2002, Schwartz and Shechter, 2010). Unfortunately, therapeutic approaches based on immunotherapeutic targeting of plaques (anti-Aβ antibodies) or regulation of Aβ (γ- or β-secretase inhibitors) have either failed at clinical trials due to adverse effects or have uncertain efficacy (Castello and Soriano, 2014, Menting and Claassen, 2014, De Strooper and Chavez Gutierrez, 2015). Hence new insights into the underlying molecular mechanisms of AD are needed to identify novel disease-modifying therapeutic targets.

1.2 Neuroinflammation in AD

Neuroinflammation is a hallmark associated with numerous neurodegenerative disease and nervous system pathologies (Glass et al., 2010). The term "neuroinflammation" describes inflammation that is observed in neurological diseases mainly mediated by glial cells such as microglia and astrocytes in response to lesions or insults (Ransohoff and Brown, 2012). These cells become activated at the site of damage, synthesizing or releasing pro-inflammatory cytokines, chemokines and ROS generators in the process known as gliosis (O'Callaghan et al., 2008). Neuroinflammation, often coined as a double-edged sword, is supposed to play a defensive role in response to insults, facilitating recovery. However, under uncontrolled situations with prolonged glial activation, it could exert detrimental effects in the central nervous system (CNS).

Microglia activation and astrocyte dysfunction has been observed way before clinical symptoms of AD and MCI (Figure 1.4), suggesting that neuroinflammation is present even in the preclinical phases of AD (Lichtenstein et al., 2010). In AD, gliosis is observed near Aβ plaques and high expression of inflammatory mediators have been detected around plaques and NFT (Akiyama et al., 2000, Heneka et al., 2015). Inflammation has been shown to induce tau hyperphosphorylation and exacerbate tau pathology in AD mouse model (Kitazawa et al., 2005). These various studies suggest that neuroinflammation in AD may accelerate the disease progression or may even be a disease trigger.

Epidemiological studies that found association between chronic use of non-steroidal anti-inflammatories (NSAIDs) and reduced risk of AD have sparked interest of using NSAIDs, such as ibuprofen, for the treatment of AD, highlighting the involvement of neuroinflammation in the disease (Stewart et al., 1997, Vlad et al., 2008). It is only in recent decades that the importance of neuroinflammation in AD has been appreciated in the field. Although key players of neuroinflammation have been identified, the exact roles of what glial cells play and immune-related changes in AD have not been fully understood (Heppner et al., 2015). A better understanding of neuroimmune pathways is required to grasp a fuller picture of the disease, thus broadening the therapeutic approaches for AD.

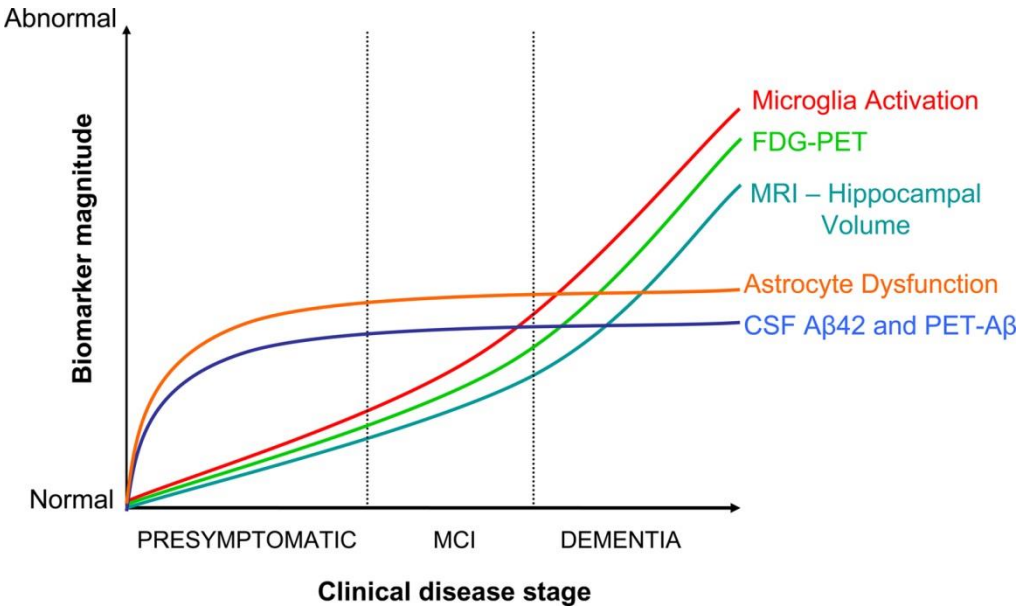

Figure 1.4 Dynamic model of AD evolution. Microglia activation due to Aβ accumulation and neuronal damage as well as astrocyte dysfunction occurs from the pre-symptomatic stage in AD. Figure adapted from (Lichtenstein et al., 2010).

1.2.1 Microglia in AD

Ubiquitously distributed in the CNS, microglia are known as the resident phagocytes in the brain, constituting about 5 to 10% of the cells in the normal brain (Mittelbronn et al., 2001). They are derived from peripheral mesodermal (myeloid) tissue, unlike neurons, astrocytes and oligodendrocytes which are originated from the neuroectoderm (Chan et al., 2007). During "resting state", microglia are usually ramified in morphology, having small cell body and thin elaborated processes, acting as surveillants in the CNS. They also support tissue maintenance by secreting factors and participate in the protection and remodelling of synapses (Ji et al., 2013).

In AD, microglia undergo activation in the presence of pathological stimuli such as neuronal death or Aβ aggregates and transform into phagocytic cells with amoeboid morphology (Giulian et al., 1995, Chan et al., 2007). The detection of soluble Aβ and its aggregates by microglia is mediated by the activation of a series of receptors which triggers internalization of Aβ as well as the production of a plethora pro-inflammatory cytokines and ROS (El Khoury et al., 1996, Chan et al., 2007, Heneka et al., 2015). The critical role of microglia in neuroinflammation in AD was further supported by recent Genome Wide Association Studies that discovered at least 20 gene variants associated with increased risk of late-onset AD which were highly encoded by microglia (Karch and Goate, 2015, Villegas-Llerena et al., 2015). In particular, the triggering receptor expressed on myeloid cells 2 (TREM2) is of high interest in the field. TREM2 is a highly expressed cell surface receptor of the immunoglobulin superfamily and is also involved in phagocytosis in microglia (Rivest, 2015, Wang et al., 2015). Mutation of TREM2 was associated with

increased risk of late-onset AD, similar extent to ApoE risk factor (Guerreiro et al., 2013).

However, in many neurodegenerative diseases including AD, chronic neuroinflammation and "over activation" of microglia can lead to dysfunctional phagocytosis, exacerbating neuronal damage due to the secretion of a range of neurotoxins that includes pro-inflammatory mediators, nitric oxide and ROS (Liu et al., 2002, Streit et al., 2004, Luo and Chen, 2012).

1.2.2 Astrocytes in AD

Astrocytes are the most abundant and heterogeneous type of glial cells which occupy up to 50% of the brain volume (Davis, 2002). These stellate cells play supportive functions in the CNS and are also involved in pathologic processes (Eddleston and Mucke, 1993). Physiologically, astrocytes interact with endothelial cells in the blood brain barrier (BBB); regulating BBB function, participate in ion homeostasis, antioxidant defence of the brain as well as transmitter synthesis and removal of glutamate. They also act as storage cells for glycogen, which serves as a reserve when glucose is in short supply in the brain, providing metabolic support for neurons (Davis, 2002, Schousboe and Waagepetersen, 2005, Abbott et al., 2006, Brown and Ransom, 2007).

For a long period of time, astrocytes were thought to play only neurosupportive roles in the CNS. Increasingly, numerous studies in recent decades have highlighted their importance especially in the context of neuroinflammation. Astrocytes are activated or become reactive in response to many CNS insults and pathologies, such as neurodegeneration, stroke or tumour growth (Pekny and Nilsson, 2005). Upon activation, they display

morphological changes, increase proliferation and size (hypertrophic) and express elevated levels of molecules, one of which is the glial fibrillary acidic protein (GFAP), an intermediate filament cytoskeletal protein specific to astrocytes (Eddleston and Mucke, 1993). This process is termed reactive astrogliosis, a prominent hallmark of many neurodegenerative diseases. Furthermore, due to their immunocompetent nature, they are able to produce cytokines and chemokines when activated (Fuller et al., 2010). In AD, the extent of astrogliosis was found to be associated with increasing Braak staging (Simpson et al., 2010).

In vitro experiments have demonstrated the ability of reactive astrocytes to phagocyte and degrade Aβ deposits (Wyss-Coray et al., 2003). Although this is the case, activated astrocytes during chronic inflammation in AD appear to neglect their neurosupportive functions, enhance excitotoxicity and exhibit prolonged inflammatory signals, creating an inflammatory cascade (Fuller et al., 2010). Moreover, gliosis that causes excessive scar formation around lesions hinders axonal growth and neuronal recovery (Hamill et al., 2005). Although the role of astrocytes in neuroinflammation is not as well established as that of microglia, the sheer abundance of astrocytes in the CNS already suggests that astrocytes may have a more critical and sustained role as compared to microglia in prolonged neuroinflammatory processes in AD.

1.2.3 Inflammatory mediators in AD

There are several types of inflammatory mediators that can be expressed and secreted by microglia, astrocytes and even neurons in AD. These include cytokines and chemokines, caspases, prostanoids, complement system and reactive oxygen species (Rubio-Perez and Morillas-Ruiz, 2012, Heneka et al.,

2015). Prolonged or overactivation of neuroinflammation in the brain aggravates synaptic dysfunction which correlates with memory decline observed preceding neuronal death associated with late stages of AD (Agostinho et al., 2010).

Cytokines were originally known as lymphokines and monokines due to their initial discovery in hematopoietic cells. They are small proteins with molecular weight ranging from 8 to 40 kDa with biological activities that are important in host responses to disease, infection and immunomodulation (Dinarello, 2000). In AD, numerous studies have consistently shown that many cytokines including TNFα (Tumour necrosis factor alpha), IL-1β (interlukin-1 beta), IL-6, IL-8 and TGFβ (transforming growth factor beta) appeared to be upregulated in AD (Akiyama et al., 2000).

1.2.4 TNFα in AD

TNFα is a pleiotropic cytokine that has been found to be elevated in the serum, CSF, cortex of AD patients and Aβ stimulated microglial cultures (Fillit et al., 1991, Tarkowski et al., 1999, Bhaskar et al., 2014). Elevated levels of soluble TNFα were also observed in those with MCI, indicating TNFα possible participation in the pathogenesis of AD even at an early stage (Tarkowski et al., 2003). Paracrine stimulation by TNFα can lead to expression of other inflammatory cytokines such as IL-1β, IL-6, IL-8, potentiating the inflammatory cascade (Perry et al., 2001).

In the brain, TNFα physiological roles include regulation of BBB integrity, febrile responses, mediation of glutamatergic transmission as well as synaptic plasticity and synaptic scaling (Beattie et al., 2002, Pickering et al., 2005,

Stellwagen and Malenka, 2006, McCoy and Tansey, 2008). However, under pathological conditions, TNFα can activate both microglia and astrocyte during injury and was identified as the main neurotoxic agent resulting from Aβ-induced pro-inflammatory transcriptional changes (Combs et al., 2001, McCoy and Tansey, 2008). Moreover, it has been demonstrated that TNFα works cooperatively with interferon γ to increase production of Aβ while inhibiting secretion of the neuroprotective soluble APPs and is required for the suppression of long-term potentiation (LTP) by Aβ in vitro (Blasko et al., 1999, Rowan et al., 2007). In AD patients, increased TNFα in serum has been linked to accelerated deterioration and aggravated psychiatric symptoms (Perry et al., 2007, Holmes et al., 2009, Holmes et al., 2011).

These findings have made TNFα and possibly even its downstream mediators potential therapeutic targets for AD in the aspect of neuroinflammation. Etanercept (Enbrel™), a recombinant TNFα receptor: Fc fusion protein that binds and inactivates TNFα (Weinblatt et al., 1999) has been approved by US Food and Drug Administration for the treatment of several autoimmune diseases including rheumatoid arthritis. A 6 month, open-label pilot study in patients with AD ranging from mild to severe showed that perispinal administration of etanercept could sustain clinical improvement with better cognitive outcomes (Tobinick et al., 2006). However, this approach has not been evaluated in randomized controlled trial and remains controversial. Based on the hypothesis of modifying long-term, low grade peripheral systemic inflammation, Butchart et al., has recently completed a double-blind, randomized, placebo-controlled phase II trial of subcutaneous administration of etanercept on patients with mild to moderate AD. Although there were no

statistical significant differences in the improvement of cognition, behaviour, or global function, there were trends favouring the treatment group as compared to placebo. According to the authors, further testing was required in a larger and more heterogeneous AD patient population for validation (Butchart et al., 2015).

1.2.5 IL-1 in AD

Similar to TNFα, IL-1 is another pleiotropic pro-inflammatory cytokine that is upregulated in the brain of AD patients and also in people with Down's syndrome before AD neuropathological changes are observed (Griffin et al., 1989). The two major effectors of the IL-1 family, IL-1α and IL-1β are distinct isoforms that exert similar biological effects by acting on IL-1 receptor IL-1RI (Gibson et al., 2004, Luheshi et al., 2011). IL-1β is commonly described as the classical pro-inflammatory cytokine in the brain and frequently measured in numerous studies (Rothwell, 1991, Luheshi et al., 2009). Physiologically, IL-1 is known as a very potent pyrogenic agent and is involved in hypothalamic-pituitary adrenal activation in response to stress (Murakami et al., 1990, van der Meer et al., 1996).

In AD, IL-1 is overexpressed in microglia surrounding Aβ plaques next to neurons in brain tissues (Griffin et al., 1995). The overexpression appeared to occur early in plaque pathology and can be observed in diffuse, non-neuritic Aβ deposits in brain samples from foetuses and young children with Down's syndrome suggesting its role in plaque formation in AD (Griffin et al., 1995, Sheng et al., 1997). Parallel to this, *in vitro* experiments have shown that IL-1 was able to induce APP gene expression (Goldgaber et al., 1989).

Although microglia is the predominant source of IL-1 in the brain, it can also be produced by many other cells including astrocytes, oligodendrocytes, neurons, endothelial cells and infiltrating leukocytes (Vela et al., 2002, Basu et al., 2004, Shaftel et al., 2008). Moreover, IL-1β can exert both autocrine and paracrine feedback to propagate inflammation including self- induction of IL-1 (Spranger et al., 1990, Shaftel et al., 2008).

1.2.6 IL-6 in AD

IL-6 is another cytokine frequently described to be elevated in AD (Baranowska-Bik et al., 2008). It has been reported that IL-6 immunoreactivity could be detected in AD cortical neuritic plaques and not observed in age-matched control brains (Bauer et al., 1991, Huell et al., 1995). Together with both TNFα and IL-1, they are known to be the key inflammatory cytokines induced during the acute-phase response during inflammation (Heinrich et al., 1990).

Astrocytes, microglia, neurons and endothelial cells of the CNS are capable of expressing IL-6 (Frei et al., 1989, Marz et al., 1998, Van Wagoner et al., 1999). Astrocytes, in particular, are known to exhibit strong induction of IL-6 in the presence of both TNFα and IL-1β (Van Wagoner et al., 1999). Physiological roles of IL-6 include facilitating oligodendrocyte differentiation, generation of astrocytes from cortical precursor cells and acting as neurotrophic factor for the CNS (Kahn and De Vellis, 1994, Hirota et al., 1996, Islam et al., 2009).

Although IL-6 has several beneficial properties in the CNS, it is generally considered as a destructive pro-inflammatory mediator in neurodegenerative diseases. Transgenic mice with GFAP promoter driven expression of IL-6

displayed deficits in learning accompanied with neuropathological changes including the loss of synapse and gliosis (Fattori et al., 1995, Heyser et al., 1997). In relation to AD, a Japanese study group has found that a genetic polymorphism of the IL6 gene promoter that showed tendency of higher IL-6 expression was associated with increased risk of sporadic AD (Shibata et al., 2002). In addition, not only does Aβ induces IL-6 expression in glial cells, IL-6 could also similarly stimulate the expression of APP (Ringheim et al., 1998, Toro et al., 2001, Vukic et al., 2009).

1.2.7 Inflammatory pathways in AD

Nuclear factor-kappa B (NF-κB), commonly labelled as the "master regulator of inflammation" is activated in numerous neurodegenerative diseases where chronic neuroinflammation is prominent (Granic et al., 2009). Particularly in AD, neurons and glial cells around Aβ plaque displayed NF-κB activation with surrounding microglial and astrocytes expressing elevated levels of inflammatory cytokines, including TNFα, IL-1β, IL-6 and free radicals in an NF-κB dependent pathway (Terai et al., 1996, Kaltschmidt et al., 1997, Akama et al., 1998), Aβ peptides were also found to induce NF-κB activation in cultured neurons and rat brains (Kaltschmidt et al., 1997, Carrero et al., 2012). The two classical pro-inflammatory cytokines, TNFα and IL-1β that are upregulated in AD, strongly activate NF-κB, propagating the canonical signalling pathway that results in the expression of a plethora of pro-inflammatory cytokines and chemokines (Moynagh, 2005, Lawrence, 2009). Both cytokines though having their own receptors (TNFR1 and IL1RI), converges on an upstream IKK complex (inhibitor of kappa B (IκB) kinase complex) that eventually phosphorylates the NF-κB inhibitory protein IκB,

releasing NF-κB into the nucleus to activate transcription of pro-inflammatory genes (see Figure 1.5) (Verstrepen et al., 2008). In the case of astrocytic NF-κB activation, evidence have shown that suppression of NF-κB transcriptional activity in astrocytes could reduce inflammation and improve recovery which makes astrocytic inhibition of NF-κB an attractive target for AD therapy (Medeiros and LaFerla, 2013, Steardo et al., 2015),.

Given that neuroinflammation in AD is chronic, other pathways could likewise contribute to the inflammatory response observed in AD. One example would be the activation of Mitogen-Activated Protein Kinases (MAPKs) signalling pathway. THE MAPK family consist of various kinases which includes extracellular signal–regulated kinase (ERK), c-Jun N-terminal kinase (JNK), and p38 kinase (p38) (Krishna and Narang, 2008). Increased levels of p38 kinase activity has been observed in post-mortem brain tissues of AD patients and was associated with NFT and Aβ plaque pathology and could be also detected at even early stages (Braak stages IV-V) of the disease indicating its involvement in AD pathogenesis (Hensley et al., 1999, Sun et al., 2003). MAPKs can also be activated by oxidative stress triggered by ROS, promoting tau hyperphosphorylation via p38 signalling (Peel et al., 2004, Sekine et al., 2006).

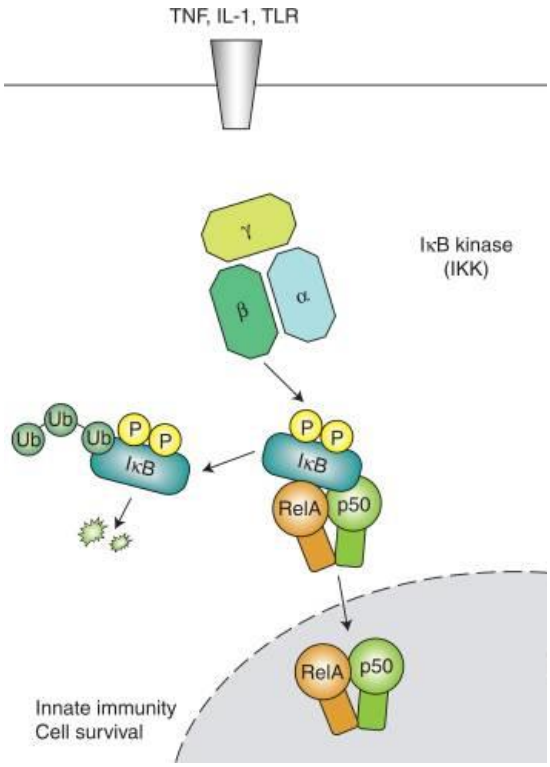

Figure 1.5 Canonical NF-κB signalling pathway. This figure illustrates the canonical signalling pathway for NF-κB activation. It can be triggered by cytokines and Toll-like receptors (TLRs), resulting in the activation of RelA/ NF-κB p65 that regulates expression of inflammatory and cell survival genes. IKK (in this case IKKβ) regulates activation of the canonical pathway through phosphorylation of IκBs. Figure adapted with permission from Cold Spring Harb Perspect Biol 2009;1:a001651, with copyright to Cold Spring Harbor Laboratory Press.

1.3 Fyn tyrosine kinase

Fyn, the non-receptor tyrosine kinase of the Src family has important roles in the activation of various signal transduction pathways. The Src family kinase (SFK) has nine members consisting of Blk, Fgr, Fyn, Hck, Lck, Lyn, Src, Yes and Yrk, with many members having oncogenic properties after mutation (Parsons and Parsons, 2004). They share a conserved region made up of three domains namely SH1 (Src homology 1), SH2 and SH3 and a unique amino-terminal sequence ranging between 60 and 90 amino acids in length which distinguishes them (See Figure 1.6A) (Kefalas et al., 1995). Fyn was isolated as a cDNA from normal human fibroblast and possesses translational product

highly similar to c-Src at an identity of 86% at its Carboxyl-terminal (Kawakami et al., 1986, Semba et al., 1986, Kawakami et al., 1988).

1.3.1 Fyn isoforms and their kinase activity

There are three transcripts variants of Fyn namely FynB, FynT and FynΔ7 as a result of alternative splicing (Goldsmith et al., 2002). Exon 7A and 7B are mutually exclusive exons for FynB and FynT isoforms respectively, they both encode a short sequence that differs in approximately 50 amino acids, spanning across the end of the SH2 domain, the SH2-kinase linker segment and the beginning of SH1-kinase domain (Figure 1.6). FynB is highly expressed in the brain and other tissues whereas FynT, the thymic isoform, is known to be predominantly expressed in cells of hematopoietic origins like in T cells (Resh, 1998). FynΔ7, on the other hand, is a newly discovered transcript variant that lacks exon 7 and hence is presumed to have no kinase activity (Goldsmith et al., 2002).

Like other SFKs, Fyn tyrosine kinase also contains two conserved tyrosine residues, Y416 and Y527, which have opposing effects upon phosphorylation. Autophosphorylation of Y416 within the kinase domain (corresponding to Y417 in FynT and Y420 in FynB) results in a conformational change to promote substrate binding and thus increase kinase activity (Figure 1.6B). Hence, phosphorylated Y416 has been used as a determinant of SFK catalytic activity. On the other hand, phosphorylation of Y527 (corresponding to Y528 in FynT and Y531 in FynB) stabilizes a closed conformation of SFK, which suppresses kinase activity towards substrates. Consistently, dephosphorylation of Y531 in Fyn, results in kinase activation (Kramer-Albers and White, 2011).

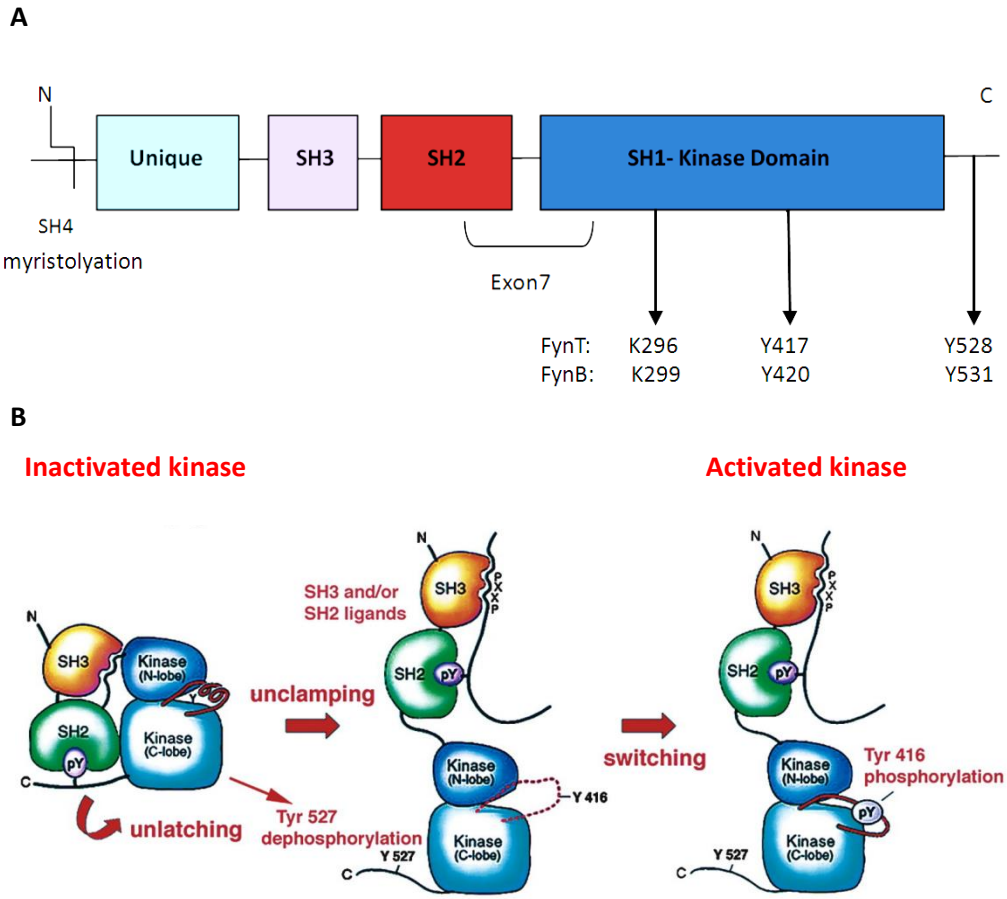

Figure 1.6 Structure of Fyn tyrosine kinase. **(A)** Primary structure of Fyn tyrosine kinase with major features that include a site at SH4 (src homology domain 4) required for myristoylation and association with the plasma membrane; a unique domain; SH3 and SH2 domains; a kinase region, including sites for phosphotransfer (lysine 296/299, K296/K299) and auto-phosphorylation (tyrosine 417/420, Y417/Y420); and a carboxy-terminal regulatory domain including the major site of tyrosine phosphorylation (tyrosine 528/531, Y528/Y531) (Picard et al., 2004). Exon 7 spans across SH2 and kinase domain which encompasses a linker region. The two isoforms, FynB and FynT differ by 52 amino acids in this region. (Diagram not drawn to scale) **(B)** SFKs, including Fyn tyrosine kinase, are activated through dephosphorylation of Y527 (corresponding to Y528 in FynT and Y531 in FynB) and phosphorylation of Y416 within the kinase domain (corresponding to Y417 in FynT and Y420 in FynB), resulting in a switch from a close conformation to an active conformation. Figure adapted from (Harrison, 2003) with permission from Elsevier.

The linker region between the SH2 domain and kinase domain (illustrated in Figure 1.6) is highly variable within the SFKs including FynB and FynT. This region is important in regulating the autoinhibitory mechanism of the kinase through facilitating inter-domain interactions thereby allowing the conformation of the kinase to be switched between activated and inactivated states (Xu et al., 1997, Xu et al., 1999). Structural analyses revealed that the linker region of FynB engages the SH3 domain with higher affinity and favours a closed auto-inhibited conformation, whereas FynT has a relatively loose autoinhibitory conformation (Brignatz et al., 2009). The observation suggested that FynT may interact with substrates with higher affinity and exhibit enhanced kinase activity compared to FynB. Indeed, it has been reported that FynT, but not FynB, interact with and phosphorylate the RNA-binding protein Sam68 (Brignatz et al., 2009). On the other hand, Davidson et al. attributed the variability of the N-terminus of the kinase domain and identified that FynT facilitated the mobilization of cytosolic calcium and lymphokine secretion upon T cells stimulation (Davidson et al., 1992, Davidson et al., 1994). In addition, genetically knock-out model of mice lacking just the thymic isoform FynT, similarly showed defective T-cell signalling in terms of reduced calcium mobilization upon T-cell activation, altered patterns of phosphotyrosine accumulation, and defective proliferation when T-cell receptor were stimulated with anti-CD3 antibodies (Appleby et al., 1992). Although only a few studies have specifically investigated the isoform-specific role of Fyn, these independent studies have highlighted the functional differences of FynB and FynT as a consequence of alternative splicing of exon should not be overlooked.

1.3.2 The roles of Fyn in the brain

The biological functions of Fyn are diverse, ranging from T cell signalling, cell adhesion, mitogenic signalling, pro-inflammatory mediator production and also in brain function; with some of its functions appearing to be isoform-specific (Davidson et al., 1994, Resh, 1998, Picard et al., 2004, Rajasekaran et al., 2013). Based on observations in Fyn mutant and knockout mouse models, Fyn has been proposed to have several critical roles in the brain. Fyn is involved in LTP induction and maintenance, which are associated with spatial learning and memory (Grant et al., 1992). It was also found that Fyn regulates dendritic spine number and morphology, indicating its role in synaptic function (Babus et al., 2011). In addition, Fyn phosphorylates subunits of the NMDA receptor which are involved in mediating tolerance to ethanol-induced sedation in Fyn knockout mice (Yaka et al., 2003). Furthermore, Fyn kinase activity is also required for the regulation of normal myelination by oligodendrocytes (Sperber et al., 2001) as well as in oligodendrocyte differentiation (Osterhout et al., 1999).

1.3.3 The pathogenic roles of Fyn in AD

Fyn was first reported in relation to the disease by Sherin K. Shirazi and John G. Wood in 1993. They discovered the co-localization of Fyn to a subset of neurons stained positively with hyperphosphorylated tau (Shirazi and Wood, 1993). Following their discovery, subsequent studies found that Fyn could directly interact and phosphorylate tau at Tyrosine 18 residue (Lee, 1998, Lee et al., 2004). A quantitative study on Fyn protein expression conducted later found that Fyn level was increased in the insoluble fraction of AD brain lysate while synapse expression of Fyn was decreased (Ho et al., 2005).

On the other hand, independent studies focusing on the toxic effects of Aβ, revealed that Fyn knockout (KO) mice were protected against diffusible Aβ oligomers neurotoxicity in the hippocampus (Lambert et al., 1998). With the introduction of transgenic mouse models of AD, double transgenic mouse model of Fyn and APP was utilize in experiments to study the effects of Fyn in memory, learning and even in seizures (Chin et al., 2005, Um, 2012). It has been shown that Fyn kinase could induce cognitive and synaptic impairment in these mice (Chin et al., 2005).

More recently, Aβ, tau and Fyn has been studied in greater details to investigate their possible interaction in AD (Ittner, 2010, Roberson, 2011, Minami et al., 2012). In 2010, Ittner et al. reported that Fyn played a critical role in tau-dependent Aβ toxicity at the postsynapse (Ittner, 2010). Similarly, Roberson et al. showed that Fyn, Aβ and tau were found to co-operatively impair synaptic and network function in multiple mouse models of AD (Roberson, 2011). Moreover, Stephen M. Strittmatter and his group has identified Fyn as a mediator of signal transduction downstream of the

cellular prion protein (PrP^C)-Aβ oligomer complex requiring the metabotropic glutamate receptor mGluR5 which are involved in Aβ-Induced dendritic spine lost and neuronal toxicity (Um et al., 2012, Um et al., 2013). These studies have supported the hypothesis of Fyn inhibition as a therapeutic approach in AD and were also in line with proposed hypothesis of Fyn-Tau-Amyloid toxic triad proposed by Christian Haass and Eckhard Mandelkow (Haass, 2010).

1.3.4 Current status of Fyn as a therapeutic target in AD

The studies discussed above have emphasized the importance of regulation of Fyn expression and activity in memory and plasticity. Currently, several tyrosine kinase inhibitors such as Masitinib, Saracatinib that are being tested in AD clinical trials are capable of inhibiting Fyn although they are not specific to targeting Fyn exclusively. Therefore, special note has to be taken to consider potential side-effects of these drugs.

Masitinib, currently in use in clinical trial to target mast cells found on both sides of the blood-brain barrier, is proposed as drug for reducing neuroinflammation and restoring compromised BBB functions in AD (Silverman et al., 2000, Nautiyal et al., 2008, Piette et al., 2011). It was found to be reasonably well tolerated in a phase II dose-ranging trial in France involving mild-to-moderate AD patients and was associated with cognitive improvement after 12 and 24 weeks (Piette et al., 2011). The launch of an international, multicenter phase 3 clinical trial has begun in 2013 to evaluate the safety and efficacy of masitinib in a larger group of mild-to-moderate AD patients (Nygaard et al., 2014).

On the other hand, saracatinib (AZD0530), proposed as a drug to target Aβ mediated synaptotoxicity through Fyn, has completed phase Ib trial in patients with AD and was also shown to be well tolerated and reasonably safe. An ongoing larger Phase IIa clinical trial of Saracatinib for the treatment of patients with AD has recently been launched (Nygaard et al., 2015).

1.4 Preliminary data showing isoform-specific role of FynT in AD

With the proposed putative pathogenic roles of Fyn in AD, one would assume that the brain-predominant FynB isoform is involved in the disease. Hence, no study has attempted to delineate possible isoform-specific roles of Fyn in AD. Our laboratory has previously reported genome wide profiling of AD versus control brains transcriptome using Affymetrix exon array platform (Tan et al., 2010). An analysis of alternative splicing events associated with AD using the same database revealed that Fyn was differentially spliced in AD temporal cortex (Lai et al., 2014). Interestingly, we observed that FynT was specifically upregulated in AD while FynB remained unchanged (see Figure 1.7). These findings were intriguing as FynT is known to be expressed predominantly in cells of hematopoietic origin but not in the CNS (Cooke and Perlmutter, 1989). Furthermore, gene ontology term enrichment analyses of the exon array data (Table 1.1) and cellular markers correlation (Table 1.2) revealed that FynT was positively correlated with markers associated to reactive astrogliosis and negatively correlated with neuronal function. Hence, we felt the urge to unravel the facts and impacts of FynT induction in AD brain.

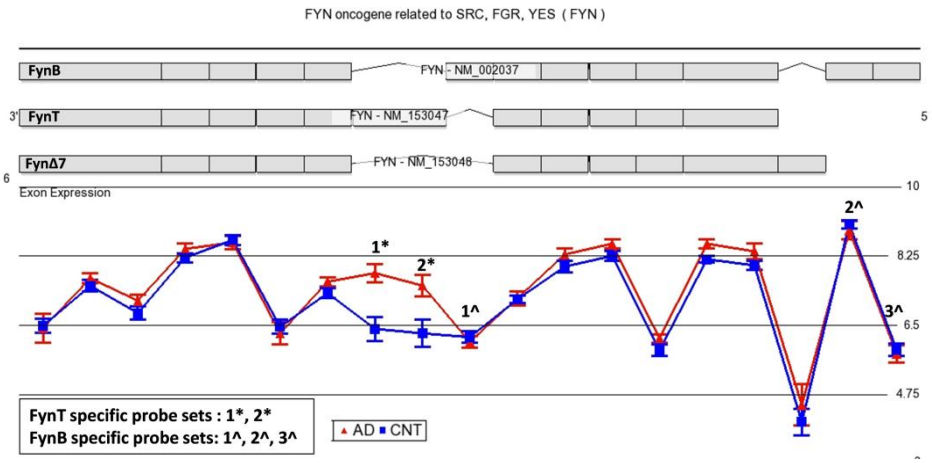

Figure 1.7 Gene View display on the selective upregulation of FynT isoform expression in AD brain. A Gene View display of differential alternative splicing of Fyn was generated from Affymetrix exon array data with AD (red) and control (blue) samples (n = 8 for both groups). Two FynT-specific probeset IDs (1* and 2*) were significantly up-regulated in AD as compared to control samples. FynB specific probeset IDs (1^, 2^ and 3^) showed no significant changes in AD. The y-axis is a log2 scale intensity value. Figure adapted from (Lee et al., 2015) with permission from John Wiley and Sons.

Table 1.1 Genes which correlate with FynT expression in AD categorized by GO terms

Genes positively correlated with FynT expression				
GO Term ID (Category) [1]	**Description**	**Count** [2]	**Fold Enrichment** [3]	**Benjamini *p*** [4]
GO:0008092 (MF)	Cytoskeletal protein binding	44	3.011	7.20E-08
GO:0015629 (CC)	Actin cytoskeleton	26	3.479	4.83E-05
GO:0048522 (BP)	Positive regulation of cellular	96	1.708	3.39E-05
GO:0007010 (BP)	Cytoskeleton organization	36	2.742	3.18E-05
GO:0016323 (CC)	Basolateral plasma membrane	22	3.900	4.17E-05
GO:0042127 (BP)	Regulation of cell proliferation	51	2.152	6.50E-05
GO:0006928 (BP)	Cellular component movement	36	2.517	1.30E-04
GO:0048523 (BP)	Negative regulation of cellular process	84	1.681	1.77E-04
GO:0031012 (CC)	Extracellular matrix	27	2.817	3.01E-04
GO:0007155 (BP)	Cell adhesion	44	2.088	6.18E-04
GO:0016563 (MF)	Transcription activator activity	29	2.440	4.21E-03
Genes negatively correlated with FynT expression				
GO Term ID (Category)	**Description**	**Count**	**Fold Enrichment**	**Benjamini *p***
GO:0043005 (CC)	Neuron projection	43	3.454	7.04E-10
GO:0045202 (CC)	Synapse	41	3.173	1.66E-08
GO:0031982 (CC)	Vesicle	53	2.173	8.18E-06
GO:0019717 (CC)	Synaptosome	15	4.849	6.04E-05
GO:0005794 (CC)	Golgi apparatus	58	1.827	2.75E-04
GO:0016192 (BP)	Vesicle-mediated transport	46	2.076	1.13E-03
GO:0050804 (BP)	Regulation of synaptic transmission	19	3.632	1.21E-03

[1]Gene ontology (GO) category: biological process (BP), cellular component (CC), molecular function (MF).

[2]Total number of genes correlated with FynT in the GO term.

[3]Fold enrichment is used for measuring the magnitude of enrichment.

[4]*p*-values adjusted for multiple testing using a false-discovery rate of 5% (see (Huang da et al., 2009a, Huang da et al., 2009b)).

Table adapted from (Lee et al., 2015) with permission from John Wiley and Sons.

Table 1.2 Expression of specific cellular markers in AD vs Ctrl brain (n=8 per group), as well as their significant correlation with FynT expression in Exon array

Exon array Transcript ID	Gene symbol	Specific cellular marker	[1] log_2 base intensity		AD vs Ctrl		[2] # probesets correlated with FynT (p<0.01)	Pearson correlation coefficient (*r*)
			Ctrl	AD	Fold	p-value		
3393744	CD3D	T cell	1.846	1.995	1.11	0.27349	none in 6	
3351280	CD3E	T cell	3.258	3.168	-1.06	0.62740	none in 6	
3351300	CD3G	T cell	1.729	2.124	1.32	0.05716	1 out of 4	*0.62503*
3402786	CD4	T cell	3.746	3.746	1.00	0.99716	none in 12	
2562932	CD8A	T cell	4.080	4.276	1.15	0.13054	1 out of 11	*0.62481*
2562965	CD8B	T cell	1.460	1.571	1.08	0.40684	none in 4	
2328841	LCK	T cell	3.361	3.668	1.24	0.02322*	none in 17	
2495187	ZAP70	T cell	2.894	3.231	1.26	0.01812*	none in 17	
2373842	CD45	hematopoietic	2.812	2.872	1.04	0.64841	none in 38	
3655109	CD19	B cell	3.289	3.539	1.19	0.17463	none in 19	
2878437	CD14	monocyte/ macrophage	6.573	6.637	1.05	0.86321	none in 4	
3442706	CD163	monocyte/ macrophage	3.143	4.475	2.52	0.01540*	3 out of 18	*0.65404 to 0.71018*
3656990	CD11b	microglia	3.431	3.627	1.15	0.16383	none in 2	
2902444	Iba1	microglia	4.235	4.271	1.03	0.87870	none in 9	
2806643	GLAST	astrocyte	8.805	9.132	1.25	0.25089	9 out of 15**	*0.65104 to 0.79985*
3759410	GFAP	astrocyte	10.729	11.327	1.51	0.02510*	14 out of 14**	*0.65573 to 0.78003*
2525533	MAP2	neuron	8.721	8.091	-1.55	0.02259*	2 out of 26	*-0.63944 to 0.64138*
3128271	NEFL	neuron	9.035	8.076	-1.94	0.02170*	10 out of 12**	*-0.62376 to -0.73384*
3090436	NEFM	neuron	8.965	8.186	-1.71	0.04663*	2 out of 11	*-0.65343 to -0.71241*
3432394	RPH3A	neuron	7.737	5.986	-3.37	0.00045*	27 out of 28**	*-0.64750 to -0.88786*
3674504	TUBB3	neuron	5.686	5.409	-1.21	0.10308	1 out of 6	*-0.65120*

[1] Log_2 base intensity is gene-level data.

[2] Correlation between cellular markers and FynT expression was analysed at the exon-level using probesets in each transcript ID. Only those with significant correlation ($p<0.01$) were indicated with Pearson correlation coefficient (r) in last column.

[*] indicated significant differentially expressed between AD vs Ctrl ($p<0.05$).

[**]indicated cellular marker with more than half of the probesets showing significant correlation with FynT expression.

Table adapted from (Lee et al., 2015) with permission from John Wiley and Sons.

1.5 Hypotheses and objectives of the project

This project aims to identify an isoform-specific role of FynT in AD and the possible impacts of FynT induction in disease progression. We employed post-mortem brain tissues, primary cortical cultures and recombinant approaches which can be found in the thesis Chapter 3, 4 and 5, respectively, to address our specific objectives.

Chapter 3- An isoform-specific role of FynT tyrosine kinase in Alzheimer's disease

- Hypothesis:

  FynT induction in AD may be associated with reactive astrogliosis and neurodegeneration.

- Objective:

  To determine FynT immunoreactivity in association with cellular markers and neuropathological hallmarks in post-mortem AD brains.

Chapter 4- Isoform-specific modulation of FynT tyrosine kinase expression in astrocytes under Aβ and TNFα treatment

- Hypothesis:

  Pathological conditions of AD can specifically induce FynT expression in primary cortical cultures.

- Objective:

  To study the modulation of differential FynT versus FynB expression in primary mixed cortical cultures and astrocytes cultures under Aβ and TNFα treatment.

Chapter 5- The functional role of FynT tyrosine kinase in modulating TNFα-induced inflammatory response in astrocytes

- Hypothesis:

  FynT kinase activity may modulate inflammatory responses at the late phase of TNFα treatment in astrocytes.

- Objective:

  To study the role of FynT kinase activity in modulating TNFα-induced inflammatory signalling using recombinant FynT mutant approaches in immortalized normal human astrocyte.

In brief, studies on post-mortem AD brains revealed that FynT induction was independently associated with neurofibrillary degeneration and reactive astrogliosis (Chapter 3). We thus aimed to delineate the isoform-specific role of FynT in neurons and astrocytes using primary cortical culture exposed to pathological conditions associated with AD (Chapter 4). The observation of TNFα-induced FynT expression in primary astrocytes prompted us to speculate that aberrant FynT induction may modulate astrocyte-associated neuroinflammatory response in AD. Hence, we focused on characterizing the role of FynT kinase activity in modulating TNFα signalling pathway using recombinant approaches (Chapter 5).

CHAPTER 2-
Materials and Methods

CHAPTER 2- Materials and Methods

2.1 Materials

2.1.1 Brain tissues

Post-mortem brain tissues were derived from twelve AD patients (five women, seven men) and eight elderly controls (three women, five men) originally recruited by OPTIMA (Oxford Project to Investigate Memory and Ageing, http://www.medsci.ox.ac.uk/optima). Additional control tissues (n=3; from two women and one man) were obtained from the Newcastle Brain Tissue Resource (NBTR), Newcastle upon Tyne, UK, both sites being part of the UK Brains for Dementia Research (BDR) network (see Table 2.1). Informed consent had been obtained from the patients' next-of-kin before collection of brains, and appropriate Institutional Review Board approvals were obtained for work carried out in Singapore (SingHealth IRB 2011/576/A). One hemisphere of each subject was processed for pathological assessments, including confirmation of AD using the Consortium to Establish a Registry for AD (CERAD) criteria (Mirra et al., 1991) as well as Braak staging (Braak and Braak, 1991) while the other hemisphere was fresh frozen for research. In this study, fresh frozen tissues samples from prefrontal (Brodmann area 9) and temporal (Brodmann area 22) were used as these areas were known to be affected by AD pathology. BA9 tissues were frozen in Optimal Cutting Temperature compound (OCT) for subsequent sectioning and immunofluorescence (IF). BA22 tissues were stored at -80°C in TRIzol® reagent (Invitrogen, P/N 15596-018) before processing for real-time reverse transcription polymerase chain reaction (RT-PCR).

Table 2.1 Demographic and disease variables in AD and control subjects

ID	Tissue Source	Group	Age	Sex	PMI	Braak
OP450	OPTIMA	AD	78	M	88	III/IV
OP80	OPTIMA	AD	88	F	30	III/IV
OP133	OPTIMA	AD	69	M	44	V/VI
OP332	OPTIMA	AD	62	M	97	V/VI
OP340	OPTIMA	AD	63	F	48	V/VI
OP357	OPTIMA	AD	71	M	49	V/VI
OP378	OPTIMA	AD	85	F	76	V/VI
OP417	OPTIMA	AD	67	M	30	V/VI
OP91	OPTIMA	AD	66	M	42	V/VI
OP107*	OPTIMA	AD	67	F	107	V/VI
OP279*	OPTIMA	AD	78	F	94	V/VI
OP388*	OPTIMA	AD	83	M	29	V/VI
188/96	Newcastle	Control	82	F	26	0
102/05	Newcastle	Control	72	M	17	I/II
144/94	Newcastle	Control	86	F	40	I/II
OP1112	OPTIMA	Control	78	M	63	I/II
OP1151	OPTIMA	Control	77	M	20	I/II
OP243	OPTIMA	Control	77	M	54	I/II
OP346	OPTIMA	Control	88	F	115	I/II
OP9	OPTIMA	Control	79	F	29	I/II
OP1044*	OPTIMA	Control	85	M	16	0
OP1132*	OPTIMA	Control	81	F	47	I/II
OP1146*	OPTIMA	Control	87	M	30	I/II

Age, age of death (in years); *Braak*, neuropathologic staging according to Braak & Braak (Braak and Braak, 1991); *PMI*, post-mortem interval (in hours). *Samples used for immunofluorescence.

2.1.2 Animals for primary cultures

Pregnant Sprague Dawley rats were purchased from InVivos Pte Ltd and housed at SingHealth Experimental Medicine Centre with protocols approval from the SingHealth Institutional Animal Care and Use Committee prior the start of the experiments (2014/SHS/950). Embryonic brains (embryonic day 18, E18) were used to establish primary cortical mixed cultures (see 2.2.1.1) and postnatal brains (Postnatal day 0 to 1, P0-1) were used to establish primary astrocyte cultures (see 2.2.1.2).

2.1.3 Cell lines

Immortalized normal human astrocytes (iNHA) were primary human astrocytes stably transfected with constructs encoding E6, E7 and human telomerase reverse transcriptase (hTERT) which were kindly provided by Dr. Russell O. Pieper from University of California, San Francisco (Sonoda et al., 2001). Human embryonic kidney 293T cells (HEK293T), human glioma U-251 MG, human glioma U-87 MG and neuroblastoma SH-SY5Y cell lines were obtained from the American Type Tissue Culture Collection (ATCC, USA).

2.1.4 Plasmid constructs

Open reading frame of FynT-WT (wild-type) (NM_153047) with C-terminal tagged of Myc-FLAG, carried by pCMV6 Entry vector was purchased from OriGene Technologies. Expression vector carried mutant forms of FynT-CA (constitutively active mutant, also known as FynT-Y528F, changed the coding position 1583 from A to T which mutated amino acid position 528 from tyrosine (T<u>A</u>C) to phenylalanine (T<u>T</u>C)) and FynT-KD (kinase dead mutant, also known as FynT-K296M, changed the coding position 887 from A to T

which mutated amino acid position 296 from lysine (AAG) to methionine (ATG)) (Davidson et al., 1992) were both generated by site-directed mutagenesis and confirmed by DNA sequencing previously.

For NF-κB luciferase reporter assay, Renilla luciferase control reporter vector (pRL-CMV) was purchased from Promega while NF-κB(1) luciferase Reporter Vector (pNF-κB-luc) comprising five tandem repeats of NF-κB transcription responsive elements was purchased from Panomics.

2.1.5 Custom-made antibodies

Custom-made rabbit polyclonal antibodies raised specifically against FynB and FynT were generated by GenScript Corporation. FynB and FynT-specific rabbit polyclonal antibodies were prepared against synthetic peptide CRESLQLIKRLGNGQ (NP_002028, residues 268-281) and QTSGLAKDAWEVAC (NP_694592, residues 252-264), respectively, which are conserved between human, mouse and rat. Both peptides were conjugated with keyhole limpet hemocyanin to increase immunogenicity for immunization. Pre-immune serum and test bleed serum from rabbits after third immunization with enzyme-linked immunosorbent assay (ELISA) titer of 1:256,000 were tested for FynB and FynT-specificity using Western blot analyses with lysates derived from FynB or FynT transfected HEK293T. The antibodies with low background and high specificity were then affinity purified and dissolved in phosphate buffer saline (PBS), pH 7.4 at a concentration of 0.428 mg/ml with 0.02% sodium azide as preservative. Aliquots were stored at -80 ºC until use.

2.1.6 Other commercially available antibodies

Table 2.2 Primary and secondary antibodies used

Antibody Name (Catalog #)	Species	Dilution	Company
FynB-specific (custom-made)	rabbit pAb	1:100 (IF); 1:1000(WB)	Genscript
FynT-specific (custom-made)	rabbit pAb	1:100 (IF); 1:1000(WB)	Genscript
Total Fyn (#4023)	rabbit pAb	1:1000 (WB)	Cell Signaling
β-actin (13E5), HRP conjugate (#5125)	rabbit mAb	1:3000 (WB)	Cell Signaling
THE™ c-Myc Tag (A00704)	mouse mAb	1:500 (IF)	Genscript
Myc-Tag (71D10)(#2278)	rabbit mAb	1:1000 (WB)	Cell Signaling
GFAP (GA5) (#3670)	mouse mAb	1:100 (IF)	Cell Signaling
Anti-NeuN antibody (ABN78)	rabbit pAb	1:100 (IF)	Millipore
Anti-NeuN antibody, clone A60 (MAB377)	mouse mAb	1:100 (IF)	Millipore
Anti-NeuN antibody, clone A60 Alexa Fluor® 555 Conjugate (MAB377A5)	mouse mAb	1:100 (IF)	Millipore
Anti-MAP2, clone AP20 (MAB3418)	mouse mAb	1:100 (IF)	Millipore
Phospho PHF-Tau (AT8) (MN1020)	mouse mAb	1:100 (IF)	Thermo Scientific
Anti-Phospho-Tau (Tyr18) (MM-0194-P)	mouse mAb	1:200 (IF)	Medimabs
Phospho-NF-κB p65 (Ser536) (93H1) (#3033)	rabbit mAb	1:1000 (WB)	Cell Signaling
NF-κB p65 (D14E12) XP® (# 8242)	rabbit mAb	1:1000 (WB)	Cell Signaling
IκBα (L35A5) Mouse mAb (#4814)	mouse mAb	1:1000 (WB)	Cell Signaling
Anti-mouse IgG, Alexa Fluor 555 conjugate (#4408)	goat pAb	1:1000 (IF)	Cell Signaling
Anti-rabbit IgG, Alexa Fluor 488 conjugate (#4412)	goat pAb	1:1000 (IF)	Cell Signaling
Anti-mouse IgG, Alexa Fluor 647 conjugate (A21235)	goat pAb	1:1000 (IF)	Thermo Scientific
Anti-mouse IgG, HRP-linked Ab (#7076)	goat pAb	1:3000 (WB)	Cell Signaling
Anti-rabbit IgG, HRP-linked Ab (#7074)	goat pAb	1:3000 (WB)	Cell Signaling

mAb= monoclonal antibody, pAb=polyclonal antibody, IF= Immunofluorescence staining, WB=Western blot analysis).

2.1.7 Primer sets

Table 2.3 Primers and primer sequences

Primer Name	Forward primer seq (5'-3')	Reverse primer seq (5'-3')
FynB	CTGCTGCCGCCTAGTAGTTC	GTGTTTCCATTCCAGGTACC
FynT	CATCGAGTTGTACCCCACAA	GTGTTTCCATTCCAGGTACC
Fyn*	GGCCCAGTTTGAAACACTTC	56-FAM/TGTTTCCATTCCAGGTACC
CCL2	GCCTCCAGCATGAAAGTCTC	AGATCTCCTTGGCCACAATG
CCL5	CGCTGTCATCCTCATTGCTA	GAGCACTTGCCACTGGTGTA
CCL7	CCTCCAACATGAAAGCCTCT	CCAGCCTCTGCTTAGGGATT
CXCL10	AGGAACCTCCAGTCTCAGCA	CAAAATTGGCTTGCAGGAAT
CXCL12	TGAGAGCTCGCTTTGAGTGA	CACCTTGCCAACAGTTCTGA
CSF3	ACGAGGGTCAGGACTGTGAC	GTGACAGTGGAGGGGACACT
GMCSF	ATGTGAATGCCATCCAGGAG	AGGGCAGTGCTGCTTGTAGT
IL1B	AGCCAGGACAGTCAGCTCTC	AAGCGGTTGCTCATCAGAAT
IL1ra	ACCAATATGCCTGACGAAGG	GTGACCAGGTTGTTGTGACG
IL6	GTCCACTGGGCACAGAACTT	CAAACTGCATAGCCACTTTCC
IL8	TAGCAAAATTGAGGCCAAGG	AAACCAAGGCACAGTGGAAC
IL23	GTGGGACACATGGATCTAAGAGAA	TCAGACCCTGGTGGATCCTT
LIF	CCCTGGTCCCTACTCAACAA	CTGGACCCTGACACCCTAAA
TNFR1	GTGCCTACCCCAGATTGAGA	TGTCGATTTCCCACAAACAA
18S rRNA	CCTGCGGCTTAATTTGACTC	CGCTGAGCCAGTCAGTGTAG
α-tubulin	ATGGAGCCCTGAATGTTGAC	ACATCTTTGGGAACCACGTC
β-actin	ACTGGAACGGTGAAGGTGAC	AGAGAAGTGGGGTGGCTTTT
GAPDH	TGACATCAAGAAGGTGGTGAAG	TTACTCCTTGGAGGCCATGTG
Rat FynB	CTGCTGCCGTCTAGTAGTTC	GTGTTTCCATTCCAGGTACC
Rat FynT	CATCAAGTTGTACCCCACAA	GTGTTTCCATTCCAGGTACC
Rat Fyn*	GGCCCAGTTTGAGACCCTTC	56-FAM/TGTTTCCATTCCAGGTACC
Rat CD11B	CAGCATCAGTACCAGTTCAACA	CTGCAACAGAGCAGTTCAGC
Rat GFAP	TGAGGCAGAAGCTCCAAGAT	CTCGAACTTCCTCCTCATGG
Rat GLAST	ATCCAGGCCAACGAAACACT	CTTCATGTTTCCGATCACGA
Rat GLT-1	CTGGGAAGAAGAACGACGAG	AGTTTCTTCAGGGGCCTCAT
Rat NeuN	TTCCCACCACTCTCTTGTCC	ATCAGCAGCCGCATAGACTC
Rat TUBB3	CCCCAGCTTACCTTCCTACC	CAGGCCTGGAGCCATAATAA
Rat ENO2	ATGACCTGACGGTGACCAAC	AACGTGTCCTCGGTTTCTCC
Rat MAP2	GGTCTAGATGTTGCTGCCAAGA	CGTGGCTGGACTCAATACCC
Rat β-actin	ACTGGAACGGTGAAGGCGAC	TGCCGTGGATACTTGGAGTG
Rat GAPDH	GGCATTGCTCTCAATGACAA	TGTGAGGGAGATGCTCAGTG
Rat 18S rRNA	CCTGCGGCTTAATTTGACTC	CGCTGAGCCAGTTCAGTGTA

*Primers used for Capillary electrophoresis

2.1.8 DsiRNA duplexes

Dicer-substrate RNAs (DsiRNA) were purchased from Integrated DNA Technologies selected using IDT's online Predesigned DsiRNA Search Tool available on https://sg.idtdna.com/Scitools/Applications/Predesign/.

Table 2.4 DsiRNA duplex sequences

	DsiRNA duplex sequences*
FynT specific_1	5′- GGAUUGGCUAAAGAUGCUUGGGAag-3′ 3′-GACCUAACCGAUUUCUACGAACCCUUC-5′
FynT specific_2	5′- ACUUAACUGUGAUUGCAUCGAGUtg-3′ 3′-AUUGAAUUGACACUAACGUAGCUCAAC-5′
FynT specific_3	5′- GUGUUUCGCUGAAGUGUGGCUUGgt-3′ 3′-CCCACAAAGCGACUUCACACCGAACCA-5′
NC1 Control Duplex	5′- CGUUAAUCGCGUAUAAUACGCGUat-3′ 3′-CAGCAAUUAGCGCAUAUUAUGCGCAUA-5′

* DsiRNAs are asymmetric 25/27-mer RNA duplexes with a 3' two-nucleotide overhang on the antisense strand and a blunt end modified with DNA bases (shown in lower case).

2.1.9 Factors and Chemicals used for cell treatment

Table 2.5 Factors/ Chemicals used for cell treatment

Name	Source (Cat #)	Solvent	Stock concentration	Treatment concentration
Cytosine ß-D-Arabinofuronoside (AraC)	Sigma (C1768)	Ultrapure water[1]	10 mM	1 μM
$A\beta_{25-35}$	Sigma (A4559)	Ultrapure water[1]	1 mM	5 to 40 μM
$A\beta_{35-25}$	Sigma (A2201)	Ultrapure water[1]	1 mM	5 to 40 μM
Cycloheximide (CHX)	Sigma (C7698)	Dimethyl sulfoxide (DMSO)	10 mg/ml	1 and 10 ug/ml
PP2	Sigma (P0042)	DMSO	20 mM	0.01 to 50 μM
Recombinant Human TNF-α	Peprotech (300-01A)	Ultrapure water[1]	50 mg/ml	5 to 100 ng/ml
Recombinant Rat TNF-α	Peprotech (400-14-20)	Ultrapure water[1]	20 mg/ml	5 and 50 ng/ml

[1]Ultrapure water was obtained from ELGA®'s PURELAB® flex water purification system

2.1.10 Multiplex immunoassay analytes

Table 2.6 Multiplex immunoassays analytes

Analytes	MILLIPLEX® Multiplex Assays Panel P/N
CCL2/MCP-1	MPXHCYTO-60K
CCL3/ MIP-1α	MPXHCYTO-60K
CCL4/ MIP-1β	MPXHCYTO-60K
CCL5/RANTES	MPXHCYTO-60K
CCL7/ MCP-3	MPXHCYTO-60K
CXCL10/ IP-10	MPXHCYTO-60K
CXCL12/ SDF-1	HCYP2MAG-62K
FGF-2	MPXHCYTO-60K
CSF2 /GM-CSF	MPXHCYTO-60K
CSF3/ G-CSF	MPXHCYTO-60K
IL-1Ra	MPXHCYTO-60K
IL-1β	MPXHCYTO-60K
IL-6	MPXHCYTO-60K
IL-8	MPXHCYTO-60K

2.2 Methods

2.2.1 Cell cultures and cell based assays related methods

2.2.1.1 Rat cortical culture

Primary rat cortical cultures were established from embryonic (E18) Sprague Dawley rats after protocol approval from the SingHealth Institutional Animal Care and Use Committee (2014/SHS/950). Briefly, cortices were dissected and meninges were removed in ice cold Hank's balanced salt solution (HBSS). The cortices were then digested using a papain dissociation system (Worthington Biochemical Corporation, P/N LK003150), according to the manufacturer's protocol. Dissociated cells were then centrifuged and resuspended in Neurobasal (NB) medium (Invitrogen, P/N 21103-049) supplemented with 2.5% B27 (Invitrogen, P/N 17504044), 0.25% GlutaMAX™ (Invitrogen, P/N 35050061), 1x penicillin-streptomycin (Invitrogen, P/N 15140-122) and with 0.1 to 1% heat-inactivated HyClone™ Fetal Bovine Serum (FBS) (GE healthcare, P/N SH30088.03) or without FBS. Cells were seeded at densities of approximately 1×10^6 cells per well in 6-well plates or 3.4×10^4 cells per well in 96-well plates coated with 0.1 mg/ ml Poly-D-lysine hydrobromide (Sigma, P/N P6407) and cultured at 37°C in a humidified 5% CO_2 incubator. Half-change of media was performed on DIV4 (days in vitro) and 1 μM AraC (mitotic inhibitor) (Sigma, P/N C1768) could be added at this point to obtain a purer neuronal culture. At DIV 7, culture medium was replaced with NB medium minus phenol red (Invitrogen, P/N 12348017) supplemented with 2.5% B27 without antioxidants (Invitrogen,

P/N 10889-038), 0.25% GlutaMAX™ (Invitrogen, P/N 35050061) and the respective FBS concentrations.

2.2.1.2 Rat astrocyte culture

For primary astrocyte cultures, cultures were prepared from cortical tissues of P0-1 Sprague Dawley rats after protocol approval from the SingHealth Institutional Animal Care and Use Committee (2014/SHS/950). Isolated cortices were separated from the meninges in ice cold PBS, and then dissociated with 0.05% trypsin (Biowest, P/N X0915-100) with 0.5 mM EDTA (Ethylenediaminetetraacetic acid) in 1x PBS. Trypsin digestion was terminated by the addition of DMEM-F12 (Biowest, P/N L0090-500) supplemented with 10% HyClone™ FBS (GE healthcare, P/N SH30088.03) and 1 mM L-Glutamine (GIBCO, P/N 25030-081) with 1% Penicillin-Streptomycin (10,000 U/mL) (GIBCO, P/N 15140-122). The cell suspension was filtered through Falcon 40 mm nylon cell strainer (BD Biosciences, P/N 352340). The resultant filtrate was centrifuged and resuspended in fresh media, plated at 1×10^7 cells per 75 cm^2 flask. The cells were grown in 5% CO_2 incubator at 37°C and media was changed on DIV3. Subsequent media changes were performed once every 2 days until the glial culture reached confluency (12-14 days). Astrocytes were enriched by vigorously shaking the cell culture flasks at 250 rpm in a shaker maintained at 37°C for 24 h with inclusion of one media change before overnight shaking to remove microglial and oligodendrocytes (McCarthy and de Vellis, 1980, Tamashiro et al., 2012). The purity of astrocytes was assessed by immunofluorescence with anti-GFAP, an astrocytes marker and DAPI nuclear stain (Vector Laboratories). This protocol of astrocytes culturing yielded up to 97% purity. For treatment, the

astrocytes were trypsinized and re-plated at a density of 5 x10^5 cells per well in 6-well plates and treated in culture medium with reduced FBS (0.5%).

2.2.1.3 Cell culture

All cell lines were maintained in DMEM High Glucose w/ L-Glutamine w/ Sodium Pyruvate (Biowest, P/N L0104-500) supplemented with 10% Heat-inactivated FBS (Hyclone, P/N SH30088.03) and 1x MEM non-Essential Amino Acids (Biowest, P/N X0557) except for SH-SY5Y which was maintained in DMEM - F12 (Biowest, P/N L0090-500) supplemented with 10% heat-inactivated HyClone™ FBS (GE healthcare, P/N SH30088.03) and 1 mM L-Glutamine (GIBCO, P/N 25030-081). The cells were grown in a 37 ºC humidified incubator with 5% CO2 and passaged at 80-90% confluence using 0.25% trypsin (Biowest, P/N X0915-100) with 1 mM EDTA in 1x Dulbecco's Phosphate Buffered Saline (Biowest, P/N X0515-500). For keeping of cell stock, cells were resuspended in cryovials containing 600 µl of 10% DMSO (Sigma, P/N D8418) in culture media and kept at -80 ºC or transferred to liquid nitrogen for long-term storage.

2.2.1.4 Stable clone generation

For establishing stable clones of iNHA expressing FynT wild type (WT), kinase constitutively active (CA), kinase dead forms (KD) or pCMV6 Entry empty vector (EV), iNHA were transfected in 6-well plates (steps similar to transient transfection, see 2.2.1.5). One day after transfection, iNHA were trypsinized and seeded at a lower density in 10 cm dishes and treated with 600 µg/ml of Geneticin® (Invitrogen) for more than two weeks to select the clones that stably expressed the transgene. Well separated individual clones in the dishes were picked, clonally expanded and confirmed for positive expression

using Western blot analyses. In this study, at least two independent stably transfected clones of FynT-WT, -CA, -KD and EV were selected for further analyses.

2.2.1.5 Transfection

For gene overexpression or gene silencing, lipofection was performed in 6-well plates with cell densities of 2-3× 10^5 cells per well in 2 ml culture medium using HilyMax transfection reagent (Dojindo Laboratories, P/N H357) in accordance to the manufacturer's protocol. Briefly, 9 µl of HilyMax reagent was added to 120 µl Opti-MEM® I Reduced-Serum Medium (GIBCO, P/N 31985070) containing either 3 µg of plasmid DNA or 3 µl of DsiRNA (20 µM), respectively, mixed well and incubated for 15 min at RT. The mixture was then added to each well and the cells were placed back into the 37°C, humidified 5% CO_2 incubator. Cells were proceeded with other treatment one day after transfection, or harvested for further analysis two days after transfection. For gene silencing experiments, a second transfection was required to be performed one day after the initial transfection to effectively knockdown the overexpressed gene.

2.2.1.6 $A\beta_{25-35}$ preparation

$A\beta_{25–35}$ (Sigma, P/N A4559) and $A\beta_{35–25}$ (Sigma, P/N A2201) were dissolved in ultrapure water at a stock concentration of 1 mM and stored at -80 °C. Before treatment, the peptides were aged by incubating at 37°C for 24 h and added directly to the primary rat mixed cortical cultures.

2.2.1.7 Cell Viability Assay

Primary rat mixed cortical cultures seeded in 96-well plates which underwent Aβ treatment were tested for cell viability at 48 h using Cell Counting Kit-8 (CCK-8) (Dojindo Molecular Technologies, P/N CK04-11). The CCK-8 assay relies on dehydrogenase activity in live cells to convert water-soluble tetrazolium salt (WST-8) into orange WST-8 formazan dye which amount can be quantitated by absorption spectroscopy. Briefly, 10 µl of CCK-8 reagent was added to each well of the 96-well plates containing 100 µl of culture medium and placed back into the incubator for 2 h before measuring absorbance at 450 nm using Benchmark Plus Microplate Spectrophotometer System (Bio-Rad Laboratories). Percentage of cell viability was calculated as (optical density of treated) / (optical density of untreated), after deduction of background.

2.2.2 RNA isolation and gene expression assay related methods

2.2.2.1 Human brain RNA isolation

Frozen brain tissue samples were homogenized in 1 ml TRIzol reagent (Invitrogen, P/N 15596-018). After homogenization, an additional 500 µl of TRIzol reagent and 300 µl of chloroform: isoamyl alcohol (24: 1) were added and vortexed vigorously for 1 min. The mixture was incubated at room temperature (RT) for 10 min and then centrifuged at 16 000 g for 10 min at 4°C. After centrifugation, the top aqueous phase was transferred to a new microcentrifuge tube containing 600 µl of acid phenol and 200 µl of chloroform: isoamyl alcohol (24:1), followed by vortexing for 1 min and centrifugation at 16 000 g for 5 min at RT. After centrifugation, the top aqueous phase was extracted with 500 µl of chloroform: isoamyl alcohol (24:1) by vortexing for 1 min, and centrifugation at 16 000 g for 2-3 min at RT. Again, the top aqueous phase was transferred to another new tube. RNA was precipitated by mixing the aqueous phase with an equal volume of isopropanol, incubation at RT for 30 min and centrifugation at 16 000 g for 10 min at 4^{o}C. The RNA pellet was then rinsed with 75% ethanol, air dried and resuspended in nuclease-free water. Quantitation of RNA isolates was performed using Nanodrop ND-1000 spectrophotometer (Thermo Scientific). The resuspended RNA was stored at -80^{o}C until use.

2.2.2.2 Cell culture RNA isolation

Culture media was removed from cells growing in 6-well plates. 1 ml of TRIzol reagent (Invitrogen, P/N 15596018) was added to each well to lyse the cells and transferred to a microcentrifuge tube. 200 µl of chloroform: isoamyl alcohol (24: 1) was added and vortexed vigorously for 1 min. The mixture was

incubated at RT for 10 min and then centrifuged at 16 000 g for 10 min at 4°C. After centrifugation, 500 µl of the top aqueous phase were transferred to a new microcentrifuge tube containing 500 µl of 70% ethanol and pipetted up down to mix well. RNA isolation was proceeded using NucleoSpin® RNA kit (Macherey-Nagel, P/N 740955) according to manufacturer's instruction. Briefly, the mixture was passed through the NucleoSpin® RNA Column and rinsed with 350 µl of Membrane Desalting Buffer. 95 µl of DNase reaction mixture was added into the column to for DNA digestion and rinsed with 200 µl RAW2. The column was then washed with RAW3 twice and spun dry before the RNA were eluted in 30 µl of RNase-free water. Quantitation of RNA isolates was performed using Nanodrop ND-1000 spectrophotometer (Thermo Scientific). The resuspended RNA was stored at -80^{o}C until use.

2.2.2.3 Reverse Transcription

Total RNA was extracted from human brain tissue (2 µg) or cell culture (1 µg) was reverse-transcribed (RT) using High-Capacity cDNA RT kit (Applied Biosystems, P/N 4368814) in accordance to the manufacturer's protocol. Briefly, the RNA was reconstituted in 10 µl of nuclease-free water. 10 µl of 2 X RT master mix consisting of RT Buffer, dNTP Mix, RT Random Primers, MultiScribe™ Reverse Transcriptase and nuclease free water was added to the reconstituted RNA to give a final volume of 20 µl per reaction mixture. The conditions for the thermal cycler were as follows: 25°C for 10 min, 37°C for 120 min and 85°C for 5 min. After reverse transcription, cDNA products were diluted with 20 µl of nuclease-free water to reduce salt interference in subsequent real-time PCR experiments.

2.2.2.4 Primer Design

The mRNA sequences (REFSEQ) of genes of interest were obtained from NCBI's Entrez Nucleotide database (http://www.ncbi.nlm.nih.gov/nucleotide/) and used as templates for primer design. The forward and reverse primers were generated using Primer3 (v. 0.4.0) online software available at http://frodo.wi.mit.edu/primer3/. The product size range was set at approximately 150-300 nucleotides. Primer specificity was assessed using NCBI's Primer-BLAST search tool available at: http://www.ncbi.nlm.nih.gov/tools/primer-blast/ (Ye et al., 2012). Further confirmation was done by running a standard PCR followed by gel electrophoresis on a 2% agarose gel containing GelRed Nucleic Acid Gel Stain (Biotium, P/N 41003) and visualized by UV on the Gel Doc™ machine (Bio-Rad Laboratories). Only primer sets that yield PCR products with the correct predicted sizes were used for real-time RT-PCR.

2.2.2.5 Real-Time PCR

Amplification of each 1 µl of diluted cDNA was done in a 15 µl reaction mix containing 1x SYBR Green PCR master mix (Applied Biosystems, P/N 4309155) or GoTaq® qPCR Master Mix (Promega, P/N A6002) with 200 nM each of the respective forward and reverse primers (Table 2.3). Real-time PCR was carried out using the 7500 Fast Real-Time PCR Machine (Applied Biosystems). The temperature program used was as follows: 50°C for 2 min, 95°C for 2 min and 40 cycles of 95°C for 15 s and 60°C for 1 min. All real-time PCR assays were performed in duplicate. Standard curves of each gene were generated independently by 10x serial dilution of template DNA. The relative signal intensity of each sample was calculated according to the

corresponding standard curve. Melting curves were analysed for each sample to check for product specificity. Normalization was performed in each sample by dividing the relative signal intensity of gene of interest to 18S rRNA (human brain samples), or geometric mean of β-actin, GAPDH and 18S rRNA (primary rat culture and human cell culture).

2.2.2.6 Capillary Electrophoresis

PCR was first performed on 1 µl of diluted cDNA product in a 20 µl master mix containing 1x Colourless GoTaq ® Flexi buffer (Promega), 1.5 mM $MgCl_2$, 200 µM dNTP, 1 unit of GoTaq® Flexi DNA Polymerase (Promega, P/N M8295), 250 nM of forward primer and 56-FAM labelled reverse primer (see Table 2.3). The temperature program used was as follows: 94°C for 3 min, 55°C for 1.5 min, 72°C for 2 min and 22-25 cycles of 94°C for 1 min, 55°C for 1 min, 72°C for 1 min. The reaction ended with 72°C for 10 min and was maintained at 4°C until collection. Capillary electrophoresis was then performed using Applied Biosystems PRISM – 310 Genetic Analyzer or Applied Biosystems 3500xL Genetic Analyzer. 1 µl of PCR product was added to 12 µl of Hi-Di™ formamide (Applied Biosystems, P/N 4311320) and 1 µl of ABI GeneScan 500 Rox size standard (Applied Biosystems, P/N 4310361). The samples were incubated at 95°C for 4 min and immediately placed on ice to prevent DNA renaturation. The product size and quantity of each DNA amplicon in the capillary electropherograms was analysed using GeneScan analysis software (Applied Biosystems). Peak areas of FynT (219 bp DNA amplicon) and FynB (228 bp DNA amplicon) in each electropherogram were translated into expression level and used to determine ratios of FynT to FynB expression.

2.2.2.7 High Throughput Real-Time PCR

High Throughput Real-Time PCR was performed using a BioMark HD system (Fluidigm Corporation) to simultaneously study 192 samples of their expression of 24 genes using a 192.24 Dynamic Array™ integrated fluidic circuit (IFC) for Gene Expression (Fluidigm, P/N 100-6266). Specific target amplification (STA) was first carried out on each cDNA sample to increase the number of copies of target DNA. This step involved mixing cDNA with all the target primer pairs (pooled in advanced) at a final concentration of 0.05 μM in 1x PreAmp Master Mix (Fluidigm Corporation, P/N 100-5580). The mixture was then placed into a thermal cycler for 10 cycles of amplification of the genes of interest. The temperature program used was as follows: 95°C for 2 min and 10 cycles of 95°C for 15 s and 60°C for 4 min. The reaction was maintained at 4°C until collection. After STA, a clean-up step was performed to remove unincorporated primers using treating with approximately 1 U/μl Exonuclease I (New England BioLabs, P/N M0293S) for 37°C for 30 min, and followed by 80°C for 15 min to stop the reaction. The end product was diluted 10-fold in TE buffer (10 mM Tris-HCI, 1.0 mM EDTA, Invitrogen) and stored at -20°C until use. To prepare samples for high throughput real-time PCR, 1.8 μl of each diluted ExoI-treated STA product was added to 96-well plate containing mixture of 2 μl of 2x SsoFast EvaGreen Supermix with low ROX (Biorad, P/N 1725211) and 0.2 μl of Delta Gene Sample Reagent (Fluidigm, P/N 100-6653), vortex and remove bubbles prior adding to IFC. To prepare assay mix, 0.4 μl of each primer set (50 μM) was added to 96-well plate containing mixture of 2 μl of 2x Assay loading reagent (Fluidigm, P/N 100-5359) and 1.6 μl of 1x DNA suspension buffer (10mM Tris, 0.1 mM EDTA,

pH8.0), vortex and remove bubbles prior adding to IFC. Preparation and loading of 192.24 Dynamic Array IFC was performed according to the manufacturer's instructions based on Fluidigm 192.24 DELTAgene™ Fast/Standard Gene Expression Workflow (PN 100-7222 C1). Briefly, the IFC was made ready by injecting 150 μl of control line fluid into the dedicated accumulator with a provided syringe and removing the blue protective film from the bottom of IFC, followed by pipetting 3 μl of each primer reaction assay mix and 3 μl of each sample into the respective inlets without generating air bubbles. Lastly, Actuation Fluid and Pressure Fluid were pipetted into the respective wells with indicated volume based on instructions. The 192.24 Dynamic Array IFC was then loaded into IFC Controller RX by running the Load Mix (169x) script to complete the mixing of samples and assays and then transferred to BioMark HD system for real-time PCR and melting curve analysis. The temperature program used was as follows: 95°C for 1 min and 30 cycles of 96°C for 5 s and 60°C for 20 s. The melting curve analysis consisted of 3 s at 60°C followed by heating up to 95°C with a ramp rate of 1°C/ 3 s. A pooled template DNAs for all the primer sets were 10x serial diluted to generate standard curves for each gene. The relative signal intensity of each sample was calculated according to the corresponding standard curve. Normalization was performed in each sample by dividing the relative signal intensity of gene of interest to geometric mean of α-tubulin, β-actin, GAPDH and 18S rRNA. Primer sequences used are listed in Table 2.3.

2.2.2.8 Dual luciferase reporter assay

To measure the NF-κB activity in FynT clones, 3 μg of pNF-κB-luc and 0.03 μg of pRL-CMV were co-transfected 24 h prior treatment with TNFα. Culture

medium was carefully removed at the respective time points post treatment and the cells were rinsed with 1x PBS. Dual-Luciferase® Reporter Assay Kit (Promega, P/N E1910) was used for investigating the activity. Briefly, cells were lysed in 250 µl of 1x Passive Lysis Buffer using a cell scraper. The lysate was transferred to a new tube and kept at -80°C before processing. One cycle of freeze and thaw was performed by thawing the frozen cell suspension in 37 °C water bath to accomplish complete lysis of the cells. The cell lysate was centrifuged at 16 000 g for 30 s to remove cell debris and 10 µl aliquots of the cell lysates were prepared in clear 1.5 ml microcentrifuge tubes for triplicate readings. Luminescent signals were measured by DLR-INJ-0 Promega protocol on Promega Glomax luminometer (2 s pre-measurement delay, followed by 10 s measurement period for each reporter). For the first reading, 50 µl Luciferase Assay Reagent II was added to the aliquot of cell lysis, mixed well and Firefly luciferase reading was measured in the luminometer. The second read was obtained after addition of 50 µl Stop & Glo® Reagent and the Renilla luciferase reading was measured. NF-κB derived luciferase activities were determined by Firefly luciferase readings after normalizing for transfection efficiency for Renilla luciferase readings.

2.2.3 Protein expression assay related methods

2.2.3.1 Preparation of brain tissue for immunofluorescence

Microscope slides (Marienfeld Superior, P/N 1005200) were coated with 0.01% Poly-L-lysine (Sigma, P/N P8920) for 5 min and dried at RT. Brain tissues from Brodmann area 9 embedded in optimum cutting temperature (OCT) were sectioned at thickness of 10 or 20 µm with cryostat (Leica CM1850, USA) and mounted onto the coated microscope slides.

2.2.3.2 Immunofluorescence (IF) staining

Samples (cells seeded on coverslips or brain sections) were first fixed in 3.7% formaldehyde (Sigma, P/N F8775) in PBS for 10 min and rinsed twice with PBS. Cells on coverslips were permeabilized via incubation with 0.1% Triton X-100 in PBS for 5 min while the brain sections were permeabilized in ice-cold acetone: methanol (1:1) for 10 min. After rinsing twice with PBS, samples were then blocked with 10% normal goat serum in PBS at RT for 1 h followed by incubation with primary antibodies (Table 2.2) overnight at 4^{o}C. The excess primary antibodies were washed off with PBS and proceed with incubation of secondary antibodies (Table 2.2) at RT for 1 h. For brain sections, an additional treatment with autofluorescence eliminator reagent (Millipore, P/N 2160) was performed according to the manufacturer's instructions to reduce autofluorescence. Briefly, sections were immersed in 70% ethanol for 5 min, then incubated with autofluorescence eliminator reagent for 5 min at RT, and washed with 70% ethanol for two times. Samples were then mounted in 4',6-diamidino-2-phenylindole (DAPI, blue nuclear stain) containing Vectashield mounting medium (Vector Laboratories, P/N H-1200), then visualized and captured using the Nikon A1R confocal microscopy system. The images were processed using Nikon NIS-Elements software.

2.2.3.3 Preparation of protein lysates and protein quantitation

Samples were lysed with 2X Laemmli Sample Buffer (Bio-Rad Laboratories, P/N 1610737) containing 65.8 mM Tris-HCl, pH 6.8, 2.1% SDS, 26.3% (w/v) glycerol, 0.01% bromophenol blue with addition of 5 % of β-mercaptoethanol and boiled for 5 min. The lysates were quantitated using 2-D Quant Kit (GE Healthcare, P/N 80-6483-56) which allows quantitation of protein in the

presence of detergents, reductants, and chaotropes. Briefly, standard curve (0–50 µg) was prepared using the 2 mg/ml BSA standard solution. 4 µl of sample was added in a microcentrifuge tube with 250 µl of precipitant followed by 250 µl of co-precipitant. The precipitated sample was centrifuged for 5 min at 10 000 g and the supernatant was carefully removed. 50 µl of alkaline copper solution and 200 µl of deionized water was added and vortexed to dissolve the protein pellet. 500 µl of colour reagent was added and mixed instantaneously. The colour reagent reacts to unbound cupric ions resulting in colour density change that is inversely related to the concentration of the protein sample. Absorbance was read at 480 nm after 15 min of incubation at RT using Benchmark Plus Microplate Spectrophotometer System (Bio-Rad Laboratories). Protein concentration was estimated by comparison to the standard curve.

2.2.3.4 Western blot analyses

SDS-PAGE (sodium dodecyl sulfate polyacrylamide gel electrophoresis) was carried out in vertical gel composed of 10% polyacrylamide resolving gel and 5 % stacking gel. Electrophoresis was performed in 1x Tris/glycine SDS buffer (f/c of 2.5 mM Tris, 19.2 mM glycine, and 0.01% (w/v) SDS, pH 8.3) (Biorad, P/N 1610732) at 120 V. PageRuler™ Plus Prestained Protein Ladder (Thermo Scientific, P/N SM0671) was electrophoresed alongside with the samples for molecular weight determination. The transfer of proteins onto nitrocellulose membranes were carried out using iBlot® Dry Blotting System with transfer stacks (Invitrogen, P/N IB301001) using program P3 and a 7 min transfer time. After transfer, the membranes were first rinsed with Tris-Buffered Saline with 0.1% (v/v) Tween 20 (TBST) and blocked with Bløk-PO

Noise Cancelling Reagents (Millipore, P/N WBAVDP001) for 1 h at RT. After blocking, the membranes were rinsed three times with TBST. The membranes were then incubated overnight at 4^{o}C with primary antibodies in the blocking solution at indicated dilutions (Table 2.2). Following that, the membranes were washed three times with TBST. Secondary antibodies conjugated with horseradish peroxidase (HRP) diluted in blocking solution were then added to the membrane and incubated for 1 h at RT. After washing three times in TBST, Immobilon Western Chemiluminescent HRP Substrate (Millipore, P/N WBKLS0500) was added and chemiluminescence was captured by UVIchemi image analyser (UVItec, Cambridge UK).

2.2.3.5 Multiplex immunoassays

TNFα-induced the release of cytokines and chemokines in iNHA was determined using multi-analyte profiling system. Tissue culture media of iNHA with or without TNFα treatment were collected at day 3, centrifuged to remove cell debris for 10 min at 4°C and stored at $–80^{0}$C until use. Inflammatory markers were measured using MILLIPLEX® Multiplex Human Cytokine/Chemokine Panel I Immunoassay (Millipore, P/N MPXHCYTO-60K) and MILLIPLEX® Multiplex Human Cytokine/Chemokine Magnetic Bead Panel II Immunoassay (Millipore, P/N HCYP2MAG-62K) (see Table 2.6 for the list of analytes) according to the manufacturer's instruction. Briefly, wells on plates were pre-wetted with Assay Buffer for 10 min at RT before vacuum drying or decanting. First, 25 µl of Standards, QC Controls or Assay buffer were added to the respective wells. 25 µl of pure culture medium was added to the Blank, Standards and QC Control wells, while 25 µl of neat or diluted samples (100 fold with culture media) were added to the respective

wells containing Assay buffer. The plate was then incubated with agitation overnight at 4°C. Subsequently, the samples were washed twice with 200 µl of wash buffer and incubated with 25 µl of detection antibodies for 1 hour at RT with agitation. The samples were then incubated with 25 µl Streptavidin-Phycoerythrin for 30 min at RT with agitation. Finally, the plate was washed twice with 200 µl of Wash buffer, and incubated with 150 µl of sheath fluid for 5 min before reading. The results were read using xPONENT® Software Version 3.1 on the Luminex LX200 instrument (Millipore). Analysis was performed using MILLIPLEX® Analyst Software Version 3.4 (Millipore).

2.2.4 Data Analyses

2.2.4.1 Image quantitation

Five representative images per sample from three AD and three control brains were analysed using 'Object Count' to obtain total cell count as well as mean fluorescence intensity of individual cell in each channel using Nikon's NIS-Elements Advanced Research software. For primary culture imaging, three representative images per treatment derived from 4 independent experiments were analysed using the 'Threshold' function to obtain the mean fluorescence intensity of ROI (Regions of interest) after applying a fixed signal intensity cut-off across all samples.

2.2.4.2 Graphs and statistical analyses

Statistical differences for gene expression of AD and control groups were analysed using Mann-Whitney tests. Statistical differences for unmatched or matched groups ($N \leq 5$) were performed using Student's *t*-tests or Student's paired *t*-test respectively. For comparisons of gene expression between

different groups or treatments, one-way analyses of variance (ANOVA) with Bonferroni's *post-hoc* tests was performed. For comparisons of gene expression or protein secretion between different groups with and without treatment, two-way analyses of variance with Bonferroni's *post-hoc* tests were performed. To perform multiple comparison to a control, one-way analyses of variance (ANOVA) with Dunnett's post-hoc test were performed. To demonstrate the presence of a positive or negative significant correlation between two parameters, Pearson's Correlation was employed for two continuous data. For all analyses, two-tailed *p*-values of < 0.05 were considered to be statistically significant. Three-dimensional PCA plots and two-dimensional unsupervised hierarchical clustering analysis were generated using Partek® Genomics Suite Version 6.6 software. All other graphs were plotted and statistical analyses were performed using GraphPad PRISM® Version 5 software.

CHAPTER 3-
An isoform-specific role of FynT tyrosine kinase in Alzheimer's disease

CHAPTER 3- An isoform-specific role of FynT tyrosine kinase in Alzheimer's disease

3.1 Background

Exon array demonstrated differential alternative splicing of Fyn in AD, with significant increase of FynT but no change of brain-predominant FynB in AD brain. In addition, gene ontology term enrichment analyses on the exon array data revealed that FynT expression correlated negatively with neuronal function and positively with reactive astrogliosis.

3.2 Hypothesis

FynT induction in AD may be associated with reactive astrogliosis and neurodegeneration.

3.3 Experimental designs/ Approaches

1. To confirm FynT induction in AD using real-time RT-PCR and FynT and FynB ratio using capillary electrophoresis. (See Results at 3.4.1)
2. To investigate the expression profiles of FynB and FynT in primary neurons and astrocytes by capillary electrophoresis and immunofluorescence. (See Results at 3.4.2 and 3.4.3)
3. To characterize specificity of custom-made FynT and FynB antibodies by Western blotting and immunofluorescence. (See Results at 3.4.3)
4. To determine FynT immunoreactivity in association with cellular markers and neuropathological hallmarks in post-mortem AD brains. (See Results at 3.4.4 to 3.4.7)

3.4 Results

3.4.1 Selective upregulation of FynT isoform expression in AD brain

To validate the exon array data that FynT was significantly upregulated in AD, real-time RT-PCR using FynB- and FynT-specific primer sets and capillary electrophoresis was performed. Real-time PCR confirmed that FynT was significantly upregulated in AD (p =0.0155, Mann-Whitney test), whereas there were no significant changes for FynB (Figure 3.1A). Furthermore, relative levels of FynB and FynT transcripts in each sample were measured by RT-PCR followed by capillary electrophoresis and showed that an elevated FynT peak in AD compared with negligible FynT in control (Figure 3.1B), consistent with the finding of significantly higher FynT to FynB ratio in AD compared to controls (p=0.0009, Mann-Whitney test, Figure 3.1C).

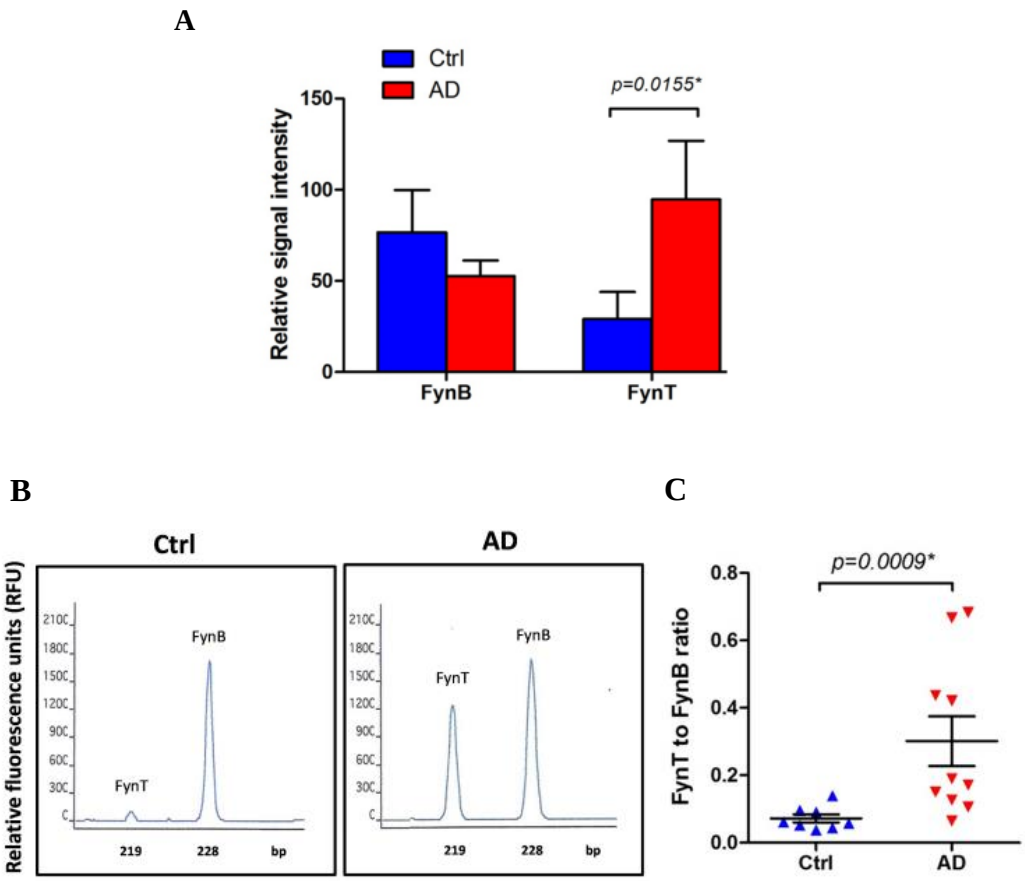

Figure 3.1 Selective upregulation of FynT isoform expression in AD brain. **(A**) Real-time RT-PCR determined the relative signal intensity of FynB and FynT in AD and control brain. **(B)** The proportional amount of FynT and FynB in AD and control brain was determined by RT-PCR followed by capillary electrophoresis. A representative electropherogram showed the relative fluorescence units (RFU) of FynT peak (219bp DNA amplicon) and FynB peak (228bp DNA amplicon) in AD and control samples. **(C)** Peak areas of FynT and FynB in each electropherogram were translated into expression level and used to determine FynT to FynB ratio of expression. The dot plot showed that AD samples have significantly higher FynT to FynB ratio than control samples (p=0.0009, Mann-Whitney test). Available samples for RT-PCR and capillary electrophoresis were 10 AD and 8 controls.

3.4.2 Higher proportions of FynT expression in cells of astrocytic origin

Our preliminary data obtained from the exon array database showed that FynT was positively and significantly correlated with genes associated with cytoskeleton organization, cell adhesion, cellular movement and extracellular matrix (Table 1.1), as well as astrocytic markers including GFAP and GLAST (Table 1.2), suggesting that FynT induction in AD may be associated with astrocyte activation. On the other hand, FynT was negatively correlated with synaptic vesicles and various neuronal markers (Table 1.1). Although FynB has been known to be the brain predominant isoform of Fyn, the expression of FynT has never been explored in the brain. The observation of opposite trends of FynT correlation in astrocytes and neurons, prompted us to determine the expression profiles of FynB and FynT in these two main cell types of the brain. First, we obtained pure cultures of primary neurons and astrocytes, as well as cell-lines derived from neuronal and astrocytic origins. RT-PCR was performed using common primers spanning the alternative spliced exon of Fyn, followed by capillary electrophoresis.

Higher proportions of endogenous FynT expression were found in primary rat astrocytes and cell lines of astrocytic lineage as compared to primary rat neurons and neuronal cell lines as illustrated in Figure 3.2A with representative electropherograms of neurons and astrocytes illustrated in Figure 3.2B.

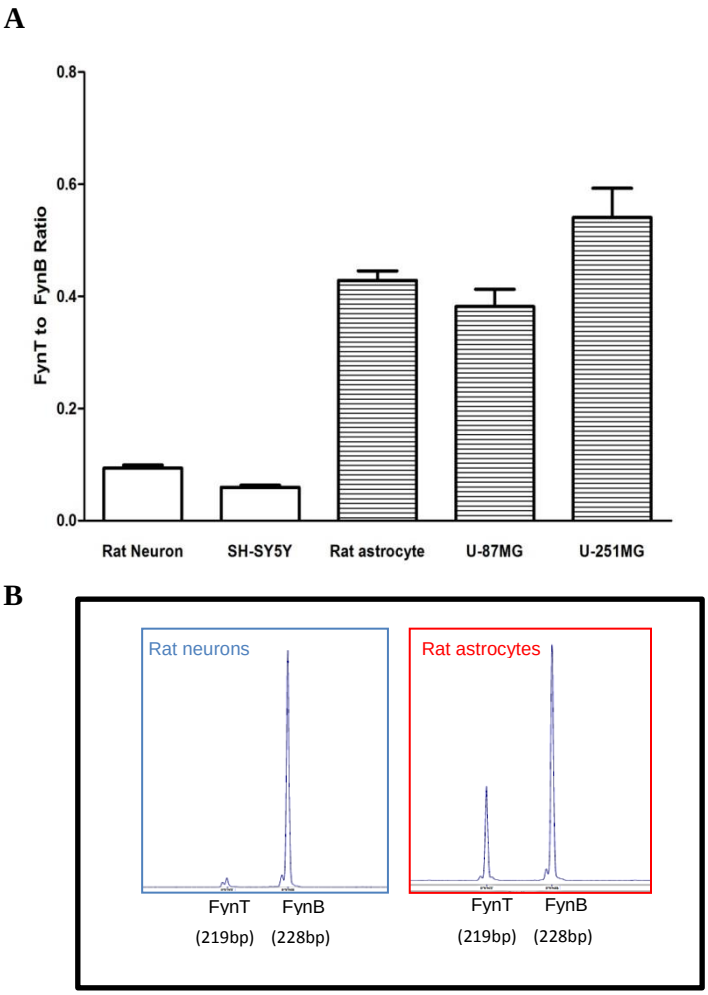

Figure 3.2 Higher proportions of FynT expression in cells of astrocytic origin. **(A)** Endogenous FynT to FynB ratios were determined by RT-PCR followed by capillary electrophoresis in untreated cells of neuronal (primary rat neurons, SH-SY5Y line) or astrocytic (primary rat astrocytes, U-87MG and U-251MG lines, shaded bars) origin. Data are mean ± SEM of at least three independent experiments for each cell type. **(B)** The proportional amount of FynT and FynB in rat neurons and rat astrocytes was determined by RT-PCR followed by capillary electrophoresis. Representative electropherograms showed the relative fluorescence units (RFU) of FynT peak (219bp DNA amplicon) and FynB peak (228bp DNA amplicon) in rat neurons and rat astrocytes.

3.4.3 Custom-made FynB and FynT antibodies were able to specifically identify their respective Fyn isoforms

There are no commercially available Fyn isoform-specific antibodies. To facilitate our study, we generated custom-made rabbit polyclonal FynB and FynT-specific antibodies. The characterization of antibody specificities was done by Western blot analyses and immunostaining using HEK293T cells transiently transfected with either FynB or FynT construct that tagged with Myc-FLAG. Western blot analyses demonstrated that FynB and FynT antibodies were able to specifically identify their respective isoforms (Figure 3.3A). Most importantly, FynT antibody did not cross-react with FynB, and vice versa. Using double IF staining, all successfully transfected cells that were stained positive for Myc-tag antibody were also specifically detected by their corresponding Fyn isoform-specific antibodies (Figure 3.3B).

The observation of higher FynT to FynB ratio in astrocytes compared to neurons suggested that stronger FynT immunoreactivity may be detected in astrocytes. Mixed rat cortical culture with triple immunofluorescence staining of FynT-specific antibody, NeuN neuronal marker and GFAP astrocytic marker revealed that astrocytes indeed exhibited higher FynT immunoreactivity as compared to neurons (arrows in Figure 3.4).

Before proceeding to investigate FynT and FynB protein expression in AD brain sections of prefrontal cortices, peptide neutralization was performed to demonstrate the specificity of FynT and FynB antibodies in the brain sections. To perform peptide neutralization, the antibodies were pre-incubated with a five-fold (by weight) excess of the respective synthetic immunizing peptides

(sequences can be found in Chapter 2- Materials and Methods under 2.1.5) overnight at 4°C in incubation buffer (10% normal goat serum in PBS), before proceeding with IF in brain tissues. The absence of positive immunoreactives in the AD brain sections after peptide neutralization procedure validated antigenic-specificity of both FynT and FynB antibodies in human brain tissue (Figure 3.5).

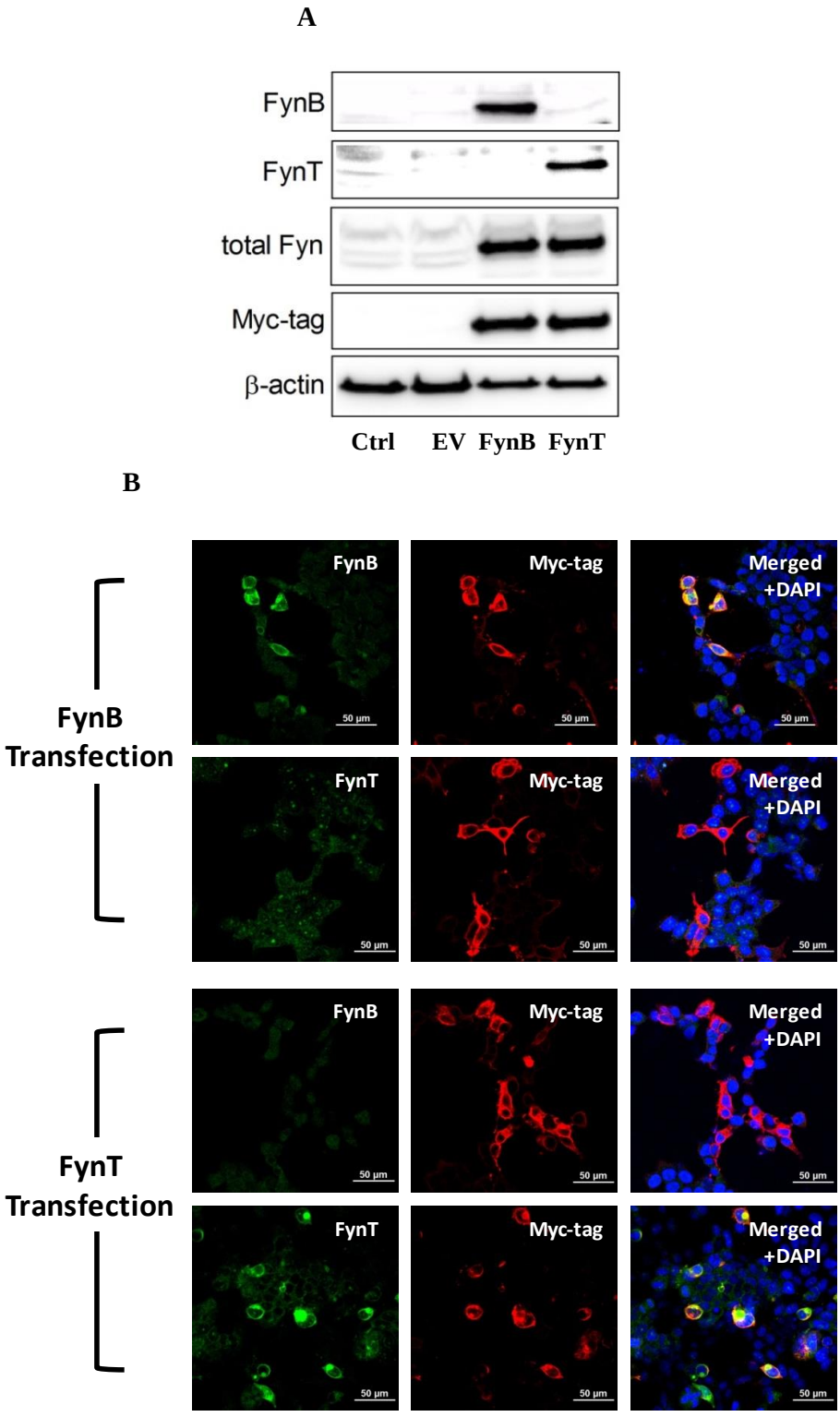

Figure 3.3 Characterization of FynB and FynT isoform-specific antibodies. Custom-made FynB and FynT isoform-specific polyclonal antibodies were characterized using transiently transfected HEK293T cells over-expressing either FynB or FynT tagged with Myc-FLAG. **(A)** Western blot analyses using total lysates harvested by direct lysis with Sample buffer

from HEK293T non-transfected cells (Ctrl), cells transfected with empty pCMV6-Entry vector (EV), or cells transfected with the tagged FynB or FynT constructs, were probed with custom-made anti-FynB or FynT polyclonal antibodies as well as with total Fyn and Myc-specific antibodies. Detection of Myc-tag and total Fyn confirmed successful transfection. **(B)** Double IF staining with FynB or FynT-specific polyclonal antibodies (green) and Myc-tag antibodies (red) were demonstrated in FynB- (top two panels) and FynT- (bottom two panels) transfected HEK293T. The right most column depicts merged channels with nuclei staining by DAPI (blue). Co-staining could be observed as yellow. Scale bars =50 µm.

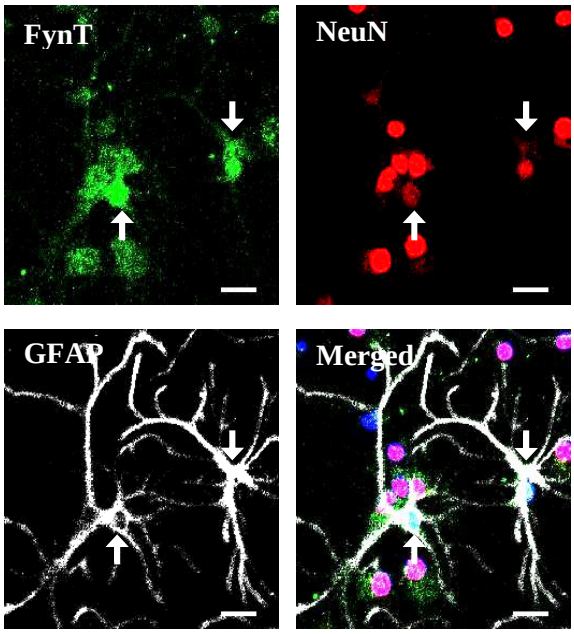

Figure 3.4 Astrocytes exhibited higher FynT immunoreactivity as compared to neurons. Triple IF staining of FynT-specific polyclonal antibodies (green), neuronal marker NeuN (red) and astrocytic marker GFAP (white) was performed on mixed rat cortical culture. Cell nuclei stained by DAPI (blue) were shown in the merged images. White arrows indicate astrocytes which are stained positively with GFAP. Scale bars = 20 µm.

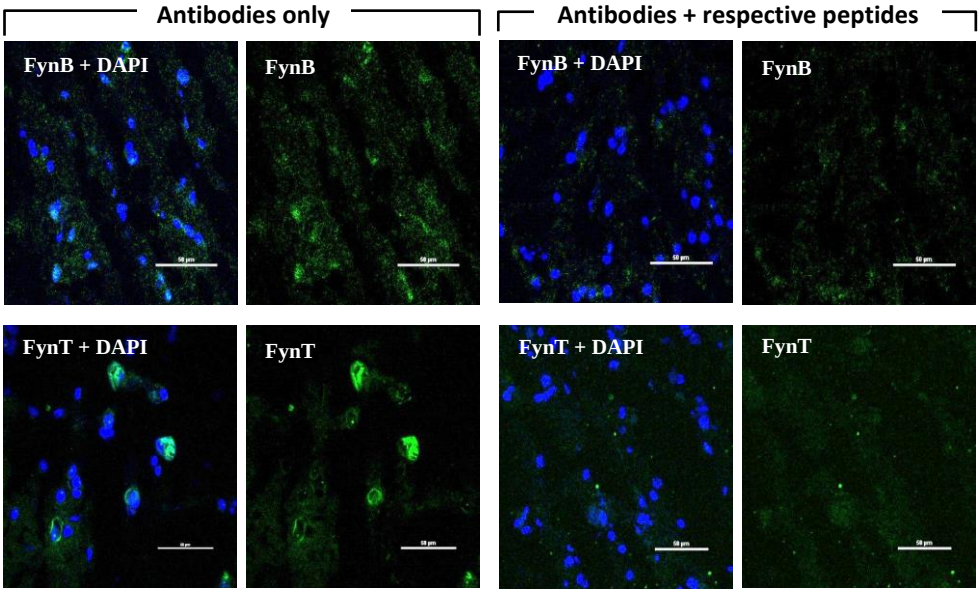

Figure 3.5 FynB and FynT isoform-specific antibodies demonstrated antigen-specific immunoreactivity in human brain tissues. Custom-made FynB and FynT isoform-specific polyclonal antibodies (green) costained with nuclear DAPI counterstain (blue) showed specific positive immunoreactivites in prefrontal cortex brain sections (left panel) obtained from AD patients which could be blocked by their respective immunizing peptides (right panel). Scale bars = 50 μm.

3.4.4 Increased FynT immunoreactivity in AD prefrontal cortex

To localize Fyn induction in AD, we employed FynB and FynT-specific antibodies for IF staining on prefrontal cortex (BA9) brain sections obtained from patients with AD and control. In general, weak FynT immunoreactivity was found in control prefrontal cortex (top left panel in Figure 3.6A); whilst in AD, a subgroup of cells with intense staining could be detected (Figure 3.6A, top right panel). Image quantitation revealed that a significantly higher percentage of strong FynT-staining cells (4.8 ± 0.6%) was found in AD (Figure 3.6B, red circle) compared to control brains (0.8 ± 0.5%, Figure 3.6B, blue circle). In contrast, FynB immunoreactivities were uniformly prominent in both AD and control sections (Figure 3.6A, bottom panels), with no significant differences in percentage of stained cells (Figure 3.6B, red and blue triangles).

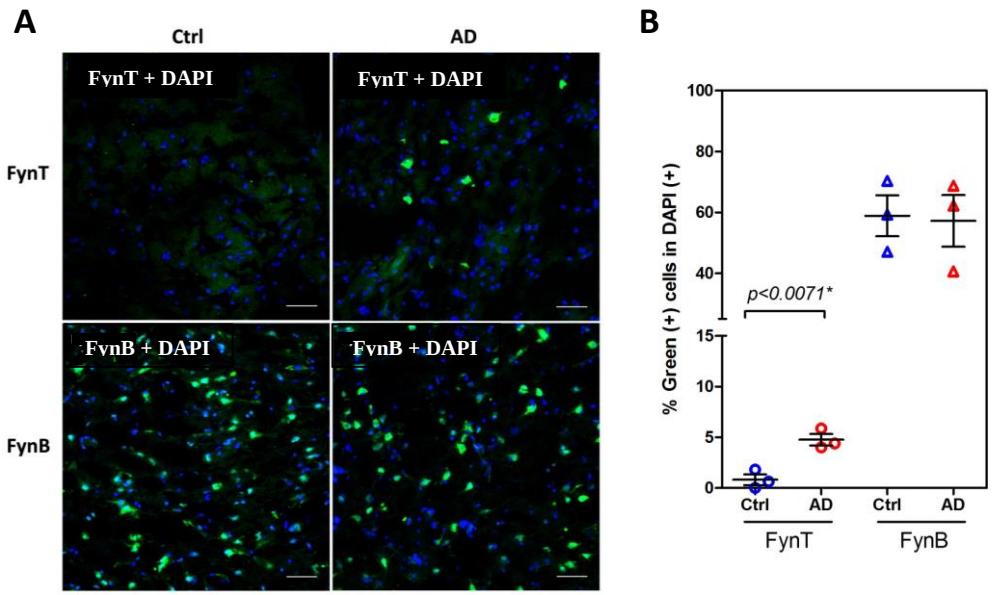

Figure 3.6 Increased FynT immunoreactivity in AD prefrontal cortex. (A) Representative IF staining of prefrontal cortex using FynT-specific antibody (green, upper panel) or FynB-specific antibody (green, lower panel) with nuclear DAPI counterstain (blue) were compared between AD and control. Scale bars = 50 µm. **(B)** Dot plot presents the mean of percentage of cells (defined by DAPI-positive staining) that stained positive for FynB (circle) and FynT (triangle) in AD (red, n=3) and control (blue, n=3) prefrontal cortex. The mean value in each sample is calculated by the percentage of positive cells in five representative images. *Significantly different (Student's *t*-tests).

3.4.5 FynT localization to a subset of neurons in AD

To determine whether FynT upregulation in AD could be localized to neurons, double IF staining was performed using Fyn isoform-specific antibodies and neuronal marker NeuN in AD and control prefrontal cortex. The strong FynT immunoreactivities were localized in NeuN-positive stained neurons (Figure 3.7A, white arrows). Only a subset of NeuN-positive neurons co-stained with FynT. In contrast, the majority of neurons stained positive for FynB (Figure 3.7B), supporting the previously established neuronal localization for FynB (Cooke and Perlmutter, 1989). Therefore, FynT upregulation in AD seems to occur in a subset of neurons, most of which showed unchanged levels of FynB.

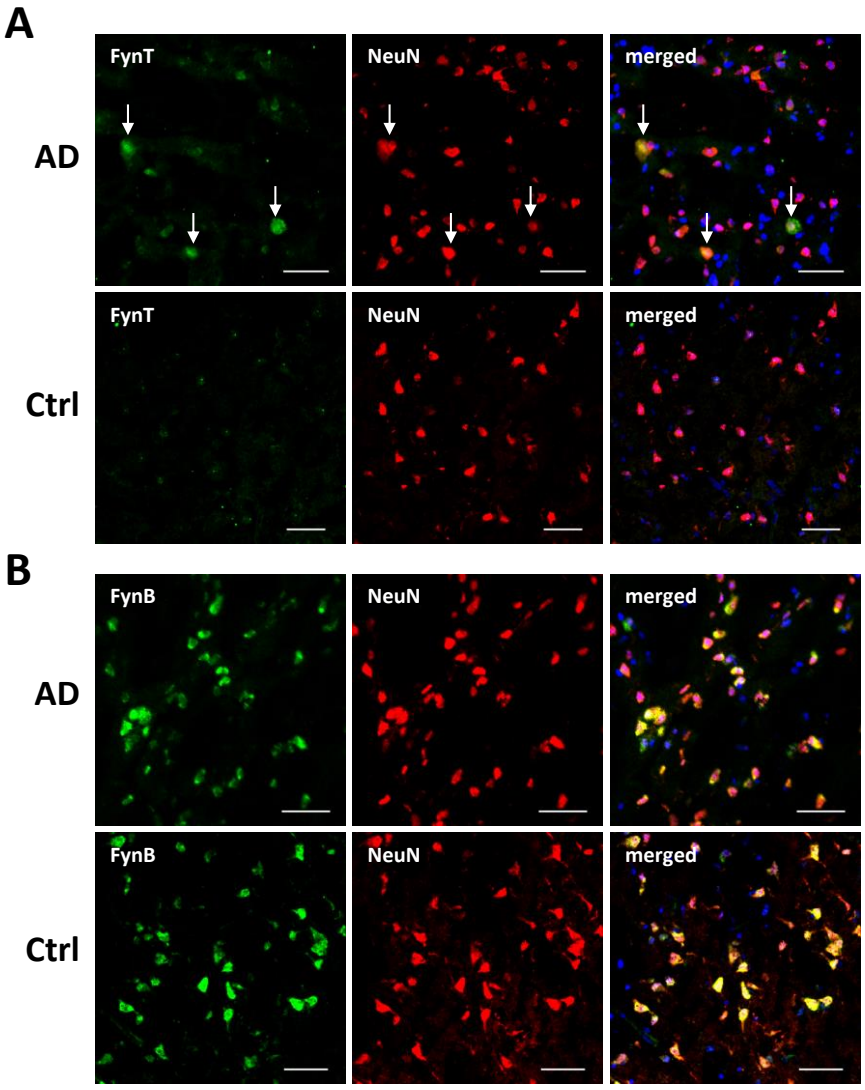

Figure 3.7 FynT localization to a subset of neurons in AD. Representative double IF staining of **(A)** FynT and **(B)** FynB (green) with neuronal marker NeuN (red) in AD and control prefrontal cortex. Nuclei were counterstained with DAPI (blue). White arrows in (A) indicated cells that were positively co-stained with FynT and NeuN. Scale bars = 20 μm.

3.4.6 FynT localization to reactive astrocytes in AD

Besides neurons, Figure 3.8 shows that FynT immunoreactivities were localized to cells that stained positive for GFAP at the thickened processes (white arrows in top panels) and hypertrophic cytoplasm (white arrows in middle panels), both of which are characteristic of reactive astrocytes. FynT immunoreactivity was observed to be relatively stronger in hypertrophic cytoplasm than in the GFAP-positive processes. However, the weaker but specific FynT staining of the astrocytic processes in AD brain could still be resolved (white arrows, Figure 3.8 top left panel) even in the presence of strong FynT signals in adjacent non-GFAP cells (putatively neurons, see Figure 3.7A). On the other hand, corresponding GFAP-positive processes in control brain appeared thinner and showed non-specific background stain for FynT (Figure 3.8, white arrows in bottom panels). This data showed that at least a proportion of FynT immunoreactivities were localized to reactive astrocytes in AD brain.

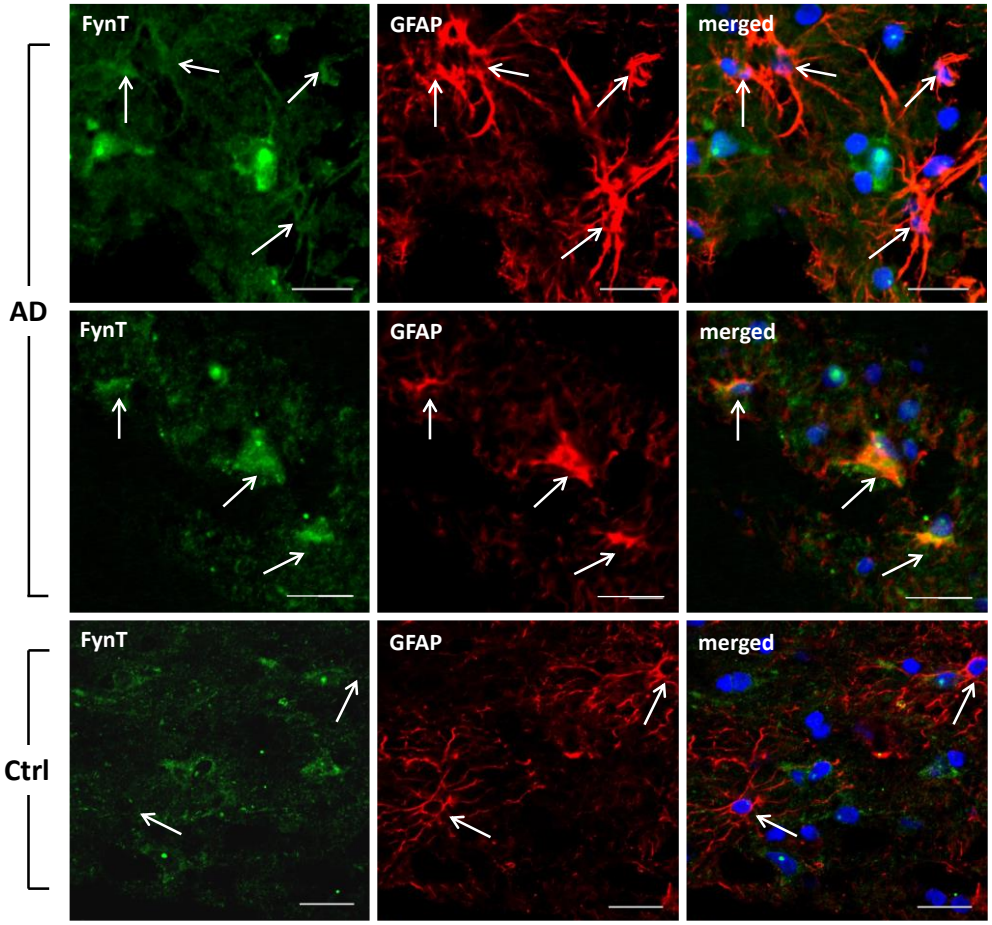

Figure 3.8 FynT localization to reactive astrocytes in AD. Representative double IF staining of FynT (green) and astrocytic marker GFAP (red) in the prefrontal cortex of AD (first two panels) and control brain (last panel). Nuclei were counterstained with DAPI (blue). White arrows indicated astrocytes. Scale bars = 20 μm.

3.4.7 Increased FynT in NFT-bearing neurons concomitant with decreased FynB immunoreactivity

Fyn is known to co-stain with NFTs (Shirazi and Wood, 1993, Ho et al., 2005). Using FynT and FynB-specific antibodies, Fyn isoform-specific association with NFT could now be examined. The AT8 antibody which recognizes phosphorylated tau at Serine 202 and Threonine 205 detects both neuropil threads as well as NFT-bearing neurons in AD prefrontal cortex (Figure 3.9A, red channels). Interestingly, cells with intense FynT immunoreactivity in AD sections were exclusively co-stained with AT8, manifesting as yellow fluorescence signals of NFT-bearing neurons in merged images (Figure 3.9A top right panel, white arrows). In contrast, FynB immunoreactivity was relatively weak in NFT-bearing neurons (Figure 3.9A bottom panels, white arrows) compared to the adjacent AT8-negative stained neurons. Mean fluorescence intensities of FynB and FynT in AT8-positive versus adjacent AT8-negative cells were both significantly different with increased FynT and decreased FynB in AT8-positive cells (Figure 3.9B). Furthermore, FynT immunoreactivity also co-localized with another antibody (Tyr18) specific for tau phosphorylated at tyrosine 18 (pY18), a site previously shown to be directly phosphorylated by Fyn (Lee, 2004), see Figure 3.10.

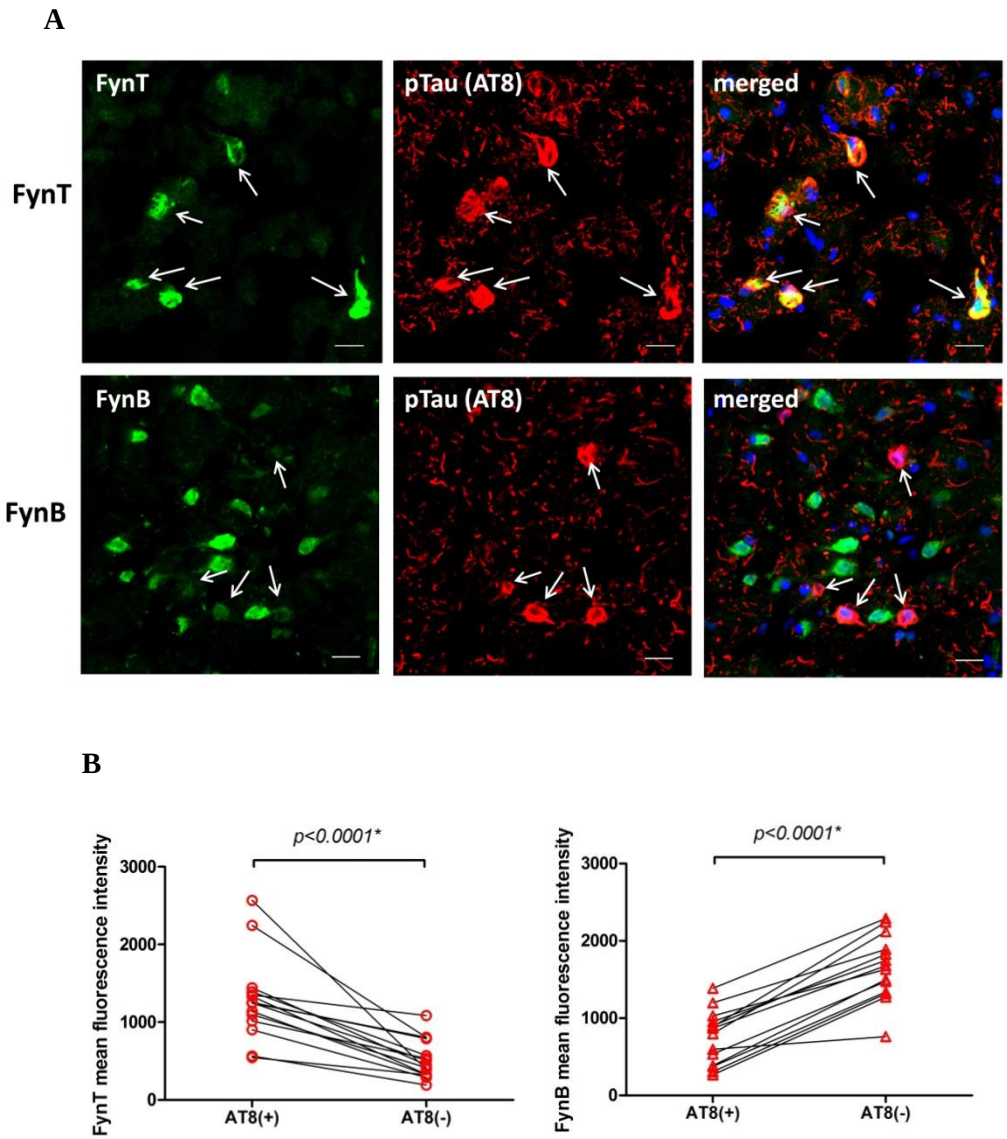

Figure 3.9 Increased FynT in NFT-bearing neurons concomitant with decreased FynB immunoreactivity. (A) Representative double IF staining of phosphorylated tau marker AT8 (red) and FynT (green, top panel) or FynB (green, bottom panel) counterstained with DAPI (blue) in the prefrontal cortex of AD brain. White arrows indicated NFT-bearing cells. Scale bars = 20 µm. **(B)** Mean fluorescence intensities of FynT or FynB in NFT-bearing neurons (defined by AT8-positive staining) and surrounding AT8-negative cells within each representative image are analysed in pairs. Five representative images were included in each sample. Three AD samples were under studied. *Significantly different (Student's paired *t*-tests).

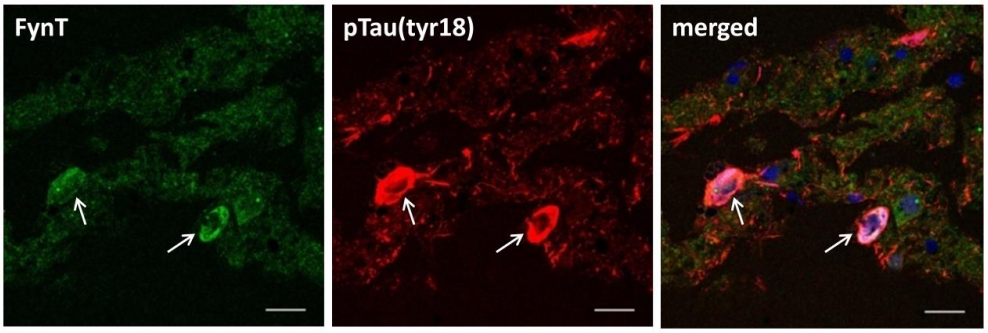

Figure 3.10 FynT co-localized with pTau (Tyr18) immunoreactivity in NFT-bearing neurons. Representative double immunofluorescence staining of FynT (green) and pTau (Tyr18) (red) counterstained with DAPI (blue) in the prefrontal cortex of AD brain. White arrows indicated NFT-bearing cells. Scale bars = 20 μm.

3.5 Discussion

3.5.1 FynT upregulation in AD

Fyn kinase is postulated to be involved in several aspects of AD pathogenesis, and the current study has elucidated an isoform-specific role for Fyn by identifying a selective upregulation of the FynT isoform in AD brain. In view of a previous report showing an increase of Fyn kinase activity but no change of Fyn protein levels in AD brain (Larson et al., 2012), it can be postulated that the abundant, unchanged expression of FynB in AD could have masked an increase in FynT expression when using non isoform-specific antibodies. It is also possible that the reported increase in Fyn kinase activity in AD could be contributed by FynT upregulation because FynT has been shown to exhibit enhanced kinase activity as compared to FynB (Davidson et al., 1994, Brignatz et al., 2009).

An independent finding showed that the differential expression of Fyn in AD brain was only observed in brain tissue processed with fractionation, showing increased expression in insoluble fraction and decreased expression in soluble fraction (How et al, 2005). We observed that specific upregulation of FynT isoform in NFT-bearing neurons, suggesting that FynT is likely to be found in the insoluble fractions of AD brain.

3.5.2 FynT in association with tau phosphorylation and NFT formation

A major finding this chapter is the neuronal FynT induction in association with tau pathology in AD. In consistency with a previous report showing phosphorylation of Fyn-catalysed Tyr18 on tau was localized in NFT but not neuropil threads (Lee, 2004), we also showed that FynT stained NFT but not neuropil threads (Figure 3.8). Hence, it is conceivable that FynT may be the

major modulator of tau hyper-phosphorylation in addition to direct phosphorylation at Tyr18, as pTau immunoreactivities (AT8 and Tyr18) colocalized exclusively with FynT, but not with adjacent neurons strongly staining for FynB. Furthermore, Bhaskar *et al.* (Bhaskar et al., 2005) also demonstrated that Fyn may bind tau isoforms with different affinities, suggesting the possibility of complex interactions between Fyn and tau isoforms. An independent study demonstrated that Tyr18 phosphorylation is important in mediating Fyn-tau interaction and influences the cellular trafficking of tau to detergent-resistant membrane microdomains (Usardi et al., 2011), suggesting that Fyn may modulate tau solubility. However, whether the co-staining of FynT and phosphorylated tau may implicate their interaction and affect their cellular trafficking is unknown which warrant further investigation.

It has also been proposed that aberrant hyper-phosphorylated tau is closely associated with cell cycle re-entry in post-mitotic neurons which may account for a substantial fraction of neuronal loss in AD brain, and that the process involves the activation of three kinases including Fyn (Seward et al., 2013). Inhibition of Fyn kinase or mutation at the Fyn-catalysed Tyr18 on tau, were both able to block the BrdU uptake of primary neurons, suggesting that Fyn kinase activity could be essential for ectopic neuronal cell cycle re-entry (Seward et al., 2013). The demonstrated link between FynT expression and NFT-bearing neurons prompts us to postulate that FynT may modulate the ectopic cell cycle re-entry and subsequently lead to neuron degeneration.

Furthermore, whilst previous studies reported higher Fyn immunoreactivity in NFT-bearing neurons in AD (Shirazi and Wood, 1993, Lee, 2004, Ho et al.,

2005), our data now suggest that FynT is the predominant isoform associated with the NFT. Intriguingly, the increased FynT expression was accompanied by apparently weaker FynB immunoreactivity in the NFT-bearing neurons (Figure 3.9), suggesting that the upregulated FynT reflects a modulation of the alternative splicing machinery which favours the FynT isoform, and that this 'switching' to FynT may be associated with AD pathogenesis. Differential alternatively-spliced transcripts in human brains associated with aging and neurodegeneration including AD have been detected simultaneously with altered expression of various splicing regulators (Tollervey et al., 2011). Furthermore, aberrant tau exon 10 splicing found in some sporadic AD was associated with a dysregulation of alternative splicing (Glatz et al., 2006). In view of the close relationship between FynT and tau in NFT-bearing neurons, we speculate that during NFT formation, alternative splicing machinery may be activated to modulate tau exon 10 splicing, as well as Fyn exon 7 splicing to favour FynT expression.

3.5.3 FynT in association with reactive astrogliosis

Another important finding of this chapter relates to FynT and astrocyte activation. Astrocyte-mediated neuroinflammation responses have long been postulated to play a role in AD (Fuller et al., 2009, Steele and Robinson, 2012, Medeiros and LaFerla, 2013). In this study, we speculate that the increased FynT expression may be partly due to higher numbers of reactive astrocytes in the AD brain supported by significant positive correlation between FynT and astrocytic markers in our preliminary data. Furthermore, higher proportions of endogenous FynT expression were found in primary rat astrocytes and glioma cell lines as compared to primary rat neurons and neuroblastoma cell lines

(Figure 3.2). Additionally, while comparing the modulation of astrocytic FynT expression between AD and control prefrontal cortex, we observed that FynT immunoreactivity was clearly localized to the thickened processes and hypertrophic cytoplasm of activated astrocytes in the AD brain (in addition to NFT-bearing neurons), compared to only weak signals in the control sections. Given that astrogliosis is a hallmark of AD, where astrocytes increase in proliferation and size alongside with the elevation of genes expression (Eddleston and Mucke, 1993, Fuller et al., 2010), these results further supports our hypothesis that the upregulation of FynT expression in AD brain is associated with astrocyte activation.

3.6 Summary

This chapter provides evidence that isoform-specific upregulation of FynT may be independently associated with neurofibrillary degeneration and reactive astrogliosis in AD. Furthermore, alternative splicing of Fyn may be an important mechanism in disease pathogenesis or response. However, further studies are needed to elucidate the upstream signalling and molecular mechanisms underlying FynT modulation as well as the precise nature of its involvement in NFT formation and astrocyte activation.

CHAPTER 4-
Isoform-specific modulation of FynT tyrosine kinase expression in astrocytes under Aβ and TNFα treatment

CHAPTER 4- Isoform-specific modulation of FynT tyrosine kinase expression in astrocytes under Aβ and TNFα treatment

4.1 Background

In the previous chapter, it was demonstrated that FynT upregulation in AD was associated with tau pathology as well as reactive astrogliosis. In this chapter, we would like to recapitulate the abnormal induction of FynT expression in AD brain using an *in vitro* system, by exposing primary mixed cortical or astrocytic culture to pathological conditions associated with AD including Aβ and TNFα treatment and monitoring the changes in FynT and FynB expression.

4.2 Hypothesis

Pathological conditions of AD can specifically induce FynT expression in primary cortical cultures.

4.3 Experimental designs/ Approaches

1. To establish an *in vitro* system for studying effects of Aβ using primary rat mixed cortical cultures with $A\beta_{25-35}$ treatment. (See Results at 4.4.1 and 4.4.2).
2. To investigate FynT versus FynB tyrosine kinase modulation by Aβ treatment in primary rat mixed cortical cultures. (See Results at 4.4.3)
3. To determine whether FynT induction could be associated with increased number of astrocytes in primary rat mixed cortical cultures, the cultures were maintained in media with increasing FBS concentration and monitored for FynB and FynT expression. (See Results at 4.4.4)

4. To investigate FynT versus FynB tyrosine kinase modulation by Aβ and TNFα treatment in primary rat astrocyte cultures. (see Results at 4.4.5 and 4.4.6)
5. To determine the possible regulatory mechanisms of astrocytic FynT induction in TNFα. (see Results at 4.4.7)

4.4 Results

4.4.1 $A\beta_{25-35}$ exhibited a cytotoxic effect on primary rat mixed cortical culture

Aβ treatment is known to induce neuronal degeneration and activate astrocytes *in vitro* (Pike et al., 1992, Pike et al., 1994, Pike et al., 1996). $A\beta_{25-35}$, the toxic moiety of Aβ was used for treatment of primary neuronal culture (Kaminsky et al., 2010). An optimization experiment was performed on $A\beta_{25-35}$ -treated primary rat mixed cortical culture to determine the suitable concentration of $A\beta_{25-35}$ used for subsequent experiments, significant reduction in cell viability was observed at a concentration of 20 μM (ANOVA $p < 0.05$) and above for $A\beta_{25-35}$ peptide at the 48 h time point (Figure 4.1A). In contrast, the inverse peptide $A\beta_{35-25,}$ did not result in any significant reduction of cell viability even at 40 μM, indicating that the toxic effect of the short $A\beta_{25-35}$ was sequence specific. Visible disintegration of dendrites could also be observed in the presence of $A\beta_{25-35}$ (Figure 4.1B).

A

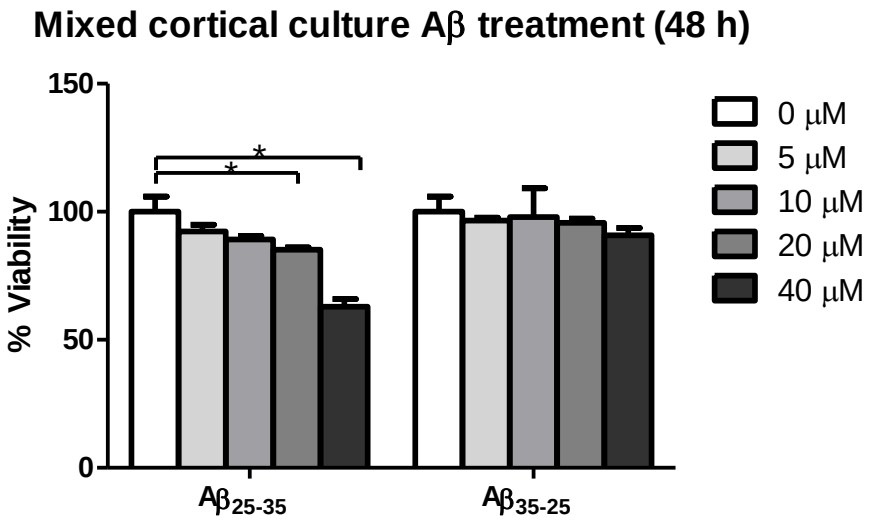

B

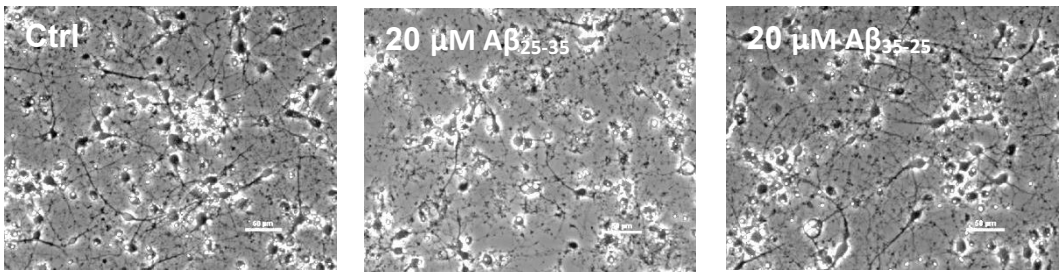

Figure 4.1 $A\beta_{25-35}$ exhibited cytotoxic effect on rat mixed cortical culture. **(A)** Cell viability upon Aβ treatment was determined using CCK-8 assay. Bar charts represent the percentage of cell viability which set the OD measurement of untreated control (0 μM) to 100%. Mixed cortical cultures were treated with 0, 5, 10, 20 and 40 μM $A\beta_{25-35}$ or $A\beta_{35-25}$ for 48 h. Values are mean ± SEM of five replicates. *Significantly different (one-way ANOVA with Dunnett's *post-hoc* test $p < 0.05$). **(B)** Phase contrast images of rat mixed cortical cultures without treatment (Ctrl), with 20 μM $A\beta_{25-35}$ or 20 μM $A\beta_{35-25}$ treatment were compared at 48 h. Scale bars = 50 μm.

4.4.2 $A\beta_{25-35}$ treatment modulated neuronal and astrocytic markers expression in primary rat mixed cortical culture

Expression levels of neuronal and astrocytic markers in a primary rat mixed cortical culture treated with $A\beta_{25-35}$ were measured using real-time RT-PCR. At 48 h, significant induction of astrocytic markers GLAST and glutamate transporter GLT1 (ANOVA $p<0.05$), as well as trends toward increased GFAP expression (ANOVA $p = 0.0858$) were observed after treatment with $A\beta_{25-35}$, but not with the peptide sequence control, $A\beta_{35-25}$ (Fig. 4.2), suggestive of Aβ-induced astrocyte activation. The inconsistency between the changes in the expression profile of these astrocytic markers could be attributed to the heterogeneity of astrocytes in these mixed cultures. Different subtypes of astrocytes are known to express varying levels of the astrocytic markers and therefore may respond differently upon treatment with Aβ (Walz and Lang, 1998, Perego et al., 2000, Abe and Misawa, 2003, Scimemi et al., 2013). On the other hand, $A\beta_{25-35}$, but not $A\beta_{35-25}$ reduced expression of neuronal marker tubulin β3 (TUBB3, ANOVA $p < 0.05$), with trends toward decreases in RBFOX3 (NeuN gene, ANOVA $p = 0.0618$) and microtubule-associated protein 2 (MAP2, ANOVA $p = 0.0976$, see Fig. 4.2), suggestive of Aβ-induced neurotoxic effects.

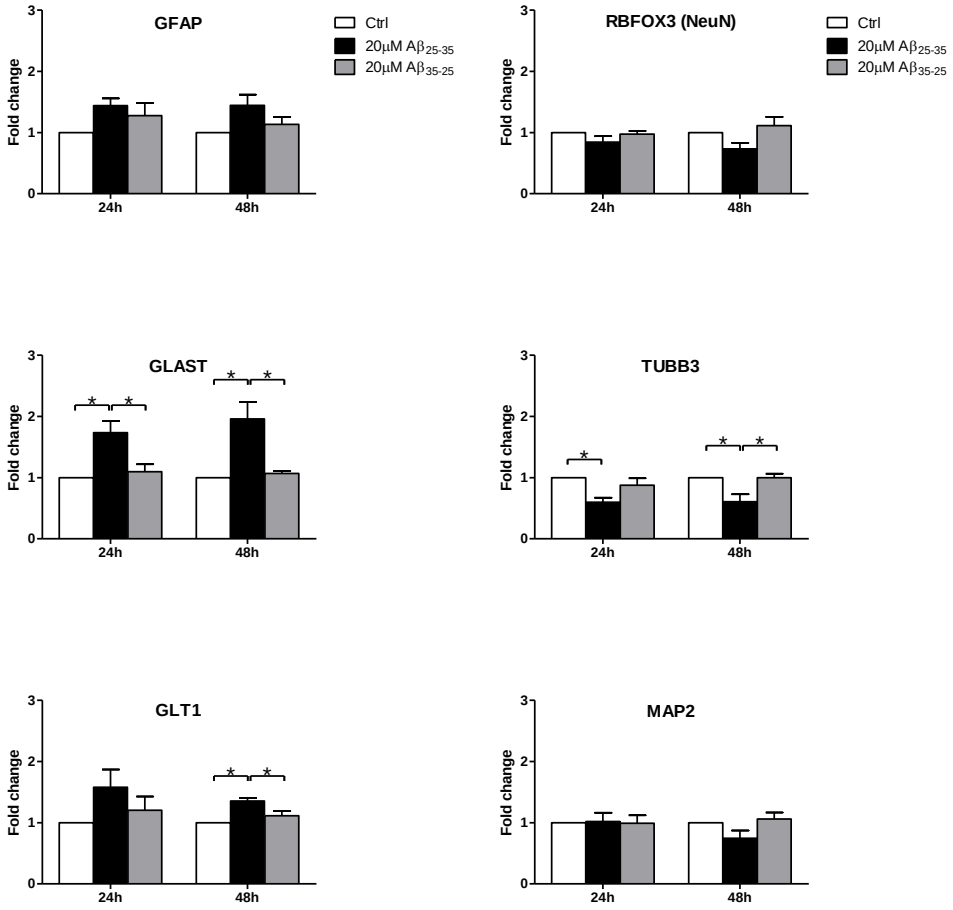

Figure 4.2 Gene expression changes in $A\beta_{25-35}$-treated primary rat mixed cortical culture. Primary rat mixed cortical cultures were treated with 20 μM $A\beta_{25-35}$ or $A\beta_{35-25}$ or without treatment (Ctrl) for 24 h and 48 h and monitored for gene expression using real-time RT-PCR for astrocytic markers GFAP, GLAST and GLT1, and neuronal markers RBFOX3/NeuN, TUBB3 and MAP2. Fold change was calculated by setting the normalized relative signal intensity of Ctrl as 1. Values are mean ± SEM of 3-4 independent experiments. *Significantly different (one-way ANOVA with Bonferroni's *post-hoc* test $p < 0.05$).

4.4.3 $A\beta_{25-35}$-induced astrocytic FynT induction in primary rat mixed cortical culture

Interestingly, $A\beta_{25-35}$ treatment selectively upregulated FynT expression while FynB remained unchanged (Figure 4.3A). The experiment was repeated once using full length $A\beta_{1-42}$ and $A\beta_{42-1}$ control peptides with comparable results (data not shown). Similarly, IF staining of $A\beta_{25-35}$-treated primary mixed cortical culture showed pronounced FynT immunoreactivity with no detectable changes in FynB immunoreactivity (Figure 4.3B). Furthermore, quantitative image analyses showed increased FynT mean fluorescence intensity in $A\beta_{25-35}$-treated primary mixed culture compared to untreated control (Figure 4.3C).

In order to identify the cell types associated with induced FynT immunoreactivity after $A\beta_{25-35}$ treatment, FynT was co-stained separately with astrocytic and neuronal markers. Pronounced FynT immunoreactivity was localized to GFAP-positive astrocytes after $A\beta_{25-35}$ treatment, showing clearly discernible yellow signals in the merged image (Figure 4.4A, top right panel). In contrast, image captured using fixed microscope and camera settings demonstrated that only weak FynT immunoreactivity was detected in GFAP-positive cells treated with control peptide $A\beta_{35-25}$ treatment (Figure 4.4A, bottom right panel), suggesting that $A\beta_{25-35}$ was able to induce FynT expression in astrocytes. For neurons, MAP2 was selected as a marker as it is a neuron-specific cytoskeletal protein highly enriched in dendritic processes (Kosik and Finch, 1987). Under control peptide $A\beta_{35-25}$ treatment, the outline of the neurons including cell bodies and elongated processes can be clearly labelled by MAP2 (Figure 4.4B, bottom panels). Upon $A\beta_{25-35}$ treatment,

reductions in neuronal processes were evident as MAP2 staining was confined to cell bodies (Figure 4.4B, top panels), suggestive of an Aβ-induced neuritic dystrophy (Pike et al., 1992). Interestingly, FynT immunoreactivity did not seem to be modulated by $A\beta_{25-35}$ treatment in MAP2-positive cells (Figure 4.4B, white arrows in top panel), suggesting that under *in vitro* conditions, the induction of FynT expression by $A\beta_{25-35}$ was localized to astrocytes.

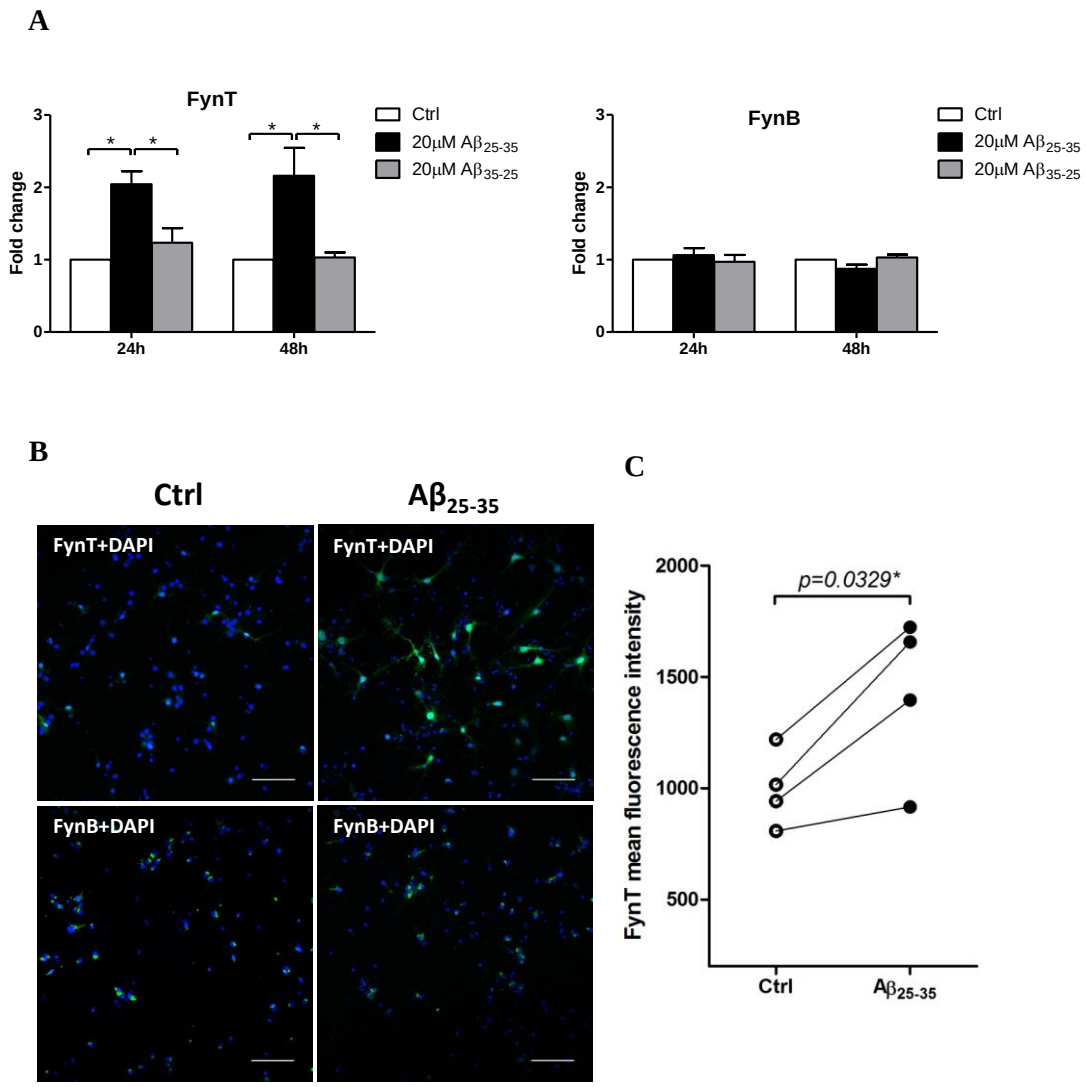

Figure 4.3 Specific upregulation of FynT in $A\beta_{25-35}$-treated primary rat mixed cortical culture. Primary rat mixed cortical cultures were treated with 20 μM $A\beta_{25-35}$ or $A\beta_{35-25}$ or without treatment (Ctrl) for 24 and 48 h and monitored for FynT and FynB expression. **(A)** Real-time RT-PCR results as represented by fold change, was calculated by setting the normalized relative signal intensity of Ctrl as 1. Values are mean ± SEM of 3-4 independent experiments. *Significantly different (one-way ANOVA with Bonferroni's *post-hoc* test $p < 0.05$). **(B)** At 48h, Ctrl and $A\beta_{25-35}$ treated primary rat mixed cortical cultures were stained for FynT or FynB (green). Cell nuclei stained by DAPI (blue) were shown to ensure similar cellular content in each tissue section. Scale bars = 100 μm. **(C)** The paired dot plot presents the mean of FynT mean fluorescence intensity in $A\beta_{25-35}$-treated primary culture and vesicle treatment control in 4 independent experiment (*p=0.0329*, Student's paired *t*-test). The mean value in each experiment is calculated by the FynT mean fluorescence intensity in three representative images.

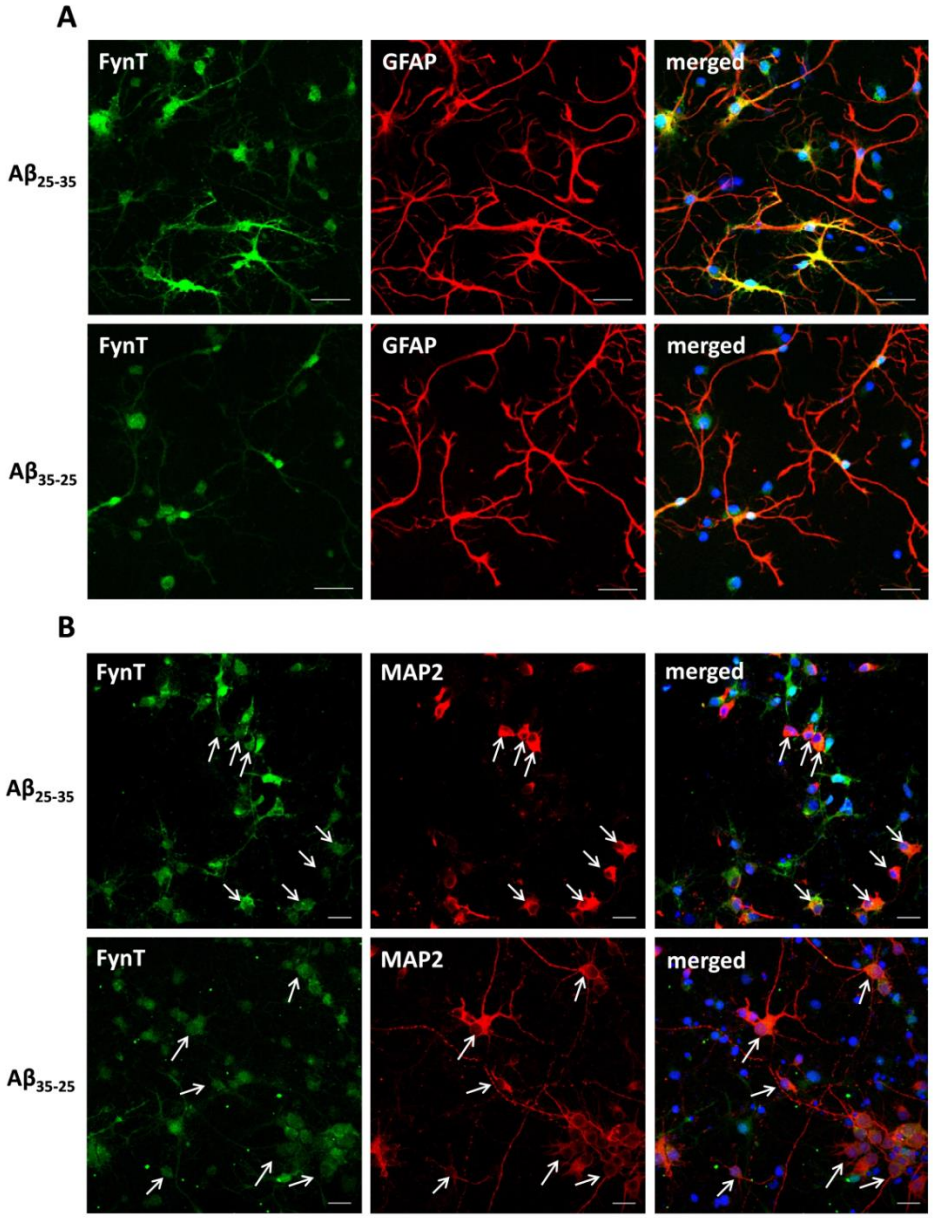

Figure 4.4 Increased FynT immunoreactivity in $A\beta_{25-35}$-treated astrocytes but not neurons. Primary rat mixed cortical cultures were treated with 20 μM $A\beta_{25-35}$ or $A\beta_{35-25}$ for 48 h. Representative double IF staining of treated cells was demonstrated for FynT (green) and **(A)** astrocytic marker, GFAP (red) or **(B)** neuronal marker, MAP2 (red). Cell nuclei stained by DAPI (blue) were shown in the merged images. White arrows indicated selected neurons. Scale bars = 20 μm.

4.4.4 FynT expression significantly and positively correlated with glial markers in primary mixed cortical culture

To determine whether FynT induction under treatment could be associated with increased astrocyte population in the mixed cortical culture, we maintained the culture in the presence of AraC mitotic inhibitor to inhibit astrocyte propagation, as well as in media with increasing FBS concentration to promote astrocyte propagation and monitored for FynB and FynT expression. Three batches of DIV 7-10 mixed cortical cultures were investigated. Immunofluorescence was performed using anti-GFAP and anti-NeuN antibody to qualitatively detect the relative amount of astrocytes and neurons, respectively in the mixed rat cortical cultures containing AraC or different FBS concentrations (Figure 4.5A). IF staining revealed that 1 μM AraC could effectively inhibit astrocyte propagation, as shown by the absence of GFAP immunoreactivity compared with other culture conditions without AraC (Figure 4.5A). The addition of FBS in culture increased amount of astrocytes as shown by the corresponding elevation of GFAP immunoreactivity (Figure 4.5A).

In line with the IF data, real-time RT-PCR data showed that in the absence of AraC, increased expression of astrocytic markers GFAP and GLAST were detected correspondingly with the increase of FBS concentration in the cultures, with the greatest increment at 1% FBS (Figure 4.5B). Similar trend of expression was also found for microglial marker CD11B. On the other hand, neuronal marker RBFOX3/NeuN appeared to decrease in the presence of FBS, with the lowest expression at 1% FBS (Figure 4.5B).

Interestingly, a corresponding increment of FynT expression was also detected in mixed cultures maintaining in increasing FBS concentration in the absence of AraC, with the greatest increment at 1% FBS (Figure 4.5B). On the other hand, FynB expression remained unchanged in all culture conditions. A similar trend of expression between FynT and glial markers prompt us to speculate that increase of FynT expression may be associated with the increased propagation of astrocyte or microglia population in the mixed culture in response to FBS. We thus carried out correlation analysis for FynT and cellular markers to access the possible link. Note that correlation analysis was performed in a batch wise manner due to variability across the different batches of cortical cultures, seen in Table 4.1. Significant positive correlation of FynT with both astrocytic markers GFAP and GLAST (Pearson correlation coefficient (r) 0.6795 to 0.7886, $p \leq 0.01$) was consistently found in all three batches of culture. We also identified positive correlation between FynT and microglial marker CD11B in two batches of the culture (Pearson correlation coefficient (r) between 0.5709 to 0.7322, $p < 0.01$). As for neuronal marker RBFOX3/NeuN, significant negative correlation of FynT with RBFOX3/NeuN was found in one of the batches (Pearson correlation coefficient (r) -0.4691, 0.0369 $p < 0.05$).

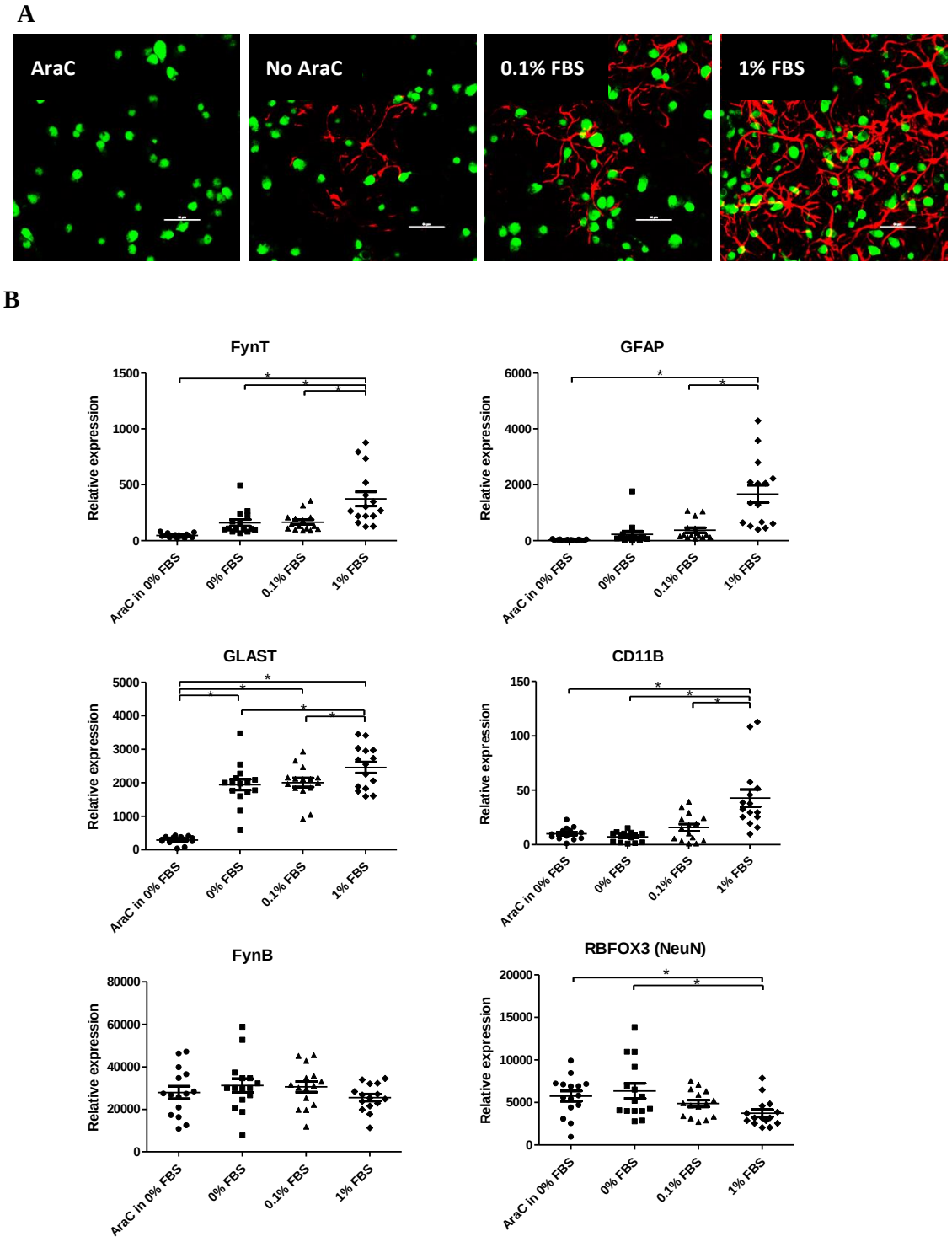

Figure 4.5 Increased astrocyte propagation concomitant with induction of glial markers and FynT expression in primary rat mixed cortical culture. **(A)** Double IF staining revealed that increased GFAP (red) positive astrocytic population concomitant with increase serum concentration (0, 0.1 and 1% FBS) in primary rat mixed cortical cultures and decreased in the presence of 1 μM AraC (mitotic inhibitor), whereas no obvious changes of NeuN (green)

positive population under these conditions. Scale bars =50 µm. **(B)** Real-time RT-PCR determined expression of astrocytic markers (GFAP and GLAST), microglial marker (CD11B), and neuronal marker (RBFOX3/NeuN), as well as FynT and FynB in four culture conditions mentioned in (A), in three independent batches of DIV 7-10 cortical cultures. Horizontal lines with error bars in dot plots indicate mean and SEM. *Significantly different (one-way ANOVA with Bonferroni's *post-hoc* test $p < 0.05$).

Table 4.1 FynT expression significantly and positively correlated with astrocytic and microglial markers in primary rat mixed cortical cultures as determined using Pearson's correlation

		Batch 1		Batch 2		Batch 3	
	Specific Cellular Marker	Pearson correlation coefficient (r)	P-value	Pearson correlation coefficient (r)	P-value	Pearson correlation coefficient (r)	P-value
GFAP	Astrocyte	0.6795*	0.0010	0.7886*	< 0.0001	0.7418*	0.0002
GLAST	Astrocyte	0.7000*	0.0006	0.7584*	0.0001	0.7494*	0.0001
CD11B	Microglia	0.1715	0.4696	0.5709*	0.0086	0.7322*	0.0002
RBFOX3 (NeuN)	Neuron	-0.07265	0.7608	-0.2645	0.2597	-0.4691*	0.0369

* indicates significant correlation with FynT expression

4.4.5 $A\beta_{25-35}$ may not act directly on astrocytes to induce FynT expression

As seen earlier (see 4.4.3), FynT induction in primary rat mixed cortical culture by $A\beta_{25-35}$ treatment was found to be localized in astrocytes but not in neurons (Figure 4.4). In this study, we would like to further validate the Aβ effects on astrocytic FynT induction using relatively pure primary rat astrocyte cultures (more than 97% purity, determined by GFAP-positive cells). We observed no significant changes of FynT expression in the astrocyte culture treated with $A\beta_{25-35}$ over 24 h and 48 h, whereas FynB appeared to be slightly increased after $A\beta_{25-35}$, although the increase was also not significant (Figure 4.6). We have performed independent batches of experiment and confirmed the findings. Our findings suggested that $A\beta_{25-35}$ may not act directly on astrocytes to induce FynT expression.

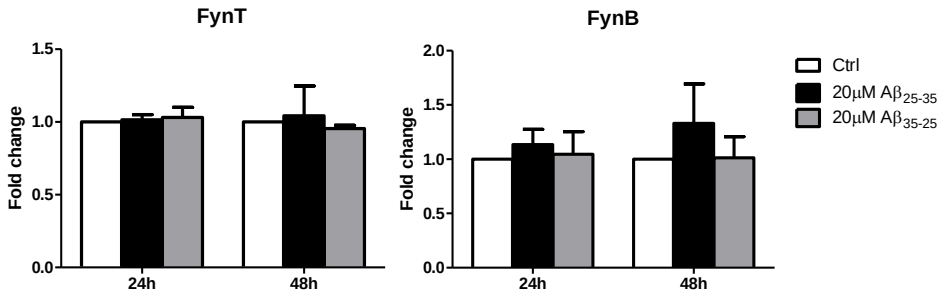

Figure 4.6 $A\beta_{25-35}$ may not act directly on astrocytes to induce FynT expression. Primary rat astrocyte cultures were treated with 20 μM $A\beta_{25-35}$ or $A\beta_{35-25}$ or without treatment (Ctrl) for 24 and 48 h and monitored for FynT and FynB expression. Real-time RT-PCR results as represented by fold change, was calculated by setting the normalized relative signal intensity of Ctrl as 1. Values are mean ± SEM of 3 independent experiments.

4.4.6 Selective induction of FynT expression in astrocytes by TNFα treatment

TNFα has been shown to be associated with the pathogenesis of AD. It is known to stimulate glial response resulting in the activation of pro-inflammation pathways and secretion of inflammatory mediators, which plays an important role during neuroinflammation (Olmos and Llado, 2014). In this study, primary rat astrocyte cultures were treated with TNFα and gene expression of both FynT and FynB were monitored from 1 h up to 72 h. Interestingly, we observed that TNFα significantly induced FynT expression at 24 h and maintained the elevation at later time points, whereas no significant changes were detected for FynB expression at all time-points (Figure 4.7).

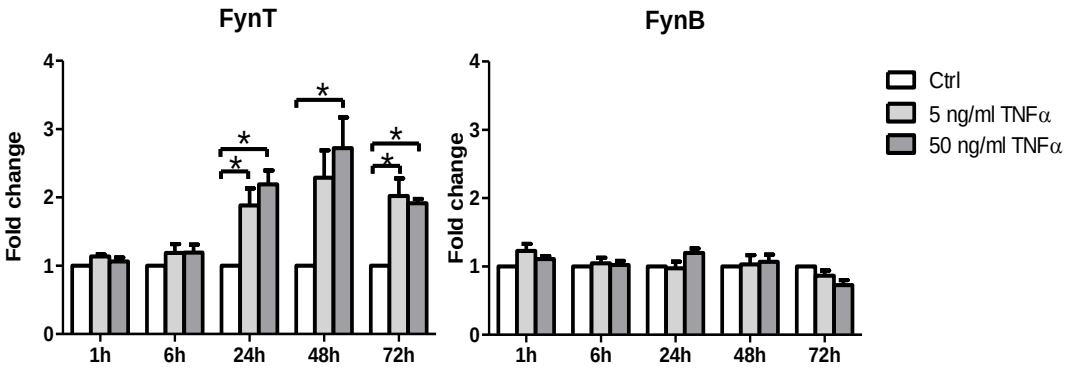

Figure 4.7 Selective induction of FynT expression in astrocytes by TNFα treatment. Primary rat astrocyte cultures were treated with 5 or 50 ng/ml of TNFα or without treatment (Ctrl) for various time points (1 h, 6 h, 24 h, 48 h and 72 h) and monitored for gene expression using real-time RT-PCR for FynT and FynB. Fold change was calculated by setting the normalized relative signal intensity of Ctrl as 1. Values are mean ± SEM of 3 independent experiments. *Significantly different (one-way ANOVA with Bonferroni's *post-hoc* test $p < 0.05$).

4.4.7 TNFα-induced alternative expression of FynT and FynB in astrocytes may be dependent on *de novo* protein synthesis

We would like to explore the possible mechanism underlying alternative expression of FynT and FynB under TNFα treatment. We identified that cycloheximide (CHX) was able to completely block TNFα-induced FynT mRNA expression (Figure 4.8), suggesting that *de novo* protein synthesis was required for FynT mRNA induction under TNFα treatment. Furthermore, TNFα-induced inflammatory cytokines gene expression of IL1B and IL6 were also attenuated by CHX treatment (Figure 4.8). Most interestingly, the inhibition of FynT expression by CHX was accompanied by the induction of FynB expression, in a dose-dependent manner (Figure 4.8).

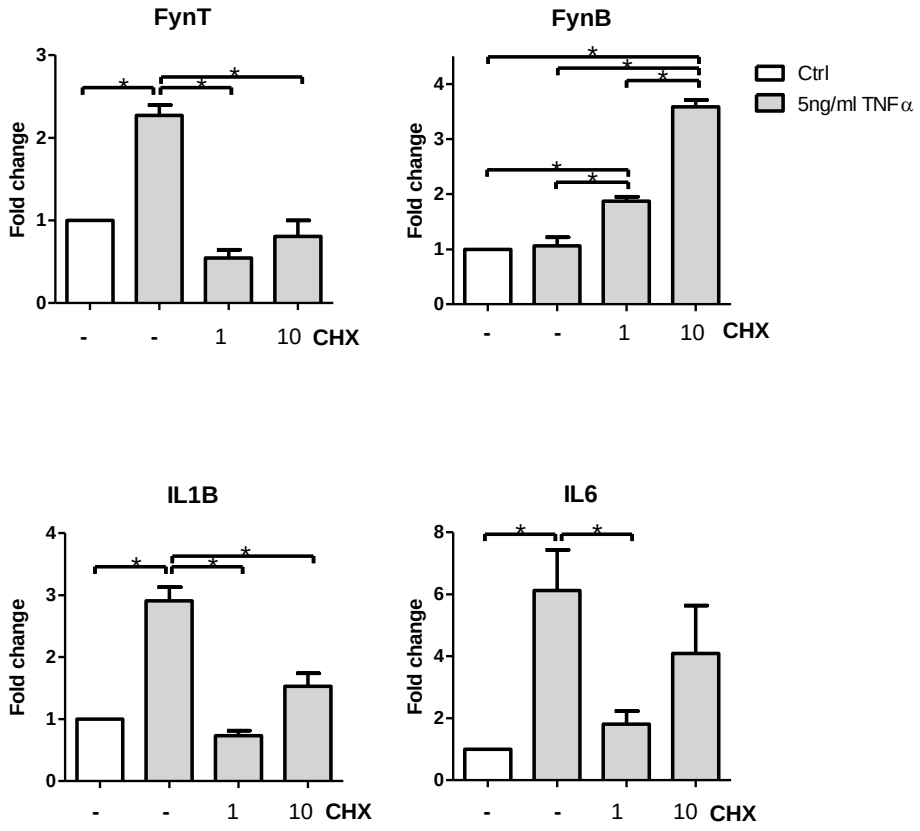

Figure 4.8 TNFα-induced alternative expression of FynT and FynB, as well as pro-inflammatory cytokines expression were modulated by *de novo* protein synthesis. Rat primary astrocytes were pre-incubated with 1 or 10 μg/ml of Cycloheximide (CHX) or vehicle control for 2 h, followed by additional of 5 ng/ml of TNFα treatment for 24 h. Gene expression was monitored using real-time RT-PCR for FynT, FynB, IL1B and IL6. Fold change was calculated by setting the normalized relative signal intensity of Ctrl as 1. Values are mean ± SEM of 3 independent experiments. *Significantly different (one-way ANOVA with Bonferroni's *post-hoc* test $p < 0.05$).

4.5 Discussion

4.5.1 Limitations of using *in vitro* approach to recapitulate AD-associated neuronal FynT induction.

Accumulating evidence suggests that Fyn is a crucial player mediating Aβ-induced neuronal dysfunction (Ittner, 2010, Roberson, 2011, Yang, 2011, Um et al., 2012, Wang et al., 2013a, Xia and Gotz, 2014). Moreover, results from the previous chapter revealed that NFT-bearing neurons displayed high FynT immunoreactivity concomitant with reduced FynB immunoreactivity, suggesting an induction of alternative splicing of Fyn that favoured FynT transcript in these neurons. We aimed to recapitulate AD-associated neuronal FynT induction through treating neuron-enriched primary cortical culture with Aβ. However, when primary cortical culture was treated with $A\beta_{25\text{-}35,}$ no changes of FynB and FynT expression in neurons was observed. It can be speculated that this *in vitro* approach may not be able to recapitulate the induction of alternative splicing machinery and/or NFT formation as found in the AD brain. Alternatively, the negative results may be due to differences in the nature or extent of Fyn isoform regulation by alternative splicing between human and rodent.

4.5.2 $A\beta_{25\text{-}35}$ induced astrocytic FynT induction in mixed cortical culture but not in astrocyte-enriched culture.

To the best of our knowledge, no study has been done on determining the role of Fyn in astrocytic activation in association with AD. We identified that Aβ-induced FynT induction was localized in astrocytes in mixed cortical culture. However, Aβ may not act directly on astrocytes to induce FynT expression because we failed to detect FynT induction in astrocyte-enriched cultures

under the same Aβ treatment. There is abundant literature on how astrocytes modulate neuronal events but little is known about the impacts of neurons on co-cultured astrocytes (Wiedemann, 2009). For example, the expression of glutamate transporter GLT1 in astrocytes is dependent on axonal interactions (Yang et al., 2009). In addition, *in vitro* astrocytes co-cultured with neurons possess process-bearing morphology that is more characteristic of astrocytes *in vivo* and hence can be considered more differentiated (Swanson et al., 1997). Taken together, these findings suggest to us that cell-cell interaction between neurons and astrocytes can possibly affect Aβ-induced responses in astrocytes.

With regards to why Aβ could induced FynT expression in astrocytes of mixed cortical cultures, the etiologic links remain unclear, and may involve both pathogenic (e.g., neurotoxicity) and adaptive (e.g., response to oxidative stress) components. Nevertheless, the consistent observations of FynT association with astrocytic markers in our preliminary data (Table 1.2) suggest that up-regulation of FynT expression in AD may be associated in part with astrocytic activation which could likely be more evident in the mixed culture. Given that astrocytes have been shown to participate in cerebral innate immunity and inflammatory responses (Aschner, 1998, Farina et al., 2007), and that studies of FynT-specific knockout mice have demonstrated the crucial role of FynT in modulating the immune system (Cooke et al., 1991, Davidson et al., 2004, Chaimowitz et al., 2013), it can be postulated that the modulation of FynT expression may be associated with astrocyte-mediated neuroinflammatory responses in AD.

4.5.3 FynT expression significantly and positively correlated with astrocyte markers in primary mixed cortical culture

Increasing serum concentration is known to induce astrocyte proliferation and GFAP expression in embryonic and neonatal cortical culture (Sakai et al., 1990, Vergeli et al., 1995). Our *in vitro* approach made use of AraC and FBS to inhibit and promote astrocyte propagation, respectively in mixed cortical cultures, which allowed us to determine the significant correlation between FynT expression and astrocytic markers GFAP and GLAST in all batches of cortical cultures (Table 4.1). This observation was in line with our first hypothesis from chapter 3 that FynT upregulation is associated with astrogliosis in AD where astrocytes also increase in numbers and GFAP expression, conceding that the *in vitro* observation here is related to developmental regulation while post-mortem association was linked to pathological reactions. Nevertheless, all findings point towards that astrocytes do contribute to significant expression of FynT in the brain.

A recent paper (Panicker et al., 2015) has reported that microglia expressed significantly more Fyn as compared to astrocytes using Western blot analyses of total Fyn levels, with no mention of the predominant Fyn isoform. Therefore, correlation analysis was also performed to look at the association of FynT with microglia marker CD11B. Of note, FynT was found to have positive significant correlation in only two batches of the mixed cortical cultures (Table 4.1). We speculate that the recovery of microglia, the minority cell type in embryonic cortex, may varied greatly between different batches of mixed cortical cultures preparation, thus resulted in inconsistency. It is difficult to conclude at this point whether microglial expression of FynT could

also contribute significantly to the overall increase in FynT expression in the mixed cortical culture since they constitute much lesser proportion of the cells as compared to astrocytes in brain and in culture (Hansson, 1984, Perry, 1998).

4.5.4 TNFα-induced alternative expression of FynT and FynB in astrocytes may be dependent on *de novo* protein synthesis.

Astrocytes are known to mediate innate immunity in the CNS and contribute to neuroinflammation. Hence, primary astrocyte cultures were treated with TNFα over a course of three days. Strikingly, specific transcriptional induction of FynT but not FynB was detected at 24 h and beyond but not at earlier time points (Figure 4.7). In line with our findings, Fyn expression was also reported to be induced by prolonged TNFα or lipopolysaccharide (LPS) stimulation in microglia alongside increased Fyn kinase activity although specific isoforms expression was not investigated (Panicker et al., 2015). Furthermore, the same group also found that Fyn-knockout mice as well as Fyn knockdown microglia culture exhibited diminished inflammatory cytokines expression when stimulated with both TNFα and LPS, ascertaining Fyn involvement in neuroinflammation (Panicker et al., 2015).

TNFα is known to orchestrate gene expression in a time dependent manner and can be classified as "early", "middle" and "late" response genes (Tian et al., 2005). "Early" genes, generally consisting of cytokines encoding genes, are induced within an hour of stimulation, "middle" genes are genes with expression profiles peaking at three hours, while "late" genes consisting of cell surface receptors, adhesion molecules and signal adapters that peak at six hours or beyond. Based on Figure 4.7, FynT induction by TNFα was detected only after 6 h, and maintained up to 3 days of treatment, suggesting that it is a

"late" response gene likely to function as a signalling molecule (Tian et al., 2005). Specific induction of FynT maintained after prolonged stimulation of TNFα suggests that FynT might possess a role in chronic neuroinflammation. Unlike "early" response genes, many "late" response genes induced by inflammatory stimuli require *de novo* synthesis of proteins involving in "late" genes transcription, which explains the temporal delay in their induction (Weinmann et al., 1999, Ramirez-Carrozzi et al., 2006, Tullai et al., 2007). Consistently, we observed that CHX was able to inhibit or attenuate FynT, as well as IL1B and IL6 expression induced by TNFα (Figure 4.8).

This compelling observation of the reduction of FynT with concurrent induction of FynB suggests that CHX did not only inhibit *de novo* protein synthesis triggered by TNFα but also influenced the modulation of the alternative splicing machinery which apparently favoured the FynB isoform. To determine whether CHX on its own would also influence FynT and FynB basal expression without TNFα stimulation, rat cortical astrocytes were treated with CHX for 24 hours and FynT/FynB expression was determined with quantitative RT-PCR. Interestingly, CHX similarly lowered basal FynT while elevating FynB expression (data not shown). Protein synthesis inhibitors have been reported to regulate alternative splicing of a number of genes including Bcl-x, CD45, TRPM-2 (Kimura and Yamamoto, 1996, Lynch and Weiss, 2000, Boon-Unge et al., 2007), however, whether alteration of Fyn splicing by CHX is solely dependent on its *de novo* protein synthesis inhibition property or by other mechanisms of action is still not clear. Further experiments using other protein synthesis inhibitors (e.g. puromycin), is required to validate this.

4.6 Summary

Using *in vitro* approaches, by treating mixed cortical culture with Aβ, or exposing astrocyte-enriched culture to TNFα, we were able to recapitulate astrocytic FynT induction in associated with pathogenesis of AD. Astrocytes have been known to mediate neuroinflammation, which has been one of the hallmarks of AD. The strong correlation between FynT and astrocytic markers, as well as the late FynT induction by TNFα treatment prompt us to speculate that FynT may play a role in chronic neuroinflammatory response in astrocytes.

CHAPTER 5-
The functional role of FynT tyrosine kinase in modulating TNFα-induced inflammatory response in astrocytes

CHAPTER 5- The functional role of FynT tyrosine kinase in modulating TNFα-induced inflammatory response in astrocytes

5.1 Background

We observed FynT induction in association with reactive astrogliosis in post-mortem AD brains (Chapter 3). Furthermore, TNFα-induced FynT expression in astrocytes at the late phase was likely to be associated with chronic inflammatory response (Chapter 4). Fyn is well recognized as a signalling molecule in various signalling pathways, including modulation of inflammatory markers expression (Davidson et al., 1994, Resh, 1998, Picard et al., 2004, Rajasekaran et al., 2013, Panicker et al., 2015). In this study, we would like to use recombinant approach to study whether FynT kinase activity might have a role in modulating inflammatory markers expression in response to TNFα stimulation in astrocytes.

5.2 Hypothesis

FynT kinase activity may modulate inflammatory responses at the late phase of TNFα treatment in astrocytes.

5.3 Experimental designs/ Approaches

1. To generate immortalized normal human astrocyte (iNHA) clones stably expressing FynT mutants of kinase constitutively active (CA) or kinase dead (KD) for studying the role of FynT tyrosine kinase activity in modulating TNFα-induced expression and secretion profiles of inflammatory markers, as determined by real-time RT-PCR and multiplex immunoassays. (See Results at 5.4.1 to 5.4.3)

2. To validate FynT kinase activity in facilitating TNFα-induced inflammatory responses at the late phase, iNHA FynT clones were treated with either PP2 tyrosine kinase inhibitor or specific DsiRNAs for silencing FynT and monitored for the attenuation of TNFα-induced inflammatory responses. (See Results at 5.4.4 and 5.4.5)
3. To determine whether FynT kinase activity modulates TNFα-induced NF-κB signalling by employing luciferase-based genetic reporter assay and Western blot analyses. (See Results at 5.4.6)

5.4 Results

5.4.1 FynT kinase activity may facilitate TNFα-induced biphasic induction of pro-inflammatory cytokines expression at the late phase

Selective FynT induction was detected in astrocytes at the late phase of TNFα treatment (Figure 4.7). In order to determine the functional role of FynT tyrosine kinase activity in modulating TNFα signalling, we generated immortalized normal human astrocytes (iNHA) clones that stably expressed FynT-wild type (WT), FynT mutants of kinase constitutively active (CA) or kinase dominant negative/ kinase dead (KD), as well as empty vector (EV), and compared their responses to TNFα treatment. As shown in Figure 5.1, positive immunoreactivities of Tyr-416 antibodies were detected solely in representative FynT-WT and FynT-CA clones that exhibited autophosphorylation of tyrosine 417, but not in representative FynT-KD and EV clones which were devoid of ectopic FynT kinase activity.

TNFα is a known strong activator of NF-κB signalling which mediates the transcription of a vast array of proteins involved in inflammatory response (Lawrence, 2009). First, we investigated TNFα-induced inflammatory responses in parental iNHA cells, using high and low concentrations of TNFα for treatment and monitored the mRNA expression profiles of IL1B and IL6 pro-inflammatory cytokines from early time points (as short as 15 min) to 3 days. Consistent with reported findings, TNFα treatment stimulated IL1B and IL6 induction at the early time points, which peaked at 6h and 1h post-treatment, respectively (Figure 5.2). However, we observed that only higher concentrations of TNFα (50, 100 ng/ml) treatment were able to exhibit biphasic induction of IL1B and IL6 expression, with the late phase induction

detected at day 3 post-treatment (Figure 5.2). Subsequent studies were performed by treating the iNHA clones with 50 ng/ml TNFα.

When comparing TNFα-induced pro-inflammatory responses between the iNHA clones, FynT-CA clone demonstrated greatest induction of IL1B and IL6 expression at the late phase (red line in Figure 5.3A), as compared to basal induction found in EV and FynT-KD clones (green and blue lines in Figure 5.3A). In contrast, there were no obvious differences in the induction of IL1B and IL6 at the early phase between the iNHA clones (Figure 5.3A), suggesting that FynT kinase activity may facilitate IL1B and IL6 induction only at the late phase of TNFα treatment. Using independent batches of TNFα treatment, we confirmed that FynT-CA clone demonstrated significantly higher fold change for IL1B and IL6 induction as compared to EV and FynT-KD clone (Figure 5.3B).

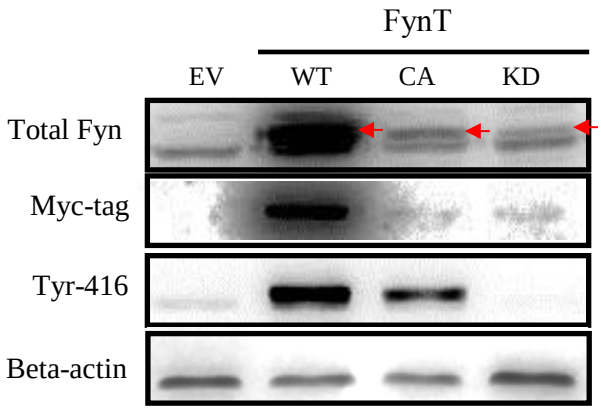

Figure 5.1 Establishment and characterization of iNHA clones that stably expressed empty vector (EV), FynT-wild type (WT), FynT mutants of constitutively active (CA) or kinase dead (KD). Exogenous expression of the Myc-FLAG tagged FynT transgenes were detected by total Fyn antibody (red arrows) and anti-Myc-tag antibody in representative clones. Autophosphorylation of tyrosine-417 corresponding to FynT kinase activity was determined by immunoreactivity of Tyr-416. β-actin was served as an endogenous loading control.

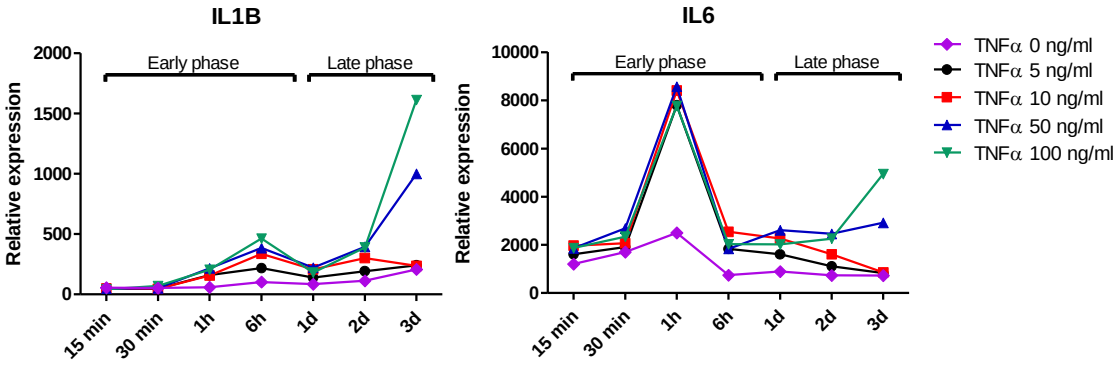

Figure 5.2 iNHA exhibited biphasic induction of pro-inflammatory cytokines expression under TNFα treatment. iNHA treated with 0, 5, 10, 50 and 100 ng/ml TNFα were monitored for IL1B and IL6 mRNA expression at early time points (15 min, 30 min, 1 h, 6 h) and late time points (1 day, 2 day and 3 day) using real-time RT-PCR. Relative expressions of genes were normalized by geometric means of housekeeping genes. This was a representative data of two independent studies.

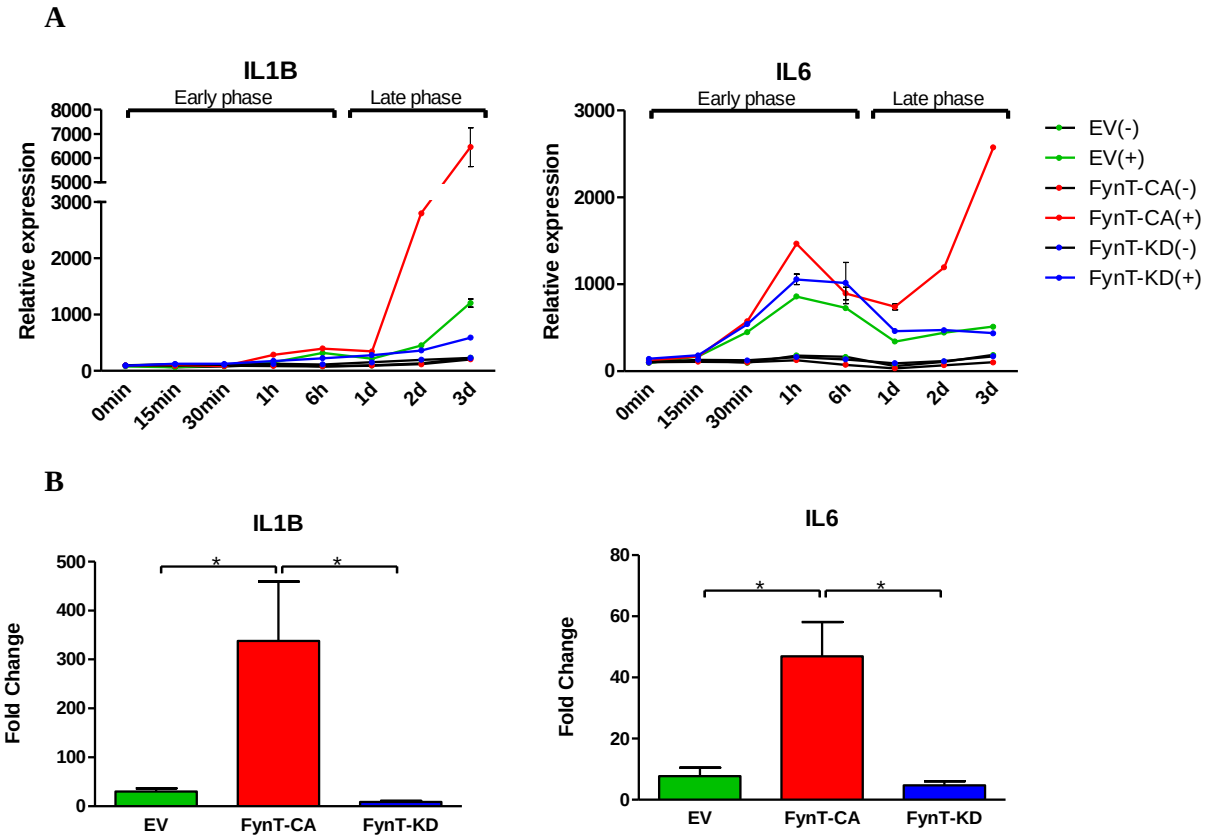

Figure 5.3 FynT kinase activity may facilitate TNFα-induced biphasic induction of pro-inflammatory cytokines expression at the late phase. (A) iNHA clones stably expressing empty vector (EV, green) or FynT mutants of constitutively active (FynT-CA, red) or kinase dead (FynT-KD, blue) were treated with 50 ng/ml TNFα (+, coloured lines) or without TNFα (-, black lines) and monitored for IL1B and IL6 mRNA expression at early time points (0min, 15min, 30min, 1h and 6h) and at late time points (1d, 2d and 3d) using real-time RT-PCR. Relative expressions of genes were normalized by the geometric means of housekeeping genes, setting the expression level of non-treated control of each clone at 0 min as 100. This was a representative data of two independent studies. **(B)** iNHA clones were treated with or without 50 ng/ml TNFα for 3 days and determined for IL1B and IL6 expression by real-time RT-PCR. Fold changes were shown as the means and ± SEM from seven independent experimental repeats. *Significantly different (one-way ANOVA with Bonferroni's *post-hoc* test p <0.05).

5.4.2 FynT tyrosine kinase activity facilitated TNFα-induced differential expression of inflammatory markers

To reinforce the observation that FynT tyrosine kinase activity facilitates TNFα-induced pro-inflammatory cytokines expression at the late phase, EV control, FynT-WT, FynT-CA and FynT-KD clones were treated with or without TNFα for 3 days and subjected to expression profiles of a panel of 14 inflammatory markers using Biomark HD system's high-throughput real-time RT-PCR. The inflammatory markers investigated could be broadly categorized into pro-inflammatory chemokines (CCL2, CCL5, CCL7, CXCL10, CXCL12, IL8), pro-inflammatory cytokines (CSF2, CSF3, IL1B, IL6, IL23), anti-inflammatory cytokines (IL1ra, LIF) and TNFα receptor, TNFR1 (Quan et al., 2003, Klein, 2004, Knapp et al., 2004, Pan et al., 2008, Soria and Ben-Baruch, 2008, Thompson and Van Eldik, 2009, Timotijevic et al., 2012, Vom Berg et al., 2012, Ramesh et al., 2013, Shiomi and Usui, 2015). Of note, some of these inflammatory markers are known to exhibit divergent pro- as well as anti-inflammatory functions depending on different cell types and the state of disease progression (e.g. CXCL12, CSF3, IL6, LIF) (Knight, 2001, Knapp et al., 2004, Scheller et al., 2011, Timotijevic et al., 2012).

Using Principal component analysis (PCA), the variation of TNFα-induced differentially expressed inflammatory markers in iNHA clones with different FynT kinase activity could be clearly visualized in a 3D scatter plot, allowing the clones with distinct expression profiles to be identified easily. In Figure 5.4A, the PCA 3D scatter plot showed to account for 81% of the variation in the dataset. Most of the untreated clones (spheres) were visibly clustered together and well separated from TNFα-treated clones (cubes), suggesting a

general observation of TNFα-induced differential expression of inflammatory markers (Figure 5.4A). Furthermore, we observed that upon TNFα treatment, FynT-CA clone (red cubes) exhibited the greatest distance from the other clones (Figure 5.4A), suggesting that FynT kinase activity may facilitate TNFα-induced inflammatory responses.

We also employed unsupervised hierarchical clustering to allow delineation of clones that share similar characteristics in response to TNFα treatment. Using the 14 inflammatory markers, samples could be well clustered into two independent branches, as untreated (-) and treated (+) on the left dendrogram (Figure 5.4B). Consistently, FynT-CA was shown to exhibit greater gene changes of inflammatory-associated markers in response to TNFα treatment as compared to others, and was found to cluster as an independent sub-branch in the dendrogram (Figure 5.4B).

A

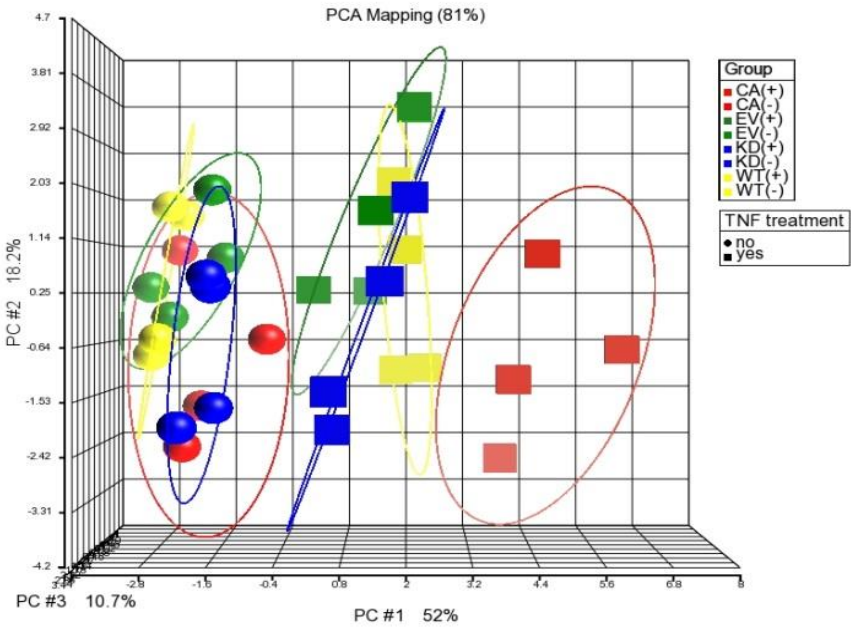

B

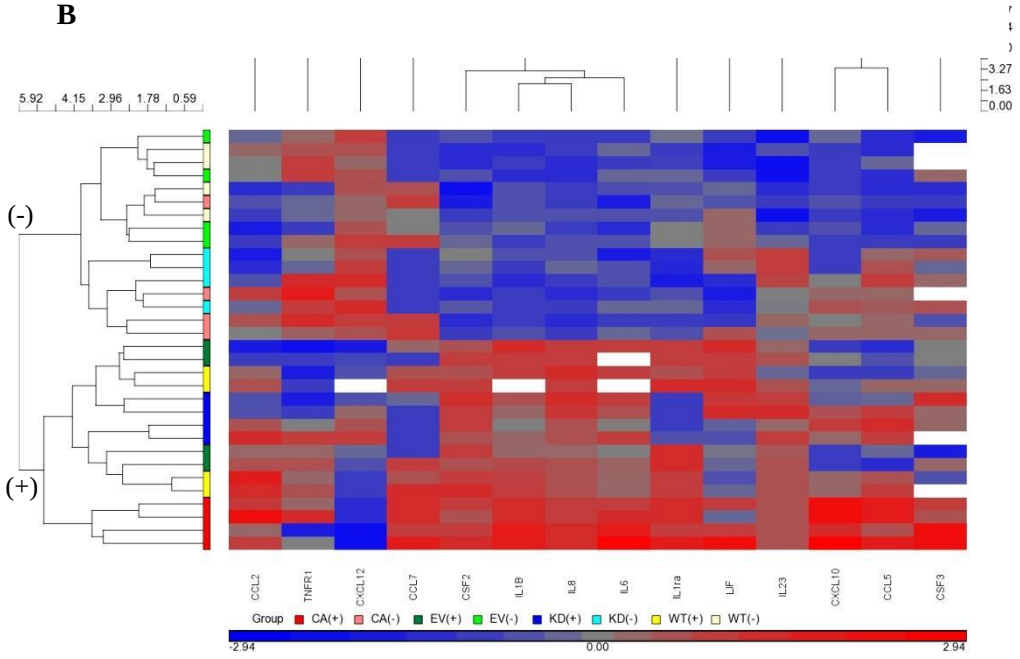

Figure 5.4 FynT tyrosine kinase activity facilitated TNFα-induced differential expression of inflammatory markers. iNHA stable clones with different FynT kinase activity (empty vector (EV), FynT wild-type (WT), FynT kinase constitutively active (CA) and FynT kinase dead (KD)) were treated with or without 50 ng/ml of TNFα for 3 days in four independent experiments and determined the expression profile of a panel of inflammatory markers (CCL2, CCL5, CCL7, CXCL10, CXCL12, CSF2, CSF3, IL1B, IL1ra, IL6, IL8, IL23, LIF, TNFR1) using Biomark HD high-throughput real-

time RT-PCR system. **(A)** Principal component analysis (PCA) identified the first 3 principal components (PCs) that explained 81% of the variation in the dataset. Each object represents an iNHA stable clone (EV= green, WT= yellow, CA= red, KD= blue) with TNFα (cubes) or without TNFα treatment (spheres). The variation of four biological replicates in each clone could be visualized by the size of each ellipse. TNFα-treated clones (cubes) were well-segregated from untreated clones (spheres), with TNFα-treated FynT-CA showing the greatest distance from the others. **(B)** Two-dimensional unsupervised hierarchical clustering analysis for segregation of iNHA clones based on their characteristics in response to TNFα treatment. The gene expression levels of 14 inflammatory-associated markers were shown with the columns (genes) and rows (samples) in cluster order. The relative value to the median among all samples are shown in colour with a continuum of expression levels from dark blue (lowest) to bright red (highest) and missing data are shown in white. Corresponding gene names are listed at the bottom. The left dendrogram lists the clones studied and provides a measure of the relatedness (untreated (-) and treated (+)) of expression in each clone.

5.4.3 FynT tyrosine kinase activity facilitated TNFα-induced secretion of inflammatory markers

To investigate whether FynT kinase activity may facilitate the TNFα-induced secretion of inflammatory markers, culture media collected from iNHA clones at day 3 post-treatment were examined for 14 inflammatory markers (gene expression of the majority of the genes were covered earlier) using multiplex immunoassays (MILLIPLEX®). PCA 3D scatter plot showed to account for 76.8% of the variation in the dataset (Figure 5.5A), showing clear segregation of untreated clones (spheres) from treated clones (cubes). Under TNFα treatment, FynT-CA clone (red cubes) exhibited the greatest distance from the others (Figure 5.5A), consistent with the findings from the expression profile of inflammatory markers (Figure 5.4A). At a closer look at four inflammatory markers secretion profiles plotted in bar charts, FynT-CA clone consistently showed the greatest secretion of all four inflammatory markers IL-1β, IL-6,

CSF3 and CXCL10 upon TNFα treatment (Figure 5.5B). Of note, even though TNFα-induced significant secretion of IL-1β in all clones, the secretion level of FynT-CA was still the highest (Figure 5.5B). On the other hand, although FynT-CA clone exhibited greater IL6 induction as compared to other clones at the late phase (Figure 5.3), the detected IL-6 secretion was similar to other clones, indicating that the measured inflammatory markers might not be solely derived from the late phase.

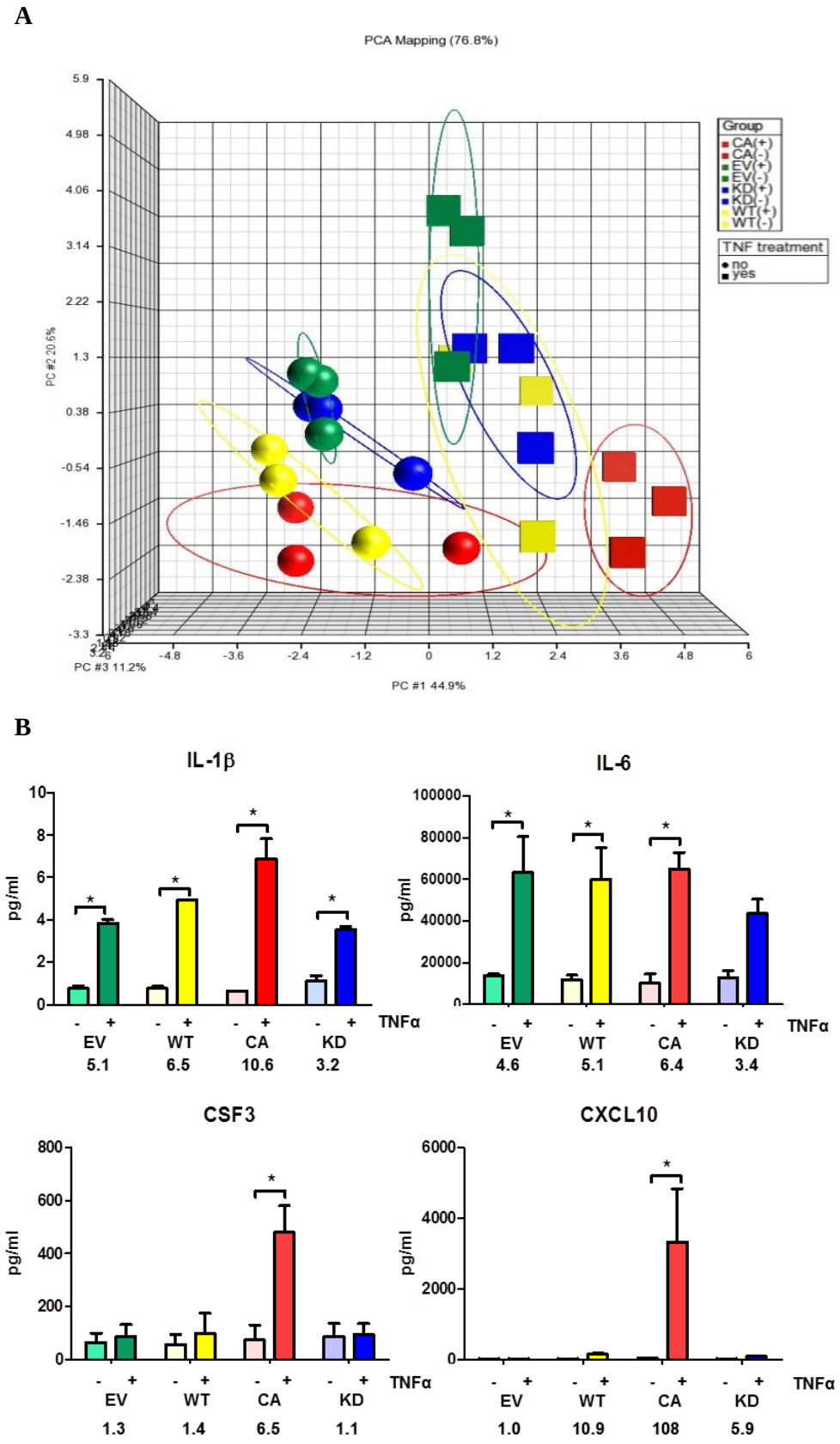

Figure 5.5 FynT tyrosine kinase activity facilitated TNFα-induced secretion of inflammatory markers. iNHA stable clones with different FynT kinase activity (empty vector (EV), FynT wild-type (WT), FynT kinase constitutively active (CA) and FynT kinase dead (KD)) were treated with or

without 50 ng/ml of TNFα for 3 days in three biological replicates and determined for secretion profile of a total of 14 inflammatory markers (CCL2, CCL3, CCL4, CCL5, CCL7, CXCL10, CXCL12, FGF, CSF2, CSF3, IL-1Ra, IL-1β, IL-6, IL-8) using MILLIPLEX® Multiplex Assays with Luminex platform. **(A)** Principal component analysis (PCA) identified the first 3 PCs that explained 76.8% of the variation in the dataset. Each object represents an iNHA stable clone (EV= green, WT= yellow, CA= red, KD= blue) with TNFα (cubes) or without TNFα treatment (spheres). The variation of three biological replicates in each clone could be visualized by the size of each ellipse. TNFα-treated clones (cubes) are well-segregated from untreated clones (spheres), with TNFα-treated FynT-CA (red cubes) showing the greatest distance from the others. **(B)** Bar charts display modulation of TNFα-induced secretion of IL-1β, IL-6, CSF3 and CXCL10 in iNHA FynT clones. Data shown are the means and ± SEM taken from three independent experimental repeats. *Significantly different (two-way ANOVA with Bonferroni's *post-hoc* test $p < 0.05$).

5.4.4 Pharmacological inhibition of Fyn tyrosine kinase activity decreased TNFα-induced inflammatory markers expression in FynT-CA clone

To validate that ectopic FynT kinase activity plays the main role in modulating TNFα-induced inflammatory responses at the late phase in FynT-CA clone, we treated the clone with PP2, a selective SFK inhibitor and monitored for the attenuation of TNFα-induced inflammatory responses. PP2 was found to inhibit FynT kinase activity in a dose dependent manner, as shown by the attenuation of Tyr-416 immunoreactivities but, without affecting total Fyn expression in FynT-CA clone (Figure 5.6A). We also observed that the inhibition of FynT kinase activity by 10 μM of PP2 was accompanied by the attenuation of TNFα-induced IL1B expression (Figure 5.6B).

FynT-CA and FynT-KD clones were then treated with PP2 to further confirm that the attenuation of TNFα-induced inflammatory responses was not associated with other endogenous SFKs. PP2 significantly attenuated TNFα-induced expression of a range of cytokines and chemokines (IL1B, IL6, CSF3 and CXCL10) (Student's paired *t*-test $p<0.05$) in FynT-CA clone (red bars in Figure 5.7), suggesting that FynT kinase activity in FynT-CA clone may play the main role in facilitating TNFα-induced inflammatory responses. Given that iNHA FynT-KD clone was already devoid of FynT kinase activity, no changes in TNFα-induction of cytokines and chemokines were observed with the addition of PP2 (blue bars in Figure 5.7).

A

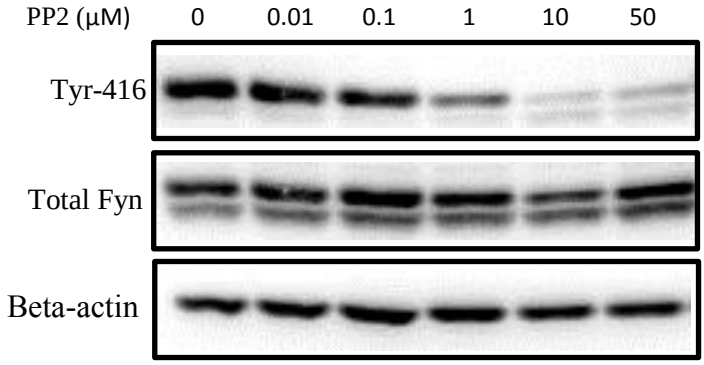

B

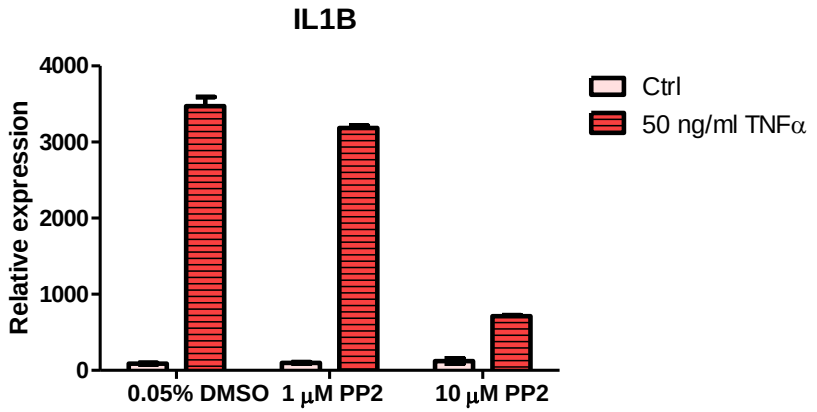

Figure 5.6 PP2 (Src-family kinase inhibitor) exhibited dose-dependent inhibition of Fyn tyrosine kinase activity in FynT-CA clone which was accompanied by the attenuation of TNFα-induced IL1B expression at the late phase. (A) FynT-CA clone treated with PP2 with concentrations of up to 50 μM were studied for inhibition of ectopic FynT tyrosine kinase activity as determined by attenuation of positive immunoreactivities of Tyr-416 using Western blot analysis. β-actin was used as a loading control. **(B)** 10 μM of PP2 effectively inhibited TNFα-induced IL1B expression in FynT-CA at 3 days post-treatment. Relative expressions of genes were normalized by geometric means of housekeeping genes. Data shown are the means and ± SEM from two independent biological replicates.

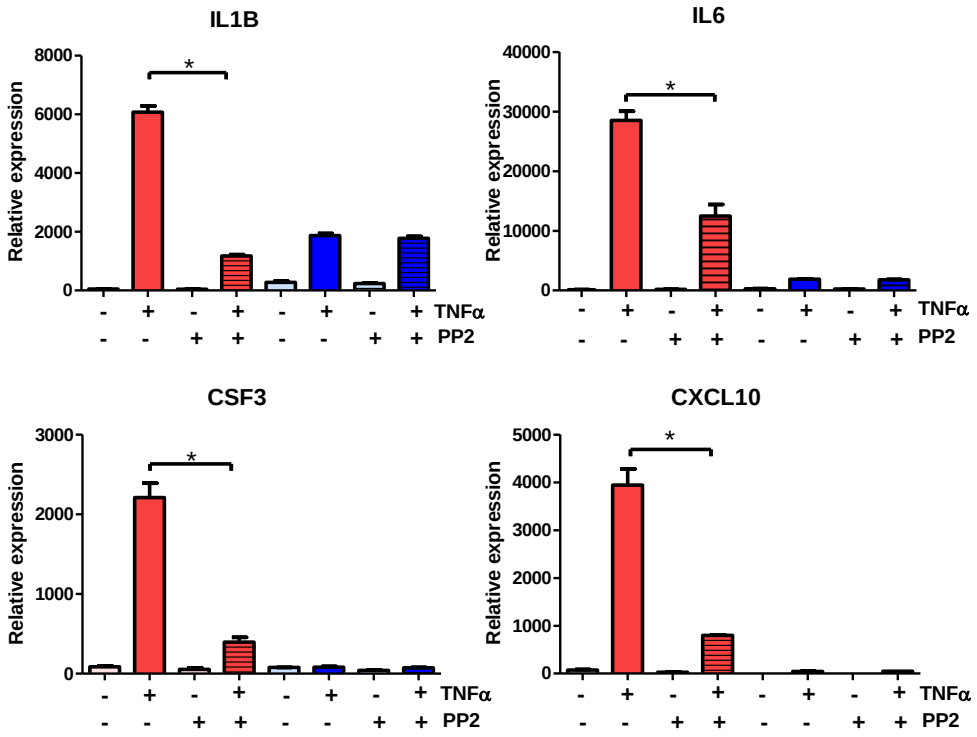

Figure 5.7 Inhibiting tyrosine kinase activity by PP2 inhibitor led to attenuated TNFα-induced inflammatory markers expression in FynT-CA clone and relatively no change in TNFα-induced inflammatory markers expression in FynT-KD clone. iNHA FynT-CA (red bars) and KD (blue bars) clones were pre-treated with 10 μM PP2 or vehicle control for 6 h, followed by treatment with (+) or without (-) 50 ng/ml of TNFα for a further 3 days and monitored for gene expression of IL1B, IL6, CSF3 and CXCL10 using real-time RT-PCR. Relative expressions of genes were normalized by geometric means of housekeeping genes. Values are the means and ± SEM of 3 independent biological replicates. *Significantly different (Student's paired *t*-test $p<0.05$).

5.4.5 Specific silencing of FynT attenuated TNFα-induced inflammatory markers expression in FynT-CA clone and increased TNFα-induced inflammatory markers expression in FynT-KD clone

To confirm that ectopic FynT mutant expression in FynT-CA contributes mainly for its sensitive response to TNFα treatment at the late phase, we tried to specifically silence FynT expression in FynT-CA clones and monitored the attenuation of TNFα-induced inflammatory markers expression.

Pooled 30 nM of Dicer-substrate RNAs (DsiRNAs) mixture consisting of three sequences specific to FynT was able to specifically silence the overexpressed FynT in iNHA FynT-CA clone with an efficiency of more than 90% as compared to control randomized sequence (NC), and showed no effect on FynB expression as determined by real-time RT-PCR (Figure 5.8). Consistently, specific silencing of FynT in FynT-CA clone was accompanied by the attenuation of TNFα-induced expression of IL1B, IL6 and CSF3 (Student's paired *t*-test $p<0.05$) (red bars in Figure 5.9). In contrast, although the overall expression of inflammatory markers in FynT-KD clone remained much lower than FynT-CA clone after FynT silencing, we observed modest increased induction of all inflammatory markers by TNFα after silencing of the ectopic kinase dead FynT mutant (blue bars in Figure 5.9). Of note, the attenuation of TNFα-induced inflammatory markers expression in FynT-CA clone was less effective by specific silencing of FynT by DsiRNA transfection as compared to inhibiting FynT kinase activity by PP2 treatment. This could be due to some unknown reasons that these clones, particularly for FynT-CA that underwent transfection procedure, had increased basal level of

inflammatory markers expression and heightened sensitivity to TNFα treatment.

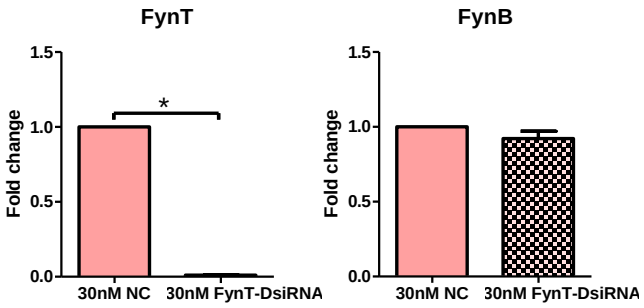

Figure 5.8 Specific silencing of FynT expression by FynT-DsiRNA in FynT-CA clone. Real-time RT-PCR was used to determine the specificity of FynT-Dicer-substrate RNAs (DsiRNAs). 30 nM of FynT-DsiRNA mixture consisting of three sequences specific to FynT was used to silence overexpressed FynT in iNHA FynT-CA clone and 30 nM of NC (randomized sequence) was used as a negative control. Relative expressions of genes were normalized by geometric means of housekeeping genes. Values are the means and ± SEM of 3 independent biological replicates. *Significantly different (Student's paired *t*-test $p<0.05$).

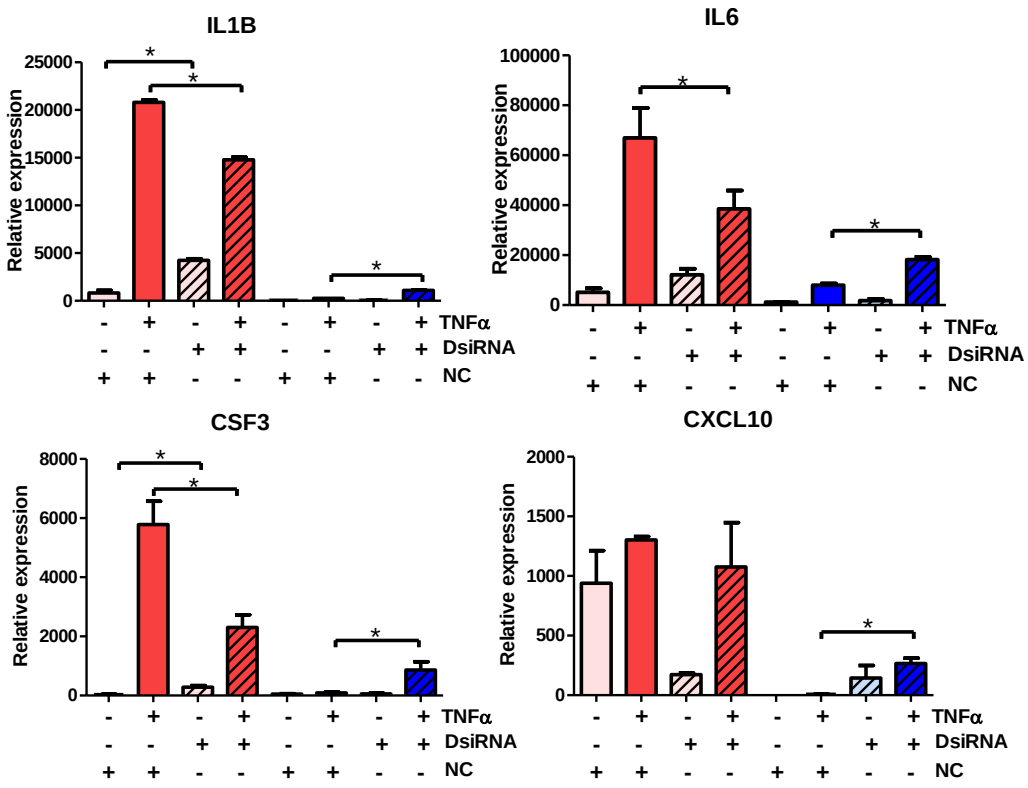

Figure 5.9 Specific silencing of FynT expression by DsiRNA led to attenuated TNFα-induced inflammatory markers expression in FynT-CA clone and increased TNFα-induced inflammatory markers expression in FynT-KD clone. iNHA FynT-CA (red bars) and FynT-KD clones (blue bars) were treated with (+) or without (-) 50 ng/ml of TNFα for 3 days in the presence of either 30 nM FynT-specific Dicer-substrate siRNAs mix (DsiRNA) or 30 nM Negative Control duplex (NC) and monitored for gene expression of IL1B, IL6, CSF3 and CXCL10 using real-time RT-PCR. Relative expressions of genes were normalized by geometric means of housekeeping genes. Values are the means and ± SEM of 3 independent biological replicates. *Significantly different (Student's paired *t*-test $p<0.05$).

5.4.6 FynT kinase activity may modulate activation of NF-κB signalling at the late phase of TNFα treatment.

NF-κB is one of the key regulators of pro-inflammatory signalling activated during inflammation and its activation is critical for TNFα-induced inflammatory response (Kempe et al., 2005, Lawrence, 2009). To determine whether FynT kinase activity may modulate TNFα-induced NF-κB signalling pathway at the early or late phase, FynT-CA and FynT-KD iNHA clones were co-transfected with inducible NF-κB-responsive firefly luciferase (pNF-κB-luc) vector and constitutively expressing Renilla luciferase (pRL-CMV) control vector and treated with TNFα for 6 hours (early phase) and 3 days (late phase). Both FynT-CA and FynT-KD showed similar induction of NF-κB activity at 6 hours post-treatment as determined by NF-κB reporter assay, indicating that FynT kinase activity may not have impact at the early phase of TNFα treatment (Figure 5.10). Interestingly, at 3 day time point (late phase), FynT-CA clone showed significantly higher NF-κB activity, in contrast to hardly any induction of NF-κB activity found in FynT-KD clone (Figure 5.10).

Activation of NF-κB signalling can also be detected by phosphorylation-dependent-IκB degradation as well as phosphorylation states of its subunits, e.g. Serine-536 of p65 subunit (Karin, 1999, Sakurai et al., 1999, Hu et al., 2004, Mattioli et al., 2004). Both FynT-CA and FynT-KD clones demonstrated an absolute degradation of IκB shortly after TNFα stimulation (15min), which was accompanied by the induction of p65 phosphorylation (Figure 5.11A), again suggesting that FynT kinase activity may not modulate activation of NF-κB signalling at the early phase. Interestingly, TNFα-induced p65 phosphorylation in FynT-CA clone at the late phase, from day 1 onwards

and were maintained up to 3 days (Figure 5.11B). In contrast, FynT-KD clone demonstrated no further induction of phospho-p65 at the late phase (Figure 5.11B and 5.11C). In addition, protein level of p65 in FynT-CA but not FynT-KD clone appeared to be increasing at late time points up to 3 days of TNFα treatment (Figure 5.11B). Taken together, these findings suggest that FynT kinase activity may modulate NF-κB activation at the late phase of TNFα treatment.

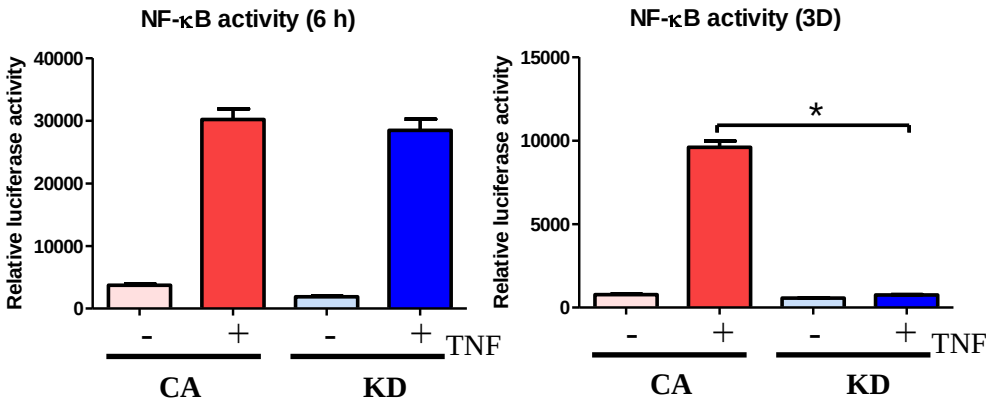

Figure 5.10. FynT kinase activity may modulate NF-κB activation at the late phase of TNFα treatment as determined by NF-κB reporter assay. iNHA FynT-CA and KD clones were co-transfected with pNF-κB-luc vector and pRL-CMV vector. 24 h post-transfection, these cells were treated with (+) or without (-) 50ng/ml TNFα for 6 h and 3 days. NF-κB derived luciferase activities were measured after normalizing for transfection efficiency against Renilla luciferase activity. Values are the means and ± SEM of 3 replicates of a representative experiment from 3 independent biological repeats. *Significantly different (Student's *t*-tests, $p<0.05$).

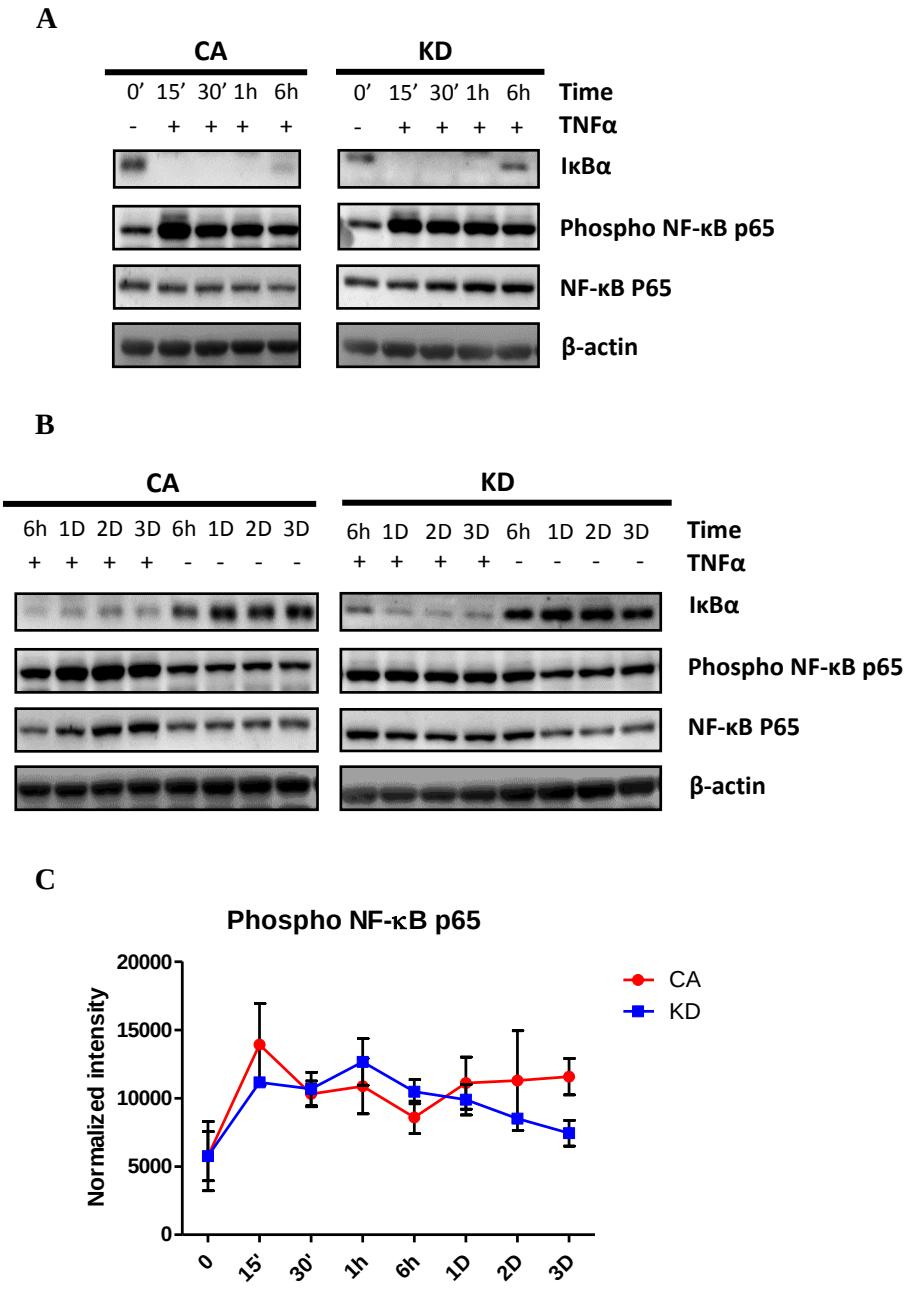

Figure 5.11 FynT kinase activity may modulate NF-κB activation at the late phase of TNFα treatment as determined by Western blot analyses. iNHA FynT-CA, FynT-KD clones were treated with (+) or without (-) 50 ng/ml TNFα and monitored for the activation of NF-κB signalling pathway using Western blot analyses at the **(A)** early time points of 0 min, 15 min, 30 min, 1 h and 6 h and **(B)** late time points of day 1, 2 and 3 (included 6 h time point for comparison). β-actin was used as a loading control. **(C)** Graph shows mean ± SEM of phosphorylated NF-κB p65 immunoreactivity normalized to β-actin in iNHA FynT-CA and FynT-KD clones treated with 50 ng/ml TNFα. Data shown are representative blots from 2 independent biological replicates.

5.5 Discussion

5.5.1 TNFα-induced biphasic induction of pro-inflammatory cytokines in iNHA

TNFα has been shown to induce biphasic induction of gene expression through activation of NF-κB in multiple types of cells including, human glioblastoma cells-U373, mouse microglial cell line-BV2, human cervical cancer cells- HeLa and murine C2C12 myoblasts (Ladner et al., 2003, Schwamborn et al., 2003, Tian et al., 2005). This biphasic induction of gene expression observed in these cell lines was attributed to the effect of oscillatory NF-κB activation by prolonged TNFα stimulation (Tian et al., 2005, Cheong et al., 2008). Biphasic activation of NF-κB has also been observed in primary murine astrocytes and is regulated by nuclear translocation of NF-κB, dependent on IκBα degradation and resynthesis (Kemler and Fontana, 1999). The time frame for biphasic activation of NF-κB and downstream activation of gene transcription differs across different cell type (Han and Brasier, 1997, Kemler and Fontana, 1999, Tian et al., 2005). In iNHA, TNFα-induced activation of NF-κB signalling occurs within 15 min of simulation as detected by IκBα degradation and phospho-p65 increment (Figure 5.11A) while downstream expression of acute inflammatory genes, IL1B and IL6 peaked at 6 h and 1 h respectively (Figure 5.2). Interestingly, when monitored up to three days post-TNFα stimulation, only higher concentrations (50 ng/ml and above) of TNFα could induce a biphasic induction of IL1B and IL6 gene expression in iNHA. It has been reported that saturating doses of TNFα is required to generate late gene expression because the expression of later genes requires persistent nuclear localization of NF-κB which is dependent on the

initial concentration of TNFα (Hao and Baltimore, 2009, Tay et al., 2010). The biological relevance of this would be in the context of chronic inflammation where persistent presence of NF-κB activating stimuli, TNFα, could surmount the inhibitory feedback mechanism leading to elevated constitutive activity of NF-κB (Hoesel and Schmid, 2013). In AD brain tissues, elevated levels of TNFα in both CSF and cortex and activated NF-κB could be detected in senile plaques even in early plaque stages as well as surrounding in neurons and astrocytes (Fillit et al., 1991, Kaltschmidt et al., 1997, Tarkowski et al., 1999). Moreover, the presence of IL-6 and IL-1β, both NF-κB inducible cytokines, were also detected in senile plaques. These evidence support the idea that persistent NF-κB activation occurs during neuroinflammation in AD (Strauss et al., 1992, Griffin et al., 1995).

5.5.2 FynT kinase activity modulates TNFα-induced biphasic induction of multiple inflammatory markers at the late phase.

In Figure 5.3A, the overt differences in the gene induction of inflammatory cytokines (IL1B and IL6) between FynT-CA and FynT-KD clone was observed only at the late phase (3 days) but not during the early phase of induction (6 h). Therefore, subsequent experiments only focused on TNFα-induced gene expression during the late phase. TNFα-induced differential expression of 14 inflammatory-associated markers were analysed using PCA which is a data reduction technique that allows the major sources of variation in a multi-dimensional dataset to be analysed without introducing inherent bias (Helmy et al., 2012), as well as using unsupervised hierarchical clustering analysis to display the gene expression data. From these data, it could be inferred that FynT-CA exhibited FynT kinase activity that facilitate TNFα-

induction in various inflammatory markers which could be easily be identified using the PCA 3D plot (Figure 5.4A) and unsupervised hierarchical clustering analysis (Figure 5.4B). These suggest that the FynT kinase activity may modulate the expression profile of TNFα-induced inflammatory markers.

Generally, mRNA transcript level can only partially correlate with protein abundance (Vogel and Marcotte, 2012). Moreover, many cytokines can only exert biological effects following secretion and binding to their respective receptors. Therefore, secretion profiles of the cytokines and chemokines from the FynT clones were examined using multiplex immunoassays on the Luminex platform. However, we need to keep in mind that the secreted inflammatory markers detected in the collected culture media at day 3 might be an accumulation of inflammatory markers that were secreted at both the early and late phase upon stimulation, which may result in inconsistency of the expression and secretion profile. Furthermore, synthesis and secretion of inflammatory markers were also dependent on downstream translation and post-translational modification; both processes could contribute to less predictable secretion profile. Nonetheless, we observed that FynT-CA could be well segregated from other clones using the expression profiles (Figure 5.4A), as well as the secretion profile of TNFα-induced inflammatory markers (Figure 5.5A) as determined by PCA 3D scatter plots. Consistently, when analysed closely, we observed that certain cytokines and chemokines (e.g. IL-1β, CSF3 and CXCL10) exhibited similar trends in both expression and secretion profiles, with FynT-CA showing the greatest response to TNFα treatment (Figure 5.4B and 5.5B). In summary, our findings supported that

FynT kinase activity may modulate TNFα-induced inflammatory response at the late phase.

Consistently, both inhibition of FynT kinase activity by PP2 treatment and specific silencing of ectopic FynT mutant by DsiRNA transfection in FynT-CA clone were able to effectively attenuate TNFα-induced inflammatory markers expression (Figure 5.7 and Figure 5.9). We noticed that during gene silencing, the transfection procedure itself affected basal expression levels of certain cytokines and hence likely to confound the findings. This observation has been previously reported where certain chemokine genes, such as CXCL10, CCL2 and CCL5 as well as type I interferons are known to be induced upon cationic liposome transfection methods of double stranded nucleic acid due to activation of innate immune response (Ishii et al., 2006). On a side note, when ectopic kinase dead FynT mutant were ablated by specific silencing of FynT, FynT-KD clone showed significant increment of TNFα-induced expression of inflammatory markers which suggest that FynT, in its kinase dominant negative form, exhibited a certain inhibitory role in the modulation of inflammatory markers (Figure 5.9). Taken together, these findings confirmed our observation that FynT kinase activity modulates TNFα-induced inflammatory markers expression at the late phase.

5.5.3 NF-κB activation is altered in clones of different FynT kinase activity at the late phase of TNFα-induction

TNFα is one of the most potent physiological inducers of the canonical signalling of NF-κB during inflammation (Lawrence, 2009). To determine whether FynT could act through NF-κB signalling to modulate TNFα-induced inflammatory markers production, NF-κB activity was investigated at both

early and late phase of induction. Both luciferase reporter assay as well as Western blot results, demonstrated that the difference between the NF-κB activities could be observed only during the late phase (3 days) of TNFα-induction, implying that early activation of NF-κB was independent of FynT kinase activity. SFKs are not known to regulate classical activation of NF-κB proteins directly (Abu-Amer et al., 1998). However, overexpression of certain SFKs (e.g. v-Src) have been shown to activate NF-κB signalling, while SFK knockouts (e.g. c-Src and Fyn), dominant negative expression of SFKs (e.g., c-Src) and SFK inhibitor PP2 are found to reduce and delay TNFα-induced NF-κB activation in vitro (Eicher et al., 1994, Abu-Amer et al., 1998, Huang et al., 2003, Itoh et al., 2005, Panicker et al., 2015). The exact mechanism on how SFKs modulate NF-κB signalling is not clear but it has been proposed that SFKs could activate upstream signalling molecules, such as protein kinase C-δ and also phosphorylate non-classical tyrosine phosphorylation of IκBα, leading to NF-κB activation (Abu-Amer et al., 1998, Panicker et al., 2015). Here, our findings demonstrated that constitutive active FynT led to prolonged NF-κB activation in iNHA even after 3 days of TNFα-induction (Figure 5.10, 5.11B and 5.11C), while dominant negative FynT kinase showed complete reversion to basal state of NF-κB activity after 3 days (Figure 5.10). These findings paralleled with previous studies to show kinase activity in SFKs positively regulates NF-κB signalling. In addition, our findings further emphasized that at least in iNHA, FynT kinase activity regulates TNFα-induction of biphasic of NF-κB activation at the late phase. This also explained why overt induction of inflammatory markers was observed in FynT-CA clone but not in FynT-KD clone during late phase of TNFα-

induction as many inflammatory markers are target genes of NF-κB signalling (Figure 5.4) (Pahl, 1999). The significance of this would be that FynT kinase activity could potentially propagate inflammatory response mediated by astrocytes in the presence of TNFα.

5.6 Summary

Using recombinant FynT mutant approaches in iNHA, FynT kinase activity was demonstrated to positively regulate inflammatory markers induction by TNFα, hence leading to increased secretion of inflammatory cytokines and chemokines during the late phase of inflammatory markers induction. This biphasic induction of inflammatory markers was found to correspond with NF-κB activity where FynT-CA clone showed biphasic induction of NF-κB which was not observed in FynT-KD clone. This indicates that ectopic FynT kinase activity can propagate prolonged inflammatory response in astrocytes leading to chronic inflammation which could potentially aggravate neurodegeneration.

CHAPTER 6-
General conclusion and future directions

CHAPTER 6- General conclusion and future directions

6.1 Summary

Numerous studies have elucidated plausible pathological roles of Fyn in AD as mentioned in the introduction in Chapter 1. This has led to strong interest in the field, delegating Fyn as a potential therapeutic in AD. Fyn is known to be alternatively spliced to generate two major isoforms, namely FynB and FynT. It is therefore convenient to assume that the brain-predominant FynB isoform is involved in the disease. This could explain why no study has attempted to delineate possible isoform-specific roles of Fyn in AD thus far.

In this thesis, the flow of my research follows a post-mortem-to-bench translational approach, where we first identified our research target from post-mortem brain tissues (Chapter 3) and then investigated and validated its function using primary cell culture (Chapter 4) and recombinant approaches (Chapter 5). Our preliminary exon array data revealed that FynT, the non-brain predominant isoform was upregulated in AD brains while FynB remained unchanged. Subsequent gene ontology term enrichment analyses of the exon array data and cellular markers correlation revealed that FynT was positively correlated with markers of associated with reactive astrogliosis and negatively correlated with neuronal function. Therefore, we hypothesized that the differentially regulated FynT in AD possess an isoform-specific role in the pathogenesis of AD. Ultimately, we aim to elucidate the isoform-specific role of FynT in AD and the possible impacts of FynT induction in disease progression.

In the first part of my findings (Chapter 3), validation of exon array data was performed using real-time RT-PCR and capillary electrophoresis to confirm that FynT is indeed upregulated in AD. Since we found FynT to be positively correlated with markers of associated to reactive astrogliosis and negatively correlated with neuronal function, cell-type specific expression of FynT versus FynB ratio in the two major cell-types of the brain (astrocytes and neurons) were determined. As anticipated, astrocytes were found to express proportionately higher amount of FynT to FynB as compared to neurons. Subsequently, FynT immunoreactivity in association with cellular markers and neuropathological hallmarks in post-mortem AD brains was investigated. This led to the first major finding of this thesis that the isoform-specific upregulation of FynT was likely to be independently associated with neurofibrillary degeneration and reactive astrogliosis in AD. The results also highlighted that the alternative splicing of Fyn may be an important mechanism in disease pathogenesis or response in AD as neurons are known to predominantly expressed FynB, but FynT was in fact increased with concomitant decrease of FynB in NFT-bearing neurons. Moreover, the observation that reactive astrocytes in AD brain displayed brighter FynT immunoreactivities as compared to control brain further emphasized FynT involvement in reactive astrogliosis. For these reasons, further studies are required to elucidate the upstream signalling and molecular mechanisms underlying FynT modulation as well as the precise nature of its involvement in NFT formation and astrocyte activation.

Based on the findings from Chapter 3, it could be speculated that certain pathological conditions in the AD brain can result in specific upregulation of

FynT. In addition, FynT expression could be associated with increased astrocyte numbers due to astrogliosis. Thus, we aimed to delineate the isoform-specific role of FynT in neurons and astrocytes using primary cortical cultures exposed to pathological conditions associated with AD. Treatment of Aβ was found to induce FynT expression in astrocytes but not in neurons from primary rat mixed cortical cultures. Although Aβ is known to induce tau hyperphosphorylation in multiple cell lines including rat neurons (Zheng et al., 2002, Hernandez et al., 2009, Tokutake et al., 2012), it is difficult to recapitulate NFT formation *in vitro* even in neurons obtained from transgenic mice that express mutant human tau protein prone to aggregation (Ko et al., 1990, Guo and Lee, 2013). This could explain why FynT was not found to be induced in neurons using this approach. On the other hand, we could still observe Aβ-induced FynT but not FynB expression in astrocyte, emphasizing that upregulation of FynT expression in AD may be associated in part with astrocytic activation. In mixed cultures with increasing numbers of astrocytes, positive correlation of FynT expression with astrocytic markers was observed, further supporting FynT as a marker of astrogliosis. Moreover, treatment of astrocytes with TNFα induced FynT upregulation at the late phase but no change in FynB expression advocates that modulation of FynT expression may be associated with astrocyte-mediated neuroinflammatory responses.

Lastly, we wanted to investigate the functional role of FynT by employing iNHA that stably expressed FynT mutants of kinase constitutively active and kinase dead to study the role of FynT kinase activity in modulating TNFα-induced pro-inflammatory signalling. Upon TNFα treatment, FynT kinase activity was found to positively regulate the expression and secretion of a

number of inflammatory markers at the late phase, likely through modulating NF-κB signalling pathway. Thus, it can be deduced that the upregulation of FynT expression in the AD brain may propagate prolonged inflammatory response and was closely associated with chronic inflammation.

In summary, our findings have added new perspectives to the pathogenic role of Fyn in AD. The identification of FynT isoform being closely associated with NFT pathology and astrocyte-mediated neuroinflammation, prompt us to speculate that FynT could be a potential pharmacotherapeutic target for AD.

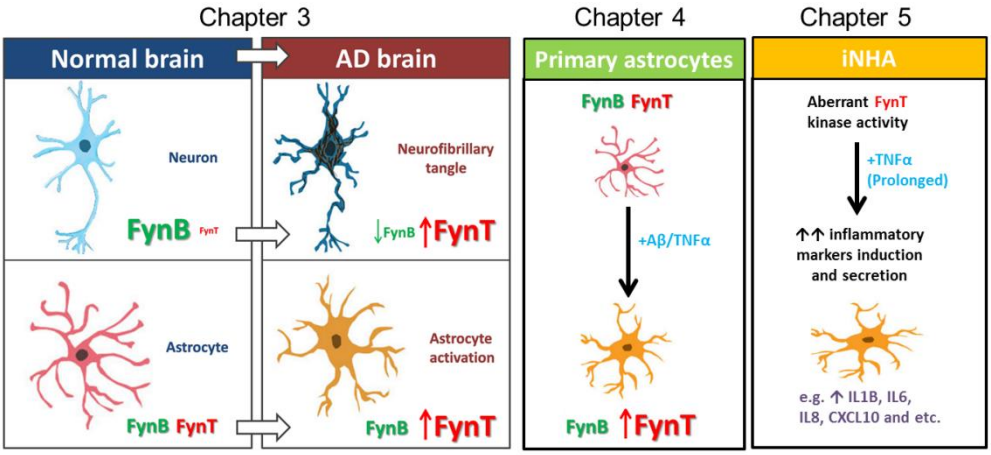

Figure 6.1 A pictorial summary of the main findings in this study. FynT mRNA and protein expression was found to be upregulated in post-mortem brain tissues, independently associated neurofibrillary degeneration and reactive astrogliosis (Chapter 3). FynT was observed to be specifically induced in Aβ-treated activated astrocytes in mixed cortical cultures as well as in TNFα-treated astrocytes cultures (Chapter 4). Aberrant FynT kinase activity in iNHA was found to facilitate prolonged TNFα-induced inflammatory response in astrocytes (Chapter 5). Figure readapted from online graphical abstract (Lee et al., 2015) with permission from John Wiley and Sons.

6.2 General Limitations

Identification of FynT and FynB protein expression in post-mortem brains:

Western blot analyses of Fyn isoforms in post-mortem brains were not included in our studies. This was because the custom-made FynB and FynT antibodies failed to detect specific immunoreactivity from the crude protein extracted from the brain tissues. We suspected that the preparation of brain lysate could be the main reason for the high background signals detected in the immunoblots. However, due to limited availability of tissues in this cohort, we did not explore different types of brain lysate preparation. We believed that localization of upregulated FynT expression in AD brain using IF could be more important than protein quantitation in the crude brain lysate using Western blot analyses. Indeed, using IF approach, we identified that FynT induction was independently localized to NFT-bearing neurons and activated astrocytes, two important hallmarks in AD pathology.

In-vitro cell culture models:

Primary cortical cultures treated with Aβ could be considered as an *in vitro* system of cellular constituents of the brain for AD studies. As the pathological characteristics of AD takes many decades to become apparent, exposing Aβ to primary cortical culture for just a few days may not be able to recapitulate the process of AD pathology. As mentioned in Chapter 4, Aβ was not able to induce FynT expression in neurons, probably because this *in vitro* system might not be able to activate alternative splicing machinery and/or NFT formation in neurons. Moreover, the observation that Aβ could induce FynT

expression in astrocytes from mixed cortical cultures and not from pure astrocyte cultures further emphasized that the induction of biological responses can be distinctively different *in vitro* and *in vivo* due to cell-cell interaction. Therefore, it is crucial to validate cell culture results with animal models when modelling disease conditions.

Overexpression of recombinant FynT in iNHA:

We have chosen iNHA over other glioma cells as a model in this study because although iNHA is immortalized, they are not transformed and are less likely to have massive genomic aberrations as compared to glioma cell lines derived from tumours. iNHA clones that stably expressing FynT-WT or FynT-mutants of CA and KD, as well as EV were established for our study. We observed that the stability of ectopic FynT expression in each clone might vary, for example FynT-CA might reduce sensitivity to TNFα treatment after long term passages in cultures. Thus, early passages of the clones were used. All clones (FynT-WT, -CA, -KD and EV) were cultured, treated at the same batch for fair comparison. We also used at least two independent clones in the beginning of the study to rule out the possibility that the observation was not due to ectopic expression of FynT but solely due to clonal differences. Due to massive cell culture involved, we only focus on one clone each for subsequent experiments. To validate our findings that the distinct responses of FynT-CA and FynT-KD to TNFα treatment were indeed due to ectopic FynT mutant expression, we showed that the phenomenon can be reverted by silencing FynT expression or inhibiting FynT kinase activity. In addition, by using an overexpression system to study functional differences in FynT kinase activity,

it is important to keep in mind that certain overt phenotypes observed in this system may not observed under physiological conditions.

6.3 Future directions

Role of FynT in neurofibrillary degeneration:

IF results in Chapter 3 revealed that the upregulation of FynT in AD was likely to be independently associated with neurofibrillary degeneration and reactive astrogliosis. This thesis, however, did not address how FynT is involved in neurofibrillary degeneration and at which stage of NFT formation. Fyn has been shown to directly phosphorylate tau at Tyrosine 18 residue (Lee, 1998, Lee et al., 2004) but isoform-specific difference has never been elucidated. It will be interesting to study regulatory mechanism of FynT induction in NFT-bearing neurons using transgenic animal models that carry tau protein mutation (e.g. P301S) (Gotz and Ittner, 2008). The greatest advantage of using animal models to study NFT pathology is that tau pathology progression can be monitored over time and expression patterns of FynB or FynT can be determined unlike in post-mortem brain tissues. Furthermore, genetic ablation of FynT can be performed by crossing the tau transgenic models with FynT knockout mice to determine if FynT regulates NFT formation.

Furthermore, it will also be meaningful to look at FynT versus FynB expression in other tauopathies such as in Frontotemporal dementias (FTD) to determine whether FynT is purely associated with NFT across different tauopathies or is only specific to AD. Tau pathology in Frontotemporal dementia with parkinsonism-17 (FTDP-17) is associated with tau mutation while in AD it is not (Wolfe, 2009); this might offer new molecular insights to

the similarities or differences in neurofibrillary degeneration across the diseases.

Role of FynT in neuroinflammation:

To address FynT role in neuroinflammation mediated by astrogliosis, *in vivo* models of neuroinflammation can be employed. Specific FynT knockout mice and wild-type mice can be subjected to inflammatory stimuli in the brain *in vivo* (e.g. intracranial injection of TNFα, LPS) and monitor the extent of astrogliosis and the expression inflammatory markers between the two groups. Similarly, to investigate role of FynT in chronic neuroinflammation related to AD, FynT knockout mice can be crossed with AD transgenic mouse models known to exhibit gliosis (e.g. APPPS1, 5XFAD, P301S) (Oakley et al., 2006, Radde et al., 2006, Yoshiyama et al., 2007) and monitor at different stages for inflammatory responses.

Studying alternative splicing mechanism of Fyn:

Currently, the exact mechanism on how Fyn undergoes alternative splicing is unknown. To identify possible regulators of Fyn splicing, samples obtained from both human as well as cell culture that displayed altered FynT expression in disease condition (e.g. NFTs and reactive astrocytes isolated by laser capture microdissection in brain tissues) or when treated with factors (astrocytes treated with Aβ or TNFα) can be collected. Subsequent proteomics (e.g. liquid chromatography-tandem mass spectrometry) and genomics technologies (e.g. exon array profiling) can be employed for the analysis of the samples, focusing on proteins or genes that regulates splicing mechanism and RNA processing.

Functional differences of FynT and FynB:

Majority of the work in this thesis have focused on FynT, since it is the isoform that is pathologically associated with AD. So far, only a few studies have pointed out that FynT and FynB exhibited functional differences which can be attributed to region encoded by exon 7 due to alternative splicing (Davidson et al., 1994, Brignatz et al., 2009). Specifically, FynB structure favours a closed auto-inhibited conformation as compared to FynT hence affecting substrate accessibility (Brignatz et al., 2009). Certain substrates of Fyn (e.g. Sam68 RNA binding protein) can bind to each isoform with different affinities and hence be phosphorylated differentially (Brignatz et al., 2009). Functional studies can be done to elucidate investigate FynT and FynB differences in substrate binding particularly those substrates that are therapeutic targets in AD which include, Tau and NMDA receptor. This can be achieved by performing co-immunoprecipitation experiments to determine binding affinities and phosphorylation statuses. It will also be worthwhile to look at whether FynB possesses equivalent roles in modulating inflammatory response as FynT in astrocytes by generating stable clones of FynB or specifically silencing each isoform and monitor for inflammatory responses. These experiments will give us an idea whether it is wise to target Fyn in diseases in a non-isoform specific manner and uncover potential unwanted side-effects.

Therapeutic potential of FynT:

Ongoing AD clinical trials targeting Fyn uses tyrosine kinase inhibitors which are not specific to Fyn are likely to result in side-effects as tyrosine kinases are ubiquitously expressed in the brain. By identifying FynT as the pathological

isoform of Fyn in AD, we hope to highlight to the field and that FynT as opposed to FynB might be a better drug target of Fyn in the FynB predominant brain tissue. Although currently there are no Fyn specific drugs, isoform-selective inhibitors for other kinases (e.g. p38αMAPK) (Roy et al., 2015) has been discovered which indicates it is possible to identify more specific inhibitors for FynT in the near future. Moreover, with the development of better drug delivery systems to the CNS, side-effects to the peripheral tissues can be reduced**.**

BIBLIOGRAPHY

Abbott, N. J., Ronnback, L. & Hansson, E. 2006. Astrocyte-endothelial interactions at the blood-brain barrier. *Nat Rev Neurosci,* 7**,** 41-53.

Abe, K. & Misawa, M. 2003. The extracellular signal-regulated kinase cascade suppresses amyloid beta protein-induced promotion of glutamate clearance in cultured rat cortical astrocytes. *Brain Res,* 979**,** 179-87.

Abu-Amer, Y., Ross, F. P., McHugh, K. P., Livolsi, A., Peyron, J. F. & Teitelbaum, S. L. 1998. Tumor necrosis factor-alpha activation of nuclear transcription factor-kappaB in marrow macrophages is mediated by c-Src tyrosine phosphorylation of Ikappa Balpha. *J Biol Chem,* 273**,** 29417-23.

Agostinho, P., Cunha, R. A. & Oliveira, C. 2010. Neuroinflammation, oxidative stress and the pathogenesis of Alzheimer's disease. *Curr Pharm Des,* 16**,** 2766-78.

Akama, K. T., Albanese, C., Pestell, R. G. & Van Eldik, L. J. 1998. Amyloid beta-peptide stimulates nitric oxide production in astrocytes through an NFkappaB-dependent mechanism. *Proc Natl Acad Sci U S A,* 95**,** 5795-800.

Akiyama, H., Barger, S., Barnum, S., Bradt, B., Bauer, J., Cole, G. M., Cooper, N. R., Eikelenboom, P., Emmerling, M., Fiebich, B. L., Finch, C. E., Frautschy, S., Griffin, W. S., Hampel, H., Hull, M., Landreth, G., Lue, L., Mrak, R., Mackenzie, I. R., McGeer, P. L., O'Banion, M. K., Pachter, J., Pasinetti, G., Plata-Salaman, C., Rogers, J., Rydel, R., Shen, Y., Streit, W., Strohmeyer, R., Tooyoma, I., Van Muiswinkel, F. L., Veerhuis, R., Walker, D., Webster, S., Wegrzyniak, B., Wenk, G. & Wyss-Coray, T. 2000. Inflammation and Alzheimer's disease. *Neurobiol Aging,* 21**,** 383-421.

Alzheimer's, A. 2015. 2015 Alzheimer's disease facts and figures. *Alzheimers Dement,* 11**,** 332-84.

Appleby, M. W., Gross, J. A., Cooke, M. P., Levin, S. D., Qian, X. & Perlmutter, R. M. 1992. Defective T cell receptor signaling in mice lacking the thymic isoform of p59fyn. *Cell,* 70**,** 751-63.

Aschner, M. 1998. Astrocytes as mediators of immune and inflammatory responses in the CNS. *Neurotoxicology,* 19**,** 269-81.

Babus, L. W., Little, E. M., Keenoy, K. E., Minami, S. S., Chen, E., Song, J. M., Caviness, J., Koo, S. Y., Pak, D. T., Rebeck, G. W., Turner, R. S. & Hoe, H. S. 2011. Decreased dendritic spine density and abnormal spine morphology in Fyn knockout mice. *Brain Res,* 1415**,** 96-102.

Baranowska-Bik, A., Bik, W., Wolinska-Witort, E., Martynska, L., Chmielowska, M., Barcikowska, M. & Baranowska, B. 2008. Plasma beta amyloid and cytokine profile in women with Alzheimer's disease. *Neuro Endocrinol Lett,* 29**,** 75-9.

Basu, A., Krady, J. K. & Levison, S. W. 2004. Interleukin-1: a master regulator of neuroinflammation. *J Neurosci Res,* 78**,** 151-6.

Bauer, J., Strauss, S., Schreiter-Gasser, U., Ganter, U., Schlegel, P., Witt, I., Yolk, B. & Berger, M. 1991. Interleukin-6 and alpha-2-macroglobulin

indicate an acute-phase state in Alzheimer's disease cortices. *FEBS Lett,* 285**,** 111-4.
Beach, T. G., Walker, R. & McGeer, E. G. 1989. Patterns of gliosis in Alzheimer's disease and aging cerebrum. *Glia,* 2**,** 420-36.
Beattie, E. C., Stellwagen, D., Morishita, W., Bresnahan, J. C., Ha, B. K., Von Zastrow, M., Beattie, M. S. & Malenka, R. C. 2002. Control of synaptic strength by glial TNFalpha. *Science,* 295**,** 2282-5.
Bhaskar, K., Maphis, N., Xu, G., Varvel, N. H., Kokiko-Cochran, O. N., Weick, J. P., Staugaitis, S. M., Cardona, A., Ransohoff, R. M., Herrup, K. & Lamb, B. T. 2014. Microglial derived tumor necrosis factor-alpha drives Alzheimer's disease-related neuronal cell cycle events. *Neurobiol Dis,* 62**,** 273-85.
Bhaskar, K., Yen, S. H. & Lee, G. 2005. Disease-related modifications in tau affect the interaction between Fyn and Tau. *J Biol Chem,* 280**,** 35119-35125.
Blasko, I., Marx, F., Steiner, E., Hartmann, T. & Grubeck-Loebenstein, B. 1999. TNFalpha plus IFNgamma induce the production of Alzheimer beta-amyloid peptides and decrease the secretion of APPs. *FASEB J,* 13**,** 63-8.
Boon-Unge, K., Yu, Q., Zou, T., Zhou, A., Govitrapong, P. & Zhou, J. 2007. Emetine regulates the alternative splicing of Bcl-x through a protein phosphatase 1-dependent mechanism. *Chem Biol,* 14**,** 1386-92.
Braak, H. & Braak, E. 1991. Neuropathological stageing of Alzheimer-related changes. *Acta Neuropathol,* 82**,** 239-59.
Brignatz, C., Paronetto, M. P., Opi, S., Cappellari, M., Audebert, S., Feuillet, V., Bismuth, G., Roche, S., Arold, S. T., Sette, C. & Collette, Y. 2009. Alternative splicing modulates autoinhibition and SH3 accessibility in the Src kinase Fyn. *Mol Cell Biol,* 29**,** 6438-48.
Brookmeyer, R., Corrada, M. M., Curriero, F. C. & Kawas, C. 2002. Survival following a diagnosis of Alzheimer disease. *Arch Neurol,* 59**,** 1764-7.
Brouwers, N., Sleegers, K. & Van Broeckhoven, C. 2008. Molecular genetics of Alzheimer's disease: an update. *Ann Med,* 40**,** 562-83.
Brown, A. M. & Ransom, B. R. 2007. Astrocyte glycogen and brain energy metabolism. *Glia,* 55**,** 1263-71.
Butchart, J., Brook, L., Hopkins, V., Teeling, J., Puntener, U., Culliford, D., Sharples, R., Sharif, S., McFarlane, B., Raybould, R., Thomas, R., Passmore, P., Perry, V. H. & Holmes, C. 2015. Etanercept in Alzheimer disease: A randomized, placebo-controlled, double-blind, phase 2 trial. *Neurology,* 84**,** 2161-8.
Butterfield, S. M. & Lashuel, H. A. 2010. Amyloidogenic protein-membrane interactions: mechanistic insight from model systems. *Angew Chem Int Ed Engl,* 49**,** 5628-54.
Carrero, I., Gonzalo, M. R., Martin, B., Sanz-Anquela, J. M., Arevalo-Serrano, J. & Gonzalo-Ruiz, A. 2012. Oligomers of beta-amyloid protein (Abeta1-42) induce the activation of cyclooxygenase-2 in astrocytes via an interaction with interleukin-1beta, tumour necrosis factor-alpha, and a nuclear factor kappa-B mechanism in the rat brain. *Exp Neurol,* 236**,** 215-27.

Castello, M. A. & Soriano, S. 2014. On the origin of Alzheimer's disease. Trials and tribulations of the amyloid hypothesis. *Ageing Res Rev,* 13**,** 10-2.

Chaimowitz, N. S., Falanga, Y. T., Ryan, J. J. & Conrad, D. H. 2013. Fyn kinase is required for optimal humoral responses. *PLoS One,* 8**,** e60640.

Chan, W. Y., Kohsaka, S. & Rezaie, P. 2007. The origin and cell lineage of microglia: new concepts. *Brain Res Rev,* 53**,** 344-54.

Cheong, R., Hoffmann, A. & Levchenko, A. 2008. Understanding NF-kappaB signaling via mathematical modeling. *Mol Syst Biol,* 4**,** 192.

Chin, J., Palop, J. J., Puolivali, J., Massaro, C., Bien-Ly, N., Gerstein, H., Scearce-Levie, K., Masliah, E. & Mucke, L. 2005. Fyn kinase induces synaptic and cognitive impairments in a transgenic mouse model of Alzheimer's disease. *J Neurosci,* 25**,** 9694-703.

Combs, C. K., Karlo, J. C., Kao, S. C. & Landreth, G. E. 2001. beta-Amyloid stimulation of microglia and monocytes results in TNFalpha-dependent expression of inducible nitric oxide synthase and neuronal apoptosis. *J Neurosci,* 21**,** 1179-88.

Cooke, M. P., Abraham, K. M., Forbush, K. A. & Perlmutter, R. M. 1991. Regulation of T cell receptor signaling by a src family protein-tyrosine kinase ($p59^{fyn}$). *Cell,* 65**,** 281-91.

Cooke, M. P. & Perlmutter, R. M. 1989. Expression of a novel form of the fyn proto-oncogene in hematopoietic cells. *New Biol,* 1**,** 66-74.

Coppola, G., Chinnathambi, S., Lee, J. J., Dombroski, B. A., Baker, M. C., Soto-Ortolaza, A. I., Lee, S. E., Klein, E., Huang, A. Y., Sears, R., Lane, J. R., Karydas, A. M., Kenet, R. O., Biernat, J., Wang, L. S., Cotman, C. W., Decarli, C. S., Levey, A. I., Ringman, J. M., Mendez, M. F., Chui, H. C., Le Ber, I., Brice, A., Lupton, M. K., Preza, E., Lovestone, S., Powell, J., Graff-Radford, N., Petersen, R. C., Boeve, B. F., Lippa, C. F., Bigio, E. H., Mackenzie, I., Finger, E., Kertesz, A., Caselli, R. J., Gearing, M., Juncos, J. L., Ghetti, B., Spina, S., Bordelon, Y. M., Tourtellotte, W. W., Frosch, M. P., Vonsattel, J. P., Zarow, C., Beach, T. G., Albin, R. L., Lieberman, A. P., Lee, V. M., Trojanowski, J. Q., Van Deerlin, V. M., Bird, T. D., Galasko, D. R., Masliah, E., White, C. L., Troncoso, J. C., Hannequin, D., Boxer, A. L., Geschwind, M. D., Kumar, S., Mandelkow, E. M., Wszolek, Z. K., Uitti, R. J., Dickson, D. W., Haines, J. L., Mayeux, R., Pericak-Vance, M. A., Farrer, L. A., Alzheimer's Disease Genetics, C., Ross, O. A., Rademakers, R., Schellenberg, G. D., Miller, B. L., Mandelkow, E. & Geschwind, D. H. 2012. Evidence for a role of the rare p.A152T variant in MAPT in increasing the risk for FTD-spectrum and Alzheimer's diseases. *Hum Mol Genet,* 21**,** 3500-12.

Cras, P., van Harskamp, F., Hendriks, L., Ceuterick, C., van Duijn, C. M., Stefanko, S. Z., Hofman, A., Kros, J. M., Van Broeckhoven, C. & Martin, J. J. 1998. Presenile Alzheimer dementia characterized by amyloid angiopathy and large amyloid core type senile plaques in the APP 692Ala-->Gly mutation. *Acta Neuropathol,* 96**,** 253-60.

Dahlgren, K. N., Manelli, A. M., Stine, W. B., Jr., Baker, L. K., Krafft, G. A. & LaDu, M. J. 2002. Oligomeric and fibrillar species of amyloid-beta peptides differentially affect neuronal viability. *J Biol Chem,* 277**,** 32046-53.

Dahm, R. 2006. Alzheimer's discovery. *Curr Biol,* 16**,** R906-10.
Davidson, D., Chow, L. M., Fournel, M. & Veillette, A. 1992. Differential regulation of T cell antigen responsiveness by isoforms of the src-related tyrosine protein kinase p59fyn. *J Exp Med,* 175**,** 1483-92.
Davidson, D., Shi, X., Zhang, S., Wang, H., Nemer, M., Ono, N., Ohno, S., Yanagi, Y. & Veillette, A. 2004. Genetic evidence linking SAP, the X-linked lymphoproliferative gene product, to Src-related kinase FynT in TH2 cytokine regulation. *Immunity,* 21**,** 707-17.
Davidson, D., Viallet, J. & Veillette, A. 1994. Unique catalytic properties dictate the enhanced function of p59fynT, the hemopoietic cell-specific isoform of the Fyn tyrosine protein kinase, in T cells. *Mol Cell Biol,* 14**,** 4554-64.
Davis, K. L. 2002. Neuropsychopharmacology the fifth generation of progress : an official publication of the American College of Neuropsychopharmacology. Philadelphia: Lippincott Williams & Wilkins,.
De Strooper, B. & Chavez Gutierrez, L. 2015. Learning by failing: ideas and concepts to tackle gamma-secretases in Alzheimer's disease and beyond. *Annu Rev Pharmacol Toxicol,* 55**,** 419-37.
Desikan, R. S., Schork, A. J., Wang, Y., Witoelar, A., Sharma, M., McEvoy, L. K., Holland, D., Brewer, J. B., Chen, C. H., Thompson, W. K., Harold, D., Williams, J., Owen, M. J., O'Donovan, M. C., Pericak-Vance, M. A., Mayeux, R., Haines, J. L., Farrer, L. A., Schellenberg, G. D., Heutink, P., Singleton, A. B., Brice, A., Wood, N. W., Hardy, J., Martinez, M., Choi, S. H., DeStefano, A., Ikram, M. A., Bis, J. C., Smith, A., Fitzpatrick, A. L., Launer, L., van Duijn, C., Seshadri, S., Ulstein, I. D., Aarsland, D., Fladby, T., Djurovic, S., Hyman, B. T., Snaedal, J., Stefansson, H., Stefansson, K., Gasser, T., Andreassen, O. A. & Dale, A. M. 2015. Genetic overlap between Alzheimer's disease and Parkinson's disease at the MAPT locus. *Mol Psychiatry,* 20**,** 1588-95.
Dinarello, C. A. 2000. Proinflammatory cytokines. *Chest,* 118**,** 503-8.
Du, H., Guo, L., Fang, F., Chen, D., Sosunov, A. A., McKhann, G. M., Yan, Y., Wang, C., Zhang, H., Molkentin, J. D., Gunn-Moore, F. J., Vonsattel, J. P., Arancio, O., Chen, J. X. & Yan, S. D. 2008. Cyclophilin D deficiency attenuates mitochondrial and neuronal perturbation and ameliorates learning and memory in Alzheimer's disease. *Nat Med,* 14**,** 1097-105.
Eddleston, M. & Mucke, L. 1993. Molecular profile of reactive astrocytes--implications for their role in neurologic disease. *Neuroscience,* 54**,** 15-36.
Eicher, D. M., Tan, T. H., Rice, N. R., O'Shea, J. J. & Kennedy, I. C. 1994. Expression of v-src in T cells correlates with nuclear expression of NF-kappa B. *J Immunol,* 152**,** 2710-9.
El Khoury, J., Hickman, S. E., Thomas, C. A., Cao, L., Silverstein, S. C. & Loike, J. D. 1996. Scavenger receptor-mediated adhesion of microglia to beta-amyloid fibrils. *Nature,* 382**,** 716-9.
Farina, C., Aloisi, F. & Meinl, E. 2007. Astrocytes are active players in cerebral innate immunity. *Trends Immunol,* 28**,** 138-45.

Farlow, M. R. & Cummings, J. L. 2007. Effective pharmacologic management of Alzheimer's disease. *Am J Med,* 120**,** 388-97.
Fattori, E., Lazzaro, D., Musiani, P., Modesti, A., Alonzi, T. & Ciliberto, G. 1995. IL-6 expression in neurons of transgenic mice causes reactive astrocytosis and increase in ramified microglial cells but no neuronal damage. *Eur J Neurosci,* 7**,** 2441-9.
Fillit, H., Ding, W. H., Buee, L., Kalman, J., Altstiel, L., Lawlor, B. & Wolf-Klein, G. 1991. Elevated circulating tumor necrosis factor levels in Alzheimer's disease. *Neurosci Lett,* 129**,** 318-20.
Frei, K., Malipiero, U. V., Leist, T. P., Zinkernagel, R. M., Schwab, M. E. & Fontana, A. 1989. On the cellular source and function of interleukin 6 produced in the central nervous system in viral diseases. *Eur J Immunol,* 19**,** 689-94.
Fukumoto, H., Cheung, B. S., Hyman, B. T. & Irizarry, M. C. 2002. Beta-secretase protein and activity are increased in the neocortex in Alzheimer disease. *Arch Neurol,* 59**,** 1381-9.
Fuller, S., Münch, G. & Steele, M. 2009. Activated astrocytes: a therapeutic target in Alzheimer's disease? *Expert Rev Neurother,* 9**,** 1585-94.
Fuller, S., Steele, M. & Munch, G. 2010. Activated astroglia during chronic inflammation in Alzheimer's disease--do they neglect their neurosupportive roles? *Mutat Res,* 690**,** 40-9.
Gibson, R. M., Rothwell, N. J. & Le Feuvre, R. A. 2004. CNS injury: the role of the cytokine IL-1. *Vet J,* 168**,** 230-7.
Giulian, D., Haverkamp, L. J., Li, J., Karshin, W. L., Yu, J., Tom, D., Li, X. & Kirkpatrick, J. B. 1995. Senile plaques stimulate microglia to release a neurotoxin found in Alzheimer brain. *Neurochem Int,* 27**,** 119-37.
Glass, C. K., Saijo, K., Winner, B., Marchetto, M. C. & Gage, F. H. 2010. Mechanisms underlying inflammation in neurodegeneration. *Cell,* 140**,** 918-34.
Glatz, D. C., Rujescu, D., Tang, Y., Berendt, F. J., Hartmann, A. M., Faltraco, F., Rosenberg, C., Hulette, C., Jellinger, K., Hampel, H., Riederer, P., Moller, H. J., Andreadis, A., Henkel, K. & Stamm, S. 2006. The alternative splicing of tau exon 10 and its regulatory proteins CLK2 and TRA2-BETA1 changes in sporadic Alzheimer's disease. *J Neurochem,* 96**,** 635-44.
Goldgaber, D., Harris, H. W., Hla, T., Maciag, T., Donnelly, R. J., Jacobsen, J. S., Vitek, M. P. & Gajdusek, D. C. 1989. Interleukin 1 regulates synthesis of amyloid beta-protein precursor mRNA in human endothelial cells. *Proc Natl Acad Sci U S A,* 86**,** 7606-10.
Goldgaber, D., Lerman, M. I., McBride, O. W., Saffiotti, U. & Gajdusek, D. C. 1987. Characterization and chromosomal localization of a cDNA encoding brain amyloid of Alzheimer's disease. *Science,* 235**,** 877-80.
Goldsmith, J. F., Hall, C. G. & Atkinson, T. P. 2002. Identification of an alternatively spliced isoform of the fyn tyrosine kinase. *Biochem Biophys Res Commun,* 298**,** 501-4.
Gomez-Isla, T., Price, J. L., McKeel, D. W., Jr., Morris, J. C., Growdon, J. H. & Hyman, B. T. 1996. Profound loss of layer II entorhinal cortex neurons occurs in very mild Alzheimer's disease. *J Neurosci,* 16**,** 4491-500.

Gotz, J. & Ittner, L. M. 2008. Animal models of Alzheimer's disease and frontotemporal dementia. *Nat Rev Neurosci,* 9**,** 532-44.
Granic, I., Dolga, A. M., Nijholt, I. M., van Dijk, G. & Eisel, U. L. 2009. Inflammation and NF-kappaB in Alzheimer's disease and diabetes. *J Alzheimers Dis,* 16**,** 809-21.
Grant, S. G., O'Dell, T. J., Karl, K. A., Stein, P. L., Soriano, P. & Kandel, E. R. 1992. Impaired long-term potentiation, spatial learning, and hippocampal development in fyn mutant mice. *Science,* 258**,** 1903-10.
Griffin, W. S., Sheng, J. G., Roberts, G. W. & Mrak, R. E. 1995. Interleukin-1 expression in different plaque types in Alzheimer's disease: significance in plaque evolution. *J Neuropathol Exp Neurol,* 54**,** 276-81.
Griffin, W. S., Stanley, L. C., Ling, C., White, L., MacLeod, V., Perrot, L. J., White, C. L., 3rd & Araoz, C. 1989. Brain interleukin 1 and S-100 immunoreactivity are elevated in Down syndrome and Alzheimer disease. *Proc Natl Acad Sci U S A,* 86**,** 7611-5.
Guerreiro, R., Wojtas, A., Bras, J., Carrasquillo, M., Rogaeva, E., Majounie, E., Cruchaga, C., Sassi, C., Kauwe, J. S., Younkin, S., Hazrati, L., Collinge, J., Pocock, J., Lashley, T., Williams, J., Lambert, J. C., Amouyel, P., Goate, A., Rademakers, R., Morgan, K., Powell, J., St George-Hyslop, P., Singleton, A., Hardy, J. & Alzheimer Genetic Analysis, G. 2013. TREM2 variants in Alzheimer's disease. *N Engl J Med,* 368**,** 117-27.
Guo, J. L. & Lee, V. M. 2013. Neurofibrillary tangle-like tau pathology induced by synthetic tau fibrils in primary neurons over-expressing mutant tau. *FEBS Lett,* 587**,** 717-23.
Guo, Z., Cupples, L. A., Kurz, A., Auerbach, S. H., Volicer, L., Chui, H., Green, R. C., Sadovnick, A. D., Duara, R., DeCarli, C., Johnson, K., Go, R. C., Growdon, J. H., Haines, J. L., Kukull, W. A. & Farrer, L. A. 2000. Head injury and the risk of AD in the MIRAGE study. *Neurology,* 54**,** 1316-23.
Haass, C. M., E. 2010. Fyn-tau-amyloid: A toxic triad. *Cell,* 142**,** 356-358.
Hamill, C. E., Goldshmidt, A., Nicole, O., McKeon, R. J., Brat, D. J. & Traynelis, S. F. 2005. Special lecture: glial reactivity after damage: implications for scar formation and neuronal recovery. *Clin Neurosurg,* 52**,** 29-44.
Han, Y. & Brasier, A. R. 1997. Mechanism for biphasic rel A. NF-kappaB1 nuclear translocation in tumor necrosis factor alpha-stimulated hepatocytes. *J Biol Chem,* 272**,** 9825-32.
Hansson, E. 1984. Cellular composition of a cerebral hemisphere primary culture. *Neurochem Res,* 9**,** 153-72.
Hao, S. & Baltimore, D. 2009. The stability of mRNA influences the temporal order of the induction of genes encoding inflammatory molecules. *Nat Immunol,* 10**,** 281-8.
Hardy, J. & Selkoe, D. J. 2002. The amyloid hypothesis of Alzheimer's disease: progress and problems on the road to therapeutics. *Science,* 297**,** 353-6.
Harrison, S. C. 2003. Variation on an Src-like theme. *Cell,* 112**,** 737-40.
Heinrich, P. C., Castell, J. V. & Andus, T. 1990. Interleukin-6 and the acute phase response. *Biochem J,* 265**,** 621-36.

Helmuth, L. 2002. New therapies. New Alzheimer's treatments that may ease the mind. *Science,* 297**,** 1260-2.

Helmy, A., Antoniades, C. A., Guilfoyle, M. R., Carpenter, K. L. & Hutchinson, P. J. 2012. Principal component analysis of the cytokine and chemokine response to human traumatic brain injury. *PLoS One,* 7**,** e39677.

Heneka, M. T., Carson, M. J., El Khoury, J., Landreth, G. E., Brosseron, F., Feinstein, D. L., Jacobs, A. H., Wyss-Coray, T., Vitorica, J., Ransohoff, R. M., Herrup, K., Frautschy, S. A., Finsen, B., Brown, G. C., Verkhratsky, A., Yamanaka, K., Koistinaho, J., Latz, E., Halle, A., Petzold, G. C., Town, T., Morgan, D., Shinohara, M. L., Perry, V. H., Holmes, C., Bazan, N. G., Brooks, D. J., Hunot, S., Joseph, B., Deigendesch, N., Garaschuk, O., Boddeke, E., Dinarello, C. A., Breitner, J. C., Cole, G. M., Golenbock, D. T. & Kummer, M. P. 2015. Neuroinflammation in Alzheimer's disease. *Lancet Neurol,* 14**,** 388-405.

Hensley, K., Floyd, R. A., Zheng, N. Y., Nael, R., Robinson, K. A., Nguyen, X., Pye, Q. N., Stewart, C. A., Geddes, J., Markesbery, W. R., Patel, E., Johnson, G. V. & Bing, G. 1999. p38 kinase is activated in the Alzheimer's disease brain. *J Neurochem,* 72**,** 2053-8.

Heppner, F. L., Ransohoff, R. M. & Becher, B. 2015. Immune attack: the role of inflammation in Alzheimer disease. *Nat Rev Neurosci,* 16**,** 358-72.

Hernandez, P., Lee, G., Sjoberg, M. & Maccioni, R. B. 2009. Tau phosphorylation by cdk5 and Fyn in response to amyloid peptide Abeta (25-35): involvement of lipid rafts. *J Alzheimers Dis,* 16**,** 149-56.

Heyser, C. J., Masliah, E., Samimi, A., Campbell, I. L. & Gold, L. H. 1997. Progressive decline in avoidance learning paralleled by inflammatory neurodegeneration in transgenic mice expressing interleukin 6 in the brain. *Proc Natl Acad Sci U S A,* 94**,** 1500-5.

Hirota, H., Kiyama, H., Kishimoto, T. & Taga, T. 1996. Accelerated Nerve Regeneration in Mice by upregulated expression of interleukin (IL) 6 and IL-6 receptor after trauma. *J Exp Med,* 183**,** 2627-34.

Ho, G. J., Hashimoto, M., Adame, A., Izu, M., Alford, M. F., Thal, L. J., Hansen, L. A. & Masliah, E. 2005. Altered p59Fyn kinase expression accompanies disease progression in Alzheimer's disease: implications for its functional role. *Neurobiol Aging,* 26**,** 625-35.

Hoesel, B. & Schmid, J. A. 2013. The complexity of NF-kappaB signaling in inflammation and cancer. *Mol Cancer,* 12**,** 86.

Holmes, C., Cunningham, C., Zotova, E., Culliford, D. & Perry, V. H. 2011. Proinflammatory cytokines, sickness behavior, and Alzheimer disease. *Neurology,* 77**,** 212-8.

Holmes, C., Cunningham, C., Zotova, E., Woolford, J., Dean, C., Kerr, S., Culliford, D. & Perry, V. H. 2009. Systemic inflammation and disease progression in Alzheimer disease. *Neurology,* 73**,** 768-74.

Hu, J., Nakano, H., Sakurai, H. & Colburn, N. H. 2004. Insufficient p65 phosphorylation at S536 specifically contributes to the lack of NF-kappaB activation and transformation in resistant JB6 cells. *Carcinogenesis,* 25**,** 1991-2003.

Huang da, W., Sherman, B. T. & Lempicki, R. A. 2009a. Bioinformatics enrichment tools: paths toward the comprehensive functional analysis of large gene lists. *Nucleic Acids Res,* 37**,** 1-13.

Huang da, W., Sherman, B. T. & Lempicki, R. A. 2009b. Systematic and integrative analysis of large gene lists using DAVID bioinformatics resources. *Nat Protoc,* 4**,** 44-57.

Huang, W. C., Chen, J. J., Inoue, H. & Chen, C. C. 2003. Tyrosine phosphorylation of I-kappa B kinase alpha/beta by protein kinase C-dependent c-Src activation is involved in TNF-alpha-induced cyclooxygenase-2 expression. *J Immunol,* 170**,** 4767-75.

Huell, M., Strauss, S., Volk, B., Berger, M. & Bauer, J. 1995. Interleukin-6 is present in early stages of plaque formation and is restricted to the brains of Alzheimer's disease patients. *Acta Neuropathol,* 89**,** 544-51.

Iqbal, K., Liu, F., Gong, C. X., Alonso Adel, C. & Grundke-Iqbal, I. 2009. Mechanisms of tau-induced neurodegeneration. *Acta Neuropathol,* 118**,** 53-69.

Ishii, K. J., Coban, C., Kato, H., Takahashi, K., Torii, Y., Takeshita, F., Ludwig, H., Sutter, G., Suzuki, K., Hemmi, H., Sato, S., Yamamoto, M., Uematsu, S., Kawai, T., Takeuchi, O. & Akira, S. 2006. A Toll-like receptor-independent antiviral response induced by double-stranded B-form DNA. *Nat Immunol,* 7**,** 40-8.

Islam, O., Gong, X., Rose-John, S. & Heese, K. 2009. Interleukin-6 and neural stem cells: more than gliogenesis. *Mol Biol Cell,* 20**,** 188-99.

Itagaki, S., McGeer, P. L., Akiyama, H., Zhu, S. & Selkoe, D. 1989. Relationship of microglia and astrocytes to amyloid deposits of Alzheimer disease. *J Neuroimmunol,* 24**,** 173-82.

Itoh, S., Lemay, S., Osawa, M., Che, W., Duan, Y., Tompkins, A., Brookes, P. S., Sheu, S. S. & Abe, J. 2005. Mitochondrial Dok-4 recruits Src kinase and regulates NF-kappaB activation in endothelial cells. *J Biol Chem,* 280**,** 26383-96.

Ittner, L. M. K., Y. D.; Delerue, F.; Bi, M.; Gladbach, A.; van Eersel, J.; Wolfing, H.; Chieng, B. C.; Christie, M. J.; Napier, I. A.; Eckert, A.; Staufenbiel, M.; Hardeman, E.; Gotz, J. 2010. Dendritic function of tau mediates amyloid-beta toxicity in Alzheimer's disease mouse models. *Cell,* 142**,** 387-97.

Iwatsubo, T., Mann, D. M., Odaka, A., Suzuki, N. & Ihara, Y. 1995. Amyloid beta protein (A beta) deposition: A beta 42(43) precedes A beta 40 in Down syndrome. *Ann Neurol,* 37**,** 294-9.

Ji, K., Akgul, G., Wollmuth, L. P. & Tsirka, S. E. 2013. Microglia actively regulate the number of functional synapses. *PLoS One,* 8**,** e56293.

Kahn, M. A. & De Vellis, J. 1994. Regulation of an oligodendrocyte progenitor cell line by the interleukin-6 family of cytokines. *Glia,* 12**,** 87-98.

Kaltschmidt, B., Uherek, M., Volk, B., Baeuerle, P. A. & Kaltschmidt, C. 1997. Transcription factor NF-kappaB is activated in primary neurons by amyloid beta peptides and in neurons surrounding early plaques from patients with Alzheimer disease. *Proc Natl Acad Sci U S A,* 94**,** 2642-7.

Kaminsky, Y. G., Marlatt, M. W., Smith, M. A. & Kosenko, E. A. 2010. Subcellular and metabolic examination of amyloid-b peptides in

Alzheimer disease pathogenesis: evidence for Ab_{25-35}. *Exp Neurol,* 221**,** 26-37.
Karch, C. M. & Goate, A. M. 2015. Alzheimer's disease risk genes and mechanisms of disease pathogenesis. *Biol Psychiatry,* 77**,** 43-51.
Karin, M. 1999. How NF-kappaB is activated: the role of the IkappaB kinase (IKK) complex. *Oncogene,* 18**,** 6867-74.
Kawakami, T., Kawakami, Y., Aaronson, S. A. & Robbins, K. C. 1988. Acquisition of transforming properties by FYN, a normal SRC-related human gene. *Proc Natl Acad Sci U S A,* 85**,** 3870-4.
Kawakami, T., Pennington, C. Y. & Robbins, K. C. 1986. Isolation and oncogenic potential of a novel human src-like gene. *Mol Cell Biol,* 6**,** 4195-201.
Kefalas, P., Brown, T. R. & Brickell, P. M. 1995. Signalling by the p60c-src family of protein-tyrosine kinases. *Int J Biochem Cell Biol,* 27**,** 551-63.
Kemler, I. & Fontana, A. 1999. Role of IkappaBalpha and IkappaBbeta in the biphasic nuclear translocation of NF-kappaB in TNFalpha-stimulated astrocytes and in neuroblastoma cells. *Glia,* 26**,** 212-20.
Kempe, S., Kestler, H., Lasar, A. & Wirth, T. 2005. NF-kappaB controls the global pro-inflammatory response in endothelial cells: evidence for the regulation of a pro-atherogenic program. *Nucleic Acids Res,* 33**,** 5308-19.
Kimura, K. & Yamamoto, M. 1996. Modification of the alternative splicing process of testosterone-repressed prostate message-2 (TRPM-2) gene by protein synthesis inhibitors and heat shock treatment. *Biochim Biophys Acta,* 1307**,** 83-8.
Kitazawa, M., Oddo, S., Yamasaki, T. R., Green, K. N. & LaFerla, F. M. 2005. Lipopolysaccharide-induced inflammation exacerbates tau pathology by a cyclin-dependent kinase 5-mediated pathway in a transgenic model of Alzheimer's disease. *J Neurosci,* 25**,** 8843-53.
Klein, R. S. 2004. Regulation of neuroinflammation: the role of CXCL10 in lymphocyte infiltration during autoimmune encephalomyelitis. *J Cell Biochem,* 92**,** 213-22.
Klein, W. L., Krafft, G. A. & Finch, C. E. 2001. Targeting small Abeta oligomers: the solution to an Alzheimer's disease conundrum? *Trends Neurosci,* 24**,** 219-24.
Knapp, S., Hareng, L., Rijneveld, A. W., Bresser, P., van der Zee, J. S., Florquin, S., Hartung, T. & van der Poll, T. 2004. Activation of neutrophils and inhibition of the proinflammatory cytokine response by endogenous granulocyte colony-stimulating factor in murine pneumococcal pneumonia. *J Infect Dis,* 189**,** 1506-15.
Knight, D. 2001. Leukaemia inhibitory factor (LIF): a cytokine of emerging importance in chronic airway inflammation. *Pulm Pharmacol Ther,* 14**,** 169-76.
Ko, L., Sheu, K. F., Young, O. & Blass, J. P. 1990. Induction of epitopes associated with neurofibrillary tangles in clonal mouse neuroblastoma (S20Y) cells. *Acta Neuropathol,* 81**,** 30-40.
Koffie, R. M., Hyman, B. T. & Spires-Jones, T. L. 2011. Alzheimer's disease: synapses gone cold. *Mol Neurodegener,* 6**,** 63.
Kosik, K. S. & Finch, E. A. 1987. MAP2 and tau segregate into dendritic and axonal domains after the elaboration of morphologically distinct

neurites: an immunocytochemical study of cultured rat cerebrum. *J Neurosci,* 7**,** 3142-53.
Kramer-Albers, E. M. & White, R. 2011. From axon-glial signalling to myelination: the integrating role of oligodendroglial Fyn kinase. *Cell Mol Life Sci,* 68**,** 2003-12.
Krishna, M. & Narang, H. 2008. The complexity of mitogen-activated protein kinases (MAPKs) made simple. *Cell Mol Life Sci,* 65**,** 3525-44.
Kubo, T., Kumagae, Y., Miller, C. A. & Kaneko, I. 2003. Beta-amyloid racemized at the Ser26 residue in the brains of patients with Alzheimer disease: implications in the pathogenesis of Alzheimer disease. *J Neuropathol Exp Neurol,* 62**,** 248-59.
Lacor, P. N., Buniel, M. C., Furlow, P. W., Clemente, A. S., Velasco, P. T., Wood, M., Viola, K. L. & Klein, W. L. 2007. Abeta oligomer-induced aberrations in synapse composition, shape, and density provide a molecular basis for loss of connectivity in Alzheimer's disease. *J Neurosci,* 27**,** 796-807.
Ladner, K. J., Caligiuri, M. A. & Guttridge, D. C. 2003. Tumor necrosis factor-regulated biphasic activation of NF-kappa B is required for cytokine-induced loss of skeletal muscle gene products. *J Biol Chem,* 278**,** 2294-303.
Lai, M. K., Esiri, M. M. & Tan, M. G. 2014. Genome-wide profiling of alternative splicing in Alzheimer's disease. *Genom Data,* 2**,** 290-2.
Lambert, M. P., Barlow, A. K., Chromy, B. A., Edwards, C., Freed, R., Liosatos, M., Morgan, T. E., Rozovsky, I., Trommer, B., Viola, K. L., Wals, P., Zhang, C., Finch, C. E., Krafft, G. A. & Klein, W. L. 1998. Diffusible, nonfibrillar ligands derived from Abeta1-42 are potent central nervous system neurotoxins. *Proc Natl Acad Sci U S A,* 95**,** 6448-53.
Larson, M., Sherman, M. A., Amar, F., Nuvolone, M., Schneider, J. A., Bennett, D. A., Aguzzi, A. & Lesne, S. E. 2012. The complex PrP^{c}-Fyn couples human oligomeric Ab with pathological tau changes in Alzheimer's disease. *J Neurosci,* 32**,** 16857-71.
Lawrence, T. 2009. The nuclear factor NF-kappaB pathway in inflammation. *Cold Spring Harb Perspect Biol,* 1**,** a001651.
Lee, C., Low, C. Y., Francis, P. T., Attems, J., Wong, P. T., Lai, M. K. & Tan, M. G. 2015. An isoform-specific role of FynT tyrosine kinase in Alzheimer's disease. *J Neurochem*.
Lee, G., Thangavel, R., Sharma, V. M., Litersky, J. M., Bhaskar, K., Fang, S. M., Do, L. H., Andreadis, A., Van Hoesen, G. & Ksiezak-Reding, H. 2004. Phosphorylation of tau by fyn: implications for Alzheimer's disease. *J Neurosci,* 24**,** 2304-12.
Lee, G. N., S. T.; Gard, D. L.; Band, H.; Panchamoorthy, G. 1998. Tau interacts with src-family non-receptor tyrosine kinases. *J Cell Sci,* 111**,** 3167-3177.
Lee, G. T., R.; Sharma, V. M.; Litersky, J. M.; Bhaskar, K.; Fang, S. M.; Do, L. H.; Andreadis, A.; Van Hoesen, G.; Ksiezak-Reding, H. 2004. Phosphorylation of tau by fyn: Implications for Alzheimer's disease. *Journal of Neuroscience,* 24**,** 2304-2312.

Lichtenstein, M. P., Carriba, P., Masgrau, R., Pujol, A. & Galea, E. 2010. Staging anti-inflammatory therapy in Alzheimer's disease. *Front Aging Neurosci,* 2**,** 142.

Liu, B., Gao, H. M., Wang, J. Y., Jeohn, G. H., Cooper, C. L. & Hong, J. S. 2002. Role of nitric oxide in inflammation-mediated neurodegeneration. *Ann N Y Acad Sci,* 962**,** 318-31.

Lorenzo, A. & Yankner, B. A. 1994. Beta-amyloid neurotoxicity requires fibril formation and is inhibited by congo red. *Proc Natl Acad Sci U S A,* 91**,** 12243-7.

Luheshi, N. M., Kovacs, K. J., Lopez-Castejon, G., Brough, D. & Denes, A. 2011. Interleukin-1alpha expression precedes IL-1beta after ischemic brain injury and is localised to areas of focal neuronal loss and penumbral tissues. *J Neuroinflammation,* 8**,** 186.

Luheshi, N. M., Rothwell, N. J. & Brough, D. 2009. Dual functionality of interleukin-1 family cytokines: implications for anti-interleukin-1 therapy. *Br J Pharmacol,* 157**,** 1318-29.

Luo, X. G. & Chen, S. D. 2012. The changing phenotype of microglia from homeostasis to disease. *Transl Neurodegener,* 1**,** 9.

Lynch, K. W. & Weiss, A. 2000. A model system for activation-induced alternative splicing of CD45 pre-mRNA in T cells implicates protein kinase C and Ras. *Mol Cell Biol,* 20**,** 70-80.

Martin Prince, A. W., Maëlenn Guerchet, Gemma-Claire Ali, Yu-Tzu Wu, Matthew Prina 2015. World Alzheimer Report 2015: The Global Impact of Dementia. London.

Marz, P., Cheng, J. G., Gadient, R. A., Patterson, P. H., Stoyan, T., Otten, U. & Rose-John, S. 1998. Sympathetic neurons can produce and respond to interleukin 6. *Proc Natl Acad Sci U S A,* 95**,** 3251-6.

Masters, C. L., Simms, G., Weinman, N. A., Multhaup, G., McDonald, B. L. & Beyreuther, K. 1985. Amyloid plaque core protein in Alzheimer disease and Down syndrome. *Proc Natl Acad Sci U S A,* 82**,** 4245-9.

Matsuoka, Y., Picciano, M., La Francois, J. & Duff, K. 2001. Fibrillar beta-amyloid evokes oxidative damage in a transgenic mouse model of Alzheimer's disease. *Neuroscience,* 104**,** 609-13.

Mattioli, I., Sebald, A., Bucher, C., Charles, R. P., Nakano, H., Doi, T., Kracht, M. & Schmitz, M. L. 2004. Transient and selective NF-kappa B p65 serine 536 phosphorylation induced by T cell costimulation is mediated by I kappa B kinase beta and controls the kinetics of p65 nuclear import. *J Immunol,* 172**,** 6336-44.

McCarthy, K. D. & de Vellis, J. 1980. Preparation of separate astroglial and oligodendroglial cell cultures from rat cerebral tissue. *J Cell Biol,* 85**,** 890-902.

McCoy, M. K. & Tansey, M. G. 2008. TNF signaling inhibition in the CNS: implications for normal brain function and neurodegenerative disease. *J Neuroinflammation,* 5**,** 45.

McLaurin, J. & Chakrabartty, A. 1997. Characterization of the interactions of Alzheimer beta-amyloid peptides with phospholipid membranes. *Eur J Biochem,* 245**,** 355-63.

Medeiros, R. & LaFerla, F. M. 2013. Astrocytes: conductors of the Alzheimer disease neuroinflammatory symphony. *Exp Neurol,* 239**,** 133-8.

Menting, K. W. & Claassen, J. A. 2014. beta-secretase inhibitor; a promising novel therapeutic drug in Alzheimer's disease. *Front Aging Neurosci,* 6**,** 165.

Millucci, L., Ghezzi, L., Bernardini, G. & Santucci, A. 2010. Conformations and biological activities of amyloid beta peptide 25-35. *Curr Protein Pept Sci,* 11**,** 54-67.

Minami, S. S., Clifford, T. G., Hoe, H. S., Matsuoka, Y. & Rebeck, G. W. 2012. Fyn knock-down increases Abeta, decreases phospho-tau, and worsens spatial learning in 3xTg-AD mice. *Neurobiol Aging,* 33**,** 825 e15-24.

Mirra, S. S., Heyman, A., McKeel, D., Sumi, S. M., Crain, B. J., Brownlee, L. M., Vogel, F. S., Hughes, J. P., van Belle, G. & Berg, L. 1991. The Consortium to Establish a Registry for Alzheimer's Disease (CERAD). Part II. Standardization of the neuropathologic assessment of Alzheimer's disease. *Neurology,* 41**,** 479-486.

Mittelbronn, M., Dietz, K., Schluesener, H. J. & Meyermann, R. 2001. Local distribution of microglia in the normal adult human central nervous system differs by up to one order of magnitude. *Acta Neuropathol,* 101**,** 249-55.

Moynagh, P. N. 2005. The interleukin-1 signalling pathway in astrocytes: a key contributor to inflammation in the brain. *J Anat,* 207**,** 265-9.

Murakami, N., Sakata, Y. & Watanabe, T. 1990. Central action sites of interleukin-1 beta for inducing fever in rabbits. *J Physiol,* 428**,** 299-312.

Musiek, E. S. & Holtzman, D. M. 2015. Three dimensions of the amyloid hypothesis: time, space and 'wingmen'. *Nat Neurosci,* 18**,** 800-6.

Nautiyal, K. M., Ribeiro, A. C., Pfaff, D. W. & Silver, R. 2008. Brain mast cells link the immune system to anxiety-like behavior. *Proc Natl Acad Sci U S A,* 105**,** 18053-7.

Nygaard, H. B., van Dyck, C. H. & Strittmatter, S. M. 2014. Fyn kinase inhibition as a novel therapy for Alzheimer's disease. *Alzheimers Res Ther,* 6**,** 8.

Nygaard, H. B., Wagner, A. F., Bowen, G. S., Good, S. P., MacAvoy, M. G., Strittmatter, K. A., Kaufman, A. C., Rosenberg, B. J., Sekine-Konno, T., Varma, P., Chen, K., Koleske, A. J., Reiman, E. M., Strittmatter, S. M. & van Dyck, C. H. 2015. A phase Ib multiple ascending dose study of the safety, tolerability, and central nervous system availability of AZD0530 (saracatinib) in Alzheimer's disease. *Alzheimers Res Ther,* 7**,** 35.

O'Callaghan, J. P., Sriram, K. & Miller, D. B. 2008. Defining "neuroinflammation". *Ann N Y Acad Sci,* 1139**,** 318-30.

Oakley, H., Cole, S. L., Logan, S., Maus, E., Shao, P., Craft, J., Guillozet-Bongaarts, A., Ohno, M., Disterhoft, J., Van Eldik, L., Berry, R. & Vassar, R. 2006. Intraneuronal beta-amyloid aggregates, neurodegeneration, and neuron loss in transgenic mice with five familial Alzheimer's disease mutations: potential factors in amyloid plaque formation. *J Neurosci,* 26**,** 10129-40.

Olmos, G. & Llado, J. 2014. Tumor necrosis factor alpha: a link between neuroinflammation and excitotoxicity. *Mediators Inflamm,* 2014**,** 861231.

Osterhout, D. J., Wolven, A., Wolf, R. M., Resh, M. D. & Chao, M. V. 1999. Morphological differentiation of oligodendrocytes requires activation of Fyn tyrosine kinase. *J Cell Biol,* 145**,** 1209-18.

Pahl, H. L. 1999. Activators and target genes of Rel/NF-kappaB transcription factors. *Oncogene,* 18**,** 6853-66.

Pan, W., Yu, C., Hsuchou, H., Zhang, Y. & Kastin, A. J. 2008. Neuroinflammation facilitates LIF entry into brain: role of TNF. *Am J Physiol Cell Physiol,* 294**,** C1436-42.

Panicker, N., Saminathan, H., Jin, H., Neal, M., Harischandra, D. S., Gordon, R., Kanthasamy, K., Lawana, V., Sarkar, S., Luo, J., Anantharam, V., Kanthasamy, A. G. & Kanthasamy, A. 2015. Fyn Kinase Regulates Microglial Neuroinflammatory Responses in Cell Culture and Animal Models of Parkinson's Disease. *J Neurosci,* 35**,** 10058-77.

Parsons, S. J. & Parsons, J. T. 2004. Src family kinases, key regulators of signal transduction. *Oncogene,* 23**,** 7906-9.

Peel, A. L., Sorscher, N., Kim, J. Y., Galvan, V., Chen, S. & Bredesen, D. E. 2004. Tau phosphorylation in Alzheimer's disease: potential involvement of an APP-MAP kinase complex. *Neuromolecular Med,* 5**,** 205-18.

Pekny, M. & Nilsson, M. 2005. Astrocyte activation and reactive gliosis. *Glia,* 50**,** 427-34.

Perego, C., Vanoni, C., Bossi, M., Massari, S., Basudev, H., Longhi, R. & Pietrini, G. 2000. The GLT-1 and GLAST glutamate transporters are expressed on morphologically distinct astrocytes and regulated by neuronal activity in primary hippocampal cocultures. *J Neurochem,* 75**,** 1076-84.

Perl, D. P. 2010. Neuropathology of Alzheimer's disease. *Mt Sinai J Med,* 77**,** 32-42.

Perry, R. T., Collins, J. S., Wiener, H., Acton, R. & Go, R. C. 2001. The role of TNF and its receptors in Alzheimer's disease. *Neurobiol Aging,* 22**,** 873-83.

Perry, V. H. 1998. A revised view of the central nervous system microenvironment and major histocompatibility complex class II antigen presentation. *J Neuroimmunol,* 90**,** 113-21.

Perry, V. H., Cunningham, C. & Holmes, C. 2007. Systemic infections and inflammation affect chronic neurodegeneration. *Nat Rev Immunol,* 7**,** 161-7.

Petersen, R. C., Smith, G. E., Waring, S. C., Ivnik, R. J., Tangalos, E. G. & Kokmen, E. 1999. Mild cognitive impairment: clinical characterization and outcome. *Arch Neurol,* 56**,** 303-8.

Picard, C., Gabert, J., Olive, D. & Collette, Y. 2004. Altered splicing in hematological malignancies reveals a tissue-specific translational block of the Src-family tyrosine kinase fyn brain isoform expression. *Leukemia,* 18**,** 1737-9.

Pickering, M., Cumiskey, D. & O'Connor, J. J. 2005. Actions of TNF-alpha on glutamatergic synaptic transmission in the central nervous system. *Exp Physiol,* 90**,** 663-70.

Piette, F., Belmin, J., Vincent, H., Schmidt, N., Pariel, S., Verny, M., Marquis, C., Mely, J., Hugonot-Diener, L., Kinet, J. P., Dubreuil, P., Moussy, A. & Hermine, O. 2011. Masitinib as an adjunct therapy for mild-to-

moderate Alzheimer's disease: a randomised, placebo-controlled phase 2 trial. *Alzheimers Res Ther,* 3**,** 16.

Pike, C. J., Burdick, D., Walencewicz, A. J., Glabe, C. G. & Cotman, C. W. 1993. Neurodegeneration induced by beta-amyloid peptides in vitro: the role of peptide assembly state. *J Neurosci,* 13**,** 1676-87.

Pike, C. J., Cummings, B. J. & Cotman, C. W. 1992. b-Amyloid induces neuritic dystrophy in vitro: similarities with Alzheimer pathology. *Neuroreport,* 3**,** 769-72.

Pike, C. J., Cummings, B. J., Monzavi, R. & Cotman, C. W. 1994. b-amyloid-induced changes in cultured astrocytes parallel reactive astrocytosis associated with senile plaques in Alzheimer's disease. *Neuroscience,* 63**,** 517-31.

Pike, C. J., Vaughan, P. J., Cunningham, D. D. & Cotman, C. W. 1996. Thrombin attenuates neuronal cell death and modulates astrocyte reactivity induced by beta-amyloid in vitro. *J Neurochem,* 66**,** 1374-82.

Platt, T. L., Reeves, V. L. & Murphy, M. P. 2013. Transgenic models of Alzheimer's disease: better utilization of existing models through viral transgenesis. *Biochim Biophys Acta,* 1832**,** 1437-48.

Qiu, C., Kivipelto, M. & von Strauss, E. 2009. Epidemiology of Alzheimer's disease: occurrence, determinants, and strategies toward intervention. *Dialogues Clin Neurosci,* 11**,** 111-28.

Quan, N., He, L. & Lai, W. 2003. Intraventricular infusion of antagonists of IL-1 and TNF alpha attenuates neurodegeneration induced by the infection of Trypanosoma brucei. *J Neuroimmunol,* 138**,** 92-8.

Radde, R., Bolmont, T., Kaeser, S. A., Coomaraswamy, J., Lindau, D., Stoltze, L., Calhoun, M. E., Jaggi, F., Wolburg, H., Gengler, S., Haass, C., Ghetti, B., Czech, C., Holscher, C., Mathews, P. M. & Jucker, M. 2006. Abeta42-driven cerebral amyloidosis in transgenic mice reveals early and robust pathology. *EMBO Rep,* 7**,** 940-6.

Rajasekaran, K., Kumar, P., Schuldt, K. M., Peterson, E. J., Vanhaesebroeck, B., Dixit, V., Thakar, M. S. & Malarkannan, S. 2013. Signaling by Fyn-ADAP via the Carma1-Bcl-10-MAP3K7 signalosome exclusively regulates inflammatory cytokine production in NK cells. *Nat Immunol,* 14**,** 1127-36.

Ramesh, G., MacLean, A. G. & Philipp, M. T. 2013. Cytokines and chemokines at the crossroads of neuroinflammation, neurodegeneration, and neuropathic pain. *Mediators Inflamm,* 2013**,** 480739.

Ramirez-Carrozzi, V. R., Nazarian, A. A., Li, C. C., Gore, S. L., Sridharan, R., Imbalzano, A. N. & Smale, S. T. 2006. Selective and antagonistic functions of SWI/SNF and Mi-2beta nucleosome remodeling complexes during an inflammatory response. *Genes Dev,* 20**,** 282-96.

Ransohoff, R. M. & Brown, M. A. 2012. Innate immunity in the central nervous system. *J Clin Invest,* 122**,** 1164-71.

Reinhard, C., Hebert, S. S. & De Strooper, B. 2005. The amyloid-beta precursor protein: integrating structure with biological function. *EMBO J,* 24**,** 3996-4006.

Resh, M. D. 1998. Fyn, a Src family tyrosine kinase. *Int J Biochem Cell Biol,* 30**,** 1159-62.

Ring, S., Weyer, S. W., Kilian, S. B., Waldron, E., Pietrzik, C. U., Filippov, M. A., Herms, J., Buchholz, C., Eckman, C. B., Korte, M., Wolfer, D. P. & Muller, U. C. 2007. The secreted beta-amyloid precursor protein ectodomain APPs alpha is sufficient to rescue the anatomical, behavioral, and electrophysiological abnormalities of APP-deficient mice. *J Neurosci,* 27**,** 7817-26.

Ringheim, G. E., Szczepanik, A. M., Petko, W., Burgher, K. L., Zhu, S. Z. & Chao, C. C. 1998. Enhancement of beta-amyloid precursor protein transcription and expression by the soluble interleukin-6 receptor/interleukin-6 complex. *Brain Res Mol Brain Res,* 55**,** 35-44.

Rivest, S. 2015. TREM2 enables amyloid beta clearance by microglia. *Cell Res,* 25**,** 535-6.

Roberson, E. D. H., B.; Yoo, J. W.; Yao, J.; Chin, J.; Yan, F.; Wu, T.; Hamto, P.; Devidze, N.; Yu, G. Q.; Palop, J. J.; Noebels, J. L.; Mucke, L. 2011. Amyloid-beta/Fyn-induced synaptic, network, and cognitive impairments depend on tau levels in multiple mouse models of Alzheimer's disease. *J Neurosci,* 31**,** 700-11.

Rothwell, N. J. 1991. Functions and mechanisms of interleukin 1 in the brain. *Trends Pharmacol Sci,* 12**,** 430-6.

Rowan, M. J., Klyubin, I., Wang, Q., Hu, N. W. & Anwyl, R. 2007. Synaptic memory mechanisms: Alzheimer's disease amyloid beta-peptide-induced dysfunction. *Biochem Soc Trans,* 35**,** 1219-23.

Roy, S. M., Grum-Tokars, V. L., Schavocky, J. P., Saeed, F., Staniszewski, A., Teich, A. F., Arancio, O., Bachstetter, A. D., Webster, S. J., Van Eldik, L. J., Minasov, G., Anderson, W. F., Pelletier, J. C. & Watterson, D. M. 2015. Targeting human central nervous system protein kinases: An isoform selective p38alphaMAPK inhibitor that attenuates disease progression in Alzheimer's disease mouse models. *ACS Chem Neurosci,* 6**,** 666-80.

Rubio-Perez, J. M. & Morillas-Ruiz, J. M. 2012. A review: inflammatory process in Alzheimer's disease, role of cytokines. *ScientificWorldJournal,* 2012**,** 756357.

Sakai, Y., Rawson, C., Lindburg, K. & Barnes, D. 1990. Serum and transforming growth factor beta regulate glial fibrillary acidic protein in serum-free-derived mouse embryo cells. *Proc Natl Acad Sci U S A,* 87**,** 8378-82.

Sakurai, H., Chiba, H., Miyoshi, H., Sugita, T. & Toriumi, W. 1999. IkappaB kinases phosphorylate NF-kappaB p65 subunit on serine 536 in the transactivation domain. *J Biol Chem,* 274**,** 30353-6.

Scheff, S. W., Price, D. A., Schmitt, F. A. & Mufson, E. J. 2006. Hippocampal synaptic loss in early Alzheimer's disease and mild cognitive impairment. *Neurobiol Aging,* 27**,** 1372-84.

Scheller, J., Chalaris, A., Schmidt-Arras, D. & Rose-John, S. 2011. The pro- and anti-inflammatory properties of the cytokine interleukin-6. *Biochim Biophys Acta,* 1813**,** 878-88.

Schousboe, A. & Waagepetersen, H. S. 2005. Role of astrocytes in glutamate homeostasis: implications for excitotoxicity. *Neurotox Res,* 8**,** 221-5.

Schwamborn, J., Lindecke, A., Elvers, M., Horejschi, V., Kerick, M., Rafigh, M., Pfeiffer, J., Prullage, M., Kaltschmidt, B. & Kaltschmidt, C. 2003.

Microarray analysis of tumor necrosis factor alpha induced gene expression in U373 human glioblastoma cells. *BMC Genomics,* 4**,** 46.
Schwartz, M. & Shechter, R. 2010. Systemic inflammatory cells fight off neurodegenerative disease. *Nat Rev Neurol,* 6**,** 405-10.
Scimemi, A., Meabon, J. S., Woltjer, R. L., Sullivan, J. M., Diamond, J. S. & Cook, D. G. 2013. Amyloid-beta1-42 slows clearance of synaptically released glutamate by mislocalizing astrocytic GLT-1. *J Neurosci,* 33**,** 5312-8.
Sekine, Y., Takeda, K. & Ichijo, H. 2006. The ASK1-MAP kinase signaling in ER stress and neurodegenerative diseases. *Curr Mol Med,* 6**,** 87-97.
Selkoe, D. J. 1991. The molecular pathology of Alzheimer's disease. *Neuron,* 6**,** 487-98.
Selkoe, D. J. 2002. Deciphering the genesis and fate of amyloid beta-protein yields novel therapies for Alzheimer disease. *J Clin Invest,* 110**,** 1375-81.
Semba, K., Nishizawa, M., Miyajima, N., Yoshida, M. C., Sukegawa, J., Yamanashi, Y., Sasaki, M., Yamamoto, T. & Toyoshima, K. 1986. yes-related protooncogene, syn, belongs to the protein-tyrosine kinase family. *Proc Natl Acad Sci U S A,* 83**,** 5459-63.
Serrano-Pozo, A., Frosch, M. P., Masliah, E. & Hyman, B. T. 2011. Neuropathological alterations in Alzheimer disease. *Cold Spring Harb Perspect Med,* 1**,** a006189.
Seward, M. E., Swanson, E., Norambuena, A., Reimann, A., Cochran, J. N., Li, R., Roberson, E. D. & Bloom, G. S. 2013. Amyloid-beta signals through tau to drive ectopic neuronal cell cycle re-entry in Alzheimer's disease. *J Cell Sci,* 126**,** 1278-86.
Shaftel, S. S., Griffin, W. S. & O'Banion, M. K. 2008. The role of interleukin-1 in neuroinflammation and Alzheimer disease: an evolving perspective. *J Neuroinflammation,* 5**,** 7.
Sheng, J. G., Mrak, R. E. & Griffin, W. S. 1997. Neuritic plaque evolution in Alzheimer's disease is accompanied by transition of activated microglia from primed to enlarged to phagocytic forms. *Acta Neuropathol,* 94**,** 1-5.
Shibata, N., Ohnuma, T., Takahashi, T., Baba, H., Ishizuka, T., Ohtsuka, M., Ueki, A., Nagao, M. & Arai, H. 2002. Effect of IL-6 polymorphism on risk of Alzheimer disease: genotype-phenotype association study in Japanese cases. *Am J Med Genet,* 114**,** 436-9.
Shiomi, A. & Usui, T. 2015. Pivotal roles of GM-CSF in autoimmunity and inflammation. *Mediators Inflamm,* 2015**,** 568543.
Shirazi, S. K. & Wood, J. G. 1993. The protein tyrosine kinase, fyn, in Alzheimer's disease pathology. *Neuroreport,* 4**,** 435-7.
Silverman, A. J., Sutherland, A. K., Wilhelm, M. & Silver, R. 2000. Mast cells migrate from blood to brain. *J Neurosci,* 20**,** 401-8.
Simpson, J. E., Ince, P. G., Lace, G., Forster, G., Shaw, P. J., Matthews, F., Savva, G., Brayne, C., Wharton, S. B., Function, M. R. C. C. & Ageing Neuropathology Study, G. 2010. Astrocyte phenotype in relation to Alzheimer-type pathology in the ageing brain. *Neurobiol Aging,* 31**,** 578-90.
Sonoda, Y., Ozawa, T., Aldape, K. D., Deen, D. F., Berger, M. S. & Pieper, R. O. 2001. Akt pathway activation converts anaplastic astrocytoma to

glioblastoma multiforme in a human astrocyte model of glioma. *Cancer research,* 61**,** 6674-8.
Soria, G. & Ben-Baruch, A. 2008. The inflammatory chemokines CCL2 and CCL5 in breast cancer. *Cancer Lett,* 267**,** 271-85.
Sperber, B. R., Boyle-Walsh, E. A., Engleka, M. J., Gadue, P., Peterson, A. C., Stein, P. L., Scherer, S. S. & McMorris, F. A. 2001. A unique role for Fyn in CNS myelination. *J Neurosci,* 21**,** 2039-47.
Sperling, R. A., Aisen, P. S., Beckett, L. A., Bennett, D. A., Craft, S., Fagan, A. M., Iwatsubo, T., Jack, C. R., Jr., Kaye, J., Montine, T. J., Park, D. C., Reiman, E. M., Rowe, C. C., Siemers, E., Stern, Y., Yaffe, K., Carrillo, M. C., Thies, B., Morrison-Bogorad, M., Wagster, M. V. & Phelps, C. H. 2011. Toward defining the preclinical stages of Alzheimer's disease: recommendations from the National Institute on Aging-Alzheimer's Association workgroups on diagnostic guidelines for Alzheimer's disease. *Alzheimers Dement,* 7**,** 280-92.
Spranger, M., Lindholm, D., Bandtlow, C., Heumann, R., Gnahn, H., Naher-Noe, M. & Thoenen, H. 1990. Regulation of Nerve Growth Factor (NGF) Synthesis in the Rat Central Nervous System: Comparison between the Effects of Interleukin-1 and Various Growth Factors in Astrocyte Cultures and in vivo. *Eur J Neurosci,* 2**,** 69-76.
Steardo, L., Jr., Bronzuoli, M. R., Iacomino, A., Esposito, G., Steardo, L. & Scuderi, C. 2015. Does neuroinflammation turn on the flame in Alzheimer's disease? Focus on astrocytes. *Front Neurosci,* 9**,** 259.
Steele, M. L. & Robinson, S. R. 2012. Reactive astrocytes give neurons less support: implications for Alzheimer's disease. *Neurobiol Aging,* 33**,** 423 e1-13.
Stellwagen, D. & Malenka, R. C. 2006. Synaptic scaling mediated by glial TNF-alpha. *Nature,* 440**,** 1054-9.
Stepanichev, M. Y., Zdobnova, I. M., Zarubenko, II, Lazareva, N. A. & Gulyaeva, N. V. 2006. Studies of the effects of central administration of beta-amyloid peptide (25-35): pathomorphological changes in the Hippocampus and impairment of spatial memory. *Neurosci Behav Physiol,* 36**,** 101-6.
Stewart, W. F., Kawas, C., Corrada, M. & Metter, E. J. 1997. Risk of Alzheimer's disease and duration of NSAID use. *Neurology,* 48**,** 626-32.
Strauss, S., Bauer, J., Ganter, U., Jonas, U., Berger, M. & Volk, B. 1992. Detection of interleukin-6 and alpha 2-macroglobulin immunoreactivity in cortex and hippocampus of Alzheimer's disease patients. *Lab Invest,* 66**,** 223-30.
Streit, W. J., Mrak, R. E. & Griffin, W. S. 2004. Microglia and neuroinflammation: a pathological perspective. *J Neuroinflammation,* 1**,** 14.
Subramaniam, M., Chong, S. A., Vaingankar, J. A., Abdin, E., Chua, B. Y., Chua, H. C., Eng, G. K., Heng, D., Hia, S. B., Huang, W., Jeyagurunathana, A., Kua, J., Lee, S. P., Mahendran, R., Magadi, H., Malladi, S., McCrone, P., Pang, S., Picco, L., Sagayadevan, V., Sambasivam, R., Seng, K. H., Seow, E., Shafie, S., Shahwan, S., Tan, L. L., Yap, M., Zhang, Y., Ng, L. L. & Prince, M. 2015. Prevalence of

Dementia in People Aged 60 Years and Above: Results from the WiSE Study. *J Alzheimers Dis,* 45**,** 1127-38.
Sun, A., Liu, M., Nguyen, X. V. & Bing, G. 2003. P38 MAP kinase is activated at early stages in Alzheimer's disease brain. *Exp Neurol,* 183**,** 394-405.
Swanson, R. A., Liu, J., Miller, J. W., Rothstein, J. D., Farrell, K., Stein, B. A. & Longuemare, M. C. 1997. Neuronal regulation of glutamate transporter subtype expression in astrocytes. *J Neurosci,* 17**,** 932-40.
Tamashiro, T. T., Dalgard, C. L. & Byrnes, K. R. 2012. Primary microglia isolation from mixed glial cell cultures of neonatal rat brain tissue. *J Vis Exp***,** e3814.
Tan, M. G., Chua, W. T., Esiri, M. M., Smith, A. D., Vinters, H. V. & Lai, M. K. 2010. Genome wide profiling of altered gene expression in the neocortex of Alzheimer's disease. *J Neurosci Res,* 88**,** 1157-69.
Tarkowski, E., Andreasen, N., Tarkowski, A. & Blennow, K. 2003. Intrathecal inflammation precedes development of Alzheimer's disease. *J Neurol Neurosurg Psychiatry,* 74**,** 1200-5.
Tarkowski, E., Blennow, K., Wallin, A. & Tarkowski, A. 1999. Intracerebral production of tumor necrosis factor-alpha, a local neuroprotective agent, in Alzheimer disease and vascular dementia. *J Clin Immunol,* 19**,** 223-30.
Tay, S., Hughey, J. J., Lee, T. K., Lipniacki, T., Quake, S. R. & Covert, M. W. 2010. Single-cell NF-kappaB dynamics reveal digital activation and analogue information processing. *Nature,* 466**,** 267-71.
Terai, K., Matsuo, A. & McGeer, P. L. 1996. Enhancement of immunoreactivity for NF-kappa B in the hippocampal formation and cerebral cortex of Alzheimer's disease. *Brain Res,* 735**,** 159-68.
Terry, R. D., Masliah, E., Salmon, D. P., Butters, N., DeTeresa, R., Hill, R., Hansen, L. A. & Katzman, R. 1991. Physical basis of cognitive alterations in Alzheimer's disease: synapse loss is the major correlate of cognitive impairment. *Ann Neurol,* 30**,** 572-80.
Thompson, W. L. & Van Eldik, L. J. 2009. Inflammatory cytokines stimulate the chemokines CCL2/MCP-1 and CCL7/MCP-3 through NFkB and MAPK dependent pathways in rat astrocytes [corrected]. *Brain Res,* 1287**,** 47-57.
Tian, B., Nowak, D. E. & Brasier, A. R. 2005. A TNF-induced gene expression program under oscillatory NF-kappaB control. *BMC Genomics,* 6**,** 137.
Tilley, L., Morgan, K. & Kalsheker, N. 1998. Genetic risk factors in Alzheimer's disease. *Mol Pathol,* 51**,** 293-304.
Timotijevic, G., Mostarica Stojkovic, M. & Miljkovic, D. 2012. CXCL12: role in neuroinflammation. *Int J Biochem Cell Biol,* 44**,** 838-41.
Tobinick, E., Gross, H., Weinberger, A. & Cohen, H. 2006. TNF-alpha modulation for treatment of Alzheimer's disease: a 6-month pilot study. *MedGenMed,* 8**,** 25.
Tokutake, T., Kasuga, K., Yajima, R., Sekine, Y., Tezuka, T., Nishizawa, M. & Ikeuchi, T. 2012. Hyperphosphorylation of Tau induced by naturally secreted amyloid-beta at nanomolar concentrations is modulated by insulin-dependent Akt-GSK3beta signaling pathway. *J Biol Chem,* 287**,** 35222-33.

Tollervey, J. R., Wang, Z., Hortobagyi, T., Witten, J. T., Zarnack, K., Kayikci, M., Clark, T. A., Schweitzer, A. C., Rot, G., Curk, T., Zupan, B., Rogelj, B., Shaw, C. E. & Ule, J. 2011. Analysis of alternative splicing associated with aging and neurodegeneration in the human brain. *Genome Res,* 21**,** 1572-82.

Toro, V. C., Tehranian, R., Zetterstrom, M., Eriksson, G., Langel, U., Bartfai, T. & Iverfeld, K. 2001. Increased gene expression of interleukin-1alpha and interleukin-6 in rat primary glial cells induced by beta-amyloid fragment. *J Mol Neurosci,* 17**,** 341-50.

Tullai, J. W., Schaffer, M. E., Mullenbrock, S., Sholder, G., Kasif, S. & Cooper, G. M. 2007. Immediate-early and delayed primary response genes are distinct in function and genomic architecture. *J Biol Chem,* 282**,** 23981-95.

Turner, P. R., O'Connor, K., Tate, W. P. & Abraham, W. C. 2003. Roles of amyloid precursor protein and its fragments in regulating neural activity, plasticity and memory. *Prog Neurobiol,* 70**,** 1-32.

Um, J. W., Kaufman, A. C., Kostylev, M., Heiss, J. K., Stagi, M., Takahashi, H., Kerrisk, M. E., Vortmeyer, A., Wisniewski, T., Koleske, A. J., Gunther, E. C., Nygaard, H. B. & Strittmatter, S. M. 2013. Metabotropic glutamate receptor 5 is a coreceptor for Alzheimer abeta oligomer bound to cellular prion protein. *Neuron,* 79**,** 887-902.

Um, J. W., Nygaard, H. B., Heiss, J. K., Kostylev, M. A., Stagi, M., Vortmeyer, A., Wisniewski, T., Gunther, E. C. & Strittmatter, S. M. 2012. Alzheimer amyloid-beta oligomer bound to postsynaptic prion protein activates Fyn to impair neurons. *Nat Neurosci,* 15**,** 1227-35.

Um, J. W. S., S. M. 2012. Amyloid-ss induced signaling by cellular prion protein and Fyn kinase in Alzheimer disease. *Prion,* 6.

Usardi, A., Pooler, A. M., Seereeram, A., Reynolds, C. H., Derkinderen, P., Anderton, B., Hanger, D. P., Noble, W. & Williamson, R. 2011. Tyrosine phosphorylation of tau regulates its interactions with Fyn SH2 domains, but not SH3 domains, altering the cellular localization of tau. *FEBS J,* 278**,** 2927-37.

van der Meer, M. J., Sweep, C. G., Rijnkels, C. E., Pesman, G. J., Tilders, F. J., Kloppenborg, P. W. & Hermus, A. R. 1996. Acute stimulation of the hypothalamic-pituitary-adrenal axis by IL-1 beta, TNF alpha and IL-6: a dose response study. *J Endocrinol Invest,* 19**,** 175-82.

Van Wagoner, N. J., Oh, J. W., Repovic, P. & Benveniste, E. N. 1999. Interleukin-6 (IL-6) production by astrocytes: autocrine regulation by IL-6 and the soluble IL-6 receptor. *J Neurosci,* 19**,** 5236-44.

Vela, J. M., Molina-Holgado, E., Arevalo-Martin, A., Almazan, G. & Guaza, C. 2002. Interleukin-1 regulates proliferation and differentiation of oligodendrocyte progenitor cells. *Mol Cell Neurosci,* 20**,** 489-502.

Vergeli, M., mazzanti, B., Ballerini, C., Gran, B., Amaducci, L. & Massacesi, L. 1995. Transforming growth factor-beta 1 inhibits the proliferation of rat astrocytes induced by serum and growth factors. *J Neurosci Res,* 40**,** 127-33.

Verstrepen, L., Bekaert, T., Chau, T. L., Tavernier, J., Chariot, A. & Beyaert, R. 2008. TLR-4, IL-1R and TNF-R signaling to NF-kappaB: variations on a common theme. *Cell Mol Life Sci,* 65**,** 2964-78.

Villegas-Llerena, C., Phillips, A., Garcia-Reitboeck, P., Hardy, J. & Pocock, J. M. 2015. Microglial genes regulating neuroinflammation in the progression of Alzheimer's disease. *Curr Opin Neurobiol,* 36**,** 74-81.

Vlad, S. C., Miller, D. R., Kowall, N. W. & Felson, D. T. 2008. Protective effects of NSAIDs on the development of Alzheimer disease. *Neurology,* 70**,** 1672-7.

Vogel, C. & Marcotte, E. M. 2012. Insights into the regulation of protein abundance from proteomic and transcriptomic analyses. *Nat Rev Genet,* 13**,** 227-32.

Vom Berg, J., Prokop, S., Miller, K. R., Obst, J., Kalin, R. E., Lopategui-Cabezas, I., Wegner, A., Mair, F., Schipke, C. G., Peters, O., Winter, Y., Becher, B. & Heppner, F. L. 2012. Inhibition of IL-12/IL-23 signaling reduces Alzheimer's disease-like pathology and cognitive decline. *Nat Med,* 18**,** 1812-9.

Vukic, V., Callaghan, D., Walker, D., Lue, L. F., Liu, Q. Y., Couraud, P. O., Romero, I. A., Weksler, B., Stanimirovic, D. B. & Zhang, W. 2009. Expression of inflammatory genes induced by beta-amyloid peptides in human brain endothelial cells and in Alzheimer's brain is mediated by the JNK-AP1 signaling pathway. *Neurobiol Dis,* 34**,** 95-106.

Walz, W. & Lang, M. K. 1998. Immunocytochemical evidence for a distinct GFAP-negative subpopulation of astrocytes in the adult rat hippocampus. *Neurosci Lett,* 257**,** 127-30.

Wang, H., Ren, C. H., Gunawardana, C. G. & Schmitt-Ulms, G. 2013a. Overcoming barriers and thresholds - signaling of oligomeric Ab through the prion protein to Fyn. *Mol Neurodegener,* 8**,** 24.

Wang, J. Z., Xia, Y. Y., Grundke-Iqbal, I. & Iqbal, K. 2013b. Abnormal hyperphosphorylation of tau: sites, regulation, and molecular mechanism of neurofibrillary degeneration. *J Alzheimers Dis,* 33 Suppl 1**,** S123-39.

Wang, Y., Cella, M., Mallinson, K., Ulrich, J. D., Young, K. L., Robinette, M. L., Gilfillan, S., Krishnan, G. M., Sudhakar, S., Zinselmeyer, B. H., Holtzman, D. M., Cirrito, J. R. & Colonna, M. 2015. TREM2 lipid sensing sustains the microglial response in an Alzheimer's disease model. *Cell,* 160**,** 1061-71.

Weinblatt, M. E., Kremer, J. M., Bankhurst, A. D., Bulpitt, K. J., Fleischmann, R. M., Fox, R. I., Jackson, C. G., Lange, M. & Burge, D. J. 1999. A trial of etanercept, a recombinant tumor necrosis factor receptor:Fc fusion protein, in patients with rheumatoid arthritis receiving methotrexate. *N Engl J Med,* 340**,** 253-9.

Weingarten, M. D., Lockwood, A. H., Hwo, S. Y. & Kirschner, M. W. 1975. A protein factor essential for microtubule assembly. *Proc Natl Acad Sci U S A,* 72**,** 1858-62.

Weinmann, A. S., Plevy, S. E. & Smale, S. T. 1999. Rapid and selective remodeling of a positioned nucleosome during the induction of IL-12 p40 transcription. *Immunity,* 11**,** 665-75.

Wiedemann, C. 2009. An intimate relationship. *Nat Rev Neurosci,* 10**,** 318.

Wolfe, M. S. 2009. Tau mutations in neurodegenerative diseases. *J Biol Chem,* 284**,** 6021-5.

Wyss-Coray, T., Loike, J. D., Brionne, T. C., Lu, E., Anankov, R., Yan, F., Silverstein, S. C. & Husemann, J. 2003. Adult mouse astrocytes degrade amyloid-beta in vitro and in situ. *Nat Med,* 9**,** 453-7.

Xia, D. & Gotz, J. 2014. Premature lethality, hyperactivity, and aberrant phosphorylation in transgenic mice expressing a constitutively active form of Fyn. *Front Mol Neurosci,* 7**,** 40.

Xu, W., Doshi, A., Lei, M., Eck, M. J. & Harrison, S. C. 1999. Crystal structures of c-Src reveal features of its autoinhibitory mechanism. *Mol Cell,* 3**,** 629-38.

Xu, W., Harrison, S. C. & Eck, M. J. 1997. Three-dimensional structure of the tyrosine kinase c-Src. *Nature,* 385**,** 595-602.

Xu, W., Tan, L., Wang, H. F., Jiang, T., Tan, M. S., Tan, L., Zhao, Q. F., Li, J. Q., Wang, J. & Yu, J. T. 2015. Meta-analysis of modifiable risk factors for Alzheimer's disease. *J Neurol Neurosurg Psychiatry,* 86**,** 1299-306.

Yaka, R., Phamluong, K. & Ron, D. 2003. Scaffolding of Fyn kinase to the NMDA receptor determines brain region sensitivity to ethanol. *J Neurosci,* 23**,** 3623-32.

Yang, K. B., J.; Trepanier, C. H.; Lei, G.; Jackson, M. F.; MacDonald, J. F. 2011. Fyn, a potential target for Alzheimer's disease. *J Alzheimers Dis,* 27**,** 243-52.

Yang, Y., Gozen, O., Watkins, A., Lorenzini, I., Lepore, A., Gao, Y., Vidensky, S., Brennan, J., Poulsen, D., Won Park, J., Li Jeon, N., Robinson, M. B. & Rothstein, J. D. 2009. Presynaptic regulation of astroglial excitatory neurotransmitter transporter GLT1. *Neuron,* 61**,** 880-94.

Ye, J., Coulouris, G., Zaretskaya, I., Cutcutache, I., Rozen, S. & Madden, T. L. 2012. Primer-BLAST: a tool to design target-specific primers for polymerase chain reaction. *BMC Bioinformatics,* 13**,** 134.

Yoshiyama, Y., Higuchi, M., Zhang, B., Huang, S. M., Iwata, N., Saido, T. C., Maeda, J., Suhara, T., Trojanowski, J. Q. & Lee, V. M. 2007. Synapse loss and microglial activation precede tangles in a P301S tauopathy mouse model. *Neuron,* 53**,** 337-51.

Zheng, H. & Koo, E. H. 2011. Biology and pathophysiology of the amyloid precursor protein. *Mol Neurodegener,* 6**,** 27.

Zheng, W. H., Bastianetto, S., Mennicken, F., Ma, W. & Kar, S. 2002. Amyloid beta peptide induces tau phosphorylation and loss of cholinergic neurons in rat primary septal cultures. *Neuroscience,* 115**,** 201-11.

APPENDICES

Published paper during candidature, contributing to Thesis

Lee, C., Low, C.Y., Francis, P.T., Attems, J., Wong, P.T., Lai, M.K., & Tan, M.G., 2016. An isoform-specific role of FynT tyrosine kinase in Alzheimer's disease. Journal of Neurochemistry, 136**,** 637-650. (Attached behind)

Poster presentations

Lee, CL., Low, C.YB., Lai, M.KP., Tan, M.GK., 2013. An isoform specific role for Fyn tyrosine kinase (FynT) in astrocyte activation. The 11th International Conference AD/PD, Florence, Italy.

Lee, CL., Low, C.YB., Lai, M.KP., Tan, M.GK., 2013. An isoform specific role for Fyn tyrosine kinase (FynT) in astrocyte. International Conference on Pharmacology and Drug Development, Singapore.

Lee, CL., Tan, D.XW., Low, C.YB., Lai, M.KP., Tan, M.GK., 2015. The role of FynT tyrosine kinase in astrocytes pertaining to neuroinflammation in Alzheimer's Disease. Alzheimer's Association International Conference 2015, Washington, DC, USA.

Other published paper during candidature

Tan, M.G., **Lee, C**., Lee, J.H., Francis, P.T., Williams, R.J., Ramírez, M.J., Chen, C.P., Wong, P.T., Lai, M.K., 2013. Decreased rabphilin 3A immunoreactivity in Alzheimer's disease is associated with Aβ burden. Neurochemistry international 64, 29-36.

Journal of Neurochemistry

JOURNAL OF NEUROCHEMISTRY | 2016 | 136 | 637–650 doi: 10.1111/jnc.13429

ORIGINAL ARTICLE

An isoform-specific role of FynT tyrosine kinase in Alzheimer's disease

Chingli Lee,*,† Clara Y. B. Low,† Paul T. Francis,‡ Johannes Attems,§ Peter T.-H. Wong,* Mitchell K.P. Lai*,‡ and Michelle G.K. Tan*,†

*Department of Pharmacology, Yong Loo Lin School of Medicine, National University of Singapore, Kent Ridge, Singapore

†Department of Clinical Research, Singapore General Hospital, Outram, Singapore

‡Wolfson Centre for Age-Related Diseases, King's College London, London, UK

§Institute of Neuroscience, Newcastle University, Campus for Aging and Vitality, Newcastle upon Tyne, UK

Abstract

Alzheimer's disease (AD) is the leading cause of dementia in old age and is characterized by the accumulation of β-amyloid plaques and neurofibrillary tangles (NFT). Recent studies suggest that Fyn tyrosine kinase forms part of a toxic triad with β-amyloid and tau in the disease process. However, it is not known whether Fyn is associated with the pathological features of AD in an isoform-specific manner. In this study, we identified selective up-regulation of the alternative-spliced FynT isoform with no change in FynB in the AD neocortex. Furthermore, gene ontology term enrichment analyses and cell type-specific localization of FynT immunoreactivity suggest that FynT up-regulation was associated with neurofibrillary degeneration and reactive astrogliosis. Interestingly, significantly increased FynT in NFT-bearing neurons was concomitant to decreased FynB immunoreactivity, suggesting an involvement of alternative splicing in NFT formation. Furthermore, cultured cells of astrocytic origin have higher FynT to FynB ratio compared to those of neuronal origin. Lastly, primary rat mixed neuron-astrocyte cultures treated with $A\beta_{25-35}$ showed selective up-regulation of FynT expression in activated astrocytes. Our findings point to an isoform-specific role of FynT in modulating neurofibrillary degeneration and reactive astrogliosis in AD.

Keywords: Alzheimer's disease, dementia, Fyn tyrosine kinase, neurofibrillary tangle, reactive astrogliosis.

J. Neurochem. (2016) **136**, 637–650.

Alzheimer's disease (AD) is a complex, progressive neurodegenerative disease characterized by cognitive impairments, neuropsychiatric behaviors and loss of functional independence. Its neuropathological hallmarks include extracellular β-amyloid (Aβ)-containing neuritic plaques, intracellular neurofibrillary tangles (NFT) consisting of abnormally phosphorylated tau protein, along with neuronal loss, synaptic dysfunction, gliosis, and neuroinflammation (Whitehouse *et al.* 1982; Selkoe 2002; Perrin *et al.* 2009). Research on the amyloid cascade hypothesis, which ascribes a major pathogenic role to the accumulation of neurotoxic Aβ aggregates, has been central in advancing our understanding of AD (Reitz 2012). Recent evidence suggests that Fyn, a member of the Src family tyrosine kinases, forms part of a 'toxic triad' (Haass and Mandelkow 2010) together with Aβ and tau in exacerbating AD. For example, Fyn was shown to be an essential mediator in signaling cascades induced by binding of Aβ to postsynaptic prion protein, leading to altered phosphorylation and translocation of glutamatergic receptors and tau, together with associated impairment of synaptic plasticity and excitotoxicity (Ittner *et al.* 2010; Roberson *et al.* 2011; Yang *et al.* 2011; Pooler

Received July 30, 2015; revised manuscript received November 5, 2015; accepted November 6, 2015.

Address correspondence and reprint requests to Mitchell K. P. Lai, Department of Pharmacology, Yong Loo Lin School of Medicine, National University of Singapore, Unit 09-01, Centre for Translational Medicine (MD6), 14 Medical Drive, Singapore 117599. E-mail: mitchell.lai@dementia-research.org (or) Michelle G. K. Tan, Department of Clinical Research, Singapore General Hospital, The Academia, Level 9, Discovery Tower, 20 College Road, 169856 Singapore. E-mail: michelle.tan.g.k@sgh.com.sg

Abbreviations used: AD, Alzheimer's disease; Aβ, β-amyloid; GFAP, glial fibrillary acidic protein; GLAST, glutamate aspartate transporter; GO, gene ontology; IF, immunofluorescence; MAP2, microtubule-associated protein 2; MMSE, mini-mental state examination; NFT, neurofibrillary tangles; NGS, normal goat serum; NP, neuritic plaques.

et al. 2012; Um et al. 2012; Wang et al. 2013; Xia and Gotz 2014).

Fyn exists in two major alternatively spliced isoforms, with FynB as the predominant isoform found in the brain while FynT is mainly expressed in cells of hematopoietic origin (Cooke and Perlmutter 1989; Resh 1998). FynB and FynT differ exclusively within a short sequence of 55 and 52 amino acids, respectively, spanning the end of the SH2 region, the SH2-kinase linker segment and the beginning of the tyrosine kinase domain (Brignatz et al. 2009). Structural analyses of intramolecular interactions of Fyn revealed that the linker region of FynB engages the SH3 domain with higher affinity and favors a closed auto-inhibited conformation as compared to FynT (Brignatz et al. 2009). Correspondingly, FynT exhibits enhanced kinase activity compared to FynB (Davidson et al. 1994; Brignatz et al. 2009). Furthermore, biological functions specific to FynT, such as mobilization of cytosolic calcium and T cell-stimulated lymphokine secretion have been identified (Davidson et al. 1992, 1994).

A putative pathogenic role of Fyn in AD has been suggested by studies showing exacerbation of disease by Fyn over-expression and amelioration by Fyn depletion in transgenic models (Lambert et al. 1998; Chin et al. 2004, 2005). Increased Fyn expression in postmortem AD brain has also been demonstrated by the detection of intense Fyn immunoreactivity in NFT-bearing neurons (Shirazi and Wood 1993; Ho et al. 2005). However, no study to date has attempted to delineate possible isoform-specific roles of Fyn in AD. Interestingly, an analysis of alternative splicing events associated with AD using our previously published exon microarray data revealed Fyn to be differentially spliced in the AD temporal cortex (Lai et al. 2014), and this study now shows that the FynT isoform is specifically up-regulated in AD while FynB remains unchanged. Our data also suggest that FynT alterations may be associated with NFT and reactive astrogliosis, thus pointing to Fyn's isoform-specific involvement in AD.

Materials and methods

Brain tissues

Postmortem brain tissues were derived from twelve AD patients (five women, seven men) and eight elderly controls (three women, five men) originally recruited by OPTIMA (Oxford Project to Investigate Memory and Ageing, http://www.medsci.ox.ac.uk/optima). Additional control tissues (n = 3; from two women and one man) were obtained from the newcastle brain tissue resource, Newcastle Brain Tissue Resource (NBTR), Newcastle upon Tyne, UK, both sites being part of the UK Brains for Dementia Research (BDR) network (see Table S1). Informed consent had been obtained from the patients' next-of-kin before collection of brains, and appropriate Institutional Review Board approvals were obtained for work carried out in Singapore (Singhealth IRB 2011/576/A). One hemisphere of each subject was processed for pathological assessments, including confirmation of AD using the Consortium to Establish a Registry for AD (CERAD) criteria (Mirra et al. 1991). Additionally, neocortical tissue sections of all AD subjects also underwent semi-quantitative scoring (0–3) of neuritic plaques (NP) and NFT using a methenamine silver/modified Palmgren stain as previously described (Lai et al. 2001). The majority of AD subjects (ten of twelve) were assessed to be Braak stage V–VI (Braak and Braak 1991) while none of the controls had higher than Braak stage I–II (Table S1). Fresh frozen tissues from prefrontal (Brodmann area BA9) and temporal (BA22) cortices of the contralateral hemisphere were dissected and stored at −80°C in TRIzol® reagent (ThermoFisher Scientific, Waltham, MA, USA) before processing for real-time reverse transcription polymerase chain reaction (RT-PCR). Blocks of BA9 was also frozen in OCT medium for subsequent sectioning and immunofluorescence (IF) staining. A subset (BA22 in eight controls and eight AD) of this study cohort has been included in a previous study profiling genome-wide changes in gene expression and alternative splicing in AD (Tan et al. 2010; Lai et al. 2014).

Exon microarray data analysis and gene ontology (GO) term enrichment analysis

To identify differential expression of alternate splice-variants in AD from our previously reported microarray studies (Tan et al. 2010), a dataset was generated and analyzed using the Exon workflows of the Partek Genomics Suite 6.6 software (Partek Inc, MO, USA) (Lai et al. 2014). This dataset is publicly available from the Gene Expression Omnibus (GEO) website (http://www.ncbi.nlm.nih.gov/geo/) using accession number GSE37264. The Gene View module of the Genomic Suite was used to localize differentially expressed probesets in the context of the transcript variants of Fyn, and probesets which were highly correlated with both FynT-specific probesets (2969915 and 2969916, with Pearson's product-moment coefficients, $R > \pm 0.65$) were retrieved. Genes with at least two representative probesets found in the list of 497 FynT-positively correlated genes and 692 FynT-negatively correlated genes were included in Gene Ontology (GO) term enrichment analysis using DAVID Bioinformatics Resouces 6.7 (http://david.abcc.ncifcrf.gov/) with Benjamini's enrichment p-values adjustment for multiple testing, using false discovery rate of 5% (Huang et al. 2009a,b), before submitting to a web server REVIGO (http://revigo.irb.hr/) (Supek et al. 2011) to remove redundant GO terms.

Antibodies

Custom-made rabbit polyclonal antibodies raised specifically against FynB and FynT were generated by GenScript Corporation (Piscataway, NJ, USA). FynB and FynT-specific rabbit polyclonal antibodies were prepared against synthetic peptide CRESLQLIKRLGNGQ (NP_002028, residues 268–281) and QTSGLAKDAWEVAC (NP_694592, residues 252–264), respectively, which are conserved among human, mouse, and rat. Both peptides were conjugated with keyhole limpet hemocyanin to increase immunogenicity for immunization. Pre-immune serum and test bleed serum from rabbits after third immunization with enzyme-linked immunosorbent assay (ELISA) titer of 1 : 256 000 were tested for FynB and FynT-specificity using western blot analyses. The antibodies with low background and high specificity were affinity purified and dissolved in phosphate buffer saline (PBS), pH 7.4 at a

concentration of 0.428 mg/ml with 0.02% sodium azide as preservative. Aliquots were stored at −80°C until use. Dilutions and sources of other commercially available primary and secondary antibodies are listed in Table S2.

Primary rat mixed cortical culture and $A\beta_{25-35}$ treatment

Primary rat mixed neuron-astrocyte cortical cultures were established from embryonic (E18) Sprague Dawley rats after protocol approval from the Singhealth Institutional Animal Care and Use Committee (2014/SHS/950). Briefly, cortices were dissected and meninges were removed in ice cold Hank's balanced salt solution, then treated with 0.2 mg/mL trypsin and 40 μg/mL deoxyribonuclease in Hank's balanced salt solution supplemented with 7.4 mM glucose, 1 mM sodium pyruvate, 10 mM HEPES, 4.2 mM $NaHCO_3$, 1.2 mM $MgSO_4$, and 0.3% bovine serum albumin at 37°C for 5 min. The trypsin digestion was terminated by the addition of trypsin inhibitor before mechanical trituration using fire-polished Pasteur pipettes. Dissociated cells were then centrifuged and resuspended in Neurobasal (NB) medium supplemented with 10% heat-inactivated fetal bovine serum, 2.5% B27 and 0.25% GlutaMAX™ with penicillin-streptomycin (all reagents from ThermoFisher Scientific, Waltham, MA, USA). Cells were seeded at densities of approximately 1×10^6 cells per well in 6-well plates coated with 0.1 mg/mL poly-D-lysine and cultured at 37°C in a humidified 5% CO_2 incubator. Two hours after adherence of the cells, the medium was replaced with NB medium in the absence of fetal bovine serum. After 7 days, medium was replaced with NB medium minus phenol red supplemented with 2.5% B27 without antioxidants, 0.25% GlutaMAX™ and penicillin-streptomycin. For Aβ incubation assays, $A\beta_{25-35}$ and $A\beta_{35-25}$ (Sigma Aldrich, St. Louis, MO, USA) were dissolved in distilled water at a stock concentration of 1 mM and aged by incubating at 37°C for 24 h. Primary rat mixed cortical cultures were treated with or without 20 μM of $A\beta_{25-35}$ or $A\beta_{35-25}$ and harvested for analysis at 24 h and 48 h. Unless otherwise stated, all cell-based data were obtained from 3 to 4 independent experiments.

Real-time RT-PCR

Two micrograms of total RNA was extracted from human brain tissue or primary rat cultures using TRIzol® reagent (Life Technologies) according to manufacturer's instructions, then reverse-transcribed (RT) using High-Capacity cDNA RT kit (ThermoFisher Scientific). Semi-quantitative measurements of gene expression were performed on the Applied Biosystems 7500 Fast Real-time PCR system (ThermoFisher Scientific) using either SYBR Green PCR master mix (ThermoFisher Scientific) or GoTaq® qPCR Master Mix (Promega, Fitchburg, WI, USA). The primer sequences used in this study are listed in Table S3. All real-time RT-PCR assays were performed in duplicate. Standard curves of each gene were generated independently by 10× serial dilution of template DNA. The relative signal intensity of each sample was calculated according to the corresponding standard curve. Normalization was performed in each sample by dividing the relative signal intensity of gene of interest to 18S rRNA (human brain samples), or geometric mean of β-actin, GAPDH and 18S rRNA (primary rat culture).

Determination of FynT to FynB ratios

Using a pair of common primers spanning the alternative spliced exon of Fyn (forward: 5′-GGCCCAGTTTGAAACACTTC-3′; reverse: 5′-GTGTTTCCATTCCAGGTACC-3′ with 5′ labeled 6-FAM), both FynB and FynT isoforms were amplified under 23 cycles of RT-PCR (see above) with cDNA from human brain tissues and cultured cells. Then, 1 μL of PCR product and 1 μL of ABI Genescan 500 Rox size standard (Applied Biosystems, NY, USA) were added to 12 μL of Hi-Di™ formamide (Applied Biosystems). After denaturing at 95°C for 4 min and snapped cooling on ice, samples were assayed by capillary electrophoresis using the PRISM-310 Genetic Analyzer (ThermoFisher Scientific). The product size and quantity of each DNA amplicon in the capillary electropherograms were analyzed, using GeneScan analysis software (ThermoFisher Scientific). Peak areas of FynT (219 bp DNA amplicon) and FynB (228 bp DNA amplicon) in each electropherogram were translated into expression level and used to determine ratios of FynT to FynB expression.

Immunofluorescence (IF) staining and image analysis

10 or 20 μm brain sections from frozen control or AD postmortem brain tissues or cultured cells grown on coverslips were fixed with 3.7% formaldehyde for 10 min at 25°C. Due to limited tissue availability, only BA9 were used for IF staining. Brain tissues were post-fixed and permeabilized in ice-cold acetone: methanol (1 : 1) for 10 min, whereas cultured cells were permeabilized in 0.1% Triton-X-100 for 5 min at 25°C. After washing twice with PBS, tissue sections or cells on coverslips were blocked with 10% normal goat serum in PBS at 25°C for 1 h and incubated overnight with primary antibodies at stated dilutions (see Table S2) in 10% normal goat serum/PBS at 4°C. Detection was performed using Alexa Flour® 488 (green) or 555 (red-orange)-conjugated secondary antibody after incubated for 45 min at 25°C. Tissue sections were treated with autofluorescence eliminator reagent (Merck Millipore, Darmstadt, Germany) according to the manufacturer's instructions. Lastly, sections or culture cells were washed and mounted with Vectashield mounting medium with DAPI nuclear stain (Vector Laboratories, Cambridgeshire, UK). Samples were visualized and captured using Nikon A1R confocal microscopy system (Nikon, Japan), and images were analyzed using Nikon NIS-Element software (Nikon, Japan). Five representative images per sample from three AD and three control brains were analyzed using 'Object Count' to obtain total cell count as well as mean fluorescence intensity of individual cell in each channel. For primary culture imaging, three representative images per treatment derived from four independent experiments were analyzed using the 'Threshold' function to obtain the mean fluorescence intensity of ROI (Regions of interest) after applying a fixed signal intensity cut-off across all samples.

Statistical analyses

Bioinformatics analysis of the microarray database has been described in its own section (see above). For neurochemical, pathologic variables and gene expression levels, the differences between AD and control samples were analyzed using Mann–Whitney tests. Data are presented as mean ± SEM. Spearman's rank correlation was used to evaluate significant correlation between FynT/FynB expression and neuritic NP ratings, NFT ratings, and pre-death cognitive (MMSE, see below) scores. For comparisons of gene modulation in primary cultures among the different Aβ treatment groups, we used one-way analyses of variance (ANOVA) with Bonferroni's *post hoc* tests. For all analyses, two-tailed *p*-values of < 0.05 were considered to be statistically significant.

Results

Selective up-regulation of FynT isoform expression in AD brain

Figure 1a shows the Gene View visualization of each probe set in the context of the transcript variants of Fyn, which has been identified to be significantly and differentially spliced in AD based on analyses of our exon microarray database (Lai *et al.* 2014). The two significantly and differentially expressed probesets with up-regulated expression in AD were found to be localized to the FynT-specific exon (2969915 and 2969916, indicated as 1* and 2*, respectively in Fig. 1a). In contrast, three probesets specific for FynB (2969918, 2969958, 2969977, indicated as 1^, 2^ and 3^ respectively in Fig. 1a) showed no change between AD and controls.

We then validated the exon microarray data by real-time RT-PCR using FynB- and FynT-specific primer sets, and confirmed that expression of the FynT isoform was significantly increased in AD (p = 0.0155, Mann–Whitney test); while FynB did not show significant changes in AD (Fig. 1b). Furthermore, relative levels of FynB and FynT transcripts in each sample were measured by RT-PCR followed by capillary electrophoresis as described above. Figure 1c shows representative electropherograms of FynT and FynB, with an elevated FynT peak in AD compared with negligible FynT in control. In contrast, FynB peaks were

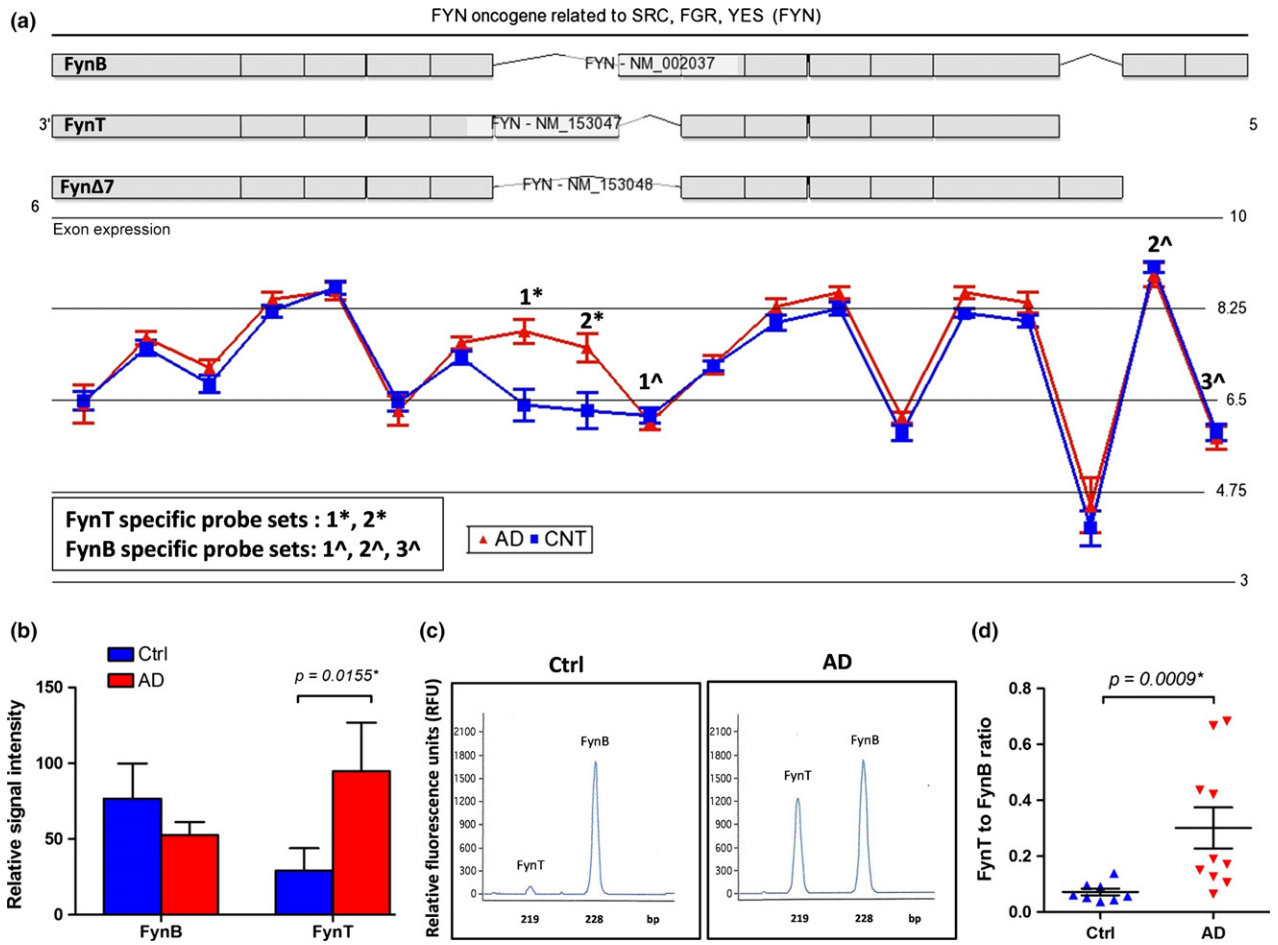

Fig. 1 Selective up-regulation of FynT isoform expression in AD brain. (a) A Gene View display of differential alternative splicing of Fyn was generated from Affymetrix exon array data with AD (red) and control (blue) samples (n = 8 for both groups). Two FynT-specific probeset IDs (1* and 2*) were significantly up-regulated in AD as compared to control samples. FynB-specific probeset IDs (1^, 2^ and 3^) showed no significant changes in AD. The y-axis is a $\log_2$ scale intensity value. (b) Real-time RT-PCR determined the relative signal intensities of FynB and FynT in AD and control brain. (c) The proportional amount of FynT and FynB in AD and control brain was determined by RT-PCR followed by capillary electrophoresis. A representative electropherogram showed the relative fluorescence units (RFU) of FynT peak (219 bp DNA amplicon) and FynB peak (228 bp DNA amplicon) in AD and control samples. (d) Peak areas of FynT and FynB in each electropherogram were translated into expression level and used to determine FynT to FynB ratio of expression. The dot plot showed that AD samples have significantly higher FynT to FynB ratio than control samples (p = 0.0009, Mann–Whitney test). Available samples for RT-PCR and capillary electrophoresis were 10 AD and 8 controls.

high in both groups. Correspondingly, AD was found to have a significantly higher FynT to FynB ratio compared to controls ($p = 0.0009$, Mann–Whitney test, Fig. 1d), thus corroborating the earlier exon array and real-time RT-PCR results and confirming the up-regulation of FynT, but not FynB isoform in AD. Lastly, correlational analyses of gene expression data with neuropathological parameters revealed that FynT levels positively correlated with semi-quantitative NP (Spearman $\rho = 0.72$, $p < 0.01$) and NFT scores ($\rho = 0.78$, $p < 0.01$), and negatively correlated with pre-death cognitive Mini-Mental State Examination (MMSE) (Folstein *et al.* 1975) scores ($\rho = -0.63$, $p = 0.012$). In contrast, there was no significant correlation between FynB gene expression and the neuropathological and cognitive scores (data not shown).

Associations of FynT expression with astrocyte activation and neuronal dysfunction

To further explore the putative role of FynT in AD, GO term enrichment analyses on FynT-correlated genes from the exon array database were performed. Table 1 shows an overview of the biological features of genes associated with FynT expression in AD (see also Table S4 for gene lists corresponding to each GO term). In summary, genes which positively correlated with FynT expression were mainly associated with cytoskeleton organization, cell adhesion, cellular movement and extracellular matrix. The positive correlated gene category with the highest fold enrichment was 'basolateral plasma membrane' (Table 1), a component of cell adhesion, cytoskeleton organization and cell movement (See Table S4). Additionally, we also observed that FynT positively correlated with astrocytic markers including glial fibrillary acidic protein (GFAP) and glutamate aspartate transporter (GLAST, see Table 2). Furthermore, higher proportions of endogenous FynT expression were found in primary rat astrocytes and cell lines of astrocytic lineage as compared to primary rat neurons and neuronal cell lines (see Fig. 2). In contrast, genes associated with synaptic vesicles and various neuronal markers were negatively correlated with FynT expression (Tables 1 and 2). Given the endogenous expression of FynT in T-lymphocytes and other hematopoietic cells (Cooke and Perlmutter 1989), the results may also reflect T-cell infiltration in the AD brain. However, expression levels of T-cell associated markers such as CD3, CD4, CD8 and CD45 were either very low or did not correlate with FynT (see Table 2). Taken together, these

Table 1 Genes which correlate with FynT expression in AD categorized by GO terms

Genes positively correlated with FynT expression				
GO Term ID (Category)[a]	Description	Count[b]	Fold Enrichment[c]	Benjamini p[d]
GO:0008092 (MF)	Cytoskeletal protein binding	44	3.011	7.20E-08
GO:0015629 (CC)	Actin cytoskeleton	26	3.479	4.83E-05
GO:0048522 (BP)	Positive regulation of cellular process	96	1.708	3.39E-05
GO:0007010 (BP)	Cytoskeleton organization	36	2.742	3.18E-05
GO:0016323 (CC)	Basolateral plasma membrane	22	3.900	4.17E-05
GO:0042127 (BP)	Regulation of cell proliferation	51	2.152	6.50E-05
GO:0006928 (BP)	Cellular component movement	36	2.517	1.30E-04
GO:0048523 (BP)	Negative regulation of cellular process	84	1.681	1.77E-04
GO:0031012 (CC)	Extracellular matrix	27	2.817	3.01E-04
GO:0007155 (BP)	Cell adhesion	44	2.088	6.18E-04
GO:0016563 (MF)	Transcription activator activity	29	2.440	4.21E-03
Genes negatively correlated with FynT expression				
GO Term ID (Category)	Description	Count	Fold Enrichment	Benjamini p
GO:0043005 (CC)	Neuron projection	43	3.454	7.04E-10
GO:0045202 (CC)	Synapse	41	3.173	1.66E-08
GO:0031982 (CC)	Vesicle	53	2.173	8.18E-06
GO:0019717 (CC)	Synaptosome	15	4.849	6.04E-05
GO:0005794 (CC)	Golgi apparatus	58	1.827	2.75E-04
GO:0016192 (BP)	Vesicle-mediated transport	46	2.076	1.13E-03
GO:0050804 (BP)	Regulation of synaptic transmission	19	3.632	1.21E-03

[a]Gene ontology (GO) category: biological process (BP), cellular component (CC), molecular function (MF).
[b]Total number of genes correlated with FynT in the GO term.
[c]Fold enrichment is used for measuring the magnitude of enrichment.
[d]p-values adjusted for multiple testing using a false-discovery rate of 5% (see Huang *et al.* 2009a,b).

Table 2 Expression of specific cellular markers in AD versus Ctrl brain ($n = 8$ per group), as well as their significant correlation with FynT expression in Exon array

Exon array Transcript ID	Gene symbol	Specific cellular marker	$\log_2$ base intensity[a]		AD vs. Ctrl		# probesets correlated with FynT ($p < 0.01$)[b]	Pearson correlation coefficient (r)
			Ctrl	AD	Fold	p-value		
3393744	CD3D	T cell	1.846	1.995	1.11	0.27349	None in 6	
3351280	CD3E	T cell	3.258	3.168	−1.06	0.62740	None in 6	
3351300	CD3G	T cell	1.729	2.124	1.32	0.05716	1 out of 4	0.62503
3402786	CD4	T cell	3.746	3.746	1.00	0.99716	None in 12	
2562932	CD8A	T cell	4.080	4.276	1.15	0.13054	1 out of 11	0.62481
2562965	CD8B	T cell	1.460	1.571	1.08	0.40684	None in 4	
2328841	LCK	T cell	3.361	3.668	1.24	0.02322*	None in 17	
2495187	ZAP70	T cell	2.894	3.231	1.26	0.01812*	None in 17	
2373842	CD45	Hematopoietic	2.812	2.872	1.04	0.64841	None in 38	
3655109	CD19	B cell	3.289	3.539	1.19	0.17463	None in 19	
2878437	CD14	Monocyte/macrophage	6.573	6.637	1.05	0.86321	None in 4	
3442706	CD163	Monocyte/macrophage	3.143	4.475	2.52	0.01540*	3 out of 18	0.65404 to 0.71018
3656990	CD11b	Microglia	3.431	3.627	1.15	0.16383	None in 2	
2902444	iba1	Microglia	4.235	4.271	1.03	0.87870	None in 9	
2806643	GLAST	Astrocyte	8.805	9.132	1.25	0.25089	9 out of 15**	0.65104 to 0.79985
3759410	GFAP	Astrocyte	10.729	11.327	1.51	0.02510*	14 out of 14**	0.65573 to 0.78003
2525533	MAP2	Neuron	8.721	8.091	−1.55	0.02259*	2 out of 26	−0.63944 to −0.64138
3128271	NEFL	Neuron	9.035	8.076	−1.94	0.02170*	10 out of 12**	−0.62376 to −0.73384
3090436	NEFM	Neuron	8.965	8.186	−1.71	0.04663*	2 out of 11	−0.65343 to −0.71241
3432394	RPH3A	Neuron	7.737	5.986	−3.37	0.00045*	27 out of 28**	−0.64750 to −0.88786
3674504	TUBB3	Neuron	5.686	5.409	−1.21	0.10308	1 out of 6	−0.65120

[a]Log_2 base intensity is gene-level data.

[b]Correlation between cellular markers and FynT expression was analyzed at the exon-level using probesets in each transcript ID. Only those with significant correlation ($p < 0.01$) were indicated with Pearson correlation coefficient (r) in last column.

*Indicated significant differentially expressed between AD vs. Ctrl ($p < 0.05$).

**Indicated cellular marker with more than half of the probesets showing significant correlation with FynT expression.

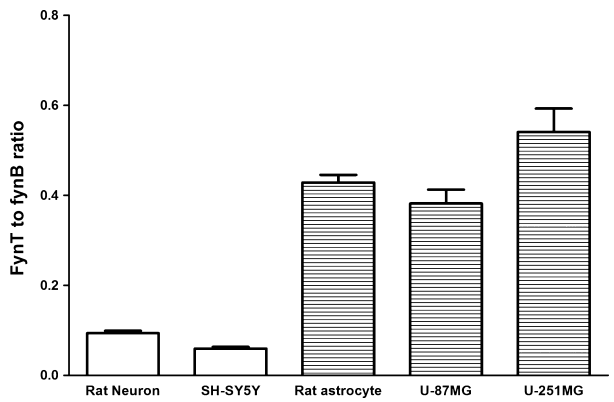

Fig. 2 Higher proportions of FynT expression in cells of astrocytic origin. Endogenous FynT to FynB ratios were determined by RT-PCR followed by capillary electrophoresis (see Methods) in untreated cells of neuronal (primary rat neurons, SH-SY5Y line) or astrocytic (primary rat astrocytes, U-87MG and U-251MG lines, shaded bars) origins. Data are mean ± SEM of at least three independent experiments for each cell type.

results suggest that up-regulation of FynT expression in AD brain is associated with astrocyte activation as well as impairment of synaptic plasticity.

Increased FynT immunoreactivity in AD prefrontal cortex

Using HEK293T cells transiently transfected with either FynT or FynB, we showed that the custom-made antibodies were able to specifically recognize their respective Fyn isoforms (see Figure S1). Furthermore, FynT but not FynB antibody stained positive in CD3-positive cells, suggesting that FynT antibody can specifically recognized endogenous FynT protein (data not shown). In subsequent IF staining with the antibodies, we observed a general, weak FynT immunoreactivity in control prefrontal (BA9) cortex (Fig. 3a, top left panel); whilst in AD, a subgroup of cells with intense staining could be detected (Fig. 3a, top right panel). Image quantitation revealed that a significantly higher percentage of strong FynT-staining cells (4.8 ± 0.6%) was found in AD (Fig. 3b, red circle) compared to control brains

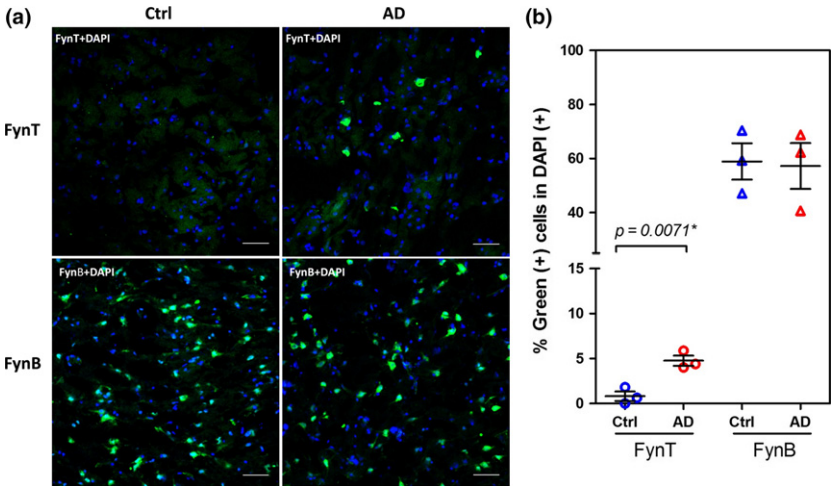

Fig. 3 Increased FynT immunoreactivity in AD prefrontal cortex. (a) Representative IF staining of prefrontal cortex using FynT-specific antibody (green, upper panel) or FynB-specific antibody (green, lower panel) with nuclear DAPI counterstain (blue) were compared between AD and control. Scale bars = 50 μm. (b) Dot plot presents the mean of percentage of cells (defined by DAPI-positive staining) that stained positive for FynT (circle) and FynB (triangle) in AD (red, $n = 3$) and control (blue, $n = 3$) prefrontal cortex. The mean value in each sample is calculated by the percentage of positive cells in five representative images. *Significantly different (Student's *t*-tests).

(0.8 ± 0.5%, Fig. 3b, blue circle). In contrast, FynB immunoreactivities were uniformly prominent in both AD and control sections (Fig. 3, bottom panels), with no significant differences in percentage of stained cells (Fig. 3b, red and blue triangles).

FynT localization to a subset of neurons in AD

To compare cell type-specific expression of FynT and FynB in AD and control brains, we performed double IF staining with neuronal marker NeuN. We observed that strong FynT immunoreactivities were found in NeuN-positive stained neurons (Fig. 4a, white arrows). Note that only a subset of NeuN-positive neurons co-stained with FynT. In contrast, the majority of neurons stained positive for FynB (Fig. 4b), supporting the previously established neuronal localization for FynB (Cooke and Perlmutter 1989). Therefore, FynT up-regulation in AD seems to occur in a subset of neurons, most of which showed unchanged levels of FynB.

FynT localization to reactive astrocytes in AD

Besides neurons, Fig. 5 shows that FynT immunoreactivities were localized to cells that stained positive for GFAP at the thickened processes (white arrows in top panels) and hypertrophic cytoplasm (white arrows in middle panels), both of which are characteristic of reactive astrocytes. We observed that FynT immunoreactivity was relatively stronger in hypertrophic cytoplasm than in the GFAP-positive processes. However, the weaker but specific FynT staining of the astrocytic processes in AD brain could still be resolved (white arrows, Fig. 5 top left panel) even in the presence of strong FynT signals in adjacent non-GFAP cells (putatively neurons, see Fig. 4a). In contrast, corresponding GFAP-positive processes in control brain appeared thinner and showed non-specific background stain for FynT (Fig. 5, white arrows in bottom panels). Our data showed that at least a proportion of FynT immunoreactivities were localized to reactive astrocytes.

Increased FynT in NFT-bearing neurons concomitant with decreased FynB immunoreactivity

Fyn is known to co-stain with NFTs (Shirazi and Wood 1993; Ho *et al.* 2005). Using FynT and FynB-specific antibodies, we can now investigate the specific isoform of Fyn involved in these associations. Neuropil threads as well as NFT-bearing neurons can be detected using AT8, a phosphorylated tau (pS202/pT205)-specific antibody in the AD prefrontal cortex (Fig. 6a, red channels). Interestingly, cells with intense FynT immunoreactivity in AD sections were exclusively co-stained with AT8, manifesting as yellow fluorescence signals of NFT-bearing neurons in merged images (Fig. 6a top right panel, white arrows). In contrast, FynB immunoreactivity was relatively weak in NFT-bearing neurons (Fig. 6a bottom panels, white arrows) compared to the adjacent AT8-negative stained neurons. Mean fluorescence intensities of FynB and FynT in AT8-positive versus adjacent AT8-negative cells were both significantly different but in opposite directions, with increased FynT and decreased FynB in AT8-positive cells (Fig. 6b). Furthermore, FynT immunoreactivity also co-localized with another antibody (Tyr18) specific for tau phosphorylated at tyrosine 18 (pY18), a site previously shown to be directly phosphorylated by Fyn (Lee *et al.* 2004), see Figure S2).

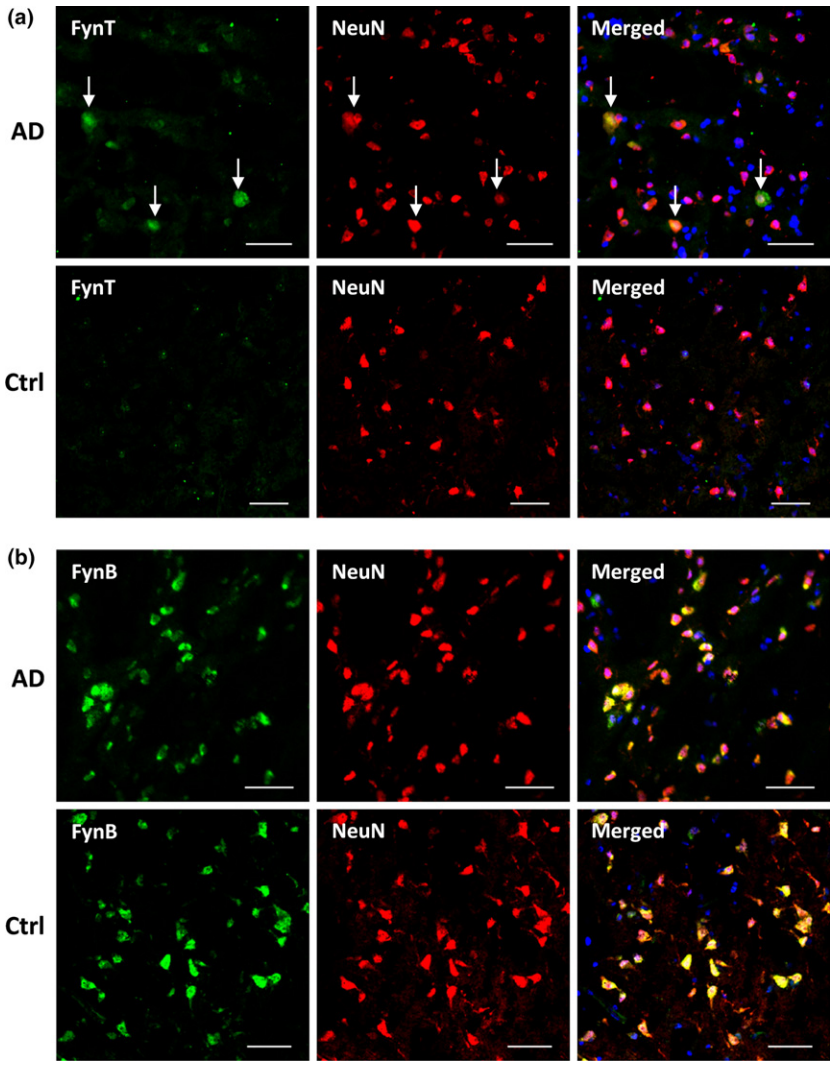

Fig. 4 FynT localization to a subset of neurons in AD. Representative double IF staining of (a) FynT and (b) FynB (green) with neuronal marker NeuN (red) in AD and control prefrontal cortex. Nuclei were counterstained with DAPI (blue). White arrows in (a) indicated cells that were positively co-stained with FynT and NeuN. Scale bars = 20 μm.

Induction FynT and astrocytic markers in primary rat mixed neuron-astrocyte cortical culture by $A\beta_{25-35}$

Aβ treatment is known to induce neuronal degeneration and activate astrocytes *in vitro* (Pike *et al.* 1992, 1994, 1996). We therefore measured expression levels of Fyn isoforms as well as neuronal and astrocytic markers in a primary rat mixed neuron-astrocyte cortical culture treated with $A\beta_{25-35}$ (the toxic moiety of Aβ, see Kaminsky *et al.* 2010) using real-time RT-PCR. At 48 h, significant induction of astrocytic markers glutamate aspartate transporter and glutamate transporter GLT1 (ANOVA $p < 0.05$), as well as trends toward increased GFAP expression (ANOVA $p = 0.0858$) were observed after treatment with $A\beta_{25-35}$, but not with the peptide sequence control, $A\beta_{35-25}$ (Fig. 7). On the other hand, $A\beta_{25-35}$, but not $A\beta_{35-25}$ reduced expression of neuronal marker tubulin β3 (TUBB3, ANOVA $p < 0.05$), with trends toward decreases in RBFOX3 (NeuN gene, ANOVA $p = 0.0618$) and microtubule-associated protein 2 (MAP2, ANOVA $p = 0.0976$, *see* Fig. 7), suggestive of Aβ-induced neurotoxic effects. Interestingly, $A\beta_{25-35}$ treatment selectively up-regulated FynT expression while FynB remained unchanged (Fig. 8a). The experiment was repeated once using full length $A\beta_{1-42}$ and $A\beta_{42-1}$ control peptides with comparable results (data not shown). Similarly, IF staining of $A\beta_{25-35}$-treated primary mixed cultures showed pronounced FynT immunoreactivity with no detectable changes in FynB immunoreactivity (Fig. 8b). Furthermore, quantitative image analyses showed increased FynT mean fluorescence intensity in $A\beta_{25-35}$-treated primary mixed culture compared to the vehicle-treated control (Fig. 8c).

Lastly, to identify the cell types associated with induced FynT immunoreactivity after $A\beta_{25-35}$ treatment, we performed FynT co-immunostaining separately with astrocytic and neuronal markers. Pronounced FynT immunoreactivity was localized to GFAP-positive astrocytes after $A\beta_{25-35}$ treatment, showing clearly discernable yellow signals in the merged image (Fig. 9a, top right panel). In contrast, the image captured using identical microscope and camera

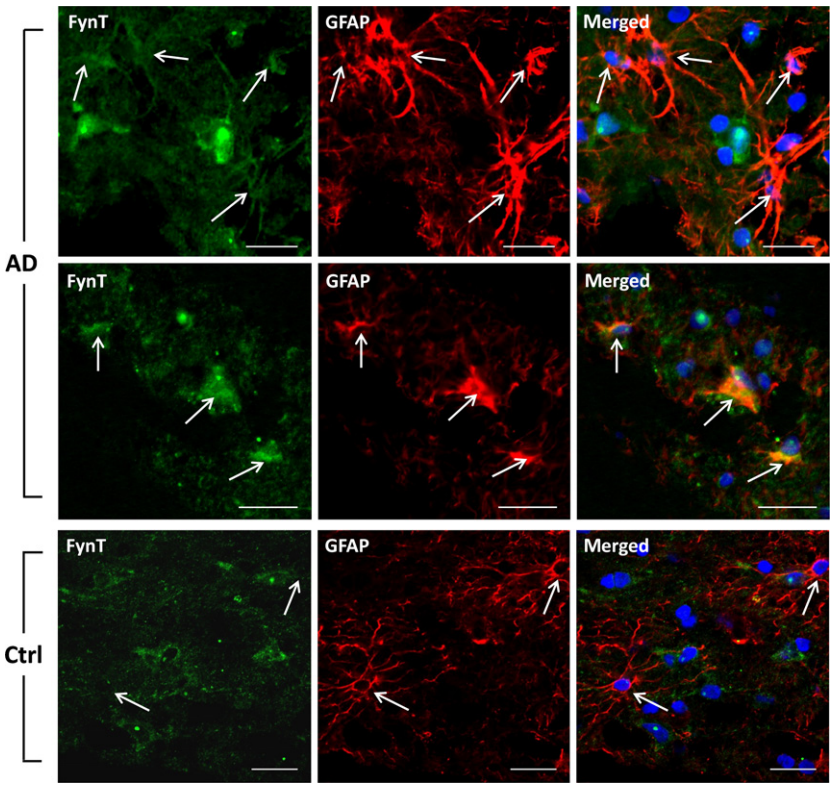

Fig. 5 FynT localization to reactive astrocytes in AD. Representative double IF staining of FynT (green) and astrocytic marker glial fibrillary acidic protein (GFAP) (red) in the prefrontal cortex of AD (top two panels) and control brain (bottom panel). Nuclei were counterstained with DAPI (blue). White arrows indicated astrocytes. Scale bars = 20 μm.

settings demonstrated that only weak FynT immunoreactivity was detected in GFAP-positive cells treated with $A\beta_{35\text{-}25}$ control peptide treatment (Fig. 9a, bottom right panel), suggesting that $A\beta_{25\text{-}35}$ was able to induce FynT expression in astrocytes. For neurons, we selected MAP2 as a marker as it is a neuron-specific cytoskeletal protein highly enriched in dendritic processes (Kosik and Finch 1987). Under control peptide ($A\beta_{35\text{-}25}$) treatment, the outline of the neurons including cell bodies and elongated processes can be clearly labeled by MAP2 (Fig. 9b, bottom panels). Upon $A\beta_{25\text{-}35}$ treatment, reductions in neuronal processes were evident as MAP2 staining was confined to cell bodies (Fig. 9b, top panels), suggestive of an Aβ-induced neuritic dystrophy (Pike *et al.* 1992). Interestingly, FynT immunoreactivity did not seem to be modulated by $A\beta_{25\text{-}35}$ treatment in MAP2-positive cells (Fig. 9b, white arrows in top panel), suggesting that under *in vitro* conditions, the induction of FynT expression by $A\beta_{25\text{-}35}$ was localized to astrocytes.

Discussion

FynT associations with tau phosphorylation and NFT formation

Fyn kinase is postulated to be involved in several aspects of AD pathogenesis, and the current study has further elucidated an isoform-specific role for Fyn in identifying a selective up-regulation of the FynT isoform in AD brain. In view of a previous report showing an increase in Fyn kinase activity but no change in Fyn protein levels in the AD brain (Larson *et al.* 2012), we postulate that the abundant, unchanged expression of FynB in AD could have masked an increase in FynT expression when using non-isoform-specific antibodies. It is also possible that the reported increase in Fyn kinase activity in AD could be contributed by FynT up-regulation because FynT has been shown to exhibit enhanced kinase activity as compared to FynB (Davidson *et al.* 1994; Brignatz *et al.* 2009).

The staining pattern of FynT in relation to tau pathology was consistent with a previous report showing phosphorylation of tau at Tyr18 was localized in NFT but not neuropil threads (Lee *et al.* 2004). Hence, it is conceivable that FynT may be the major modulator of tau hyper-phosphorylation as pTau immunoreactivities (AT8 and Tyr18) co-localized exclusively with FynT, but not with adjacent neurons strongly staining for FynB. Furthermore, Bhaskar *et al.* (2005) also demonstrated that Fyn may bind tau isoforms with different affinities, suggesting the possibility of complex interactions between the Fyn and tau isoforms. An independent study demonstrated that Tyr18 phosphorylation is important in mediating the Fyn–tau interaction and influences the cellular trafficking of tau (Usardi *et al.* 2011). However, whether the co-staining of FynT and phosphorylated tau may implicate their interaction and affecting their cellular trafficking is unknown which warrant further investigation.

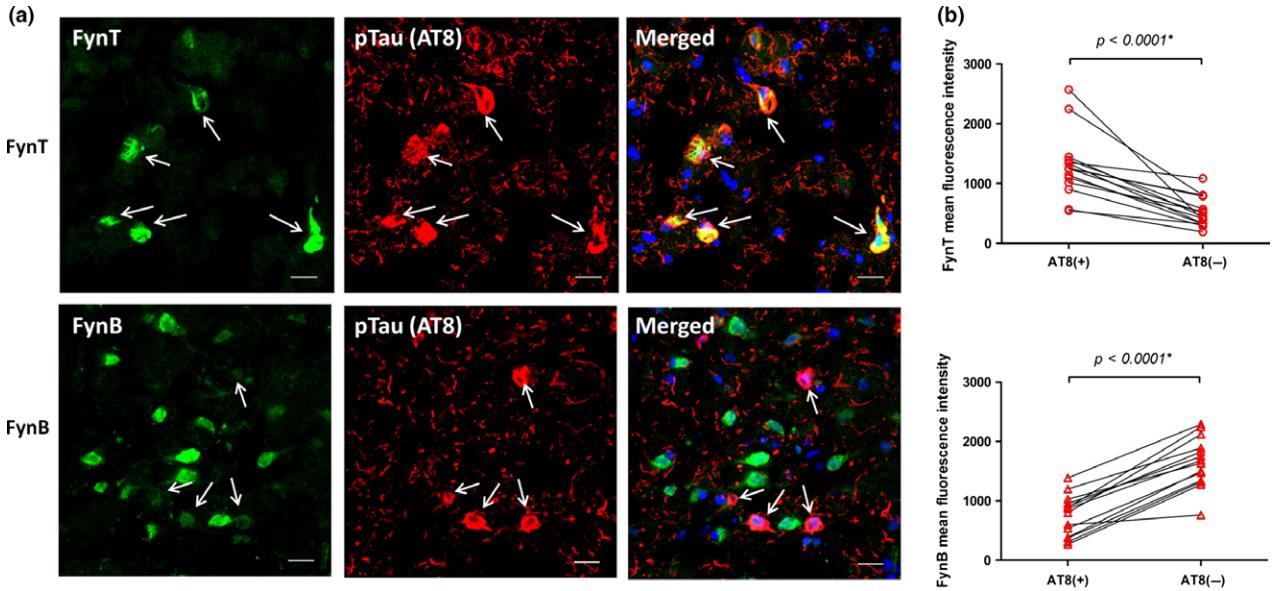

Fig. 6 Increased FynT in neurofibrillary tangles (NFT)-bearing neurons concomitant with decreased FynB immunoreactivity. (a) Representative double IF staining of phosphorylated tau marker AT8 (red) and FynT (green, top panel) or FynB (green, bottom panel) counterstained with DAPI (blue) in the prefrontal cortex of AD brain. White arrows indicated NFT-bearing cells. Scale bars = 20 μm. (b) Mean fluorescence intensities of FynT or FynB in NFT-bearing neurons (defined by AT8-positive staining) and surrounding AT8-negative cells within each representative image are analyzed in pairs. Five representative images were included in each sample for three AD subjects. *Significantly different (Student's paired *t*-tests).

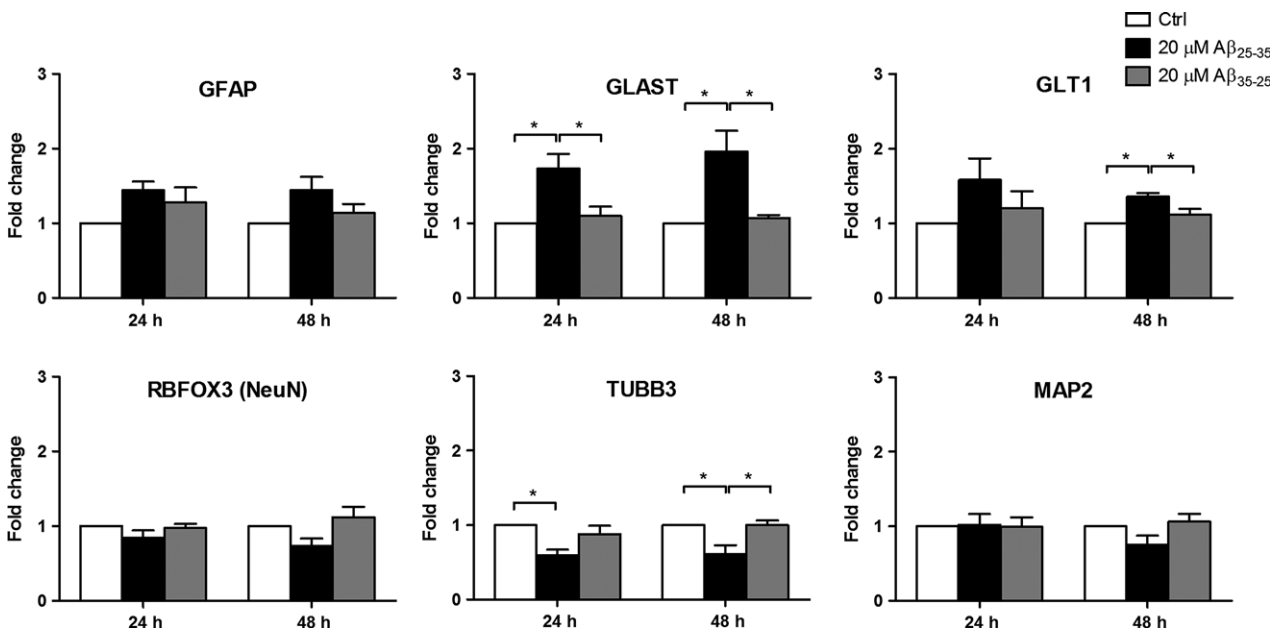

Fig. 7 Gene expression changes in $A\beta_{25\text{-}35}$-treated primary rat mixed neuron-astrocyte cortical culture. Primary rat mixed cortical cultures were treated with 20 μM $A\beta_{25\text{-}35}$ or $A\beta_{35\text{-}25}$ or without treatment (Ctrl) for 24 and 48 h and monitored for gene expression using real-time RT-PCR for astrocytic markers (GFAP, GLAST and GLT1) and neuronal markers (RBFOX3/NeuN, TUBB3 and MAP2). Fold changes were calculated by setting the normalized relative signal intensity of Ctrl as 1. Values are mean ± SEM of at least three independent experiments. *Significantly different (one-way ANOVA with Bonferroni's *post hoc* test $p < 0.05$).

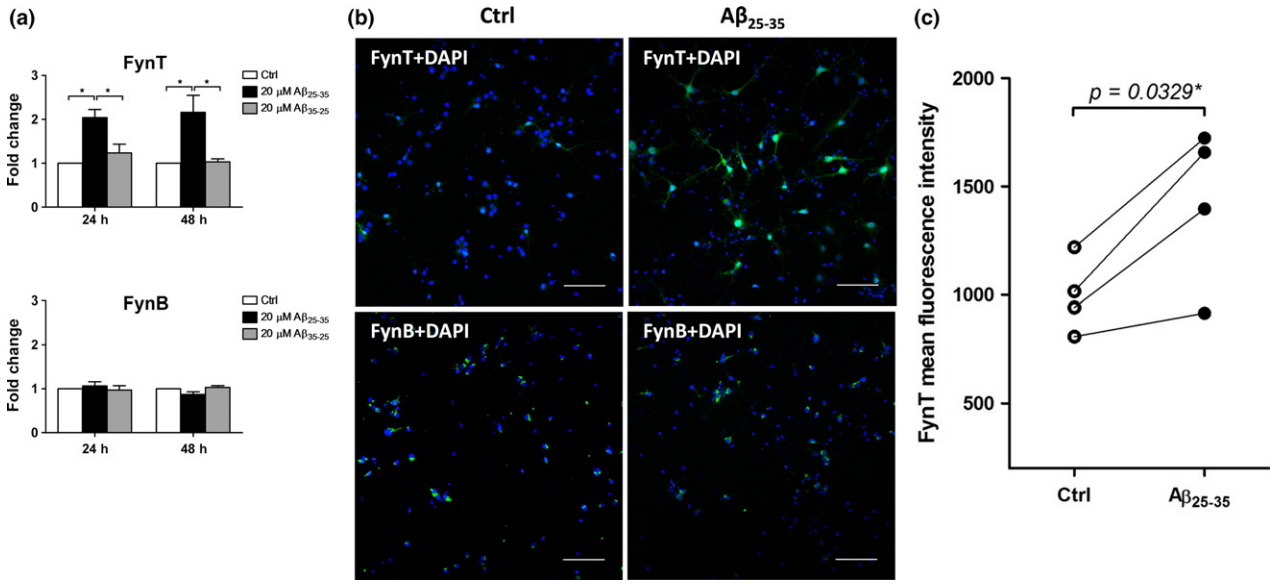

Fig. 8 Specific up-regulation of FynT in $A\beta_{25-35}$-treated primary rat mixed neuron-astrocyte cortical culture. Primary rat mixed cortical culture were treated with 20 μM $A\beta_{25-35}$ or $A\beta_{35-25}$ or without treatment (Ctrl) for 24 and 48 h and monitored for FynT and FynB expression. (a) Real-time RT-PCR results as represented by fold change, was calculated by setting the normalized relative signal intensity of Ctrl as 1. Values are mean ± SEM of 3-4 independent experiments. *Significantly different (one-way ANOVA with Bonferroni's *post hoc* test $p < 0.05$). (b) At 48 h, Ctrl and $A\beta_{25-35}$-treated primary rat mixed cortical culture were stained for FynT or FynB (green). Cell nuclei stained by DAPI (blue) were shown to ensure similar cellular content in each tissue section. Scale bars = 100 μm. (c) The paired dot plot presents the mean of FynT mean fluorescence intensity in $A\beta_{25-35}$-treated primary culture and vesicle treatment control in 4 independent experiment ($p = 0.0329$, Student's paired *t*-test). The mean value in each experiment is calculated by the FynT mean fluorescence intensity in three representative images.

Furthermore, whilst previous studies reported higher Fyn immunoreactivity in NFT-bearing neurons in AD (Shirazi and Wood 1993; Ho *et al.* 2005), our data now suggest that FynT is the predominant isoform associated with the NFT. Intriguingly, the increased FynT expression was accompanied by apparently weaker FynB immunoreactivity in the NFT-bearing neurons (Fig. 6a), suggesting that the up-regulated FynT reflects a modulation of the alternative splicing machinery which favors the FynT isoform, and that this 'switching' to FynT may be associated with AD pathogenesis. Differential alternatively spliced transcripts in human brains associated with aging and neurodegeneration including AD have been detected simultaneously with altered expression of various splicing regulators (Tollervey *et al.* 2011). Furthermore, aberrant tau exon 10 splicing found in some sporadic AD was associated with a dysregulation of alternative splicing (Glatz *et al.* 2006). In view of the close relationship between FynT and tau in NFT-bearing neurons, we speculate that during NFT formation, alternative splicing machinery may be activated to modulate tau exon 10 splicing, as well as Fyn exon 7 splicing to favor FynT expression. However, whether these are the cause or consequence associated with NFT formation is still unclear.

Aβ-treated primary cortical culture showed no changes of FynB and FynT expression in neurons. We speculate that this *in vitro* approach may not be able to recapitulate the induction of alternative splicing machinery and/or NFT formation as found in the AD brain. Alternatively, the negative results may be because of differences in the nature or extent of fyn isoform regulation by alternative splicing between human and rodent. Furthermore, association of Fyn alterations with soluble Aβ should also be investigated in the AD brain.

FynT in association with astrocyte activation

A second major finding of this study relates to FynT and astrocyte activation. Astrocyte-mediated neuroinflammatory responses have long been postulated to play a role in AD (Fuller *et al.* 2009; Steele and Robinson 2012; Medeiros and LaFerla 2013). In this study, we speculate that the increased FynT expression may be partly due to higher numbers of reactive astrocytes in the AD brain, which is corroborated by significant positive correlation between FynT and astrocytic markers, as well as cell adhesion and extracellular matrix proteins (Tables 1 and 2), both of which are known to be highly associated with reactive astrogliosis (Zamanian *et al.* 2012). Furthermore, higher proportions of endogenous FynT

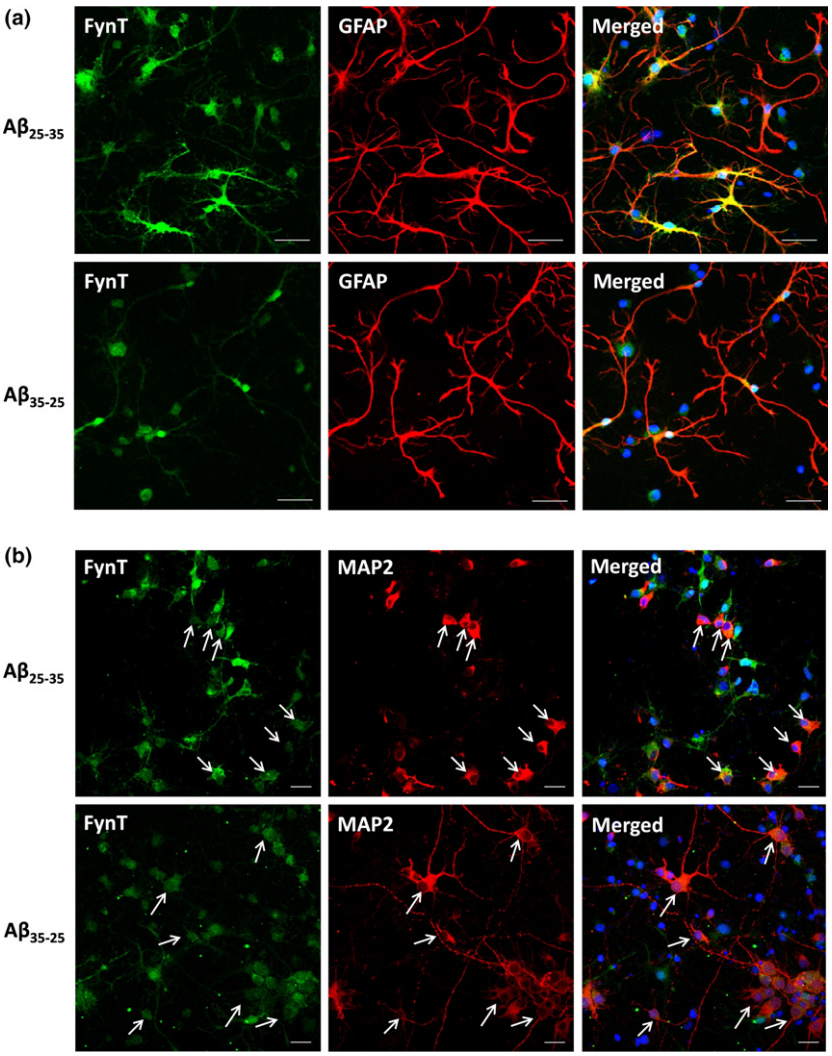

Fig. 9 Increased FynT immunoreactivity in $A\beta_{25\text{-}35}$-treated astrocytes but not neurons. Primary rat mixed cortical culture were treated with 20 μM $A\beta_{25\text{-}35}$ or $A\beta_{35\text{-}25}$ for 48 h. Representative double IF staining of treated cells was demonstrated for FynT (green) and (a) astrocytic marker, glial fibrillary acidic protein (GFAP) (red) or (b) neuronal marker, MAP2 (red). Cell nuclei stained by DAPI (blue) were shown in the merged images. White arrows indicated selected neurons. Scale bars = 20 μm.

expression were found in primary rat astrocytes and glioma cell lines as compared to primary rat neurons and neuroblastoma cell lines (Fig. 2). Additionally, while comparing the modulation of astrocytic FynT expression between AD and control prefrontal cortex, we observed that FynT immunoreactivity was clearly localized to the thickened processes and hypertrophic cytoplasm of activated astrocytes in the AD brain (in addition to NFT-bearing neurons), compared to only weak signals in the control sections, suggesting that FynT may be up-regulated during reactive astrogliosis. This postulate was further supported by the observation of increased FynT expression co-localized with GFAP in primary rat astrocytes under Aβ treatment (Fig. 9a).

Accumulating evidence suggests that Fyn is a crucial player mediating soluble Aβ-induced neuronal dysfunction (Ittner *et al.* 2010; Roberson *et al.* 2011; Yang *et al.* 2011; Pooler *et al.* 2012; Um *et al.* 2012; Wang *et al.* 2013; Xia and Götz 2014). However, to the best of our knowledge, no study has focused on the role of Fyn in astrocytic activation in association with AD. Although we observed Aβ-induced FynT expression in astrocytes of mixed cortical cultures, the etiologic links remain unclear, and may involve both pathogenic (e.g., neurotoxicity) and adaptive (e.g., response to oxidative stress) components. Nevertheless, the consistent observations of FynT association with astrocytic markers in our study suggest that up-regulation of FynT expression in AD may be associated in part with astrocytic activation. Given that astrocytes have been shown to participate in cerebral innate immunity and inflammatory responses (Aschner 1998; Farina *et al.* 2007), and that studies of FynT-specific knockout mice have demonstrated the crucial role of FynT in modulating the immune system (Cooke *et al.* 1991; Davidson *et al.* 2004; Chaimowitz *et al.* 2013), we postulate that the modulation of FynT expression may be associated with astrocyte-mediated neuroinflammatory responses in AD.

Conclusion

This study provides the initial evidence that isoform-specific up-regulation of FynT may be associated with both NFT and reactive astrogliosis in AD, and that alternate splicing may be an important mechanism in disease pathogenesis or response. However, further studies are needed to elucidate the upstream signaling and molecular mechanisms underlying FynT modulation as well as the precise nature of its involvement in NFT formation and astrocyte activation. In the longer term, characterization of the effects of FynT activity in the AD process may provide the rationale for isoform-specific targeting of Fyn in inflammation-focused therapeutic strategies.

Acknowledgments and conflict of interest disclosure

We acknowledge the contribution of patients and their families for this study from OPTIMA. Additional control brain tissues were obtained from the Newcastle Brain Tissue Resource, which is funded in part by a grant from the UK Medical Research Council (G0400074) and by Brains for Dementia Research, a joint venture between Alzheimer's Society and Alzheimer's Research UK. We also thank Dr Gloria Lee from University of Iowa for helpful discussions as well as the generous gift of tau-pY18 (Tyr18) antibody. This study is supported by grants from the Singapore National Medical Research Council (NMRC/EDG/1040/2011) and the Yong Loo Lin School of Medicine, National University of Singapore (R184-000-223-133). The authors declare that there are no conflicts of interest to disclose.

All experiments were conducted in compliance with the ARRIVE guidelines.

Supporting information

Additional supporting information may be found in the online version of this article at the publisher's web-site:

Figure S1. Characterization of FynB and FynT isoform-specific antibodies.

Figure S2. FynT co-localized with pTau (Tyr18) immunoreactivity in NFT-bearing neurons.

Table S1. Demographic and disease variables in AD and control subjects.

Table S2. Primary and secondary antibodies used in "An isoform-specific role of FynT tyrosine kinase in Alzheimer's disease".

Table S3. Primers used in "An isoform-specific role of FynT tyrosine kinase in Alzheimer's disease".

Table S4. Genes associated with FynT expression in AD brain as determined by GO term enrichment analysis.

References

Aschner M. (1998) Astrocytes as mediators of immune and inflammatory responses in the CNS. *Neurotoxicology* **19**, 269–281.

Bhaskar K., Yen S. H. and Lee G. (2005) Disease-related modifications in tau affect the interaction between Fyn and Tau. *J. Biol. Chem.* **280**, 35119–35125.

Braak H. and Braak E. (1991) Neuropathological stageing of Alzheimer-related changes. *Acta Neuropathol.* **82**, 239–259.

Brignatz C., Paronetto M. P., Opi S. *et al.* (2009) Alternative splicing modulates autoinhibition and SH3 accessibility in the Src kinase Fyn. *Mol. Cell. Biol.* **29**, 6438–6448.

Chaimowitz N. S., Falanga Y. T., Ryan J. J. and Conrad D. H. (2013) Fyn kinase is required for optimal humoral responses. *PLoS ONE* **8**, e60640.

Chin J., Palop J. J., Yu G. Q., Kojima N., Masliah E. and Mucke L. (2004) Fyn kinase modulates synaptotoxicity, but not aberrant sprouting, in human amyloid precursor protein transgenic mice. *J. Neurosci.* **24**, 4692–4697.

Chin J., Palop J. J., Puolivali J., Massaro C., Bien-Ly N., Gerstein H., Scearce-Levie K., Masliah E. and Mucke L. (2005) Fyn kinase induces synaptic and cognitive impairments in a transgenic mouse model of Alzheimer's disease. *J. Neurosci.* **25**, 9694–9703.

Cooke M. P. and Perlmutter R. M. (1989) Expression of a novel form of the fyn proto-oncogene in hematopoietic cells. *New Biol.* **1**, 66–74.

Cooke M. P., Abraham K. M., Forbush K. A. and Perlmutter R. M. (1991) Regulation of T cell receptor signaling by a src family protein-tyrosine kinase ($p59^{fyn}$). *Cell* **65**, 281–291.

Davidson D., Chow L. M., Fournel M. and Veillette A. (1992) Differential regulation of T cell antigen responsiveness by isoforms of the src-related tyrosine protein kinase p59fyn. *J. Exp. Med.* **175**, 1483–1492.

Davidson D., Viallet J. and Veillette A. (1994) Unique catalytic properties dictate the enhanced function of p59fynT, the hemopoietic cell-specific isoform of the Fyn tyrosine protein kinase, in T cells. *Mol. Cell. Biol.* **14**, 4554–4564.

Davidson D., Shi X., Zhang S., Wang H., Nemer M., Ono N., Ohno S., Yanagi Y. and Veillette A. (2004) Genetic evidence linking SAP, the X-linked lymphoproliferative gene product, to Src-related kinase FynT in TH2 cytokine regulation. *Immunity* **21**, 707–717.

Farina C., Aloisi F. and Meinl E. (2007) Astrocytes are active players in cerebral innate immunity. *Trends Immunol.* **28**, 138–145.

Folstein M. F., Folstein S. E. and McHugh P. R. (1975) "Mini-mental state". A practical method for grading the cognitive state of patients for the clinician. *J. Psychiatr. Res.* **12**, 189–198.

Fuller S., Münch G. and Steele M. (2009) Activated astrocytes: a therapeutic target in Alzheimer's disease? *Expert Rev. Neurother.* **9**, 1585–1594.

Glatz D. C., Rujescu D., Tang Y. *et al.* (2006) The alternative splicing of tau exon 10 and its regulatory proteins CLK2 and TRA2-BETA1 changes in sporadic Alzheimer's disease. *J. Neurochem.* **96**, 635–644.

Haass C. and Mandelkow E. (2010) Fyn-tau-amyloid: a toxic triad. *Cell* **142**, 356–358.

Ho G. J., Hashimoto M., Adame A., Izu M., Alford M. F., Thal L. J., Hansen L. A. and Masliah E. (2005) Altered p59Fyn kinase expression accompanies disease progression in Alzheimer's disease: implications for its functional role. *Neurobiol. Aging* **26**, 625–635.

Huang D. W., Sherman B. T. and Lempicki R. A. (2009a) Bioinformatics enrichment tools: paths toward the comprehensive functional analysis of large gene lists. *Nucleic Acids Res.* **37**, 1–13.

Huang D. W., Sherman B. T. and Lempicki R. A. (2009b) Systematic and integrative analysis of large gene lists using DAVID bioinformatics resources. *Nat. Protoc.* **4**, 44–57.

Ittner L. M., Ke Y. D., Delerue F. *et al.* (2010) Dendritic function of tau mediates amyloid-b toxicity in Alzheimer's disease mouse models. *Cell* **142**, 387–397.

Kaminsky Y. G., Marlatt M. W., Smith M. A. and Kosenko E. A. (2010) Subcellular and metabolic examination of amyloid-b peptides in Alzheimer disease pathogenesis: evidence for $Ab_{25\text{-}35}$. *Exp. Neurol.* **221**, 26–37.

Kosik K. S. and Finch E. A. (1987) MAP2 and tau segregate into dendritic and axonal domains after the elaboration of morphologically distinct neurites: an immunocytochemical study of cultured rat cerebrum. *J. Neurosci.* **7**, 3142–3153.

Lai M. K., Lai O. F., Keene J., Esiri M. M., Francis P. T., Hope T. and Chen C. P. (2001) Psychosis of Alzheimer's disease is associated with elevated muscarinic M2 binding in the cortex. *Neurology* **57**, 805–811.

Lai M. K., Esiri M. M. and Tan M. G. (2014) Genome-wide profiling of alternative splicing in Alzheimer's disease. *Genomics Data*, **2**, 290–292.

Lambert M. P., Barlow A. K., Chromy B. A. *et al.* (1998) Diffusible, nonfibrillar ligands derived from Aß1-42 are potent central nervous system neurotoxins. *Proc. Natl Acad. Sci. USA* **95**, 6448–6453.

Larson M., Sherman M. A., Amar F., Nuvolone M., Schneider J. A., Bennett D. A., Aguzzi A. and Lesne S. E. (2012) The complex PrP^{c}-Fyn couples human oligomeric Ab with pathological tau changes in Alzheimer's disease. *J. Neurosci.* **32**, 16857–16871.

Lee G., Thangavel R., Sharma V. M. *et al.* (2004) Phosphorylation of tau by fyn: implications for Alzheimer's disease. *J. Neurosci.* **24**, 2304–2312.

Medeiros R. and LaFerla F. M. (2013) Astrocytes: conductors of the Alzheimer disease neuroinflammatory symphony. *Exp. Neurol.* **239**, 133–138.

Mirra S. S., Heyman A., McKeel D. *et al.* (1991) The consortium to establish a registry for Alzheimer's disease (CERAD). Part II. standardization of the neuropathologic assessment of Alzheimer's disease. *Neurology* **41**, 479–486.

Perrin R. J., Fagan A. M. and Holtzman D. M. (2009) Multimodal techniques for diagnosis and prognosis of Alzheimer's disease. *Nature* **461**, 916–922.

Pike C. J., Cummings B. J. and Cotman C. W. (1992) b-Amyloid induces neuritic dystrophy in vitro: similarities with Alzheimer pathology. *NeuroReport* **3**, 769–772.

Pike C. J., Cummings B. J., Monzavi R. and Cotman C. W. (1994) b-amyloid-induced changes in cultured astrocytes parallel reactive astrocytosis associated with senile plaques in Alzheimer's disease. *Neuroscience* **63**, 517–531.

Pike C. J., Vaughan P. J., Cunningham D. D. and Cotman C. W. (1996) Thrombin attenuates neuronal cell death and modulates astrocyte reactivity induced by beta-amyloid in vitro. *J. Neurochem.* **66**, 1374–1382.

Pooler A. M., Usardi A., Evans C. J., Philpott K. L., Noble W. and Hanger D. P. (2012) Dynamic association of tau with neuronal membranes is regulated by phosphorylation. *Neurobiol. Aging* **33**, 431, e427–e438.

Reitz C. (2012) Alzheimer's disease and the amyloid cascade hypothesis: a critical review. *Int. J. Alzheimers Dis.* **2012**, 369808.

Resh M. D. (1998) Fyn, a Src family tyrosine kinase. *Int. J. Biochem. Cell Biol.* **30**, 1159–1162.

Roberson E. D., Halabisky B., Yoo J. W. *et al.* (2011) Amyloid-b/Fyn-induced synaptic, network, and cognitive impairments depend on tau levels in multiple mouse models of Alzheimer's disease. *J. Neurosci.* **31**, 700–711.

Selkoe D. J. (2002) Alzheimer's disease is a synaptic failure. *Science* **298**, 789–791.

Shirazi S. K. and Wood J. G. (1993) The protein tyrosine kinase, fyn, in Alzheimer's disease pathology. *NeuroReport* **4**, 435–437.

Steele M. L. and Robinson S. R. (2012) Reactive astrocytes give neurons less support: implications for Alzheimer's disease. *Neurobiol. Aging* **33**, 423, e421–e413.

Supek F., Bošnjak M., Škunca N. and Šmuc T. (2011) REVIGO summarizes and visualizes long lists of gene ontology terms. *PLoS ONE* **6**, e21800.

Tan M. G., Chua W. T., Esiri M. M., Smith A. D., Vinters H. V. and Lai M. K. (2010) Genome wide profiling of altered gene expression in the neocortex of Alzheimer's disease. *J. Neurosci. Res.* **88**, 1157–1169.

Tollervey J. R., Wang Z., Hortobagyi T. *et al.* (2011) Analysis of alternative splicing associated with aging and neurodegeneration in the human brain. *Genome Res.* **21**, 1572–1582.

Um J. W., Nygaard H. B., Heiss J. K., Kostylev M. A., Stagi M., Vortmeyer A., Wisniewski T., Gunther E. C. and Strittmatter S. M. (2012) Alzheimer amyloid-b oligomer bound to postsynaptic prion protein activates Fyn to impair neurons. *Nat. Neurosci.* **15**, 1227–1235.

Usardi A., Pooler A. M., Seereeram A., Reynolds C. H., Derkinderen P., Anderton B., Hanger D. P., Noble W. and Williamson R. (2011) Tyrosine phosphorylation of tau regulates its interactions with Fyn SH2 domains, but not SH3 domains, altering the cellular localization of tau. *FEBS J.* **278**, 2927–2937.

Wang H., Ren C. H., Gunawardana C. G. and Schmitt-Ulms G. (2013) Overcoming barriers and thresholds - signaling of oligomeric Ab through the prion protein to Fyn. *Mol. Neurodegener.* **8**, 24.

Whitehouse P. J., Price D. L., Struble R. G., Clark A. W., Coyle J. T. and Delon M. R. (1982) Alzheimer's disease and senile dementia: loss of neurons in the basal forebrain. *Science* **215**, 1237–1239.

Xia D. and Götz J. (2014) Premature lethality, hyperactivity, and aberrant phosphorylation in transgenic mice expressing a constitutively active form of Fyn. *Front. Mol. Neurosci.* **7**, 40.

Yang K., Belrose J., Trepanier C. H., Lei G., Jackson M. F. and MacDonald J. F. (2011) Fyn, a potential target for Alzheimer's disease. *J. Alzheimers Dis.* **27**, 243–252.

Zamanian J. L., Xu L., Foo L. C., Nouri N., Zhou L., Giffard R. G. and Barres B. A. (2012) Genomic analysis of reactive astrogliosis. *J. Neurosci.* **32**, 6391–6410.